New Sensing Methods for Scheduling Variable Rate Irrigation to Improve Water Use Efficiency and Reduce the Environmental Footprint

A thesis presented in partial fulfilment of the requirements for the degree of

Doctor of Philosophy

in

Soil Science

at Massey University, Palmerston North, New Zealand.

Ahmed El-Naggar

[2020]

Abstract

Irrigation is the largest user of allocated freshwater, so conservation of water use should begin with improving the efficiency of crop irrigation. Improved irrigation management is necessary for humid areas such as New Zealand in order to produce greater yields, overcome excessive irrigation and eliminate nitrogen losses due to accelerated leaching and/or denitrification.

The impact of two different climatic regimes (Hawkes Bay, Manawatū) and soils (free and imperfect drainage) on irrigated pea (*Pisum sativum*., cv. 'Ashton') and barley (*Hordeum vulgare*., cv. 'Carfields CKS1') production was investigated. These experiments were conducted to determine whether variable-rate irrigation (*VRI*) was warranted. The results showed that both weather conditions and within-field soil variability had a significant effect on the irrigated pea and barley crops (pea yield - 4.15 and 1.75 t/ha; barley yield - 4.0 and 10.3 t/ha for freely and imperfectly drained soils, respectively).

Given these results, soil spatial variability was characterised at precision scales using proximal sensor survey systems: to inform precision irrigation practice. Apparent soil electrical conductivity (EC_a) data were collected by a Dualem-421S electromagnetic (*EM*) survey, and the data were kriged into a map and modelled to predict EC_a to depth. The EC_a depth models were related to soil moisture (θ_v), and the intrinsic soil differences. The method was used to guide the placement of soil moisture sensors.

After quantifying precision irrigation management zones using *EM* technology, dynamic irrigation scheduling for a *VRI* system was used to efficiently irrigate a pea crop (*Pisum sativum*., cv. 'Massey') and a French bean crop (*Phaseolus vulgaris*., cv. 'Contender') over one season at the Manawatū site. The effects of two *VRI* scheduling methods using (i) a soil water balance model and (ii) sensors, were compared. The sensor-based technique irrigated 23–45% less water because the model-based approach overestimated drainage for the slower draining soil. There were no significant crop growth and yield differences between the two approaches, and water use efficiency (*WUE*) was higher under the scheduling regime based on sensors.

To further investigate the use of sensor-based scheduling, a new method was developed to assess crop height and biomass for pea, bean and barley crops at high field resolution (0.01 m) using ground-based *LiDAR* (Light Detection and Ranging) data. The *LiDAR* multi-temporal, crop height maps can usefully improve crop coefficient estimates in soil water balance models. The results were validated against manually measured plant parameters.

A critical component of soil water balance models, and of major importance for irrigation scheduling, is the estimation of crop evapotranspiration (ET_c) which traditionally relies on regional climate data and default crop factors based on the day of planting. Therefore, the potential of a simpler, site-specific method for estimation of ET_c using in-field crop sensors was investigated. Crop indices (*NDVI*, and canopy surface temperature, T_c) together with site-specific climate data were used to estimate daily crop water use at the Manawatū and Hawkes Bay sites (2017-2019). These site-specific estimates of daily crop water use were then used to evaluate a calibrated FAO-56 Penman-Monteith algorithm to estimate ET_c from barley, pea and bean crops. The modified ET_c–model showed a high linear correlation between measured and modelled daily ET_c for barley, pea, and bean crops. This indicates the potential value of in-field crop sensing for estimating site specific values of ET_c.

A model-based, decision support software system (*VRI–DSS*) that automates irrigation scheduling to variable soils and multiple crops was then tested at both the Manawatū and Hawkes Bay farm sites. The results showed that the virtual climate forecast models used for this study provided an adequate prediction of evapotranspiration but over predicted rainfall. However, when local data was used with the *VRI–DSS* system to simulate results, the soil moisture deficit showed good agreement with weekly neutron probe readings. The use of model system-based irrigation scheduling allowed two-thirds of the irrigation water to be saved for the high available water content (*AWC*) soil.

During the season 2018 – 2019, the *VRI–DSS* was again used to evaluate the level of available soil water (threshold) at which irrigation should be applied to increase *WUE* and crop water productivity (*WP*) for spring wheat (*Triticum aestivum* L., cv. ‘Sensas’) on the sandy loam and silt loam soil zones at the Manawatū site. Two irrigation thresholds (40% and 60% *AWC),* were investigated in each soil zone along with a rainfed control. Soil water uptake pattern was affected mainly by the soil type rather than irrigation. The soil

water uptake decreased with soil depth for the sandy loam whereas water was taken up uniformly from all depths of the silt loam. The 60% *AWC* treatments had greater irrigation water use efficiency (*IWUE*) than the 40% *AWC* treatments, indicating that irrigation scheduling using a 60% *AWC* trigger could be recommended for this soil-crop scenario.

Overall, in this study, we have developed new sensor-based methods that can support improved spatial irrigation water management. The findings from this study led to a more beneficial use of agricultural water.

Acknowledgements

This work would not be possible without the support and encouragement I got from colleagues and family.

I sincerely acknowledge the financial support of the New Zealand Ministry for Business, Innovation and Employment's "Maximising the Value of Irrigation" Programme for this PhD work and the scholarship from the Manaaki Whenua Landcare Research for completing this thesis.

I want to express my deep gratitude to my supervisors, Dr. Carolyn B Hedley, A/Prof. David Horne, Dr. Pierre Roudier and Dr. Brent E Clothier for the constant support and guidance needed throughout this study. I thoroughly appreciate the efforts of Dr. Carolyn Hedley and A/Prof. David Horne to allow me to perform research and live in New Zealand. Furthermore, I thank Jagath Ekanayake, John Dando, Paul Peterson, Kevin Sinclair and Kishor Kumar for their technical and experimental support at the field.

I would like to express my gratitude to my fellow students, the staff, and the faculty members of the School of Agriculture and Environment of Massey University for the collaboration over these four years. I am also grateful for the tremendous generosity of Manaaki Whenua Landcare Research.

Special thanks are expressed to my parents for always encouraging me to work hard towards my goals and never giving up.

Table of Contents

List of Tables

List of Figures

Abbreviations and acronyms

AWC	Available water content
SMC	Soil moisture content
PI	Precision irrigation
VRI	Variable-rate irrigation
PM	Penman-Monteith
e_a	Actual vapour pressure (kPa)
e_s	Saturation vapour deficit (kPa)
R_n	Net radiation at the crop surface (MJ m^{-2} d^{-1})
R_s	Solar radiation (MJ m^{-2} d^{-1})
G	Soil heat flux density (MJ m^{-2} d^{-1})
T	Mean daily air temperature at 2 m height (ºC)
u_2	Wind speed at 2 m height (m s^{-1})
Δ	Slope vapour pressure curve (kPa $ºC^{-1}$)
γ	Psychrometric constant (kPa $ºC^{-1}$)
K_c	Crop coefficient
K_s	Water stress coefficient
K_{cb}	Basal crop coefficient
K_e	Soil evaporation coefficient
$Z_{r,i}$	Rooting depth (mm)
$Z_{e,i}$	Effective rooting depth (mm)
RH_{min}	Daily minimum relative humidity during the growth stage (%)
ET	Evapotranspiration
ET_o	Reference evapotranspiration (mm d^{-1})
ET_c	Crop evapotranspiration (mm d^{-1})
K_{sat}	Saturated hydraulic conductivity (mm hr^{-1})
C	Soil organic carbon
GDD	Growing degree day units
SWB	Soil water balance
PAW	Plant available water (reported as mm in a prescribed depth)
DAP	Days after planting
NDVI	Normalized Difference Vegetation Index

fPAR	Fraction of Photosynthetically Active Radiation
R	Red reflectance measurements
NIR	Near-infrared reflectance measurements
WSN	Wireless sensor network
DSS	Decision support system
LEPA	Low Energy Precise Application
IWUE	Irrigation water use efficiency
WUE	Water use efficiency
WP	Water productivity
PT	Priestley-Taylor equation
EB	Surface energy balance approach
GIS	Geographic Information System
NO_3-N	nitrate nitrogen (mg kg^{-1})
NH_4-N	ammonium nitrogen (mg kg^{-1})
PCB	Printed circuit board
EMI	Electromagnetic induction
EC_a	Apparent electrical conductivity (mS m^{-1})
GPR	Ground-penetrating radar
ER	Electrical resistivity
HCP	Horizontal co-planar receiver array
PRP	Perpendicular co-planar receiver array
LIN	Low induction numbers
θ_v	Volumetric moisture content (m^3 m^{-3})
θ_g	Gravimetric moisture content (g g^{-1})
RS	Remote sensing
IRT	Infrared thermometers
LiDAR	Light Detection and Ranging
TOF	Time-of-Flight
ALS	Airborne LiDAR systems
TLS	Terrestrial or ground-based LiDAR systems
UAV	Unmanned aerial vehicles
CSM	Crop surface model
DEM	Digital Elevation Model

IDW	Inverse distance weighting
NN	Nearest Neighbourhood
FC	Field capacity
WP	Wilting point
AD	Allowable deficit (mm)
IR	Irrigation water applied (mm)
P	Precipitation (mm)
RO	Runoff from the soil surface (mm)
CR	Capillary rise from the groundwater (mm)
SWD	Soil water deficit (mm)
TAW	Total available water (mm in a prescribed depth)
θ_{FC}	Moisture content at field capacity ($m^3\,m^{-3}$)
θ_{WP}	Moisture content at wilting point ($m^3\,m^{-3}$)
FAO56-PM	Food and Agriculture Organization Irrigation and Drainage Paper 56 - Penman-Monteith equation
MPM	Modified FAO-56 Penman-Monteith equation
ΔS	Change in soil water storage
NIWA	National Institute of Water and Atmospheric Research
KS	Kolmogorov-Smirnov test of normality
ANOVA	Analysis-of-variance
σ	True electrical conductivity ($mS\,m^{-1}$)
λ	Damping factor
LAI	Leaf area index
FAR	Foundation for Arable Research
T_c	Canopy surface temperature (^oC)
Ta	Air temperature (^oC)
VPD	Vapour pressure deficit (kPa)
FD	Frequency domain capacitance sensor
TDR	Time-domain reflectometer
CWSI	Crop water stress index
ρ_b	Soil bulk density ($kg\,m^{-3}$)
R^2	Coefficient of determination
RMSE	Root-mean-square error

MSE	Mean absolute deviation
CF	Cumulative function modelling
FS	Full solution modelling
CV	Coefficient of variation
MC	Moisture content
h	Crop height (m)
Y_g	Irrigated grain yield (kg m^{-2})
Y_{gd}	Non-irrigated (rainfed) yield (kg m^{-2})
CEC	Cation exchange capacity (cmol(+) kg^{-1})
LOOCV	Leave-one-out' cross-validation approach

Chapter 1

Introduction

1.1 Overview

Irrigated agriculture is the major consumer of allocated freshwater worldwide, accounting for 70% of the total freshwater use (FAO, 2015). Water shortage is a key concern for the future of agricultural production. This is more pressing when viewed in conjunction with climate change which is expected to bring more extreme climatic conditions including droughts (Perea et al., 2018). Thus, concerns over water availability and water quality increasingly require more efficient use of water resources in irrigated agriculture (Perea et al., 2018).

In New Zealand, irrigation accounts for 78% of allocated freshwater (Booker et al., 2016). In 2017, irrigated agricultural land covered 3% (747,000ha) of New Zealand's land area. The area of irrigated agricultural land in New Zealand almost doubled between 2002 and 2017, from 384,000 ha to 747,000 ha (Statistics NZ, 2019). The use of irrigation in New Zealand has resulted in the significant expansion and intensification of a range of farming systems, with irrigation giving greater reliability of production, increased yields, and improved quality of production (e.g., larger and more consistent fruit size) (Kaye-Blake et al., 2014). In a number of primary industries, particularly cropping and horticulture, financial margins, and market demands are 'tight', and irrigation is the only means of ensuring a viable production system.

The two key problems facing freshwater management in in New Zealand are: (i) water is becoming scarce in certain catchments as demand for irrigation and urban water increases (Ministry for the Environment, 2014, Kaye-Blake et al. (2014)) (ii) water quality is deteriorating as water flows reduce and pollutant loads increase, with nitrate leaching being particularly problematic. Some important agricultural land on New Zealand's east coast, located in the rain shadow of the mountains along New Zealand's spine, receive less rainfall and are already limited by a shortage of available water (Kaye-

Blake et al. (2014); Dark et al., 2017). This includes regions such as Central Otago, coastal Canterbury and parts of the Hawkes Bay. Here the potential growth in production is limited by available water so the competition for consumptive and non-consumptive water use has become a prominent issue in recent years, especially in Canterbury where water allocations have increased by 25 million cubic metres per week (11 percent) between 2006 and 2010 (Ministry for the Environment, 2014).

Given the constraints on water availability, it is of paramount importance to increase the efficiency of water use in irrigation. Improved irrigation scheduling is the basis of greater water use efficiency. Irrigation scheduling is the process of determining the timing (frequency) and size of irrigation events. Such schedules are based on: climate, available water content (*AWC*) (Moghaddasi et al., 2010), soil water supply and infiltration rate, crop characteristics, the application rate and distribution uniformity (Delavar et al., 2011) of the irrigation equipment, and regional water allocations (the amount of water allocated to a farmer for irrigation). Freshwater needs to be conserved to maintain the environmental flow in rivers. An irrigation system could be highly efficient but if the allocation is too high – then this has a negative impact on the environment (Grafton et al., 2018). Accurate scheduling maximizes irrigation efficiency by determining the exact amount of water needed to replenish the soil moisture content (*SMC*) to the desired level for optimal plant growth.

Water needs vary spatially in fields because of spatial soil variability (texture, *AWC*, flow pathways, infiltration and drainage rate) (Al-Karadsheh et al., 2002; Evans et al., 2013). Therefore, the need for irrigation may differ between different zones of a particular field. With precision irrigation (*PI*), farmers can manage this discrepancy and irrigate differentially (e.g. targeting the lighter textured soils and avoid over-irrigating poorly drained zones) during the cropping season (Hedley et al., 2013). As *PI* equipment such as variable-rate irrigation (*VRI*) centre pivots become increasingly available to agricultural producers in New Zealand, research is needed to determine how to best manage these irrigation systems to optimize crop yield and water resources. However, optimising irrigation will depend not only on the use of *PI* systems but also on the tools that can help the farmer monitor, manage and automate irrigation scheduling, so that water is applied precisely to satisfy crop water requirements (Ekanayake & Hedley, 2018; Lea-Cox, 2012).

Wireless transmission of *SMC* and other site-specific parameters such as canopy-air temperature differences ($T_c - T_a$) and normalised difference vegetation index (*NDVI*) will inform and allow real-time water applications that precisely match the water needs in each area. In addition to wireless sensor networks (*WSN*), the use of remote (e.g. light detection and ranging (*LiDAR*)) and proximal sensing survey (e.g. electromagnetic induction (*EMI*)) technologies offers unique opportunities to make the non-invasive, non-destructive and very reliable measurements required to map soil variability and monitor crop performance at high spatial resolution (i.e. 0.01 – 5 m) (Corwin & Lesch, 2003; Friedli et al., 2016; Zhang & Grift, 2012).

1.2 Problem statement

Irrigation water requirements vary spatially and temporally within fields depending on soil properties, crop type and stage of growth, and topography. Therefore, at any irrigation event, the water requirement is likely to differ between different zones of a particular field. When travelling irrigation systems apply water at constant rates, some areas of the field may receive too much water and others not enough.

The use of *VRI* addresses this problem (i.e. it can vary the rate of water applied with individual sprinkler control), but farmers need a smart scheduling regime if they are to realise the benefits of these improved irrigation systems. In other words, precision scheduling methods are required to support the ability of *VRI* equipment to precisely apply water. Precision management is needed to match precision hardware. Research is needed to develop more accurate sensing methods and techniques, which are based on high resolution spatio-temporal information of soils and crops and/or modelling, to inform spatial *VRI* scheduling tools, models and other Decision Support Systems (*DSS*). In addition, research is needed to assess the relative benefits of smart scheduling to plant production, irrigation water use efficiency (*IWUE*) and nutrient leaching.

Research Question: Is it possible to develop new sensing technology methods to improve the spatio-temporal resolution of *VRI* decision support systems?

1.3 Aim and objectives

This research aimed to optimise the value of irrigation water by developing new sensing methods which could be practically adopted, or integrated into existing tools, to improve *VRI* scheduling.

These sensing methods focus on the fundamental soil and crop parameters used by the soil water balance (*SWB*) i.e. soil water content, soil water status, crop height, crop evapotranspiration (ET_c). Method development takes advantage of recent advances in connected sensor technologies to deliver high resolution spatio-temporal information to support the latest *VRI* hardware systems.

Individual research objectives are as follows:

1- Investigate the effects of spatial variability of water stress (waterlogging; drought) on crop growth and the possible benefits of implementing *VRI* strategies.

2- Develop and validate a novel method for mapping and characterising soil physical property variability in the field with high spatial (6 m) and depth resolution (< 0.15 m to 1.5 m) using *EMI* technology so that this variability can be accounted for in irrigation management.

3- Compare the use or integration of real-time soil moisture monitoring with a *SWB* modelling approach for irrigation scheduling.

4- Develop a novel sensing method for high resolution mapping of crop height (0.01m accuracy) to inform spatial *VRI* scheduling tools and models.

5- Investigate the use of site-specific crop sensor data (*NDVI*; T_c) to simplify and improve spatial estimations of ET_c in order to support latest *VRI* scheduling tools and models.

6- Evaluate an existing spatially explicit, decision support software tool for *VRI* systems, and the potential and need to include high resolution spatio-temporal environmental data (rain, soil, crop) including data streams developed in this study.

7- Implement the *VRI* software informed by high resolution spatio-temporal data streams (from Objective 6) to investigate the impact of two irrigation thresholds (i.e. criteria) on crop yield, irrigation demand, drainage and leaching risk.

1.4 Thesis design

This thesis is presented in ten chapters. This thesis has been developed as a collection of seven manuscripts (Chapters 3, 4, 5, 6, 7, 8 and 9):

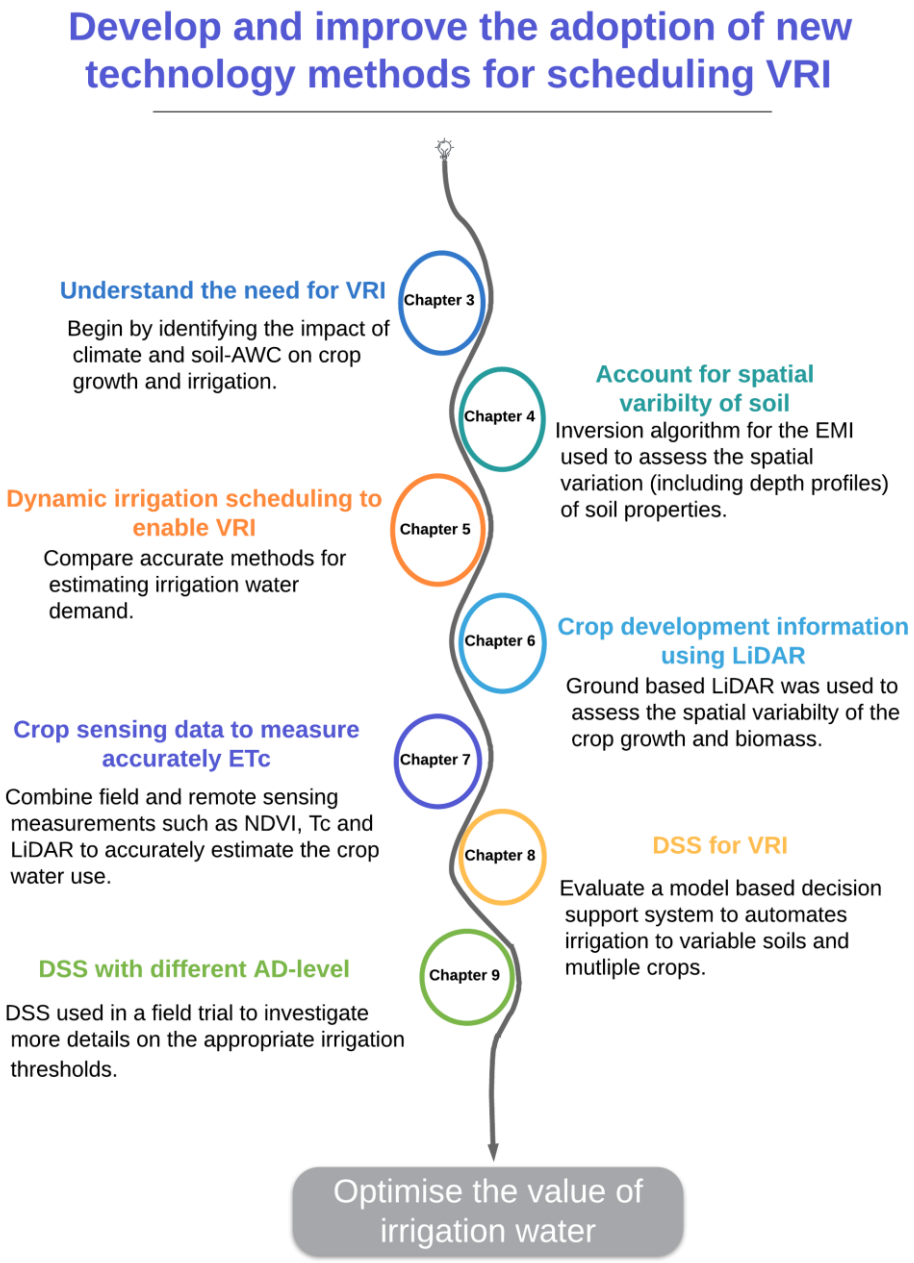

Chapter 2

Literature Review

2.1 Irrigated agriculture and water use efficiency

Cultivated land under well-managed irrigation produces greater yields per unit area than non-irrigated agriculture, by reducing crop water stress under drought conditions. Without irrigation, the same level of crop production would require a far greater area of land under cultivation (El Chami et al., 2019).

Agriculture accounts for roughly 70% of total freshwater withdrawals globally (FAO, 2015). 38% of this irrigated area depend on groundwater (Siebert et al., 2013), which has contributed to a ten-fold increase of groundwater abstraction for agricultural irrigation over the last 50 years. Water-use efficiency (*WUE*) improvements are considered instrumental to address the projected 40% gap between demand and supply and to mitigate water scarcities by 2030 (UNEP, 2011). Well managed systems that lessen negative environmental impacts such as drainage and run-off with associated nutrient losses are urgently needed in many countries (Daccache et al., 2015), including New Zealand.

The potential savings from increased *WUE* could be as high as US$115 billion annually by 2030 (Dobbs et al., 2011). Too much irrigation resulted in low crop *WUE* and effective irrigation using less water can lead to a higher yield and *WUE* (Daccache et al., 2015; Zhang et al., 2004). Irrigation delivery systems commonly include two broad categories; these are surface (gravity), and pressurized (e.g. centre pivot and linear move systems, sprinkler, and drip systems). Pressurized systems deliver water in smaller, more precise amounts than surface systems, which contributes to their greater *WUE* potential (Hedley et al., 2013). The *WUE* of pressurized systems can be enhanced by using variable rate water applicators (Perea et al., 2018), and through supervisory control and data acquisition (Ekanayake & Hedley, 2018; Ruiz-Garcia et al., 2009) to customize irrigation

based on root zone water content (*AWC*) in each portion of the field.

Rapid irrigation development has taken place in New Zealand, particularly at the turn of the 20th century, with increasing levels of investment in irrigation systems and irrigation research (Dark et al., 2017). Some regions in New Zealand, such as parts of Hawke's Bay, Canterbury, Otago, and the Wairarapa are seasonally drought limited, receiving less than 800 mm rain per year (Fig. 2.1a). In general, the introduction of new irrigation systems into these regions has been highly successful and has driven agricultural intensification in the drier areas, improving and sustaining the general well-being of rural communities. Irrigation schemes in New Zealand currently cover some 650,000 ha of land (Fig. 2.1b). In 2012, spray systems were utilised on 74% of New Zealand's land with 18% of farms still utilising flood systems (Connor, 2015), and the percentage of spray systems has probably continued to increase to the current day.

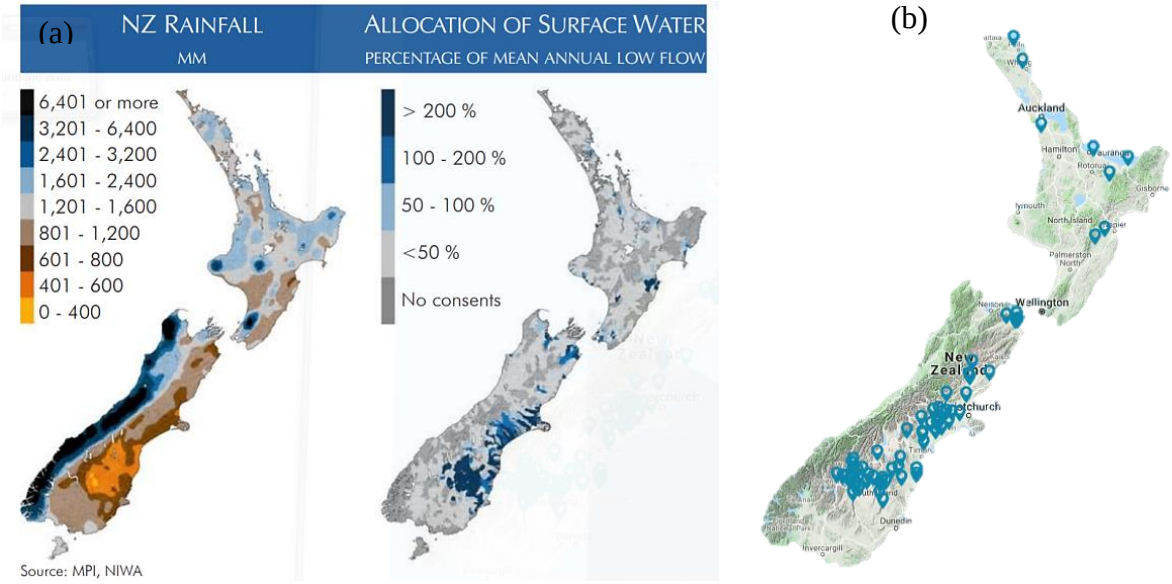

Figure 2.1: (a) the wide range of annual regional rainfalls and allocation of surface water in New Zealand (NIWA, 2018) (b) irrigation schemes in different regions of New Zealand (Irrigationnz.co.nz)

2.2 Variable-rate irrigation (*VRI*)

The major driver for variable-rate irrigation (*VRI*) is the presence of spatial variability within an irrigated field that (i) affects water availability (sufficiency or excess) to a crop and limits crop yield or quality or (ii) regulates water application due to erosion, runoff,

leaching or other environmentally sensitive problems (Daccache et al., 2015; El Chami et al., 2019). Common sources of within-field variability derive from variation in soil properties and topography, either naturally occurring or induced by human management (e.g., compaction, erosion, organic matter depletion) that in turn regulate *AWC*, soil, and terrain hydrologic properties, and nutrient supply (Perea et al., 2018; Pierce, 2010). Nielsen et al. (1973) were one of the first to quantify the within-field variability of field-measured soil-water properties in an irrigated field. According to Evans et al. (2013), *VRI* is the ability to spatially vary water application depths across a field to address specific soil, crop, and/or other conditions (e.g. see Fig. 2.2).

The majority of research into *VRI* deals with continuous move irrigation systems, primarily centre pivot and linear move systems as the platform on which sensing and control take place, recent advances have also been made for fixed irrigation systems, for example, in orchards (Coates & Delwiche, 2008). *VRI* in continuous move irrigation systems has evolved since the first system was reported in 1992 by Fraisse et al. (1993) and Duke et al. (1992) and most of the research at that time was for spatially variable application of water and fertilizers with databases of spatially referenced data being used for system control (Camp & Sadler, 1998; Duke et al., 1997; Evans et al., 1996; King & Kincaid, 1996; Sadler et al., 2000a).

For centre pivots, *VRI* is currently complemented by two techniques: (i) speed control varies the fraction of time that the outermost tower is moving, so application depth can be different in each sector of the field (*VRI* Speed Control - One slice is one sector: Figure 2.3a). (ii) nozzle control varies the fraction of time that each sprinkler or bank of sprinklers is turned on, so application depth can be different angularly and radially. Both mechanisms may be integrated for zone control *VRI* (*VRI* Zone Control -One block is one management zone: Fig. 2.3b).

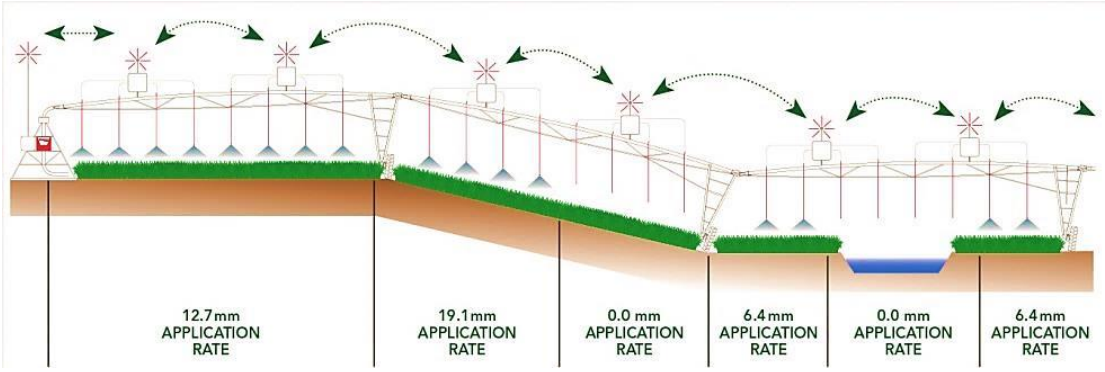

Figure 2.2: Different water application rates across a field using variable-rate irrigation (*VRI*) centre pivot under different conditions (Breneger et al. (2015), Irrigationnz.co.nz).

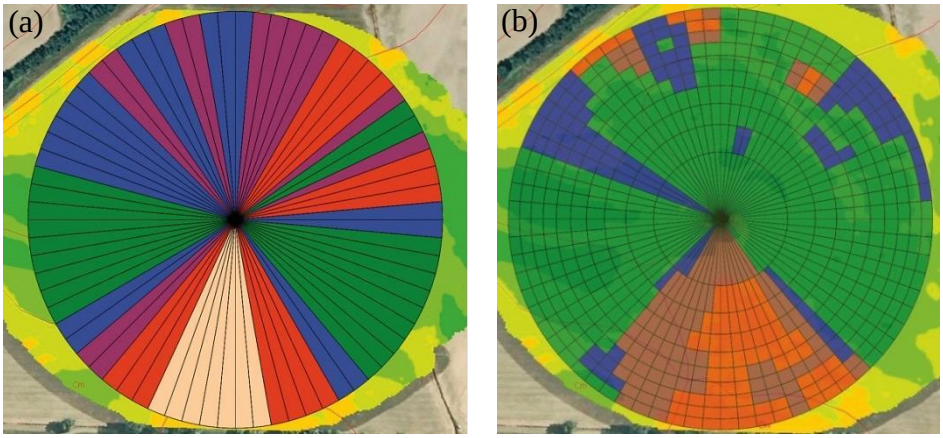

Figure 2.3: Example prescription map for A) a speed control and B) a zone control variable-rate irrigation (*VRI*) centre pivot; each color indicates a different irrigation application depth (Breneger et al. (2015), Irrigationnz.co.nz).

According to Sadler et al. (2000b), variations in water availability across a field because of different soil characteristics may cause farmers to 1) ensure that areas with the smallest *AWC* receive adequate water, 2) manage the whole field based on average soil water conditions, or 3) limit water application to avoid over-irrigating the wettest areas. All of these scenarios will cause over-irrigation or under-irrigation of other areas due to the inability of current irrigation systems to differentially apply irrigation water based on soil and plant factors within a single irrigated field. Chemical leaching below the root zone, surface runoff, or potential yield decreases in particular areas can occur under each management strategy.

Over recent years, *VRI* (i.e., site-specific centre-pivot irrigation) has emerged as an effective and convenient means of customizing irrigation to parts of a field (Evans et al., 2013). With *VRI*, the application depth, intensity, and timing, as well as the spatial extent

of each management zone, can now be controlled at levels of precision that had been infeasible in the large fields of modern agriculture (Daccache et al., 2015).

Hedley and Yule (2009a) reported that around 25% of the water savings can be achieved by efficient application of site-specific irrigation models. Oliveiria et al. (2005) reported that for tomato production in Tennessee, uniform management required 20% more applied water compared with site-specific management. Merely achieving a small but consistent yield improvement would make *VRI* adoption profitable (Marek et al., 1998), irrespective of water savings.

The impact of *VRI* benefits can reach beyond field boundaries. For example, reducing nitrogen (*N*) leaching with *VRI* not only decreases fertilizer budgets but may also improve the quality of drinking water and the environment. Meisinger and Delgado (2002) presented the principles for managing nitrate-N (NO_3-*N*) leaching where one of the key principles to reduce NO_3-*N* leaching is site-specific irrigation management. This was reported for the spatial variability of residual soil NO_3-*N* and NO_3-*N* leaching during the growing season (barley, canola, and potato) for centre-pivot irrigated systems. The residual soil NO_3-*N* in a loamy sand zone was lower than that measured for the sandy loam zone. The NO_3-*N* leached from the irrigated crops in the loamy sand zone areas was therefore assumed to be higher than for these crops grown on the sandy loam zone.

Several research studies have been carried out in the past decade using variable irrigation centre-pivots or linear moves (King et al., 1999; Sadler et al., 1996; Sadler et al., 2000b; Wall et al., 1996). Omary et al. (1997) developed an automated system for centre pivots that enabled variable application depths within 9-m long segments at a given speed. The system used three-manifolds per segment that could be operated individually or in various combinations to provide eight different application rates at any given tower velocity. McCann et al. (1997) developed a control system for centre pivots and linear move systems that enabled spatially varied water application along the lateral in a stepwise manner, using electric solenoid valves and control modules to operate multiple sprinklers with different nozzle sizes. Signals to the control modules were transmitted along a single cable by a microprocessor according to the position of the irrigation system relative to a target application map. Buchleiter et al. (1995) developed a spatially variable application system for a linear move system that used computerized control to vary the travel speed, and hence application depth, in the direction of travel. *VRI* in each half-span along the

lateral was achieved by pulsing the flow to individual manifolds with an auxiliary controller interfaced with the primary control panel.

VRI's benefits were quantified on several intensely studied fields by conducting simulations (Daccache et al., 2015; DeJonge et al., 2007; El Chami et al., 2019; Hedley & Yule, 2009b; Nijbroek et al., 2003; Perea et al., 2018) or field experiments (Hillyer & Higgins, 2014; Khalilian et al., 2008; King et al., 2006).

The *VRI* systems generally consist of the following components as described by Breneger et al. (2015) (see Fig. 2.2 and 2.3):

1- PC software: is used to create the *VRI* farm irrigation plan. The plan consists of management zones defined by layer type. Each layer defines the parameters (where/how much) that each substance is applied. This is loaded into the *VRI* controller; either manually via a communication cable, USB stick or through a wireless connection. Some advanced systems use web-based application software to reduce the need for the irrigator to have a high spec computer. This also allows the development company to upgrade/update the software without needing to visit the irrigator.

2- *VRI* controller: generally mounted on the irrigator, it reads and interprets the irrigation plan and uses data from other inputs (such as Global Positioning Systems (*GPS*) coordinates) to calculate which valves need to be actuated at any one time. It controls water outlets including individual sprinklers and the end gun. The *VRI* controller also has the ability to record and report its status and events.

3- Wiring loom: this consists of a cable that runs between nodes delivering power from the power source to the node. Different system types also use the wiring loom to connect the *VRI* controller to the valve nodes and transmit data along the length of the irrigator.

4- Valve nodes: consisting of a watertight enclosure and a printed circuit board (*PCB*) containing the processor and drivers to control relays and in turn valves.

5- Manufacturers use different hardware in this area. Some use wireless technology to control the valve node while other manufacturers use a continuous cable system linking one node to the next along the length of the irrigator.

6- Solenoid valves: require a signal from the node to actuate. There are two types of solenoids currently available:

- Continuous powered solenoids require the signal current to be either continuously on or off depending on the desired state of the valve.

- Latching solenoids require a polarity pulse to actuate the valve on or off.

7- *GPS* unit: is mounted at the end of the pivot to send a signal back to the *VRI* controller notifying it of the position of the irrigator, and allowing it to calculate the valve control signals at this point. A lateral-move irrigator will have a *GPS* on each end of the irrigator.

8- Speed control: is the part of the *VRI* software that calculates and matches the speed of the irrigator with the pulsing of the solenoid valves to maximise the application efficiency and minimise the return time of the irrigator. The combination of both the variation in ground speed and a number of nozzles operating reduces both the depth (mm/ha) and the rate (mm hr^{-1}) near the centre point where normal uniform-rate irrigators over irrigate, thus improving instantaneous application rates on longer (+500 metre) pivot irrigators.

2.3 Mapping the spatial variability of soil and crop characteristics

It is necessary for *VRI* system presented in **Section 2.2** to strategically account for the spatial variability of soil water and crop characteristics distribution in the field, therefore this Section explains how we can do this using proximal and remote sensing survey system.

2.31 Identifying soil variability by electromagnetic induction (*EMI*)

Identifying soil water content (*SWC*) and *AWC* variability in agricultural fields can be assessed in a variety of ways. Traditional core sampling provides very accurate information but induces very serious labour costs to generate high-resolution data. The geophysical technologies such as ground-penetrating radar (*GPR*), electrical resistivity

(*ER*), or electromagnetic induction (*EMI*) (Allred et al., 2008; Allred et al., 2010) have the potential to produce high-resolution data while reducing field monitoring costs and increasing efficiency.

EMI is a highly adaptable non-invasive technique that measures the apparent bulk electrical conductivity (EC_a) of the soil (De Jong et al., 1979). The principle of *EMI* sensors is to firstly generate a primary magnetic field that induces very small currents in the soil which in turn generate a secondary magnetic field. This secondary magnetic field is measured by a receiver coil in the sensor. Sensors are designed so that the secondary and primary magnetic field are linearly proportional to EC_a (Corwin & Lesch, 2005). Measurement of soil EC_a is a frequently used and very reliable method to indicate field variability in precision agriculture (Corwin & Lesch, 2003). Commercial examples of *EMI* sensors include the EM-31 and EM-38 soil conductivity meters (Geonics Ltd, Mississauga, ON., Canada) and Dualem systems (DualEM, Milton, ON, Canada). The depth of exploration of the soil profile is proportional (for homogeneous material) to the distance between the transmitting and sensing coils for *EMI* sensors. Four examples of *EMI* sensors are shown in Fig 2.4. Also, there are multi-coil *EMI* sensors e.g. "Dualem-421" which incorporates an *EM* transmitter that operated at a fixed low frequency (9 kHz) and 3 pairs of horizontal co-planar (*HCP*) and perpendicular (*PRP*) receiver arrays. The depth of EC_a measurement is, respectively, 0–1.5 (1m*Hcon*), 0–3.0 (2m*Hcon*) and 0–6.0 m (4m*Hcon*), and 1.1, 2.1 and 4.1 m (*PRP*) (Triantafilis et al., 2013a). The approximate incremental response by the depth of the *HCP* and *PRP* of the Dualem-2S and Veris 2000XA is shown in Fig. 2.5A. The EC_a measurement provided by the instrument is an integrated response to EC_a with depth, as weighted by this instrument response function (McNeill, 1980). Theoretical considerations underlying the derivation of *EMI* instrument response functions are discussed by (McNeill, 1980). These include operation at low induction numbers (*LIN*) and the instrument being located on the surface of a homogeneous half space. Integrating the response curves with respect to depth gives the cumulative fraction of the total response to depth z and clearly shows the different soil volumes examined by the sensors (Fig. 2.5B).

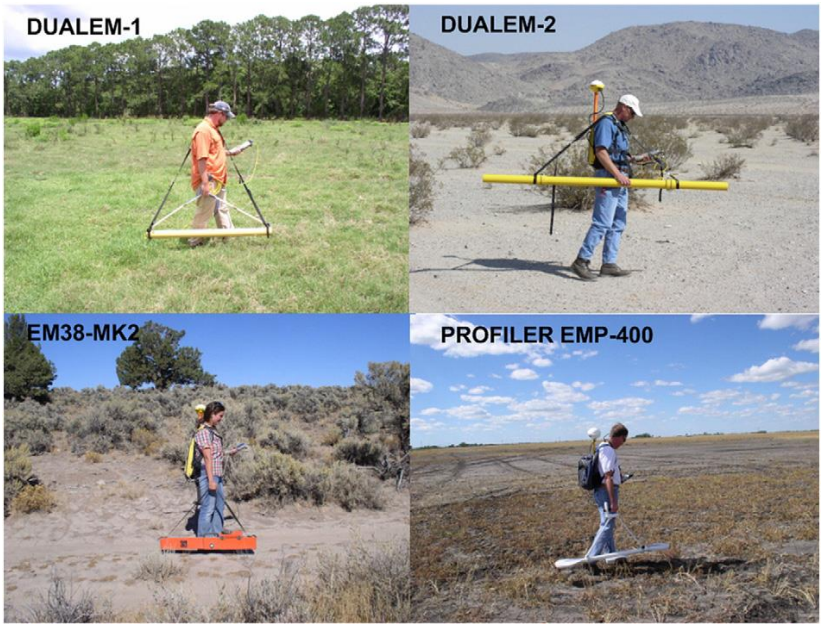

Figure 2.4: Four electromagnetic induction (*EMI*) sensors commonly used in soil investigations are the Dualem-1 meter, the Dualem -2 meter, the EM38-MK2 meter, and the Profiler EMP-400 (Doolittle & Brevik, 2014).

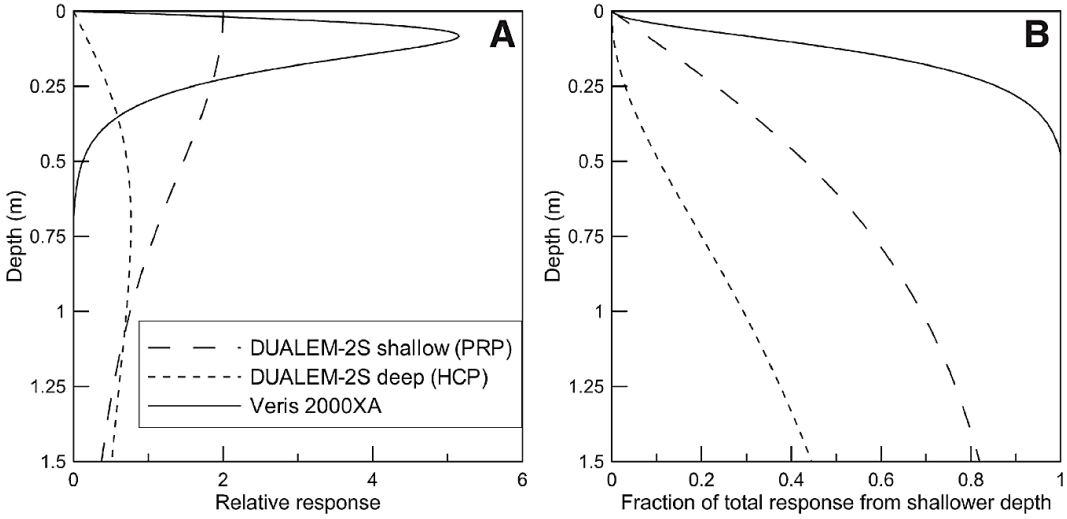

Figure 2.5: Incremental (A) and cumulative (B) response curves for the three apparent bulk electrical conductivity (EC_a) datasets used in Sudduth et al. (2013) study.

EC_a is a variable that can be measured densely by on-the-go *EMI* sensor survey systems (Adamchuk & Rossel, 2011). The surveys could be carried out in the field with hand-held or vehicle-mounted sensor instruments with *GPS* unit and the measurements are read directly from an integrated datalogger. In theory, EC_a relates to the number of conducting pathways through the soil. This is controlled by the number of charged surfaces (e.g. broken clay surfaces, soil solution); connecting pathways between minerals (including

the degree of compaction); and continuous soil solution (Rhoades et al., 1989). Variations in EC_a principally affected by the type and concentration of ions in solution, the amount and type of clays in the soil matrix, water content, and the temperature and phase of the soil water (McNeill, 1980). EC_a increases with increases in insoluble salt, water and clay contents, and temperature (McNeill, 1980). The EC_a value is dependent on the *SWC*, soil clay content, soil clay mineralogy, cation exchange capacity, soil bulk density and soil temperature (Dabas et al., 2001).

In literature, there are many examples of research that include how the EC_a data is used to delineate spatial variability (precision agriculture zones) in addition to soil properties. Ekwue and Bartholomew (2011) observed in their experiments a strong positive correlation between the EC_a and the *SWC* for three soil types evaluated in laboratory and field conditions. Brevik et al. (2006) monitored the EC_a and volumetric moisture content (θ_v) of soil and concluded that EC_a is strongly influenced by θ_v. Doerge et al. (1999) suggested that EC_a could be successfully related to *AWC*, which would be closely related to soil texture, so long as proper field verification is performed. Mertens et al. (2008) recommended that ground truth verification be performed when using EC_a data because the regression of EC_a data versus clay percentage was found to vary from site to site. Doerge et al. (1999) noted that the relationship between EC_a and crop yield was strongest when *AWC* was the main factor influencing yield differences; this suggests that EC_a should also be related to *AWC* if other variables such as salinity are consistent. EC_a is known to relate well to clay content (Sudduth et al., 2005a; B. Williams & Hoey, 1987). Sand particles have a low electrical conductivity while the charged surfaces of clay particles have a high conductivity; therefore, finely textured soils should produce high EC_a values while coarse soils should produce low EC_a values (Lund et al., 1999; Sudduth et al., 2005a). EC_a can be used to improve the estimation of soil variables, when they are spatially correlated (Moral et al., 2010). Moral et al. (2010) found a high positive correlation between EC_a and clay content. Sudduth et al., 2005a reported that soil EC_a can be calibrated to any specific soil property so long as the soil property of interest dominates the other local soil properties that influence EC_a readings. Corwin and Lesch (2003) found a correlation coefficient of 0.76 for EC_a to percent clay. Similar work performed by Fulton et al. (2011) also showed correlation coefficients between EC_a and percent clay, sand, and silt of around 0.75; however, the correlation success varied throughout the field.

Hezarjaribi & Sourell, 2007 used EC_a to predict *AWC*. This technique has been implemented using Geonics- *EMI* type sensors or Veris coulter type sensors. Also, the EC_a parameter had been used in many studies as an important secondary variable when performing in-field zoning (Fulton et al., 2011; Moral et al., 2010; Serrano et al., 2014). Hedley & Yule, 2009a used an indirect approach to first delineate the field into management zones based on the dense EC_a data and then assign a uniform *AWC* to each management zone based on *AWC* of the sampled locations within that management zone. Hezarjaribi & Sourell, 2007 used a direct approach by using regression or geostatistics to predict *AWC* throughout the field based on the *AWC* and EC_a datasets. Regardless of the approach, a strong relationship between *AWC* and EC_a is critical to the success of this technique of making *AWC* maps. If such a relationship does not exist in the field of interest, then other dense geospatial datasets would be needed. Fortes et al., 2015 indicated that EC_a is a useful tool to improve guided soil sampling for the agricultural management of soils. This information may be helpful for the planning of more efficient irrigation management, through the adaptation of the design of the irrigation installation according to soil factors.

The success of the research mentioned above that relates EC_a to *SWC, AWC* and soil texture characteristics suggest that EC_a has the potential to allow users to successfully identify precision management zones for irrigation management.

2.32 Assessing crop growth using Light Detection and Ranging (*LiDAR*)

Parameters such as crop height, leaf cover, and biomass density are relevant for the assessment of crop stands (e.g. crop yields; site-specific amount of water, fertilizers and pesticides) (Ehlert et al., 2010c). Remote Sensing (*RS*) systems have demonstrated capabilities for monitoring at finer spatial resolutions and over smaller extents, including identifying key variables relevant to crop. All proximal and *RS* information is then useful to guide soil and crop samplings and assist decision-making process regarding property management (Andreo, 2013).

Considering the growing availability of data collected by low-cost sensors installed on satellites and/or in unmanned aerial vehicles, *RS* technology represents great promise (Jha & Chowdary, 2007) for use in monitoring and managing irrigation over long periods (Santos et al., 2010). Among *RS* sensors, the most used are cameras, scanners, video cameras, Light Detection and Ranging (*LiDAR*), infrared thermometers (*IRT*), and Normalised Difference Vegetation Index (*NDVI*) sensors.

LiDAR is a non-contact optical device that measures the distance to an object in a scanning field with high accuracy (1 cm to 5 cm vertical accuracy) using a laser beam (Shrivastav, 2015). Advantages of this active *RS* method are, e.g., its non-invasive and non-destructive measurements, its capability to capture crops area-wide in high geometric detail, its ability to partly penetrate ('see-through') objects like vegetation, and its independence of lighting conditions (Hofle, 2014; Lumme et al., 2008).

LiDAR systems currently available on the market use various measuring principles: light time-of-flight, phase modulation, interferometry, and triangulation. In many cases, the first three principles are combined into the technique known as Time-of-Flight (*TOF*) measurement. Triangulation sensors measure short ranges (maximum a few meters) with high accuracy, while *TOF* sensors are suitable for both short and far range (Ehlert et al., 2009a).

LiDAR systems can be used in different ways:

(i) Satellites and airborne *LiDAR* systems (*ALS*) for detecting medium-ranged areas from aircraft (500-1,000 m) and helicopters (200-300 m). These are very costly technologies, used mainly for mapping land topography (Krabill et al., 1984); forest road alignment (Akay et al., 2014); sustainable forest management (Akay et al., 2009; Hudak et al., 2009; Lefsky et al., 2002; Woods et al., 2011) ; estimating vegetation characteristics (Nelson et al., 1988); water depth measurement (Penny et al., 1989); measuring the distances from points on earth to satellites (Hecht, 2011).

(ii) Terrestrial or ground-based *LiDAR* sensors (*TLS*) are e.g. suitable for surveying purposes such as architectural applications, for mobile road-mapping systems and for the determination of forest inventory parameters.

Agricultural crops have high growth dynamics and a short life cycle on the order of months, so with the aim to manage agricultural crop production, current information is needed - sometimes within hours or seconds. Therefore, using a low-cost sensor to perform real-time operations makes the use of *TLS* acceptable for agricultural purpose (Ehlert et al., 2009a).

LiDAR is increasingly applied in precision agriculture-related studies (Hofle, 2014; Paulus et al., 2014; Saeys et al., 2009; Zhang & Grift, 2012). Ehlert conducted various studies (Ehlert et al., 2009b; Ehlert et al., 2010c, 2010d) for measuring the crop biomass by the use of different *LiDAR* sensors. Chatzinikos et al. (2013), found a high correlation between crop biomass and mean crop heights (R^2 from 0.79 to 0.99). Hofle (2014) used *LiDAR* to detect single maize plant positions and their heights in a 132 m × 6 m field, for growth monitoring and site-specific plant treatment.

Friedli et al. (2016) studied genotypic differences between canopy height growth during the season for maize (*Zea mays*), soybean (*Glycine max*) and wheat (*Triticum aestivum*) by using *TLS*. Eitel et al. (2014) also used both *TLS* radiometry and geometry to detect the *N* status of wheat for optimizing fertilizer applications.

2.33 Spatial analysis methods in precision irrigation

Spatial analysis methods can be used to interpolate point measurements in order to create a continuous surface map or to describe the spatial pattern. Numerous studies have shown the benefits of spatial analysis techniques in agricultural management (Stewart et al., 2002). This approach provides a multitude of powerful interpolation methods with advanced analytical tools for generating optimal interpolated surfaces from discrete spatial data measurements.

There are mainly two groups of interpolation techniques: deterministic and geostatistical. Deterministic techniques use mathematical functions that form weighted averages of nearby measured values to create a surface, while geostatistical techniques use both mathematical and statistical methods and the autocorrelation of the attribute with their position in the landscape to assist the modelling process.

2.331 Deterministic interpolation technique

Deterministic methods only use the geometric characteristics of point data to create a continuous surface. There are numerous techniques to characterize and model the spatial distribution of a data set:

1- Inverse distance weighting (*IDW*)

Inverse distance weighting (*IDW*) is a simple and intuitive deterministic method for multivariate interpolation with a known scattered set of points. The un-sampled points are calculated with a weight function of the known points that include more observations. So, it is an advanced nearest neighbour theory that considers more points than only the nearest observation. It estimates values by weighted average using nearby observations. The weight decreases as distance increases (Ly et al., 2013). Therefore, the closer points have more influence on the predicted point than the further distance point, which may cause a "bulls-eye" effect. *IDW* is a simpler interpolation technique in that it does not require pre-modelling like kriging (Tomczak, 1998). By using this technique, we can obtain maps with which it is possible to perform from simple mathematical operations to more complex geostatistical analysis (Best & Leon, 2006).

1- Nearest Neighbourhood (*NN*)

The nearest neighbourhood (*NN*) is a simple and fast method of multivariate interpolation. The theory of *NN* method is to assign value to a certain grid cell from the nearest point (Sluiter, 2008). However, this method requires a dense dataset to be used successfully.

2.332 Geostatistical interpolation technique

All of the above described interpolation methods do not assume any parametric distribution for data. There is another technique; however, that assumes a continuous and normal distribution of values of a variable in the geographic space of a field. This technique is called Geostatistics. Mapping of the variables sampled using geostatistical methods and a reference grid (raster map or surface map), is a recommendable measure (Plant, 2001).

Geostatistics is a means to describe spatial patterns and to predict the values of spatial attributes at unsampled locations, where a sample is expected to be affected by its position and relationships with its neighbors. The basic concept in geostatistics is that there is a spatial correlation between two sample points that depends on the distance of the sample points, with points further apart being less likely to be related than points closer together. It is an intuitive concept that locations close to one another have values more alike than locations that are farther away. Detailed descriptions of the theory of geostatistics are given, for example, by (Cressie, 1989; Goovaerts, 1997; Journel & Huijbregts, 1978; Olea, 2000; Webster & Oliver, 2007)

Geostatistics uses the variogram or semi-variogram, as a mathematical description of the relationship between pairs of observations, at different distances. Several models may then be fit to the experimental variogram (the one based on observations in the field) which are then used as a basis for the modelling, using kriging methods (Best & Leon, 2006).

Kriging is an optimal interpolation based on regression against observed values of surrounding data points, weighted according to spatial covariance values. The advantage of kriging over other interpolation methods such as *IDW* is that kriging estimates the value at unsampled locations using a minimized estimation variance derived from a semi-variogram model, accounting for spatial correlation in the samples (Deutsch & Journel, 1998). The estimation at an unsampled location is given as the linearly weighted sum of its surrounding points. Over the past several decades kriging has become a fundamental tool in the field of geostatistics (Isaaks & Srivastava, 1989). There are different types of kriging can be used, the commonly used methods are:

1- Ordinary kriging

Ordinary kriging is the basic form of kriging interpolation. It measures values by linear combination, using a variogram to determine the weight of data and describe the spatial correlation (Yang, 2015).

2- Co-kriging

Co-kriging uses a multivariate variogram or co-variance model with additional co-varying data (Sluiter, 2008). The theory of co-kriging is based on the linear weighted sum

of all the test data to estimate a location, so when there are two or more co-variables, the method may become more complex. Moreover, the result is better when both covariables and the spatial correlation are higher.

2.333 Inversion of EMI data

Inversion of geophysical data is a mathematical procedure that seeks to obtain the distribution of one (or more) physical property in the survey area (or volume) to depth. In the *EMI* case, electrical conductivity (or resistivity) is the property of interest. Therefore, from a finite number of data (EC_a values) at more than one depth of exploration, this method investigates the distribution with depth of the data set.

Triantafilis and Santos (2010) illustrated that EM4Soil inversion software can be used to invert single frequency (EM38 and EM31) and multiple coil arrayed Dualem-421 data to produce a depth map of exchangeable sodium percentage (Huang et al., 2014), clay content (Triantafilis & Santos, 2013c) and θ_v (Huang et al., 2016)

There are three model candidates: layered earth (1D); an earth model allowing the variation of conductivity in two directions (2D) or a more realistic model allowing that the conductivity varies in the three directions (3D) (EMTOMO, 2014).

The parameterization of each model is obviously different, and the number of unknown parameters increases from 1D to 3D models. The model to be adopted depends on several factors but the most important is the geophysical array used in the data acquisition. Because this information is partial, several models can fit the data. The model can be improved and validated using additional information e.g. from boreholes or other geophysical indirect methods (EMTOMO, 2014). **Appendix A** shows the description of inversion algorithm (EM4Soil) by Santos (2004).

2.4 Monitoring the temporal changes of soil and crop water status

Recent innovations in low-voltage sensor and wireless radio frequency technologies combined with advances in Internet technologies offer tremendous opportunities for development and application of real-time management systems for agriculture (Kim et al., 2008; Q. Liang et al., 2007; O'Shaughnessy & Evett, 2010). While quantifying differences between precision management zones for irrigation management using *EMI* technology in **Section 2.3**, wireless sensor networks (*WSN*) promise to give a higher yield and lower input cost by real-time monitoring of the field soil, crop and environment conditions using sensors placed in the field management zones which send the sensed data via a gateway to a cloud-based database so that a global decision can be taken spatially and temporally about the physical environment, within near real-time.

WSNs are applied in agriculture for a variety of applications such as irrigation, cultivation, fertilizer management, pesticide spraying; animal monitoring, etc. They consist of a collection of sensor nodes used in real-time monitoring of the field soil, crop and environment conditions using different sensors and thereby improving crop cultivation, reducing time and labour costs. Each sensor node consists of five components: sensor/actuator, controller, communication device, memory, and power supply. The sensors gather the environment data, which are processed intelligently by an embedded system. The information is transmitted to a decision centre by a wireless communication network, which provides remote monitoring for management of the agricultural environment (Yu et al., 2013).

Early research:

Feedback networking control systems based on evaporation measurements were described by Phene et al. (1992) and Vermeiren and Jobling (1980). In both systems the control was accomplished by measuring the evaporation in a class “A” pan and triggering the irrigation when the water level dropped to a preset limit. The pan was refilled proportionally to the amount of water being applied through irrigation, and a feedback

networking system was installed so that the system switched off when the pan was refilled.

Phene and Howell (1984) developed a high-frequency irrigation system that can be controlled accurately by the feedback of wireless sensor soil moisture sensor installed in the crop root zone. Automatic irrigation using feedback from soil sensors makes it possible to maintain almost constant soil water potential in the root zone. This produces the desired plant responses, and hence high yields while using the exact volume of water required to maintain the crop.

Several network feedback irrigation control systems have been developed using microcomputers and data loggers as controllers (Meron et al., 1995; Phene & Howell, 1984; Shock et al., 1998; Stone et al., 1985; Testezlaf et al., 1997; Torre-Neto et al., 2000; Wessels et al., 1995; Zazueta & Smajstrla, 1992).

Recent research:

Recent major advances in *WSN* technology have been driven by the accessibility of the internet and cellular communication systems, leading to the development of low power, low cost, multifunctional sensor node systems. *WSNs* sense the environment and provide continuous data for processing elsewhere. Various sensors can be attached to the nodes, e.g. crop and soil sensors. The nodes coordinate and send sensor data to the base station. Hedley et al. (2012) developed a *WSN* soil moisture monitoring method in *EM* defined zones to provide information for irrigation scheduling. Data were presented in digital format for incorporating into the *VRI* controlling software. The irrigation was by a centre pivot irrigator with *VRI* modification. Each sprinkler was controlled individually by digital maps uploaded to a central controller. Data were relayed to a base station every 15 minutes and processed in real-time and converted to the necessary format and immediately made available through a 3G cellular modem via the internet to a webpage. End users could access the web site. This *WSN* method provided a direct measure of the *SWC* status and the need for irrigation. It has the advantages of using site-specific real-time *SWC* data and site-specific climatic conditions to schedule the irrigation.

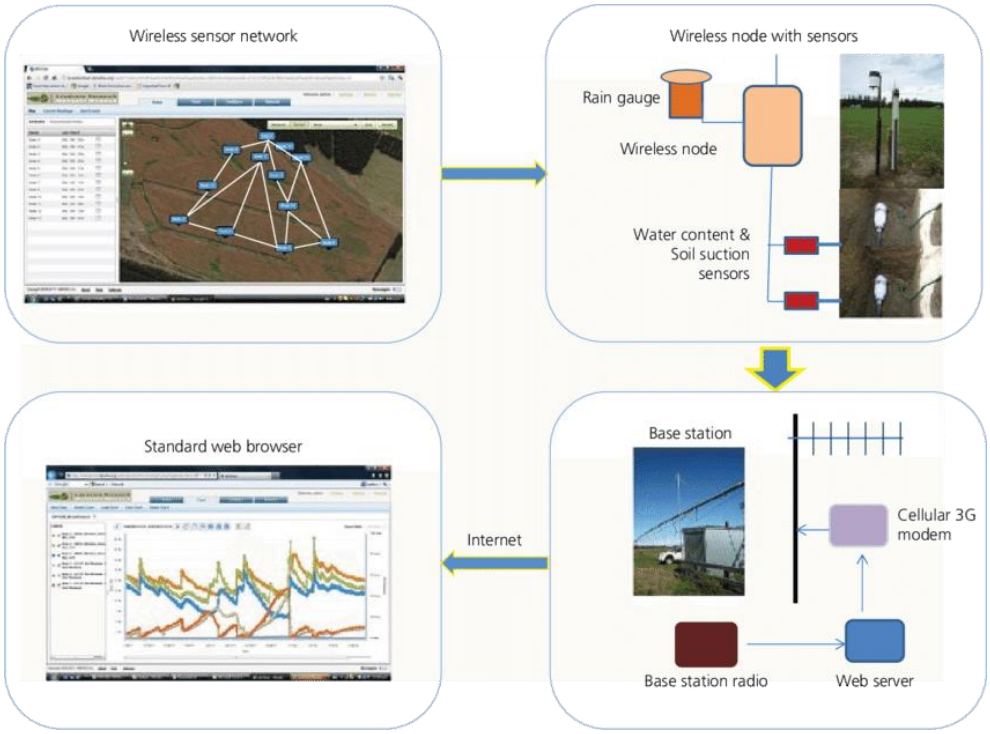

Figure 2.6: Schematic flowchart of wireless soil moisture sensor network (Hedley et al., 2012)

Also, a number of *WSN*'s for *SWC* and *IRT* sensors with various topologies (e.g. star, mesh-network) have been developed and investigated by different researchers in the past decade (Ekanayake & Hedley, 2018; Ruiz-Garcia et al., 2009) including *WSN*'s for irrigation scheduling in cotton (Vellidis et al., 2008), centre-pivot irrigation (Ekanayake & Hedley, 2018; O'Shaughnessy & Evett, 2008) and linear-move irrigation systems (Kim et al., 2008).

Ekanayake and Hedley (2018); Nikolidakis et al. (2015) reported the ideology of *WSNs* for data acquisition, Peijin et al. (2011) reported the ideology of using *WSN* to collect parameters of *SWC* and communicate with the master PC via e.g. an RS232 interface. Xuejun et al. (2013) reported on an automatic irrigation control system based on *SWC* meter. Xiao et al. (2010) reported that water-saving irrigation control is realized by using GSM (Global System for Mobile communication) technology, remote data transmission of soil moisture is realized by using General Packet Radio Service (*GPRS*), which was confirmed by Chen and Tang (2012).

More recent work in the area of *WSNs* is the usage of *IRT* to develop automatic scheduling of irrigation and control (Ekanayake & Hedley, 2018; Evett et al., 2008; Peters & Evett, 2004, 2005, 2008). Another important development in the area of *VRI* with *WSNs* is the

usage of radio transmitters and installation of Low Energy Precise Application (*LEPA*) and sprays on the same irrigation system (Camp et al., 2006). The application of water using non-stationary irrigation systems were studied in New Zealand (Hedley & Yule, 2009a; Yule et al., 2008).

2.5 Irrigation scheduling methods

Irrigation scheduling ascertains when to irrigate the crop and how much water (time and quantity) to apply (Thompson et al., 2007). Its primary purpose is to maximize the irrigation efficiency by applying the exact amount of water needed to replenish the soil moisture to a level that meets the water demands of the crop. The FAO-56 modelling approach defines the irrigation water requirement for a well-watered crop as the depth of water needed to meet water loss through ET_c of a disease-free crop under non-limiting soil conditions (Allen et al., 1998).

The success of any irrigation method depends largely on utilizing irrigation scheduling principles to develop a management plan, and on efficiently implementing the plan. Excessive irrigation leaches salts from the root zone, which is beneficial for salinity control. However, excessive irrigation may also leach nutrients important to the crop; the leached nutrients can become pollutants in groundwater and streams. Under-irrigation may limit yields, especially if it occurs during flowering and fruit development stages.

Previous studies with a variety of crops, ornamental and turf species have reported that the use of appropriate scheduling methods and *VRI* technologies can save a significant amount of water, while maintaining or increasing yield and product quality and minimise negative environmental impacts (Bacci et al., 2008; Beeson & Brooks, 2006; Blonquist et al., 2006; Fereres et al., 2003).

Appropriate methods of irrigation scheduling are necessary to improve *WUE*, especially when faced with rising competition between protection of the environment and the various end-users of water resources (Jones, 2004a). Irrigation scheduling techniques can be divided into three categories: (i) soil moisture measurements-based approach involving direct measurements of soil moisture (e.g. with neutron probes, capacitative or *TDR*-type sensors, tensiometers; Smith (2000); (ii) soil water balance (*SWB*) calculated from

meteorological data (Allen et al., 1998); and (iii) direct measurement of plant water status (Jones, 2004b).

2.51 Soil moisture-based methods

Soil moisture plays a major role in the growth of crops along with soil temperature, and knowledge of its status in the soil for irrigation scheduling is critical. *SWC* measurement methods include gravimetric and instrument sensing methods (Charlesworth, 2005). The instrument sensing methods measure other properties of the soil that vary with water content and relate it to the soil water content through calibration. There are various instrumental/sensors soil-water measurement tools available, most of which must be calibrated for the soil in which they are used.

2.511 Gravimetric method

This is the traditional, most frequently used direct method of *SWC* measurement (Charlesworth, 2005). The gravimetric method is the most satisfactory method for one time moisture-content data and for calibrating the equipment to be used in the other methods (Johnson, 1962). These methods often serve as references rather than a means for irrigation scheduling. The gravimetric method involves collecting a soil sample, weighing the sample before and after oven drying (to constant weight), and calculating its original moisture content. This moisture content is usually expressed as the ratio of the mass of water present in the soil sample to the oven dry weight of the soil sample, or on a volume basis, as the ratio of the volume of water in the sample to the total volume of the soil sample (Hillel, 1982).

The measurement of the gravimetric moisture content by weight (e.g. g water per 100 g soil) only requires auger or bulk sampling while volumetric estimation, θ_v (e.g. cm^3 water per 100 cm^3 soil) requires the use of sampling cylinders of known volume to calculate soil bulk density (g cm^{-3}). This method, which involves sampling (especially from depths greater than a few cms.), transporting and repeated weighing, is laborious and time-consuming. The accuracy of this method depends on the accuracy of sampling and drying.

Many researchers prefer instrumental methods using sensors installed into the field, which once installed and calibrated (using the gravimetric or volumetric method as a reference), permit repeated or continuous measurements of *SWC* at the same points with minimal time and labour inputs and little soil disturbance (Hillel, 1998).

2.512 Instrumental/ sensor technologies

Sensors for water content measurement require the installation of these instruments into the soil profile. Jones (2004a) noted the various types of soil moisture sensors available at that time. The variety of soil moisture sensors (e.g. tensiometric, neutron, resistance, heat dissipation, psychrometric or dielectric) has continually evolved since then; the choices are now overwhelming, since each sensor has specific strengths and weaknesses in specific situations.

Tensiometers have long been used to measure matric potential in soils (Smajstrla & Harrison, 1998). Soil matric potential can be used to define the stress limit for the plant. White (2003) found that the stress limit for grapevines is set in the range -60 to – 400 kPa, where the vines can extract water held at lower potentials, but the rate of supply is too slow for adequate physiological functioning.

A number of next-generation soil moisture sensors have become available in the past decade from various manufacturers, e.g.Theta probe and SM300 (DeltaT, Burwell, UK) and EC5, 5TM and 10HS sensors (Decagon Devices Inc., Pullman, WA, USA) which provide precise data. These sensors determine the θ_v by measuring the apparent dielectric constant of the soil. These sensors are easy to use and provide highly reproducible data (van Iersel et al., 2009). All these sensors differ in terms of use and maintenance, calibration requirements, accuracy and price (Balendonck & Hilhorst, 2001). Table 1 summarized the main indirect soil moisture methods that are currently used for irrigation scheduling.

Table 2.1: Indirect soil moisture measurement methods with some examples of different types of soil moisture sensors that are available (Jones, 2004a)

Soil moisture measurement method	Soil moisture sensor
Tension measurement sensors	Tensiometers
	Electrical resistance
Soil dielectric sensors	Water content reflectometer
	Time-domain reflectometer (*TDR*)
	Frequency domain capacitance sensor (*FD*)

- **Time-domain reflectometry (*TDR*)**

This instrument determines the apparent dielectric constant of the soil matrix and empirically relates it to the θ_v. The use of *TDR* in soil science was pioneered by Topp et al., 1980. With *TDR* instruments, such as TRASE and Campbell, a waveguide, or probe, of known length is inserted into the soil and the travel time for a generated electromagnetic pulse to traverse this length is measured. Using empirical equations (Topp et al., 1980) or dielectric mixing models, the travel time is converted into a velocity of pulse propagation. The velocity of propagation is used to determine the soil's bulk dielectric permittivity from which the θ_v is inferred. The dielectric permittivity is directly related to θ_v. According to (Jones et al., 2002), some of the advantages of using *TDR* are: (i) accurate estimations of θ_v (to within ± 2% without soil-specific calibration), (ii) minimal calibration requirements in most soils, (iii) absence of radiation hazards that are associated with neutron probe or gamma-attenuation techniques, (iv) excellent spatial and temporal resolution, and (v) ease of measurements.

- **Frequency domain capacitance sensor (*FD*)**

This device measures the soil dielectric constant by placing the soil (in effect) between two electrical plates to form a capacitor. This explains the term 'capacitance', which is commonly used to describe what these instruments measure. When a voltage is applied to the electric plates a frequency can be measured. This frequency varies with the soil dielectric constant. The soil dielectric constant, an electrical property that is highly dependent on the moisture content. The dielectric constant for the water ≈ 80, compared to dry soil ≈ 5 to 15, wet soil ≈ 30 to 40 (Allred et al., 2005) and air ≈ 1. The dielectric constant of the soil has a strong influence on the applied field which is detected by the

FD sensors (i.e. SM300), resulting in a stable voltage output that acts as a simple, sensitive measure of θ_v.

The SM300 sensor has a sealed plastic body attached to two 51 mm long sensing rods which insert directly into the soil for taking readings. When an electrical field is applied, the soil around the electrodes (or around the tube) forms the dielectric of the capacitor that completes the oscillating circuit. Changes in θ_v can be detected by changes in the circuit operating frequency. The main advantages of *FD* sensors are the immediate and accurate reading, thus they are quite suitable for automated irrigation control (Pardossi et al., 2009) and allow for the deployment of multiple sensors to take measurements at different depths.

SM200 and SM300 sensors, which are more recent than the Theta Probe, are suitable for many types of soil and substrates. Moreover, it is barely affected by soil salinity and can be used at extreme temperatures, since the operating range is between – 20 and + 60 °C. Measuring accuracy is ± 0.3% for θ_v from 0 to 0.50 m^3 m^{-3}; as a function of temperature, the accuracy is ± 0.07% at 20 °C and 0.13% in the 20 – 60°C range (Pardossi et al., 2009).

2.52 Plant-based methods

Proper monitoring of plant water stress is useful for efficient scheduling of irrigation (Yazar et al., 1999), and especially relevant in arid climates where intermittent rainfall events, that replenish soil storage, are not expected. By measuring the appropriate plant parameters, one can evaluate a plant's general health and use that information to make a decision about when to irrigate (Reginato & Howe, 1985). Neither soil water status nor the atmospheric demand accurately represents the plant water status as well as the plant itself. However, plant methods typically indicate only when to irrigate, implying that soil moisture measurements or other estimation procedures must be used to determine how much water to apply to optimize crop water use (Nielsen, 1990; Stockle & Dugas, 1992).

The response of a plant to the combined effects of soil moisture availability, evaporative demand, internal hydraulic resistance and resistance/uptake capacity of the plant/root interface is principally measured in terms of the plant water status (Aladenola, 2014).

These methods measure water loss either from a whole single plant or from a small group of plants. The plant water status can be determined by measuring either the tissue water status (i.e. potential or content) or the plant's response to a change in tissue water status (White & Raine, 2008). Plant-based sensing is classified based on what the sensors are measuring; they may measure a direct physiological indicator (e.g. plant water status) or an indirect physiological plant response induced by changes in plant water status (e.g. leaf temperature, plant organ diameter or growth) (Remorini & Massai, 2003).

One method of assessing crop water stress condition is the use of canopy surface temperature (T_c) that has been shown to reflect subtle changes in physiological processes such as cell growth and biochemical reactions associated with the damaging effects of super optimal temperature (Conaty, 2010). Phene (1986) reported the most frequently used methods for automatic irrigation control are the T_c method and the sap flow method. Sap flow measurements also provide a unique and valuable way to quantify the time course of whole-plant water use under field conditions (Smith & Allen, 1996) and this by applying heat to the stem and detecting the rate of sap flow or sap-flux density by monitoring the stem's thermal regime. The technology is utilized across a wide range of applications on diverse plant types including natural and urban forest trees (Čermák et al., 2004), woody horticultural trees and vines (Alarcón et al., 2003), and agricultural crop species (Cohen et al., 1988)

The difference between T_c and air temperature (T_a) ($T_c - T_a$) is in some way related to plant water stress (Widmoser, 2010). The $T_c - T_a$ was first studied by Ehrler (1973), who investigated the possibility of using $T_c - T_a$ as a guide for irrigation scheduling. He found that the canopy-air temperature decreased after irrigation, reaching minimum several days following irrigation, and then increased as soil water became increasingly depleted. The linear relationship between $T_c - T_a$ and vapour pressure deficit (*VPD*) led Ehrler (1973) to conclude that $T_c - T_a$ has potential as an irrigation scheduling tools. Canopy to air temperature differences has been correlated to *SWC* and stem water potential for potential use in managing deficit irrigation of peach orchards; Wang and Gartung (2010) obtained correlations with R^2 values of 0.67 to 0.70 between stem water potential and canopy to air temperature difference.

Another use of T_c to estimate crop water stress is to measure the temperature variability of a crop (González-Dugo et al., 2006). Using the deviation of mid-day T_c as an irrigation scheduling tool was suggested by Aston and Van Bavel (1972) and has been implemented in various studies (Clawson & Blad, 1982; Clawson et al., 1989). The theory behind this method is that plants deplete the available water around their roots at different rates due to variability of soil properties, rooting depth and irrigation application. The spatial variability in T_c should be low for a well-watered, non-stressed crop but increase as plant water stress increases.

Idso et al. (1981) further observed a linear relationship between T_c (measured using *IRT*) and T_a and *VPD*, which they used to develop an empirical method for quantifying crop water stress. Jackson et al. (1981) also conducted theoretical research to develop a crop water stress index (*CWSI*). Jones (2004a) confirmed that irrigation scheduling can be improved by monitoring T_c using *IRT*. The availability of precise, handheld *IRT* allows rapid monitoring of T_c to identify crop water stress (Colaizzi et al., 2003; Peters & Evett, 2007) for irrigation timing and automatic scheduling (Irmak et al., 2000).

2.521 Crop water stress index (CWSI)

CWSI is calculated from T_c, T_a and atmospheric *VPD*. This approach is based on the principle that transpiration cools the leaf surface and as water becomes limited, stomatal conductance and transpiration decrease, leading to increases in leaf temperature. However, given that ambient conditions can have a large influence on T_c; T_c is, in fact, a reflection of both plant and environmental factors (Conaty, 2010; Jones, 2006). Empirical (Idso et al., 1981) and theoretical (Jackson et al., 1988) *CWSI* approaches have been proposed to estimate the lower limiting T_c. The empirical *CWSI* uses two baselines (non-water stressed and water-stressed). The lower baseline represents $T_c - T_a$ of a well-watered crop transpiring at the maximum potential rate while the upper baseline represents $T_c - T_a$ of a non-transpiring crop. The plot of $T_c - T_a$ and *VPD* under fully watered and water-stressed crop that was used to determine the non-water stressed and maximum stressed baselines respectively are used to quantify crop water stress. The empirical *CWSI* does not account for net radiation and wind speed whereas the theoretical method is estimated based on net radiation and the aerodynamics resistance factor. O'Toole et al. (1984)

conducted a study to assess eight different methods, namely, leaf water potential, leaf diffusive resistance, transpiration rate, photosynthesis rate, T_c, canopy-air temperature, *CWSI* and leaf rolling score for assessing plant water status and concluded that *CWSI* was the best technique. Yuan et al. (2004) also stated that *CWSI* is the most frequently used index to quantify crop water stress based on the T_c. This suggests that *CWSI* is a sensitive plant water stress index and a valuable tool for making irrigation decisions along with soil water measurements.

CWSI has been widely used as a tool to indicate plant water status and for scheduling irrigation in many crops (Cremona et al., 2004; Erdem et al., 2010; Yildirim et al., 2012). Nonetheless, for *CWSI* to be an effective tool for scheduling irrigation predicting yield, it has to be determined for particular crops in specific climates, given that crop response to water stress depends on local environmental conditions (Orta et al., 2003). The application of *CWSI* in irrigation scheduling has been evaluated for different crops, including vegetables (Erdem et al., 2010; Erdem et al., 2006; Köksal, 2008). The physiological responses of plants to water stress and their relative importance for crop productivity vary with species, soil type, nutrients and climate (Akıncı & Lösel, 2012; Orta et al., 2003).

The process for calculating *CWSI* using Idso et al. (1981) function is expressed in Equations (2.1), (2.2) and (2.3)

$$\mathrm{CWSI} = \frac{(\mathrm{Tc} - \mathrm{Ta})_{\mathrm{m}} - (\mathrm{Tc} - \mathrm{Ta})_{\mathrm{l}}}{(\mathrm{Tc} - \mathrm{Ta})_{\mathrm{u}} - (\mathrm{Tc} - \mathrm{Ta})_{\mathrm{l}}} \qquad [2.1]$$

T_c: is the canopy temperature (°C), T_a is the air temperature (°C), and m, l, and u, designate measured, lower baseline (well-watered), and upper limit (completely stressed) canopy-air temperature differences, respectively

$$(Tc - Ta)_l = Intercept + Slope(VPD) \qquad [2.2]$$

$$(Tc - Ta)_u = Intercept + Slope\big(VPsat(Ta) - VPsat(Ta + Intercept)\big) \qquad [2.3]$$

VPD: is the vapor pressure deficit (kPa); *VPsat* is the saturated vapor pressure at air temperature (kPa)

2.53 Soil water balance modelling

Many crop simulation models that have been used for calculating/predicting crop water use and irrigation scheduling are currently available i.e. CropWat (Smith, 1992b), APSIM (Keating et al., 2003), AquaCrop (Steduto et al., 2009), CROPSYST (Marsal & Stöckle, 2012), DSSAT (Thorp et al., 2008) , STICS (Hadria et al., 2006; Weiss et al., 2001), SWAP (Van Dam et al., 1997), SWAT (USDA; Douglas-Mankin et al. (2010)), WOFOST (Diepen et al., 1989). The governing equations and underlying theory of these models as such are very divergent.

The mathematical formulation, structure and complexity of crop simulation models are also very different. For some models, empirical equations were sufficient to describe the processes of interest, while other models include complex mechanistic equations to capture a certain crop or soil water response (Hunink et al., 2011). However, most models contain a mixture of empirical and mechanistic concepts.

For the crop growth components of the models, the main distinction that can be made in terms of their underlying equations is whether they are (i) radiation (or light) use efficiency based, (ii) photosynthesis based, or (iii) *WUE* based (Hunink et al., 2011). The concepts behind modelling of soil water dynamics range from the use of a simple bucket-filling model to those that solve more complex and vertically algorithms, based on the Richards´ equations. Richards' equation has a clear physical basis at a scale where the soil can be considered to be a continuum of soil, air, and water. In principle, the uses of numerical solutions for the Richards´ equation are better for soils below field capacity (Hunink et al., 2011).

With the *SWB* modelling approach to irrigation scheduling, the soil water deficit (*SWD*) is tracked by accounting for all water additions (inputs) and subtractions (outputs) from the soil root zone. Major inputs are precipitation and irrigation. Water might also be transported upward by the capillary rise (*CR*) from a shallow water table towards the root zone (Allen et al., 1998). Outputs include any form of water removal with the major removal being crop water consumption or crop evapotranspiration (ET_c) (Fig. 7).

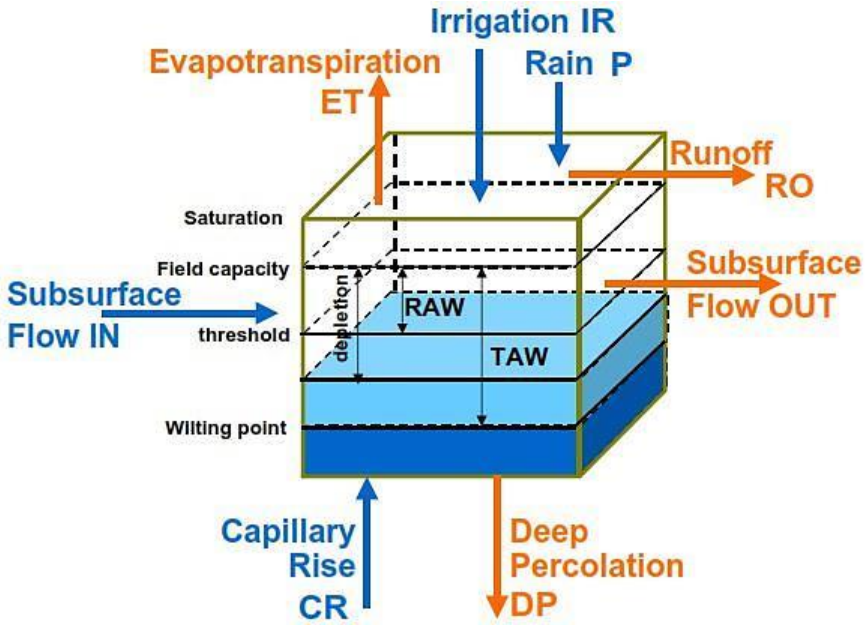

Figure 2.7 The water balance of the root zone (Allen et al., 1998)

Portions of rainfall and irrigation might be lost by surface runoff (*RO*) and by deep percolation (*DP*). *DP* losses increase depletion although this will eventually recharge the water table. The *SWB* approach is based on conservation of mass which states that the change in soil water storage (ΔS) of the root zone of a crop is equal to the difference between the amount of water added to the root zone (Q_i), and the amount of water withdrawn (Q_o) (Hillel, 1998) in a given time interval. This process is expressed in Equation (2.4) and (2.5).

Irrigation is required when ET_c exceeds the supply of water from both soil water and rainfall. The logic behind the *SWB* method is to apply irrigation with a net amount equivalent to the accumulated estimated ET_c losses since the last irrigation. ET_c is often determined as the product of reference evapotranspiration (*ET*) and crop coefficient (K_c) with the *ET* calculated from climatic parameters. At present, there are good estimates of K_c values for many horticultural crops, even though most research has been conducted on the major field crops (Allen et al., 1998). However, there are virtually no K_c values for ornamental species and most estimates of woody perennial crop water use are quite variable. Inaccuracies in K_c values can result in large potential errors in estimated *SWC* (Allen et al., 1998). The approach, therefore, works best where it is combined with regular monitoring techniques, for example of *SWC*, that can help reset the model.

The soil in the root zone has an upper and a lower limit for storing water that can be used by crops. The drained upper limit is called the field capacity (*FC*), which is the amount of water that can be held by the soil against gravity after the excess water has been drained. This is typically attained 1 – 2 days after precipitation or irrigation has saturated a soil. The time to reach *FC* increases from one for sandy soils to two to three days for heavier-textured soils that contain more silt and clay (Andales & Chavez, 2011). The lower limit is called the permanent wilting point (*PWP*), which is the soil moisture level at which plants can no longer absorb water from the soil. The *AWC*, or total available water-holding capacity, of the soil is the amount of water between these two limits (*AWC* = *FC* – *PWP*). Usually, the irrigator will set a management allowable depletion level (*AD*), which is used as a trigger to irrigate and prevents soil from reaching the yield threshold depletion level (refill point). This may be based on a percentage of available water.

$$\Delta S = Q_i - Q_o \qquad [2.4]$$

$$SWD_2 = SWD_1 - IR - P - CR + RO + ET_c + DP \qquad [2.5]$$

Where, SWD_1 and SWD_2: beginning and ending total *SWD* (mm), respectively, *IR*: irrigation (mm), *P*: precipitation (mm) *CR*: capillary rise from the groundwater (mm), *RO*: runoff from the soil surface (mm), ET_c: calculated crop water use, or evapotranspiration (mm d^{-1}), and *DP*: deep percolation or drainage out of the root zone (mm).

A particular strength of this approach is that it not only addresses scheduling issues about "when to irrigate" but also about "how much to apply". Although useful for soil-based irrigation scheduling, there may be limitations on how quickly these calculations can be manually performed (Aladenola, 2014).

It is imperative that we connect our capability for precision water applications with knowledge of real-time soil water supply and plant water use. In this study, we will work to improve our ability to predict plant water use in real-time using various technologies.

2.6 Decision support system (*DSS*) for irrigation management

Optimal irrigation water management relies on accurate knowledge of plant water consumption, water flows and soil moisture dynamics throughout the growing season (**Sections 2.51, 2.52, and 2.53**). The temporal and spatial variability of rainfall, soils, and crops cannot be reconstructed fully from field measurements or *RS*, so dynamic simulation models (**Section 2.6**) are deemed necessary to describe soil physical processes, the surface water balance, and crop growth. The decision-supporting systems (*DSS*) via an open application programming interface can integrate these models with the irrigation scheduling monitoring and control functions (a mixture of model and measurement-based). This will enable more predictive (feed-forward) management of water use, based upon the underlying plant and environmental water-use models.

Numerous *DSS* for irrigation have been developed in the last decades. The main advantages of using a *DSS* are as follows: an increased number of alternatives can be examined, a better understanding of the business/processes, identification of unexpected situations, improved communication, cost savings, better decisions, time savings, and better use of data and resources (Rinaldi & He, 2014).

DSS for irrigation are intended to utilize holistic approaches to irrigated crop management, which requires the seamless integration of the hardware (physical system), existing control and safety mechanisms, positioning systems (i.e., *GPS*), software interfacing with predictive crop models and other software tools, field data networks and various types of remotely sensed data, and wireless communications (Evans et al., 2011).

DSSs (interactive software-based system) in irrigation management applications began in the early 1990s (Liping et al., 2002). Different *DSS* (e.g. (Bergez et al., 2001; Bing et al., 2006; Brown et al., 2010; Chávez et al., 2010a, b and c; De Juan et al., 1996; Heeren et al., 2006; Kim & Evans, 2009; Kim et al., 2007; Oswald et al., 2006; Thysen & Detlefsen, 2006; Zhu et al., 2003; Zhu et al., 2005) have been developed more or less widely in the most intensive agricultural areas in the world to enhance soil water management

approaches to irrigated crop management within a single field or several fields to maximize total yield over the area.

Examples of Irrigation scheduling decision support systems at a field/farm scale on a daily basis

Smith (1992b) developed an empirical *DSS* (*CropWat*) which is well known to farmers for its easy estimation of crop water demands under different irrigation practices. The model considers climate, soil, and crop data. The model is based on the FAO Irrigation and Drainage Papers No. 56 "Crop evapotranspiration" and No. 33 "Yield response to water," The *PM* equation and respective K_c are used to calculate ET_c rates. Crop growth is simulated by the so-called linear model where gross dry matter production of a standard crop is empirically calculated and crop-dependent correction factors for climate, growth, and yield are applied (Doorenbos & Kassam, 1979). Bergez et al. (2001) developed a management-oriented cropping system model (*MODERATO*). It has been developed for use by irrigation advisors. It simulates the plant-soil system with a dynamic biophysical model and takes into account within-field variability that results from sequentially irrigating the plots in a block of irrigation. The *DSS* components are related to hydraulic context, mode of action; agronomic models; and timer and agro-economic evaluator. Bazzani (2005) described a *DSS* (*DSIRR*) created for the economic evaluation of irrigation water in Italy. *DSIRR* is working for integrating agronomic, technical, and environmental aspects with economic theory in a multi-criteria framework using mathematical programming techniques. In Denmark, a *DSS* (*PlanteInfo Irrigation manager*) for irrigation was developed by Thysen and Detlefsen (2006). *PlanteInfo Irrigation Manager* has the characteristic to be entirely Web-based in terms of input of farm and field data, automatic supply of weather data, and consulting for advice. The model runs with daily time steps. Crop growth and development are driven by three state variables, root depth, phenological stage, and leaf area index (*LAI*). Soil water is calculated by a simple system keeping for daily input of water from precipitation and irrigation and daily outputs from ET_c (evaporation from soil and crop transpiration). The *DSS* (*HydroLOGIC*) was designed in Australia (Richards et al., 2008), mainly to evaluate the consequences of several irrigation strategies and to explore options to optimize yieldand *WUE* at a field level in cotton. This information was subsequently used to assess economic and environmental consequences resulting from differences in irrigation

production practice. The *HydroLOGIC* interface main components are crop profile, climate and weather, crop observations, scenario generator, and the report generator. The *DSS* (*AquaCrop*) developed by Steduto et al. (2009) from FAO Irrigation and Drainage Paper No. 33 "Yield Response to Water" (Doorenbos & Kassam, 1979). The model is used for developing a seasonal irrigation schedule for a specific crop and field, determining the date of next irrigation, determining the seasonal water requirements and its components for various crops on a farm, developing deficit and supplemental irrigation programs at a field scale, developing water production functions, and using them in economic decision tools (Rinaldi et al., 2011). Zhang and Feng (2009) developed a timely irrigation *DSS* (*CropIrri*) in China to operate the optimal allocation of water resources in irrigation districts. *CropIrri* system was designed for dryland crops (wheat, maize, and soybean) to provide a practical decision tool for irrigation management. *CropIrri* system combines environmental conditions, like climate and soil, with crop growth characteristics as a whole, and was established using *SWB* model, crop phenology model, root growth model, crop water production function, and irrigation decision-making model. *CropIrri* concerns the date and amount of irrigation and the impact of selected irrigation schedule on crop yield. The *DSS* (*IrriSatSMS*) developed in Australia. The model uses satellite-derived crop coefficients in a daily water balance approach (Car et al., 2012). The system generates the decision support based on (i) weather data, (ii) irrigation measurement and management unit, (iii) satellite image data of land surface reflectance values and (iv) irrigation application and rainfall data. The approach in this *DSS* is not told specifically when or how much to irrigate but rather just how much they will have to irrigate, on any given day, to return their crop water deficit to zero. Barradas et al. (2012) designed a *DSS* for a drip irrigation system and analyzed the influences, which are exerted by the components of soil and some other factors on the process of irrigation decision, on irrigation scheme. *AquaTRAC*™ was developed in New Zealand by Foundation for Arable Research (*FAR*) and Plant and Food Research. Using data including crop type, soil type, weather and irrigation to date, it calculates when and how much irrigation to apply to optimise yield for each crop. It also calculates the potential economic loss if the soil moisture falls below the critical deficit. Growers need to set*AquaTRAC*™ up at the start of the season by inputting soil type, planting dates and crop types for each paddock. Weather data is imported throughout the season.

AquaTRAC™ provides a graphical representation of what has already happened in the paddock along with accurate forecasts of the amount of irrigation to apply and at what time.

These studies helped to improve crop water management and irrigation decision-making level. In general, the *DSS* systems applied in agriculture are customised for specific areas, purposes and specific crops, so it is difficult to be applied in other areas and crops (Jinyao & Shaolong, 2003; Liu & Feng, 2006) also it is difficult to determine growth period accurately, complex model parameters or large database. However, despite the successful application of *DSS* over the past decades, there is little evidence in the literature of widespread adoption or use by farmers. McCarthy et al. (2010) reported that the adaptive control of centre pivot and linear move sprinkler irrigation systems requires the integration of a decision-making process and real-time monitoring of field conditions with the irrigation system controls.

2.7 Summary of literature review and aim of this PhD study

Irrigated agriculture will be expected to help meet the food demands of projected population growth in the coming decades. At the same time, competition for water resources, land area, and pressure to lessen environmental impacts will require irrigation techniques that will improve *WUE*. The variability of rainfall events requires the application of supplemental irrigation to meet crop water demands in New Zealand; irrigation needs vary by location and crop type. Canterbury accounts for 62% of all irrigated land, followed by Otago, Marlborough and Hawke's Bay (Statistics NZ, 2019). These regions are the largest producers of dairy, arable and horticultural crops.

Variations in water availability across the field due to different soil types or crop water needs require *VRI* management to achieve optimum yields and maximise irrigation *WUE*. Determining appropriate *VRI* scheduling approaches for optimised crop production is necessary. Irrigation scheduling methods are typically based on soil moisture measurements, *SWB* calculations (Allen et al., 1998), and plant water stress indicators (Idso et al., 1981; Jackson et al., 1981). Previous research indicated that the *WUE* of

crops can be improved if irrigation is scheduled when water stress reaches a certain threshold and this threshold varies for different crops and different crop stages. T_c is a sensitive indicator of water stress and is easily measured using *IRTs* that do not contact the plant. The *CWSI* is a canopy temperature-based index that normalizes T_c for meteorological variability. A large body of research during the past two decades has investigated the *CWSI* and its ability to quantify water stress and aid irrigation scheduling. Although *WUE* can be improved by timing irrigations when a *CWSI* threshold was reached, there is no consensus on a set of threshold values appropriate for all possible crops, soils, and climates. In addition, the *CWSI* does not indicate the optimal amount of water needed per irrigation. Therefore, soil moisture sensors and *SWB* remain the basis for irrigation management. The *CWSI* may provide more meaningful information if it could be related to soil moisture.

Recent innovations in low-power sensor and *WSNs* technologies combined with advances in internet technologies offer tremendous opportunities for development and application of real-time management systems for irrigation. Irrigation management in precision agriculture requires spatio-temporal information on soil water supply and crop water demand that is timely, frequent and has sufficient spatial resolution for the existing within-field variability. Present airborne and/or ground-based sensor technologies (e.g. *LiDAR* and *NDVI*) have potential to meet these information requirements. The recent availability of *GPS*, Geographic Information Systems (*GIS*), and high-speed personal computers would make on-site data processing feasible within minutes.

Thus, the aim of this study is to develop and improve the adoption of new technology methods for scheduling *VRI* as a viable option to improve the management of irrigation scheduling to give greater *WUE* (greater yields, less water, and nutrient losses).

Connecting text to Chapter 3

Chapter 3 presents the results of trials to evaluate the impact of two different climatic regions and soils on irrigated pea and barley production. This assessment sought to determine whether this variability is sufficient to warrant the use of variable-rate irrigation.

Chapter 3

Impact of climate and soil spatial variability on pea (*pisum sativum*) and barley (*hordeum vulgare*) production in New Zealand

Abstract

Exploring the responses of crop water use and yield to climate and soil available water variability could enable growers to understand and exploit spatial variations in crop growth and yield via variable input management. The objective of this study was to determine the impact of weather and soil variability (for both freely and imperfectly drained soils) on pea (*pisum sativum*) and barley (*hordeum vulgare*) production using soil and crop sensing data. A variable-rate irrigation scenario was also simulated by a water balance CROPWAT8 program to optimize the irrigation regime of the two soil management zones without undesirable reduction of yield.

The study was conducted under centre pivot irrigation systems. The two field sites were located in contrasting climatic regions of New Zealand (site *A*, Manawatū and *B*, Hawke's Bay). Heavy rainfall during the pea crop trial meant that site *A* required no irrigation during the growing season. At site *B*, hot and dry conditions meant that irrigation was uniformly applied to barley with maximum irrigation application of 15 mm at any one time at a fixed interval (7 days) during the growing season.

Both weather conditions and soil variability had a significant effect on the crop growth and total yield of pea and barley. A period of waterlogging induced by 130 mm of heavy rainfall reduced pea yield by 58% in the poorly drained soil compared with the well-drained soil at site *A*. The irrigation application of 15 mm per week for the freely drained soil at site *B* was less than required to avoid water stress for barley. This led to reduced barley grain yield by 4 T ha^{-1} (60%) mainly through a reduction in the number of grains/

plants, compared with imperfectly drained soils.

Overall, the results revealed that soil physical properties exhibited significant spatial variability within each study site. This caused crop growth in the different soils to respond differently to rainfall and irrigation resulting in different maturity rates and final yields.

Keywords: Waterlogging; Water deficit; Wireless sensor network; Soil moisture sensors; Infrared radiometers; Variable rate irrigation; Water use efficiency; CROPWAT8

3.1 Introduction

Under New Zealand's climate conditions, fluctuations in precipitation can cause water shortages or excesses at critical stages of crop growth. The water supply that can be stored in the soil profile and supplied to the crop, is often described as the available soil water content (*AWC*) (Wong & Asseng, 2006). In coarse textured soils with a very small *AWC*, excess water can percolate quickly past the root zone, and therefore these soils require more frequent irrigation with small applications to maximize yields. Soils with a high *AWC* store more plant available water and therefore should be able to produce maximum yields with less irrigation in temperate climates, where some rainfall is expected during the period of irrigation. The *AWC* is directly related to soil texture which often varies spatially in agricultural fields (Hedley & Yule, 2009a).

The under-irrigation of crops leads to unnecessary water deficit stress and reduced yield. Heavy rainfall or over-irrigation of crops can lead to waterlogging and increased leaching and surface runoff of nutrients, fertilizers, as well as increasing the overall cost of irrigation and reducing profit. There has been considerable research conducted overseas on the response of pea and barley crops grown on different soils to applied water. The effects of waterlogging or water shortage on plants depend on the stage of its development and duration of this stress (Svobodová & Misa, 2004). The major physiological effect of waterlogging is reduced uptake and transport of mineral ions by roots (Drew & Sisworo, 1979; Slowik et al., 1979). With waterlogging, yield reductions have been reported in peas of 6-40% respectively (Belford et al., 1980; Cannell et al., 1984; Cannell et al., 1980). This yield loss appears linked most closely to hypoxia and/or anoxia where shoot

and root growth decrease, and nutrient uptake becomes inhibited (Bacanamwo & Purcell, 1999). The negative effects of water shortages on yield mainly depend upon the severity of the stress and the plant growth stage. In contrast, yield reductions due to water shortage might be due to various factors such as decreased rate of photosynthesis, disturbed assimilate partitioning, or poor flag leaf development (Jamieson et al., 1995). In an experiment in Canterbury, New Zealand, Jamieson et al. (1995) showed that water shortage caused a decrease in yield, grain number and size per spike. A significant reduction in the grain yield of barley was also observed by Samarah (2005) under drought conditions mainly because of smaller numbers of fertile tillers and grains along with less 1000 grain weight. González et al. (1999) reported that water shortage affects spike number per plant or unit area more than grain number per spike for spring barley.

Therefore, variations in water availability across a field due to different soil *AWC* and/or variation in crop needs may require site-specific management to achieve optimum yields and maximize water use efficiency (*WUE*) (Raine et al., 2007). Soil type and crop yield can now be mapped at the sub-field scale with commercially available technologies (Lawes et al., 2009; Wong et al., 2008). These technologies can be employed to develop the field management strategies, using precision irrigation equipment such as a variable rate irrigation (*VRI*) system, which has the potential to spatially optimize the irrigation regime, nutrient management, and thus yield, of areas with low *AWC* without an unnecessary reduction of yield in areas of high *AWC* (Evans et al., 2013).

The Penman and Monteith (*PM*) equation used in FAO56 (Allen et al., 1998) is the standard procedure for calculating reference evapotranspiration (ET_o) and subsequently plant water use ET_c via a crop factor K_c. Crop models such as CROPWAT (Smith, 1992) and AquaCrop (Steduto et al., 2009), many of which are based on the *PM* approach and the soil water balance (*SWB*)) (Allen et al., 1998), are often used as a practical tool to calculate the crop water use and manage irrigation..

The models are hindered with a major research shortcoming of high resolution spatial and temporal information. The actual size and duration of crop water stress need to be quantified for the development of models to describe relationships between cropproduction and field management. Recent technologies (e.g. wireless sensor networks (*WSN*)) can be used to quantify the potential impact of crop management and

soil-*AWC* on irrigation water use and crop production in the field (Hedley et al., 2012). This is because *WSNs* measure field soil and crop conditions in real-time (Ekanayake & Hedley, 2018), whether using direct soil moisture content (*SMC*) measurements with capacitance, neutron probe, *TDR* sensors (Topp & Davis, 1985) and tensiometers (Smajstrla & Harrison, 1998) or direct measurement of plant water status using infra-red radiometers (Jones, 2004a).

Canopy surface temperature (T_c) measured with infrared radiometers (*IRT*) provides a well-established, and important tool to detect water stress in a crop. The crop water stress index (*CWSI*) is the most frequently used index to quantify crop water stress based on T_c (Sezen et al., 2014). Idso et al. (1981) observed a linear relationship between T_c (measured using *IRT*) and air temperature (T_a) and vapour pressure deficit (*VPD*), which they used to develop an empirical method for quantifying crop water stress. Research has been conducted to evaluate the application of the *CWSI* in irrigation scheduling for different crops in different places (Alderfasi & Nielsen, 2001; Cremona et al., 2004; Yeşim Erdem et al., 2010), However, little research has been undertaken to evaluate the use of *CWSI* for horticultural and cereals crops in New Zealand.

The resulting information from crop models (e.g. *SWB* and *APSIM*) and *WSNs* can be used to support policies and incentives that help farmers adopt practices that reduce water and energy used for irrigation.

Therefore, our study aimed to quantify the impact of temporal variability in weather and spatial variability in soil-*AWC* on pea and barley crops using soil and crop sensing data, and to determine whether this variability is sufficient to warrant the use of *VRI* systems. The research objectives were; (i) to compare the effects of freely and imperfectly drained soils on crop growth, final yield, *WUE*, *CWSI*, drainage and nutrient concentrations for a pea and barley crop grown for one season under centre pivot sprinkler irrigation, and (ii) to simulate the benefits of a *VRI* scenario using the CROPWAT8 model (Smith, 1992) where irrigation is scheduled to the two soil-*AWC* management zones in a manner that prevents any reduction in yield.

3.2 Materials and Methods

3.21 Study sites

The first experimental site (site *A*) is 1.2 ha in size and located on Massey University's No.1 Farm near Palmerston North, New Zealand (latitude 40.22° S, longitude 175.36° E, altitude 37 m). The trial was conducted during the 2016/2017 growing season. According to the National Institute of Water and Atmospheric Research (*NIWA*) (www.niwa.co.nz), the climate is humid, and the average annual rainfall is approximately 980 mm. The soils are Fluvial Recent soils formed in greywacke alluvium (Hewitt, 2010). The existing soil map for this field (El-Naggar et al., 2017; Pollok et al., 2003) indicates the presence of two different soil types: a Manawatū fine sandy loam (free draining soil) and a Manawatū silt loam (moderated poorly drained soil) (Fig. 3.1).

The second experimental site (site *B*) is 4 ha in size and located near Otane, Hawke's Bay, New Zealand (-39. 533°S °N; 176.402°E, altitude 130 m). This site is on the east coast of the North Island of New Zealand, which is in a different climatic region to site *A*. The mean annual precipitation is 679 mm. Temperature is always the highest relative to what is typical for the time of year. There is a greater incidence that the dry summer led to the rapid depletion of soil moisture levels in this area. The trial was conducted during the 2017/2018 growing season. The soils in this study area are alluvial soils. The existing soil database for this field indicates the presence of a Twyford sandy loam and a Kaiapo silt loam (Fig. 3.1). The Twyford sandy loam is distinguished by the presence of coarse, relatively un-cohesive sands throughout the profile, and topsoil with a sandy loam texture. It is an excessively well-drained soil. The Kaiapo silt loams have a finer texture, which contributes to relatively slow internal drainage. It is classified as a poorly drained soil.

The physical characteristics of the soils at each site are given in Table 3.1

3.22 Experimental setup

Field peas (*Pisum sativum*., cv. 'Ashton') at site *A* and barley (*Hordeum vulgare*., cv. 'Carfields CKS1') at site *B* were sown on 18 October 2016 and 2 August 2017, respectively. Each experiment consisted of a randomised block design with four plots (20 x 10 m) or replicates in each soil zone (Fig. 3.1). The trial's operation management was the same in each soil zone for peas and barley crops (Table 3.2). Both sites have centre pivot irrigators. The irrigator at site *A* is 86 m long and was run with an application rate of 2.54 mm hr^{-1}. At site *B*, the irrigator has a length of 580 m and an application rate of 1.8 mm hr^{-1} was used for irrigation. These application rates were lower than the infiltration rate into the topsoil.

At site *A*, the plan was to schedule irrigation with the aid of a water balance calculation but the heavy rainfall during crop growth prevented the field from being irrigated. At site *B*, the irrigation was uniformly applied with a maximum application depth of 15 mm (due to insufficient water allocation) at a fixed interval (5-7 days) unless significant rainfall was received.

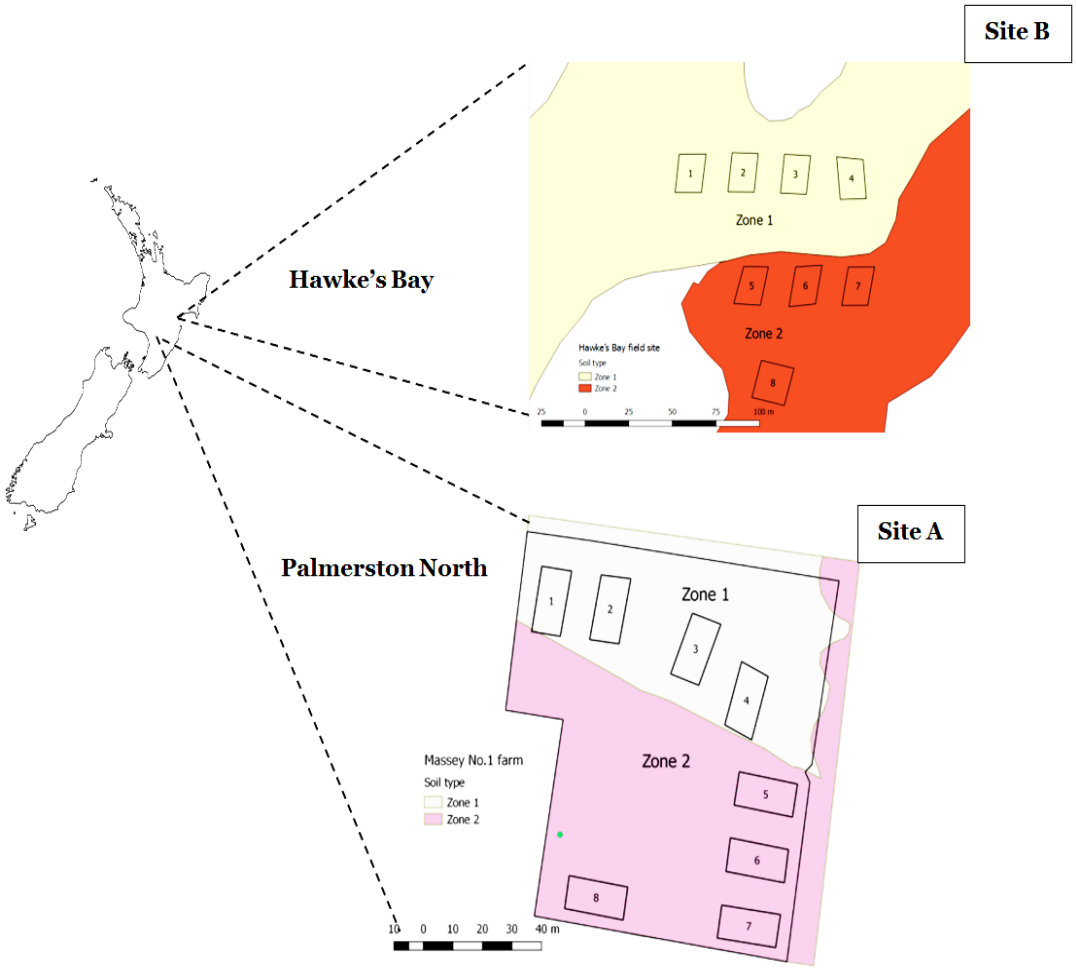

Figure 3.1: Experimental design of study areas: Two soil management zones with 4 replicates plots (10 x 20 m) in each zone based on the soil types at site *A* (block: 1.2 ha) (Zone 1: Manawatū sandy loam, Zone 2: Manawatū silt loam) (Pollok et al., 2003) and site *B* (Zone 1: Twyford fine sandy loam, Zone 2: Kaiapo silt loams) (Manderson map "unpublished").

Table 3.1: Physical properties of the soil (0 – 1m).

Properties	Site *A*		Site *B*	
	Soil types/ zones			
	Zone 1	Zone 2	Zone 1	Zone 2
Available water capacity (mm m^{-1})	123	203	190	273
Bulk density (g cm^{-3})	1.41	1.30	1.28	1.17
Sand (%)	80.6	44.9	47.3	1.3
Silt (%)	12.7	40.6	40	70.8
Clay (%)	6.7	14.5	12.8	28

Table 3.2: Management records for the pea crop trail (2016/2017) at site *A* and barley trial (2017/2018) at site *B*.

Pea trial 2016/2017	
30Sep-16	Weed control: Pre-Empt applied @ 1.7 l ha^{-1} and incorporated
18Oct-16	Fertilizer: 250 kg Cropmaster 15 applied, power harrowed (fertiliser)
18Oct-16	Planting: Peas sown @ 260 kg ha^{-1} (cultivar - Ashton)
25Nov-16	Weed control: Sprayed with Bruno @ 2.5l ha^{-1} and MCPB @ 1l ha^{-1}
09Jan-17	Harvest
Barley trial 2017/2018	
2/08/2017	Planting: Barley ('Carfields CKS1); 100 kg seed ha^{-1}
2/08/2017	Fertilizer: 200 kg ha^{-1} Yara ACTYVA (23-10-5)
15/11/2017	Fertilizer: 326 kg urea ha^{-1} (150 kg N ha^{-1})
24/01/2018	Harvest: Final barley harvest (10.5 t grain ha^{-1}; 19.7 t DM ha^{-1})

3.22 Measurements

3.221 Soil and crop sensing data

Soil moisture was measured during the crop season in each plot at the 0–10, 10–20, 20–30 and 30–40 cm soil depths at daily intervals for site *A* using frequency domain reflectometry probe (SM300- DeltaT, Burwell, UK) connected with a *WSN* developed by Ekanayake and Hedley (2018). Measurements at weekly intervals for site *B* were made using neutron-probes down to a depth of 80 cm in 10 cm depth increments. The soil sensors were calibrated against the *SMC* determined gravimetrically. *SMC* measurements started after 5 and 16 days after cultivation for pea and barley, respectively. Canopy temperatures were measured in each plot with *IRT* (Apogee Instruments, Inc., model SI-400). The instrument was installed about 1 m above ground level and directed vertically down at the plant (see Fig. 3.2). Real-time T_c measurements were recorded every one hour during most of the season using a *WSN* developed by Ekanayake and Hedley (2018). Data collection for T_c was initiated at 35 and 65 days after planting for the pea and barley crops, respectively when the plant cover percentage was nearly 70–85%. Measurements were made between 11:30 am- 2:00 pm (local standard time) to detect the crop water stress

(Idso et al., 1981; Jackson et al., 1981) at maximum solar intensity because the sun will be directed on all plants during this time. Mean values of the T_c were used for calculating *CWSI* using Idso et al. (1981) function (Equation 3.1).

$$CWSI = \frac{(T_c - T_a)_{\mathrm{m}} - (T_c - T_a)_{\mathrm{l}}}{(T_c - T_a)_{\mathrm{u}} - (T_c - T_a)_{\mathrm{l}}} \quad [3.1]$$

T_c is the canopy temperature (°C), T_a is the air temperature (°C), and m, *l*, and *u*, designate measured, lower baseline (well-watered), and upper limit (completely stressed) canopy-air temperature differences, respectively

$$(T_c - T_a)_{\mathrm{l}} = a + b(VPD) \quad [3.2]$$

$$(T_c - T_a)_{\mathrm{u}} = a + b\left(VP_{\mathrm{sat(T_a)}} - VP_{\mathrm{sat(T_a+a)}}\right) \quad (3.3)$$

Vapor pressure deficit (*VPD*, kPa) and saturated vapor pressure (VP_{sat}, kPa) at air temperature were calculated by:

$$VPD = \left(1 - \frac{RH}{100}\right) * VP_{\mathrm{sat}} \quad [3.4]$$

$$VP_{sat} = e^{\left(\frac{16.78*\mathrm{T_a} - 116.9}{\mathrm{T_a} + 237.3}\right)} \quad [3.5]$$

L for the canopy–air temperature difference (T_c–T_a) versus the vapor pressure deficit (*VPD*) relationship was determined using data collected only from the unstressed treatments. *U* was computed according to the procedures explained by Idso et al. (1981).

Figure 3.2: Typical infrared thermometers sensor arrangement in peas crop (site *A*) for measuring the crop stress. The infrared thermometers mounted at 0 degrees below horizontal which give a visible area of 1.2 m^2.

Previously twenty-four drainage flux-meters (4 sensors each plot for plots 2 – 7) (Green et al., 2010) were installed for comparing the amounts of drainage and nutrient concentrations in soil water for each treatment in site *A*. The basic device design is similar to that of (Gee et al., 2003) and (Holder et al., 1991). The drainage volume was recorded manually in order to calculate an average drainage rate (mm/day) for the scheduling treatments.

3.222 Experimental data

The effects of the soil treatments on crop performance during the growing season were assessed. Crop assessments (i.e. height, length, number of nodes, flowers, and pods) were conducted manually on a weekly basis until harvest. Three replicates of 25 to 30 plants were monitored at each time for each plot.

The actual yield difference between each soil zone was evaluated at crop maturity. In the pea trial, seed yield and aboveground plant material were measured by harvesting an area of 1 m^2 (three replicates/plot). Seed and biomass weights were measured on subsamples from this harvest. Dry biomass and yield were estimated on an oven dry-weight basis (70ºC). In the barley trial, the crop yield was determined from a yield map provided by the farmer. The map was derived from data collected by a yield monitor positioned on the harvester. The yield map was imported into Trimble Ag Software to load and analyse the performance of the plots. *WUE* (kg mm^{-1}) (Gregory, 2004) was then calculated as dry seed yield per water used per unit area.

3.23 Soil water balance model with variable rate irrigation scenario

A *SWB* model (CROPWAT8, (Smith, 1992)) has been used to simulate the crop water needs for a *VRI* scenario with barley in two soil zones for Site B i.e. irrigation was varied to the two soil zones based on critical soil water deficit (*SWD*) at both sites.

Irrigation scheduling in CROPWAT8 is based on a soil-water budget, where on a daily basis the *SWD* is determined, accounting for incoming and outgoing water in the root

zone (Hillel, 1998). The ET_c was determined as the product of ET_o and K_c. Daily weather data derived from a local on-farm climate station were used to calculate ET_o for each day of the week, using the *PM–FAO 56* method Equation (3.6 and 3.7) (Allen et al., 1998). The K_c function values were estimated as described by Allen et al. (1998).

The initial *SWD* was derived from measured *SMC* using portable TDR sensor "The MiniTrase (6050X3)". The initial depletion was near field capacity (*FC*). Any excess water in the root zone was assumed to be lost through deep percolation (*DP*). Capillary rise (*CR*) was assumed to be zero because the water table was more than about 1 m below the bottom of the root zone (Allen et al., 1998). Runoff (*RO*) was assumed to be zero. Irrigation is triggered each time *SWD* in the roots zone reaches 50% of the total available water (*TAW*) Equation (3.8). This maximum allowable *SWD* will ensure that barley crop will not be subjected to any water stress that might affect crop productivity or quality (Allen et al., 1998).

$$ET_o = \frac{0.408*\Delta*(R_n-G)+\gamma*\frac{900}{T+273}*u_2*(e_s-e_a)}{\Delta+\gamma(1+0.34*u_2)} \quad [3.6]$$

$$ET_c = K_c\, ET_o \quad [3.7]$$

Where, ET_o: reference evapotranspiration (mm d^{-1}), R_n: net radiation at the crop surface (MJ m^{-2} d^{-1}), G: soil heat flux density (taken as zero for daily calculations) (MJ m^{-2} d^{-1}), T: mean daily air temperature at 2m height (°C), u_2: wind speed at 2 m height (m s^{-1}), e_s: saturation vapour pressure (kPa), e_a: actual vapour pressure (kPa), $e_s - e_a$: saturation vapour deficit (kPa), Δ: slope of the saturated vapour pressure curve (kPa $°C^{-1}$), γ: psychrometric constant (kPa $°C^{-1}$), ET_c: crop evapotranspiration (mm d^{-1}), K_c: crop coefficient.

$$TAW = 1000\ (\theta_{FC} - \theta_{WP})_i * Z_{r,i} \quad [3.8]$$

Here, TAW is the total available soil water in the root zone (mm), θ_{FC} water content at field capacity ($m^3\,m^{-3}$), θ_{WP} water content at wilting point ($m^3\,m^{-3}$), Z_r is the rooting depth (m).

3.23 Soil sampling

To determine whether the soil zone treatments impacted differently on soil nitrate content, soil levels of nitrate and ammonium (*NO3-N*, *NH4-N*) were measured at planting and harvest, by collecting three replicated soil samples at 0.15 m intervals to a depth of 0.45 m (i.e. 0 – 0.15 m, 0.15 – 0.30 m; 0.30 – 0.45 m) from each plot.

3.24 Laboratory analyses

The plant available nitrogen was assessed using a mineral nitrogen analysis, estimated as the sum of *NH4-N* and *NO3-N* extracted with *2M KCl* using a 1:10 soil: extractant ratio and a 1-hour end-over-end shake followed by filtration (Blackmore et al., 1987) and then quantified using a QuikChem 8500 flow injection analyser.

Nutrient concentrations in soil drainage water (*NO3-N*, *NH4-N*, *P*) were determined using Lachat instruments (Lachat Instruments, 1998c 1998f) based on Standard Methods for the Examination of Water and Wastewater (FWE & APHA, 2005).

Plant nutrient concentrations of nitrogen (*N*) and phosphorus (*P*) from the harvested herbage cuts for pea crop were determined using the Kjeldahl determination method (McKenzie & Wallace, 1954).

All soil preparation and laboratory analyses were undertaken at the Manaaki Whenua soil Laboratory (http://www.landcareresearch.co.nz/resources/laboratories/) and Massey University soil Chemistry Laboratory (http://flrc.massey.ac.nz), Palmerston North, New Zealand.

3.25 Statistical analysis

Kolmogorov-Smirnov test of normality (*KS*) was carried out at 5% significance. Analysis-of-variance (*ANOVA*) at P=0.05, Tukey's HSD (data normally distributed) and Bonferroni (*Dunn*) (data non-normal distributed) were conducted to investigate significant differences in measured soil and crop measurements.

All of the data visualizations and analyses performed in this study were carried out using the R programing language (R Core Team, 2018).

3.3 Results and Discussion

3.31 Weather data

Fig. 3.3 shows the weather data of the cropping trial season and the 10 years mean derived from a local climate station, located 50 m from site *A* (http://cliflo-niwa.niwa.co.nz/) and Te Aute Drumpeel Rd climate station situated adjacent to the site *B*.

At site *A* the trial period was a relatively wet season where the rainfall for August-January was significantly higher than the mean. The rainfall received in the pea growing season (October through January) was 393.3 mm, which was higher than the long-term mean rainfall (325 mm) by 17.4%. At site *B*, rainfall in the barley growing season was significantly lower than in the mean. The rainfall in the growing season (August through January) was 214.4 mm, which was lower than the long-term mean rainfall (317.6 mm) by 32.5%. November was wetter than normal at site *A* and drier than normal at site *B* (Fig 3). Mean evapotranspiration for the pea crop was significantly lower than expected from November-January. Mean evapotranspiration records for barley were a close match with the mean except in November.

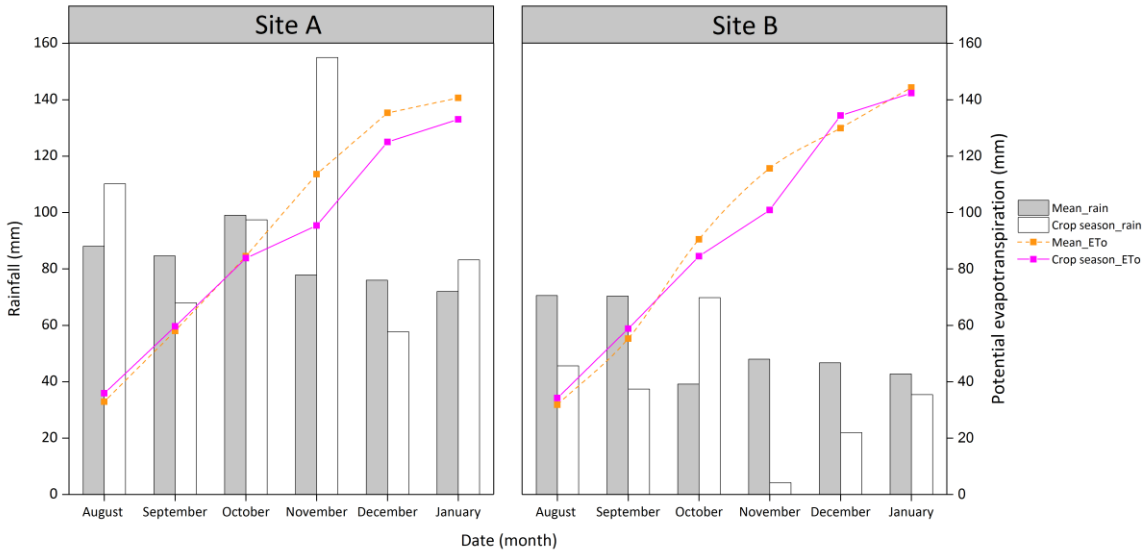

Figure 3.3: Weather data at site *A* for 2016/2017 and site *B* for 2017/2018 and 10 year mean climate data.

3.32 Comparison of soil water content for the two soil zones during each experimental trial

Profile *SMC* and *SWD* variations during the pea and barley growing seasons for each soil zone are shown in Fig. 3.4 and 3.5, respectively.

During the pea trial, the results show a period of waterlogging in Zone 2 induced when 131 mm rainfall occurred. During the development stage (emergence to bloom stage), *SMC* for Zone 2 was above *FC* (November 12-November 18) for around 7 days after 26 days of planting (Fig. 3.4). In Zone 1, there was a very short period of water shortage in late-stage (bloom to harvest) (71 days after planting) and before harvest (65% *AWC*). The highest values of *SWD* were 79 and 48 mm for Zone 1 and Zone 2, respectively.

During the barley trial, the quantity of irrigation applied to each soil zone treatment was based on a fixed interval (5-7 days). Ten irrigation treatments applied a total of 150 mm in each soil zone (Fig. 3.4). Weekly *SWD* determinations showed that *TAW* in the Zone 2 treatment was frequently between 40% and 50% especially during early flowering (stem extension to heading) whereas under Zone 1 treatment it started to be below 50%.

Soil-water extraction patterns differed among the soil zones treatments in both crop trials (Fig. 3.5). During the pea trial, the distribution of *SMC* occurred in the Zone 1 soil profile

during the experiment, showed the surface layers generally becoming wetter and deeper layers becoming drier except during the vegetative growth (waterlogging period). This increased *SWD* for Zone 1 could be explained by increasing rates of water use and to drainage during the season compared to Zone 2. For the Zone 1 treatment, this corresponded to a drainage loss of approximately 135 mm, or 40% of the used water over the season (see Fig. 3.8). During the barley trial, soil water uptake from Zone 1 treatment (Fig. 3.5) was mainly from the surface (0-0.4m) layers, but some extraction had occurred to 0.8 m depth by the end of the crop season. Soil-water extraction patterns for Zone 2 treatment showed that the amount of water extracted from deep in the profile was much greater than in the Zone 1 treatment. This increased extraction to 0.8 m depth was probably the result of deeper rooting and reduced water availability in shallower layers.

The period at development stage for pea and early flowering stage for barley were very sensitive stages where water stress through waterlogging and deficit just prior to these stages reduces the accumulated biomass and yield.

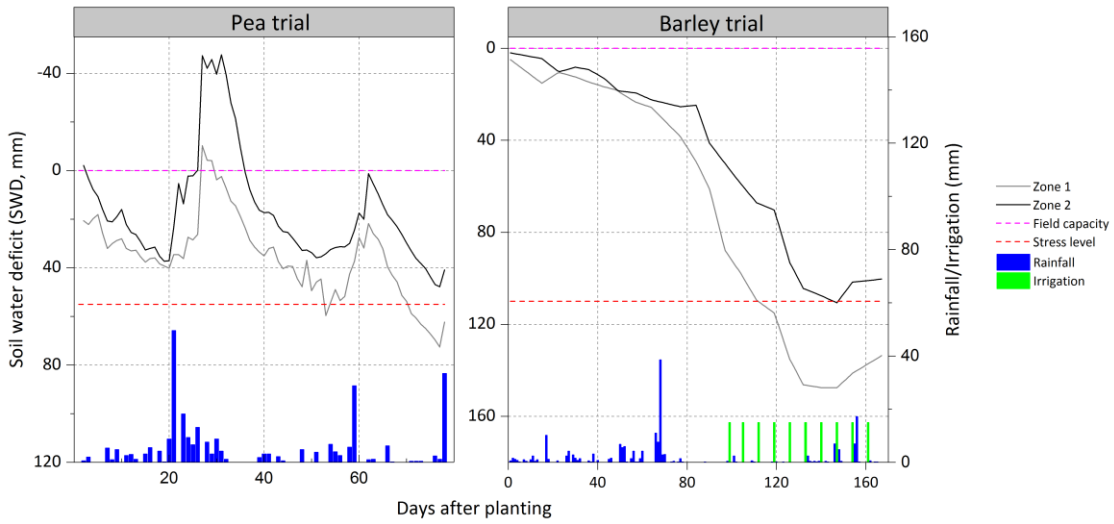

Figure 3.4: Estimated soil water deficit (*SWD*, mm) for each soil zone at site *A* and site *B*. The *SWD* was estimated by subtracting the calibrated sensor measurements from the available water of the soil.

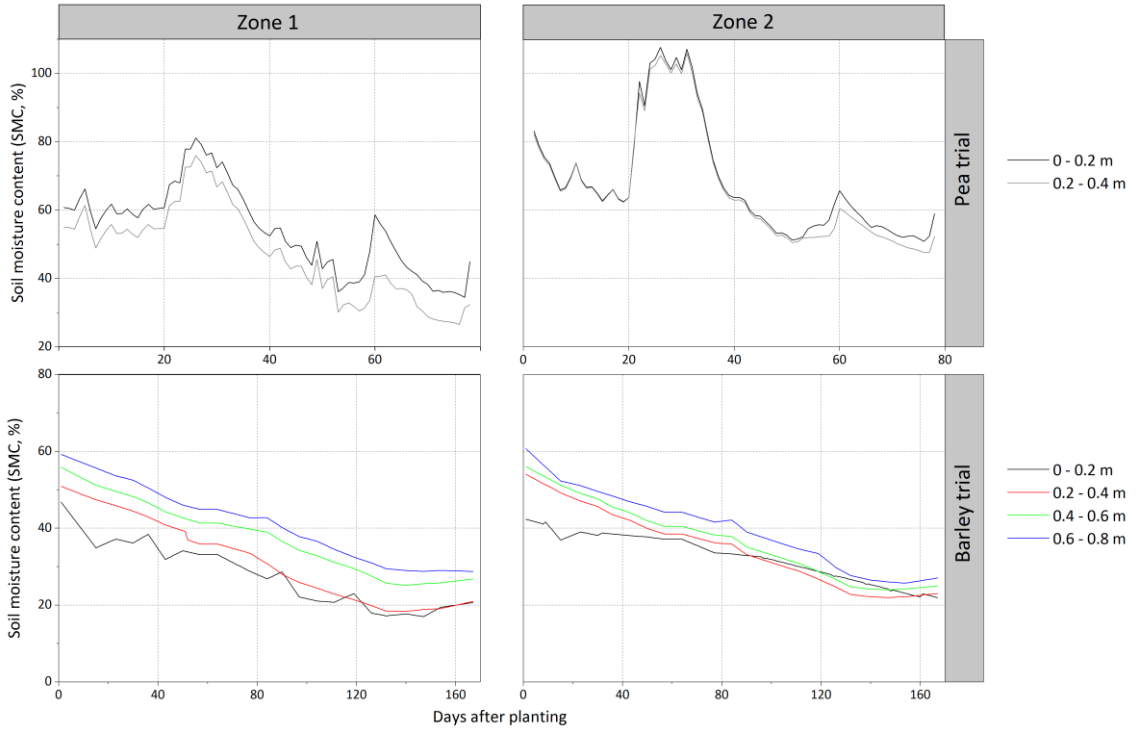

Figure 3.5: Daily average soil moisture content (*SMC*, %) at site *A* measured by SM300 sensors (3 sensors in each soil zone). Average soil moisture content trend (*SMC*, %) at site *B* measured by neutron probes (4 sensors in each soil zone).

3.33 Comparison of *CWSI* for the two soil zones during each experimental trial for Sites *A* and *B*

The non-water stressed baselines for T_c–T_a versus *VPD* for pea and barley are illustrated in Fig. 3.6. The upper limit (*U*) and lower limit (*L*) equations were developed as follows: $U = -11.73\ VPD + 23.79$ and $L = 2.67\ VPD + 0.79$ for pea. For barley, the upper limit (*U*) and lower limit (*L*) equations were: $U = -8.15\ VPD + 14.85$ and $L = 0.36\ VPD + 0.61$.

The variations in *CWSI* under each zone treatment during pea and barley growing seasons are shown in Fig. 3.7. When the stress becomes more severe, the canopy–air temperature difference will increase, and then the values of *CWSI* will increase (Sezen et al., 2014). In our study, with increasing water stress, the values of *CWSI* show the trend of increase, however, there are frequent day-to-day variations of *CWSI*.

In the pea trial, *CWSI* values ranged between 0.11 and 0.59 in Zone 1 and ranged between

0 and 0.09 in Zone 2. The seasonal mean *CWS*I values were 0.24 and 0.1 for Zone 1 and Zone 2, respectively. The variation of *CWSI* between Zone 1 and Zone 2 indicates that the crop was under a short stress period (72 – 78 days after planting) where the crop wasn't irrigated and the total rainfall (about 1.2 mm) wasn't enough to meet the root zone water depletion (mm) which gives a quite similar indication to our *SWD* data (see Fig. 3.4).

In the barley trial, *CWSI* values ranged between 0.32 and 1.86 in Zone 1 and ranged between 0.02 and 0.78 in Zone 2. Zone 1 had the highest *CWSI* among the treatments, indicating that the plants grown on this soil zone suffered greater water stress than Zone 2 which agreed with *SWD* data (Fig. 3.4). The experimental results indicated that the *CWSI* 0.4 and 0.8 for pea and barley is more reasonable for quantifying the crop water deficit so irrigating at this level of *CWSI* would result in higher pea and barley yields for both field sites.

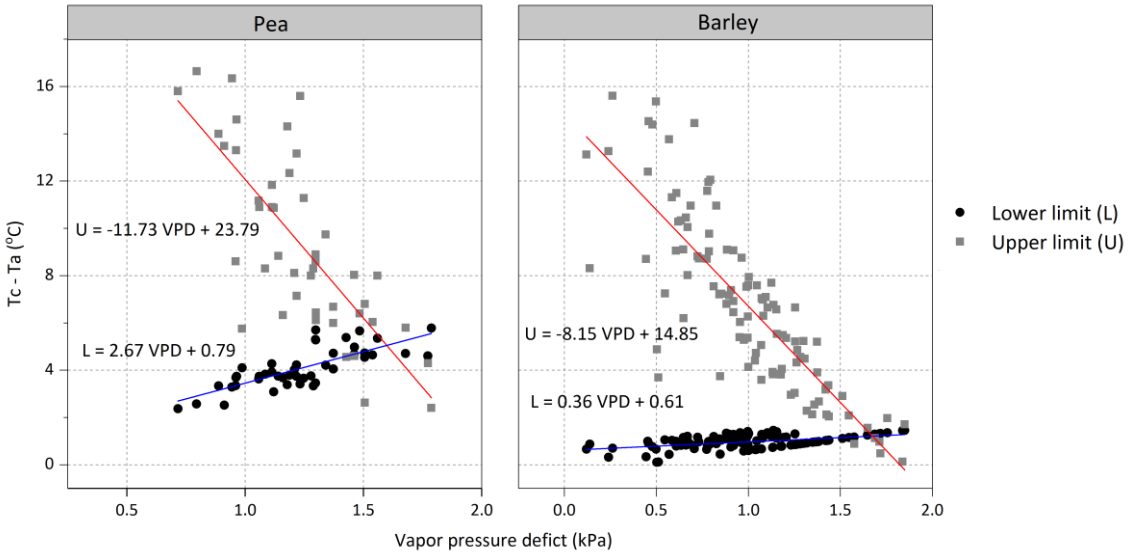

Figure 3.6: Canopy–air temperature differential (T_c–T_a) versus air vapor pressure deficit (*VPD*) for well-watered and fully stressed pea and barley. U is the upper limit base line (completely stressed), and upper limit and L is the lower limit (well-watered).

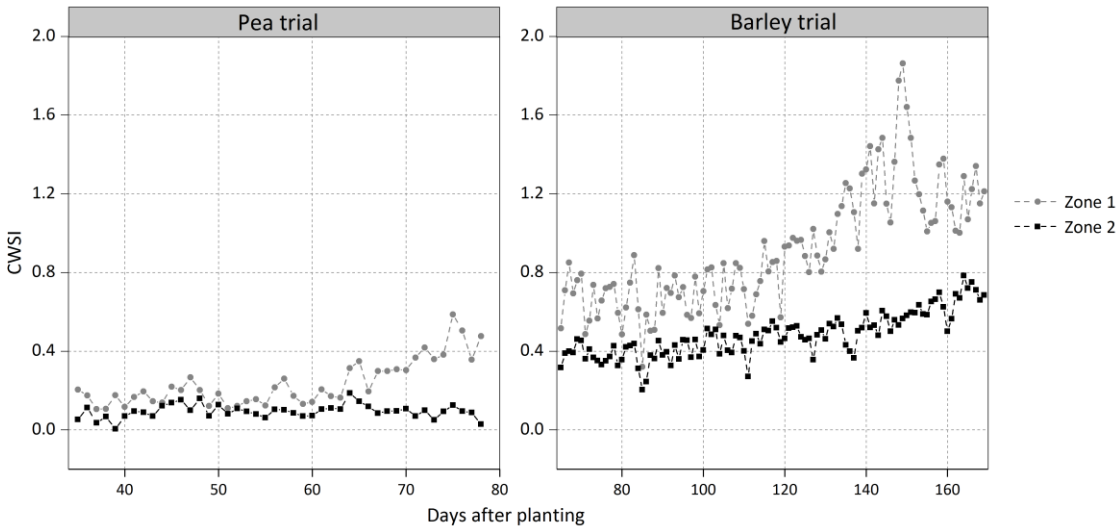

Figure 3.7: Estimated variations of *CWSI* values between the two soil zones for fresh peas at site *A* and spring barley at site *B.*

3.34 Drainage volume/analysis for the two soil zones in pea crop trial

Fig. 3.8 shows the drainage volume measured by 24 drainage flux-meters (4 sensors in each plot treatment) at site *A* and nutrient concentrations in soil water measured in the lab.

Higher drainage volumes were in the highly porous soil (135 mm) and lower in textured soils (36 mm) ($p < 0.05$). However, there were no significant differences in *NO3-N* plus *NH4-N* and *P* between the two soil zones.

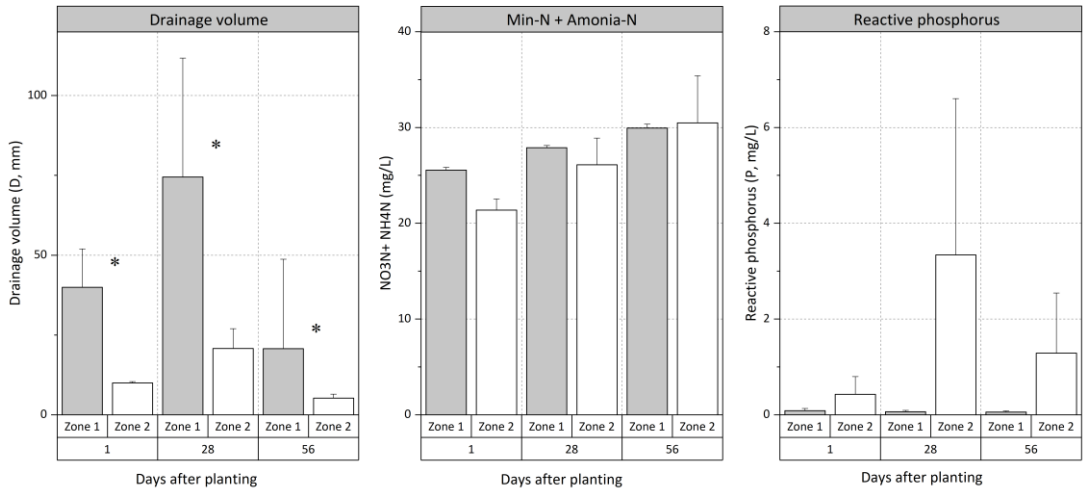

Figure 3.8: Drainage volume measured at site *A* by 24 drainage flux-meters (4 sensors in each plot treatment) and nutrient concentrations in soil water measured in the lab. "*"significant at p< 0.05.

3.35 Soil nitrate content for the two soil zones in each experimental trial

There was no significant difference in mean *NO3-N* and *NH4-N* in the top 0.45 m at pre-planting for pea and barley ($p > 0.05$) while the mean values of *NO3-N* and *NO3-N* plus *NH4-N* levels were larger in Zone 1 than in Zone 2 ($p < 0.05$) at harvest (Table 3.3). This due to waterlogging impacts which reduce the levels of nitrates in the soil by denitrification. This is in agreement with Belford et al. (1980) who reported that waterlogging increases the rate of denitrification and reduces plant uptake of *N*, *P*, *K*, and some trace elements.

Table 3.3: Average nitrate content (*NO3-N* (mg kg^{-1})) and Ammonia content (*NH4-N* (mg kg^{-1})) in the top 0.4 m at harvest for pea and barley. "*"significant at p< 0.05

Pea trial		*NO3-N*	*NH4-N*	*NO3N+NH4N*
	Zone 1	6.07 (0.41)	1.44 (0.29)	7.52 (0.54)
	Zone 2	4.07 (0.37)	1.04 (0.14)	5.12 (0.41)
	P value	P,*	NP	P,*
Barley trial				
	Zone A	3.30 (0.61)	0.54 (0.12)	3.85 (0.72)
	Zone B	4.93 (0.74)	0.30 (0.08)	5.25 (0.73)
	P value	P	NP	P

3.36 Crop assessment for the two soil zones in each experimental trial

The effects of soil variations on crop growth and yield were evaluated for each crop trial. The results are summarized in Fig. 3.9 and Table 3.4.

The pea trial results showed a reduction of crop growth in Zone 2 (where waterlogging occurred) comparing to Zone 1. There was a significant difference in mean crop height, number of flowers (see Fig. 3.9), number of nodes, and number of pods (results not included) between both soil zones at the probability level using *ANOVA* and Tukey's HSD tests. Significant effects on seed yields were reflected mainly by the number of pods/ plants. Yield differences were observed between the two Zones: the yield of Zone 2 treatment decreased by approximately 58% (Zone 1= 4.15 T ha^{-1}, Zone 2= 1.75 T ha^{-1}), and this can be explained by waterlogging through excessive rainfall to above *FC* in Zone 2. Similar findings by Belford et al. (1980) showed that yield reductions in peas were 6-40% due to waterlogging. Greenwood and McNamara (1987) found in their experiment in North Otago, New Zealand waterlogging through excessive irrigation or rainfall to above *FC* (1.5 *FC* and 2 *FC*) reduced seed yield by approximately 0.73 T ha^{-1} and treatments 3 *FC* and 4 *FC* by 1.1 T ha^{-1}. Cannell et al. (1980) and Jackson (1979) found the yield reduction of 13 to 30% which resulted from waterlogging was mainly due to a similar reduction in the number of pods/plant; Similarly in our experiment, we found a reduction in filled pods/plant (Zone 1= 96%, Zone 2= 60%). Work investigating the effect of waterlogging at different growth stages has shown that waterlogging just before flowering is most damaging (Cannell et al., 1980). In our trial, the waterlogging occurred in the development stage (emergence to bloom stage) which led to a yield reduction of 58% in Zone 2 compared to Zone 1. In Zone 1, the plant available water was below the trigger of irrigation for a short period (Fig. 4) at the maturity stage and this was before harvest (72 – 78 days after planting) compared to Zone 2 which was too wet.

In contrast, during the subsequent year (2017), rainfall was less, and irrigation was needed in both soil zones. The irrigation was applied using *VRI* scheduling system. The total amounts of irrigation were 85 and 53 mm for Zone 1 and Zone 2, respectively, and there

was no significant difference in mean pea crop yield and biomass (see Chapter 5).

The barley yield from site *B* varied between the two soil zone treatments. Irrigation with small insufficient quantities of water (15mm/7 days) by the farmer gave significant ($P< 0.01$) yield reductions for Zone 1. Grain yields (at 14% moisture content) ranged from 10.3 T ha^{-1} in the Zone 2 treatment to 4.0 T ha^{-1} in the Zone 1 treatment with the most severe water stress. Water stress gradually decreased the plant height (Fig. 3.9) where a *SWD* at 65-70% *TAW* (Fig. 3.4) produced almost 40–60% decrease in plant growth. Samarah (2005) calculated a 57% reduction in barley grain yield at severe water stress. This reduction in grain yield might be due to the shortening of the crop growth cycle that leads to early flowering under water stress. This early flowering not only shortened the grain filling period but also affected the plant vegetative growth period. Thus, this resulted in lower plant height and biomass accumulation which failed to provide sufficient photosynthates to developing grains at the grain filling stage (Alghabari & Ihsan, 2018). The current experimental findings at site *A* and *B* are in agreement with the results of Greenwood and McNamara (1987) and Jamieson et al. (1995) who stated that water stress at the development stage for pea and early flowering stage for barley has the greatest negative impact on yield and quality for pea and barley.

Concentrations of *N* and *P* in whole-pea samples from the two soil zones taken at harvest are given in Table 3.4 which shows reduced concentrations mainly of *N* and *P* and in the waterlogging soil zone (Zone 2). This in agreement with Cannell et al. (1980); Greenwood and McNamara (1987) reported that root growth appears most severely affected by waterlogging which may limit nutrient uptake.

The *WUE* values were significantly influenced by soil zone treatments. Measures of *WUE* expressed as seed yield per mm of water applied ranged from 10.6 kg mm^{-1} (Zone 1) to 4.4 kg mm^{-1} (Zone 2) for pea and from 9.10 kg mm^{-1} (Zone 1) to 22.8 kg mm^{-1} (Zone 2) for barley (Table 3.4).

Overall, pea and barley growth appeared sensitive to small amounts of excessive or restricted water, respectively. Pea plants in Zone 2 showed a delay in growth which can be explained by lack of oxygen due to waterlogging and consequent nutrient deficiencies such as nitrate-*N*, phosphorus and potassium in topsoil (Table 3.4). Also, possibly due to the nitrogen-limiting conditions, root nodules were observed on the roots of plants. Seed

yield for barley in Zone 1 was 61% lower than Zone 2 with less grain fill. The *SMC* in Zone 1 fell below the irrigation trigger level of 65-70% *TAW*, and the observed crop growth and yield indicate a significant reduction at level P< 0.01 compared to Zone 2.

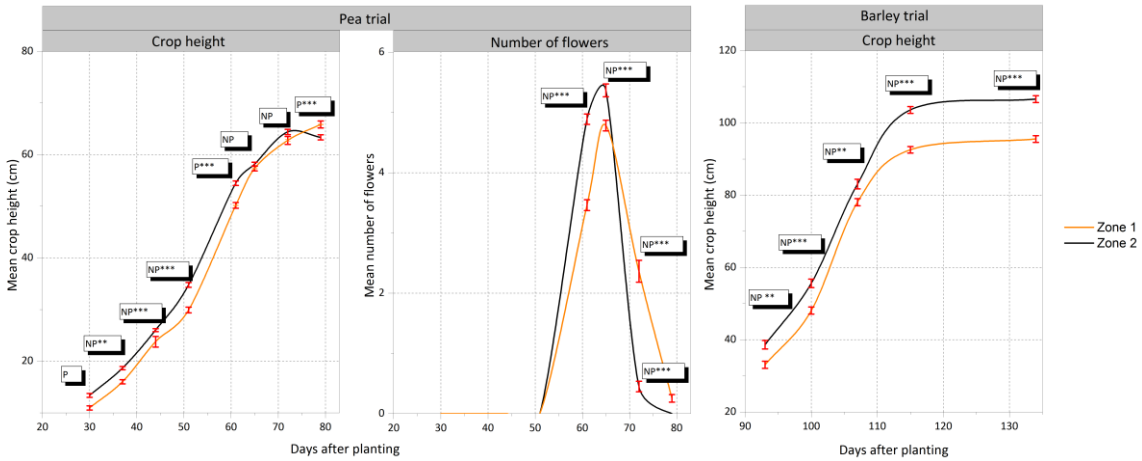

Figure 3.9: Results from One-Way *ANOVA*, Tukey's Studentized Range (HSD) Test (data normally distributed) and Bonferroni (*Dunn*) t-Tests (data non-normal distributed) tests comparing, pea and barley measurements between the two soil zones. "**"significant at p< 0.05, "***"significant at p< 0.001, *P*= parametric test, *NP*= Non parametric test.

Table 3.4: Comparison of (a) actual mean (standard error) yield for pea and barley (b) biomass and concentrations percentage of *N* and *P* between the two zones for pea. *P*= parametric test, *NP*= Nonparametric test. * indicate p > 0.05 (not significantly different).

Pea trial		Dry yield (T ha^{-1})	Dry biomass (T ha^{-1})	Nitrogen %	Phosphorus %	WUE kg mm^{-1}
	Zone 1	4.15 (o.37)	5.92 (0.49)	2.57 (0.51)	0.26(0.01)	10.6 (o.37)
	Zone 2	1.75 (0.48)	6.05 (0.35)	1.95 (0.10)	0.17(0.01)	4.4 (0.48)
	P value	P,*	NP	P,*	P,*	P,*
Barley trial						
	Zone 1	4 (0.61)	-	-	-	9.10 (0.61)
	Zone 2	10.3 (0.74)	-	-	-	22.8 (0.74)
	P-value	P				P,*

3.37 Variable-rate irrigation scenarios for barley trial using CROPWAT

Fig. 3.10 shows the *VRI* scheduling scenario in each soil zone for barley simulated by CROPWAT8 program. The irrigation requirement for the season was estimated at 180 and 135 mm for Zone 1 and 2, respectively. The average irrigation demand interval was about 3-4 days starting from the mid-season (considering the Max application depth 15 mm) for Zone 1.

In the vegetative growth stage (0 – 80 days after planting), sufficient rainfall meant that irrigation was not needed for Zone 2 and irrigation intervals varied from 7 to 15 days in Zone 1. Compared with the actual irrigation applied (fixed interval method), the *VRI* scheduling scenario used 25% less irrigation water on Zone 2.

In general, these results indicate that the timing of irrigation was important for optimizing the irrigation regime in Zone 1 for avoiding the unnecessary reduction of yield. Thus, irrigation when *SWD* falls to 30–50 % *TAW* or at irrigation intervals of 4 days during the mid-stage would seem a sensible recommendation for Zone 1 and in this experiment, it may have given higher yields and a greater irrigation response.

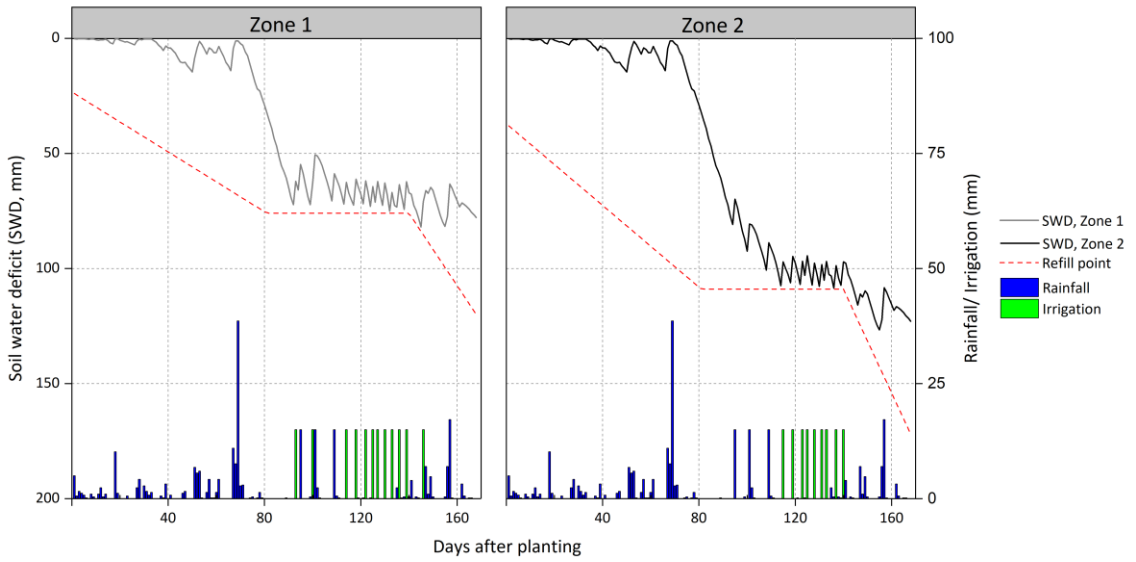

Figure 3.10: Variable rate irrigation (*VRI*) schedule scenario for barley crop 2017 to avoid crop water stress and to achieve optimum yield using CROPWAT.8 program (Penman-Monteith model).

3.4 Conclusions

The spatial variation of crop productivity across farm fields is influenced in part by the amount and distribution of rainfall and the soil's capacity to hold moisture. The present experiment was conducted to evaluate the effects of freely and imperfectly drained soils on crop growth, final yield, *WUE, CWSI*, amounts of drainage and nutrient concentrations for a pea and a barley crop using soil and crop sensing data.

The results showed that peas were very sensitive to a short period of waterlogging under these field conditions. The excessive rainfall causing the imperfectly drained soil (Zone 2) to become wetter than or at *FC* (7 days) caused substantial variations in maturity and yield at harvest, with an average of 1.75 T ha^{-1} in the imperfectly drained treatment, to 4.15 T ha^{-1} in the freely drained treatment (Zone 1). At site *B*, the amount of irrigation applied by the farmer at a fixed interval (15 mm/7 days) wasn't enough to fully restore plant available water for barley for the freely drained soil. The lower *SMC* in the freely soil profile after 83 days of planting (flowering stage) for barley resulted in both lower yield and crop growth due to water stress occurring prior to flowering compared with the other soil zone. The *VRI* scenario for barley trial indicated that irrigating when *SWD* at 30–50 % *TAW* or at irrigation intervals of 15 mm/4 days would seem an efficient method for the freely drained soil which may have given higher yields and a greater irrigation response. The *CWSI* of 0.4 for pea and 0.8 for barley quantified the crop water deficit during the growing season so irrigating at this level of *CWSI* would be optimize yield production for pea and barley in both field sites.

Overall, the current experimental findings for pea and barley yield variability, visual observations and crop measurements indicated significant *AWC* variability due to varying soil textures between the two soil zones at each site. Waterlogging and water stress adversely affected pea and barley growth and grain yield. The results for the early waterlogging for pea and crop water stress for barley could have important implications for models aiming to simulate the effects of stress types on cereal growth and water use. With declining water resources, future research must focus on using new technologies such as *VRI* systems and *WSN* with specific crop management options that increase irrigation *WUE* and crop production.

Connecting text to Chapter 4

Given the results from Chapter 3, it is concluded that it is desirable to account for the spatial variability of soil water and crop characteristics at fine scales, if possible. If variable-rate irrigation (*VRI*) is advantageous, how can it be achieved or implemented? As a first step to answer this question, Chapter 4 develops a method using apparent soil electrical conductivity (EC_a) survey data to investigate and quantify this soil variability. The EC_a data was kriged into a map and modelled to predict EC_a to depth, using an inversion modelling technique. This chapter was presented in conference proceedings:

(i) New Zealand Society of Soil Science& Soil Science Australia (NZASSS) conference in Queens town, New Zealand (2016). Poster presentation.

(ii) Fertilizer and Lime Research Centre conference (Report No. 30) in Massey University, Palmerston North, New Zealand (2017). Conference paper.

(iii) 7th Asian-Australasian conference on precision agriculture in Hamilton, New Zealand (2017). Conference paper.

This chapter is under review in March 2020 at the Precision Agriculture Journal.

Chapter 4

Imaging the electrical conductivity of the soil profile and its relationships to soil water content

Abstract

A quasi-2dimensional (*quasi-2D*) apparent electromagnetic conductivity (EC_a) model, capable of modeling EC_a information down the entire soil profile, was developed using EC_a data collected by a multi-coil Dualem-421S sensor. The optimal relationships between true electrical conductivity (σ) and volumetric soil moisture content (θ_v) were established by using all coil arrays of the Dualem-421S, a damping factor of 0.04, an initial model of 35 mSm^{-1}, and with ten iterations. A leave-one-out cross-validation was used to assess the regression models. The predicted θ_v showed a significantly higher correlation and lower biases and errors with the measured θ_v (R^2 = 0.66, bias = 0.00 cm^3 cm^{-3}, *RMSE* = 0.04 cm^3 cm^{-3}). These relationships were then used to derive soil profile images of these properties. As expected, θ_v and σ follow similar trends down the soil profile.

The derived soil profile images for θ_v have potential use for irrigation scheduling to two EC_a-derived soil management zones under a variable-rate irrigation system at this case study site. They reflect the intrinsic soil differences that occur between texture, texture transitions and drainage characteristics. The method can also be used to guide the placement of soil moisture sensors for in-season soil moisture monitoring to monitor spatiotemporal variations of θ_v. This soil σ imaging method showed good potential for predicting *2D* depth profiles of certain soil properties and can support soil, plant and irrigation management.

Keywords: Soil electrical conductivity; Dualem-421S; Soil volumetric water content; Soil texture; quasi-2D inversion; EM4Soil

4.1 Introduction

Recent developments in sensor technologies coupled with software packages are improving our ability to map the fundamental, yet spatially and temporally dynamic soil property, soil moisture (θ). The soil must contain adequate θ to maintain plant growth, avoid yield reduction and facilitate nutrient uptake. Thus, nutrient uptake and crop yield can be maximized when the θ is known, and well characterized across a field (Grote et al., 2010) and used to inform irrigation scheduling.

For appropriate irrigation management, θ measurements should be taken frequently at least to the depth of the managed root zone. The soil water pattern in the topsoil may not match that of the subsoil and this spatial variability in soil water patterns down the soil profile as well as across the landscape needs to be determined. The spatial variability of θ is attributed to the influence of varying soil properties such as texture, structure and drainage characteristics, as well as topography (Hedley & Yule, 2009a; Vachaud et al., 1985).

The θ measurement methods include gravimetric and sensing techniques. Gravimetric measurement is the reference method against which other methods are compared (Charlesworth, 2005). It involves collecting a soil sample, weighing the sample before and after oven drying, and calculating gravimetric water content, (θ_g) (Hillel, 1982). This method, which requires physical soil sampling, transporting, laboratory analysis and repeated weighing, is laborious and time-consuming. It also needs to be converted to volumetric water content (θ_v) for irrigation scheduling to inform how much water to apply to soil (Evett et al., 2008). Sensing methods use a surrogate property (e.g. dielectric constant) that is then related to θ_v through a calibration (Evett et al., 2007). These sensing methods are rapid and provide highly reproducible data. In order of accuracy, they include neutron-probes (Kodikara et al., 2013), time domain reflectometry (*TDR*) methods (Wraith et al., 2005) and capacitance sensor techniques (van Iersel et al., 2009). Sensors measure soil water content at one position or in a network of positions (e.g. (Ekanayake & Hedley, 2018)) but for precision irrigation, the spatial variability of θ_v across the area to be irrigated is also important.

Emerging technologies for estimating the spatial distribution of soil water include the use of satellite data (Corbari et al., 2019; Thi et al., 2019), although its use for precision irrigation has been limited by its spatial and temporal resolution. With the recent emergence of constellations of small CubeSat-based satellite systems, these constraints are lessening, with daily 3 km resolution optical data a reality for earth observation (Aragon et al., 2018). However, an enduring limitation of satellite data is that it largely responds to surface soil conditions. In contrast, electromagnetic induction (*EMI*) instruments can be used to map θ_v to depth. The sensor is affected by other soil properties as well as θ_v (de Lara et al., 2019). These include clay content, compaction, and cation exchange capacity in non-saline soils (Corwin & Lesch, 2003; Hedley et al., 2004; Sudduth et al., 2005a). These other factors often co-relate to moisture content so that researchers have successfully established correlations between apparent electromagnetic conductivity (EC_a) and θ_v. Kachanoski et al. (1988) first established correlations between EC_a and θ_v measured by a *TDR*. Ekwue and Bartholomew (2011) observed a strong positive relationship between the EC_a and the θ_v for three soil types evaluated in laboratory and field conditions. Hedley et al. (2013) mapped θ_v (to 0.5 m) across an irrigated field of uniform sandy soils using an EM38 survey, and Robinson et al. (2009) mapped θ_v at a depth of 0.4 m. However, these *EMI* survey methods were unable to resolve the relationship of EC_a to θ_v content with depth.

Therefore, although the successful mapping of θ_v has been achieved, most correlations were established between EC_a and profile-average θ_v. Characterisation of the depth specific variation in θ_v is ideally needed to guide the best placement of soil moisture sensors to accurately represent the variation that exists in a field, e.g. for precision irrigation scheduling.

More recently studies have demonstrated how EC_a data coupled with quasi-2 dimensional (*quasi-2D*) inversion modeling software (Santos et al., 2010) can be used to characterise depth specific variation of soil properties, including exchangeable sodium percentage (Huang et al., 2014), clay (Triantafilis et al., 2013a), θ_v (Huang et al., 2016; Huang et al., 2017a), soil salinity (Davies et al., 2015; Huang et al., 2015), and cation exchange capacity (Koganti et al., 2017).

In principle, *EM* inversion is a mathematical procedure that aims to obtain the distribution of EC_a property in soil volume (Santos, 2004). The inversion modelling tools (i.e. Santos et al. (2010)) calculate the EC_a changes with depth using Maxwell's equations that are based on the low induction number approximation and because the measured EC_a is a weighted average value over the coil configuration specific penetration depth; this enables the estimations for EC_a over different depths (von Hebel et al., 2014). In general, there are three inversion models: a layered earth (*1D*), an earth model allowing the variation of conductivity in two directions (*2D*) and a more realistic model allowing that the conductivity varies in the three directions (*3D*). The parameterisation of each model is different, and the number of unknown parameters increases from *1D* to *3D* models. The model to be adopted depends on several factors, but the most important are the geology and the geophysical array used in the data acquisition (Santos, 2004; Triantafilis et al., 2013a).

The main focus of our research trial was to investigate the use of the *EMI* method and inversion algorithm approach (EMTOMO, 2014) for high-resolution imaging of vertical soil variability under a variable-rate irrigation (*VRI*) system to inform scheduling decisions for two EC_a delineated irrigation management zones. Although the inversion algorithm approach has been shown to be successful in mapping depth-specific dynamics in homogeneous sandy soil (Huang et al., 2017a), and in a field with varying soil texture (Huang et al., 2017b), little work has been undertaken to relate the *EMI* image outputs to soil drainage characteristics in an area of different soil texture and drainage characteristics. Therefore, our study aimed to use EM4Soil inversion software (EMTOMO, 2014) to generate a two-dimensional depth profile model from the EC_a values measured by a multi-coil *EM* sensor survey, and then develop a relationship between the calculated vertical profile of true electrical conductivity (σ) and the measurements of θ_v for two irrigation management zones of differing texture and drainage characteristics. We were interested to investigate its ability to interpret drainage characteristics because vertical and lateral distribution of soil water in a soil profile impacts on effective management of irrigated land.

4.2 Materials and Methods

4.21 Study sites

The study field is located at Massey University in Palmerston North, New Zealand, (lat. 40°22′57″S, long. 175°35′38″E). The study field is 1.2 ha and was cultivated and sown with ryegrass (*Lolium perenne L.*) and white clover (*Trifolium repens*). According to the New Zealand Soil Classification (Hewitt, 2010), the soils are Fluvial Recent soils formed in greywacke alluvium, which correspond to Fluvisols in the FAO World Soil Reference Base (Michéli et al., 2006), and to Fluvents in the USDA Soil Taxonomy (USDA & Soil Conservation Service, 1975). This field is known to be non-saline and variable in texture, so it was expected that the *EM* survey data would be predominantly influenced by variation in the soil texture and soil water content. The existing soil map for this field (Pollok et al., 2003) indicated the presence of two different soil types: a Manawatū fine sandy loam (Zone 1) and a Manawatū silt loam (Zone 2) (Fig. 4.1b).

4.22 *EM* survey

The *EM* survey was carried out at 6 m swath widths across the field and along two transects using a Dualem-421S mounted on a wheeled frame at a height of 0.15 m above the surface (Fig. 4.1a). The Dualem-421S (Dualem Inc., Milton, Ontario, Canada) instrument incorporates an *EM* transmitter that operates at a fixed low frequency (9 kHz) with three pairs of horizontal, co-planar (*HCP*) and perpendicular (*PRP*) receiver arrays. The distances from the transmitters to the *PRP* receivers are 1.1, 2.1 and 4.1 m. The depth of EC_a measurement is, respectively, 0–1.5 (1m*Hcon*), 0–3.0 m (2m*Hcon*) and 0–6.0 m (4m*Hcon*), and 0.5, 1 and 2 m (*PRP*) (Dualem Inc 2008). The georeferenced EC_a data were collected every second at six depths using a Trimble RTK GPS system with 2 cm accuracy. The elevation data collected by the RTK GPS system was also interpreted to predict slope angles and other topographic details.

4.23 Soil sampling

To calibrate the inverted EC_a models, 20 sites were selected (Fig. 4.1a). Twelve of these sites were positioned along two transects (transect 1: locations 1 – 6; transect 2: locations 7 – 12) so that the calibration model could be used to predict longitudinal depth profiles of EC_a for these two transects. The remaining eight sites were selected using stratified random sampling of the *EM* survey data. Undisturbed soil samples of known volume (intact cores) were taken at 0.30 m intervals to a depth of 1.5 m at each site, on the same day as the *EM* survey. On transect 1, soil samples were collected at 15.6 m intervals while on transect 2 they were collected at 17 m intervals. Both the soil sampling and the *EM* survey were carried out on September 22nd, 2016.

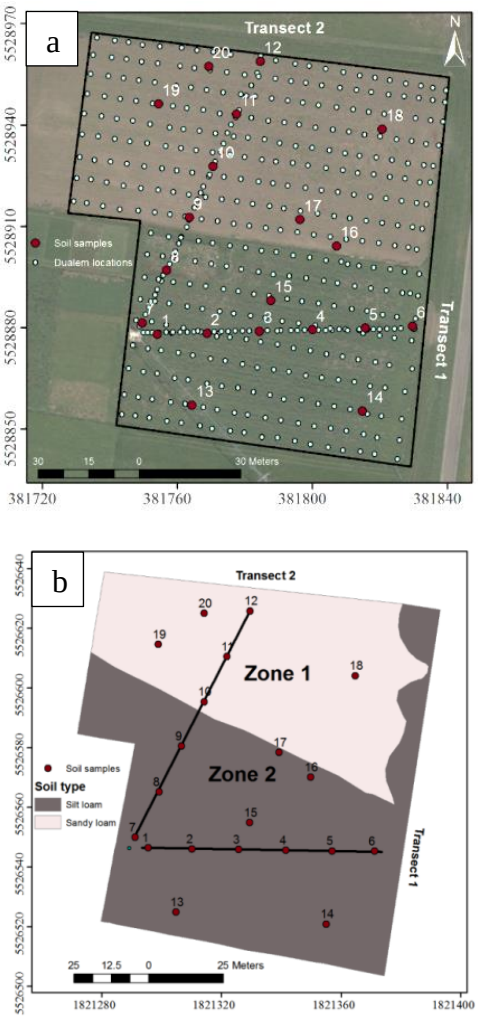

Figure 4.1: a) Google Map image of the study field with the locations of the Dualem-421S measurements and 20 soil sampling points, b) Soil map for Massey University arable experimental field site (Palmerston North, New Zealand) where a variable rate irrigation (*VRI*) centre pivot has been installed (Zone 1: Manawatū fine sandy loam, Zone 2: Manawatū silt loam. Source: (Pollok et al., 2003)

4.24 Laboratory analysis

Laboratory analyses of the calibration samples were (i) soil bulk density (ρ_b, g cm^{-3}) and gravimetric soil water content (θ_g, g g^{-1}) on an oven dry-weight basis (105◦ C), these calculations were then converted to θ_v (cm^3 cm^{-3}) (Gardner, 1986).

All soil preparation and laboratory analyses were undertaken at the Manaaki Whenua Environmental Chemistry Laboratory, Palmerston North, New Zealand.
(http://www.landcareresearch.co.nz/resources/laboratories/environmental-chemistry-laboratory)

4.25 EM4Soil and *2D* inversion of EC_a data

EM4Soil is a software package (EMTOMO, 2014) which was developed to invert EC_a data acquired at low induction numbers. The algorithm is described by Santos et al. (2010). In this study, we used the *quasi-2D* inversion modeling approach to generate a model of the σ at specific depths and *2D* electromagnetic images (*EMIs*) of both transects. Briefly, the algorithm generates *EMIs* by applying a *1D* inversion algorithm with the σ constrained by neighboring locations in *quasi-2D* or *-3D* (Santos et al., 2011).

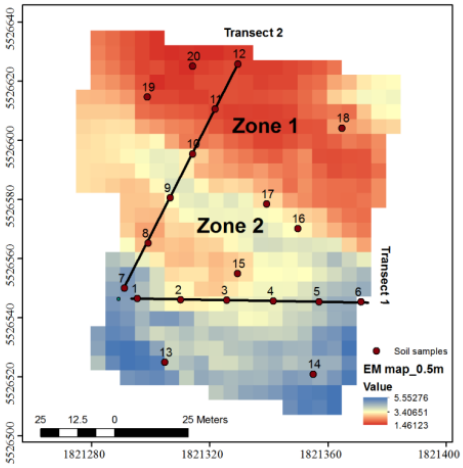

Figure 4.2: Electromagnetic (EM) map at a 5-m spatial resolution from the EM survey using ordinary kriging in R version 3.4 (R Core Team, 2018) in the gstat package (Pebesma, 2004).

To determine an optimal inversion, a number of factors were used including forward modeling, inversion algorithms, size of damping factor (λ), number of iterations (Triantafilis et al., 2013b; Triantafilis & Santos, 2013c; Triantafilis et al., 2013a). In our study, we selected the EM4Soil parameters which achieve the maximum coefficient of determination (R^2) for the linear correlation between σ and soil properties θ_v. We varied the forward modeling (*CF* and *FS*), the value of λ (e.g., 0.04, 0.07, 0.3, 1, 1.5 and 3), available coil arrays (4, 2 and 1) and inversion algorithms (*S1* and *S2*).

The *CF* model is based on the EC_a cumulative response and is used to convert depth-profile conductivity to EC_a under low induction number conditions (McNeill, 1980). The *FS* model is based on the Maxwell equations (Kaufman & Keller, 1983) and is not limited to the low induction number condition. The inversion algorithms (*S1* and *S2*) are based upon the Occam regularization method (e.g. (deGroot-Hedlin & Constable, 1990; Sasaki, 1989)), where *S2* constrains *EMI* around a reference model and produces smoother results than *S1*.

The optimal combinations of inversion for the *quasi-2D* inversion of EC_a were forward modeling based upon 'full-solution' of *EM* fields (*FS*), a damping factor of 0.04, an initial model (σ = 35 mSm^{-1}), all available coil arrays data and with 10 iterations.

4.26 Predicting θ_v and validation of prediction accuracy

Analysis of variance on measured θ_v between the two soil zones was carried out, and the significance of differences was estimated using the Least Significant Difference (*LSD*) at 5% probability level. In addition, a linear regression was performed to develop the calibration relationship between σ with θ_v for (i) both transects, and (ii) available data of 20 sites (n= 99). The performance of the regression models was assessed using a 'leave-one-out' cross-validation (*LOOCV*). In this case, the model was repeatedly refitted leaving out a single observation and then used to derive a prediction for the left-out observation. Within the literature, it is widely appreciated that *LOOCV* is a sub-optimal method for cross-validation, as it gives estimates of the prediction error that are more variable than other forms of cross-validation, but we consider that it is a useful and appropriate method for relatively small datasets, such as this one (Friedman et al., 2001). The predictive power of the model was described by the average coefficient of determination (R^2), root-mean-square error (*RMSE*) and mean error (*ME*) as measures of the bias determined using LOOCV.

All of the data visualizations and analyses performed in this study were carried out using R version 3.4 (R Core Team, 2018).

4.3 Results and Discussion

4.31 Comparison of θ_v data

Table 4.1 shows the summary statistics for measured θ_v between the two soil zones. Significant differences were observed in four of the five soil layers for θ_v. In particular, θ_v of Zone 2 were significantly ($p < 0.05$) higher than those of Zone 1. However, there were no significant differences in the surface θ_v (0 – 0.3 m) between the two soil zones. Use of the skewness values of soil properties to inspect for normality suggests that the data for both soil properties are moderately skewed.

The analysis of results shows considerably more variation in θ_v with depth in Zone 2 than Zone 1. In Zone 1, the larger θ_v for the 0 – 0.3 m depth compared to the rest of the profile is likely due to the coarser texture, higher organic matter content and higher available water content (*AWC*) of this soil depth as has been observed in a previous investigation (Pollok et al., 2003).

Table 4.1: The summary statistics of volumetric water content (θ_V, $cm^3\ cm^{-3}$) for Zone 1 (locations 10 – 12 and 18 – 20) and Zone 2 (locations 1 – 9 and 13 –17). The mean values θ_V in depths with P values >0.05 are not significantly different between the two soil zones.

	Zone 1					Zone 2					
Depth(m)	Mean	Min	Max	SD	Skew-ness	Mean	Min	Max	SD	Skew-ness	P value
volumetric water content (θ_V, $cm^3\ cm^{-3}$)											
0 – 0.3	0.22	0.18	0.28	0.04	0.90	0.25	0.22	0.30	0.03	-0.35	0.067
0.3 – 0.6	0.10	0.07	0.17	0.04	2.15	0.18	0.12	0.25	0.04	0.26	0.000
0.6 – 0.9	0.09	0.07	0.12	0.02	0.58	0.15	0.09	0.24	0.05	0.53	0.011
0.9 – 1.2	0.09	0.07	0.13	0.02	0.48	0.16	0.08	0.25	0.07	-0.02	0.034
1.2 – 1.5	0.09	0.06	0.17	0.04	2.05	0.21	0.08	0.32	0.09	-0.71	0.008

4.32 Comparison of the EC_a data

Table 4.2 shows the mean EC_a values were lower for the coarser textured soil (Zone 1) and higher for the finer- textured soils sites (Zone 2). Similar to the soil properties data, the *EM* data distributions also appeared to be moderately skewed except *Hcon* (1.5m) which is right-skewed. The highest coefficient of variation (*CV*) was for Zone 1 and the smallest for Zone 2 showing that Zone 1 conductivity (0 – 1.5 m) was more variable than Zone 2 conductivity.

With respect to the transects, EC_a values for transect 2 (in the north-eastern section) are lower than those of transect 1 in Zone 2 (Fig. 4.3). We attributed these observed variations between the two sections to the varying texture of the soil profiles.

In addition, elevation is a natural proxy for the underlying factors that could drive the observed differences in EC_a. For example, in transect 2, EC_a was larger at low elevation positions than in the higher elevations, which is possibly indicative of lateral water movement downslope at this position.

The descriptive statistics of the measured θ_v (Table 4.1) for Zone 1 and Zone 2 can be used to confirm and explain the variation in EC_a (Table 4.2, Fig. 4.2 and Fig 4.3) where the low values of EC_a coincide with the lower θ_v of the coarser textured soil.

Table 4.2: The summary statistics of apparent electrical conductivity (EC_a, mSm^{-1}) measured for the 20 sites by a Dualem-421S. Zone 1 (locations 10 – 12 and 18 – 20) and Zone 2 (locations 1 – 9 and 13 –17)

	Zone 1						Zone 2					
	Mean	Min	Max	SD	CV	Skew-ness	Mean	Min	Max	SD	CV	Skew-ness
Pcond(0.5m)	1.73	0.20	6.42	0.80	0.49	1.02	4.43	2.20	10.1	1.12	0.26	0.42
Pcond(1m)	1.30	0.13	4.51	0.80	0.66	1.20	4.10	2.40	10.9	1.00	0.25	1.31
Hcon(1.5m)	1.60	0.10	4.80	0.92	0.57	0.94	4.3	2.70	11.4	1.30	0.31	1.45
Hcon(2m)	2.19	0.50	3.70	1.10	0.55	-0.18	5.23	3.20	8.20	0.87	0.27	1.36
Pcond(3m)	1.69	1.20	2.60	0.52	0.53	0.81	4.53	2.30	7.10	0.84	0.14	0.82
Hcon(6m)	2.04	0.60	3.70	1.08	0.31	-0.01	4.93	3.20	7.80	0.68	0.19	0.93

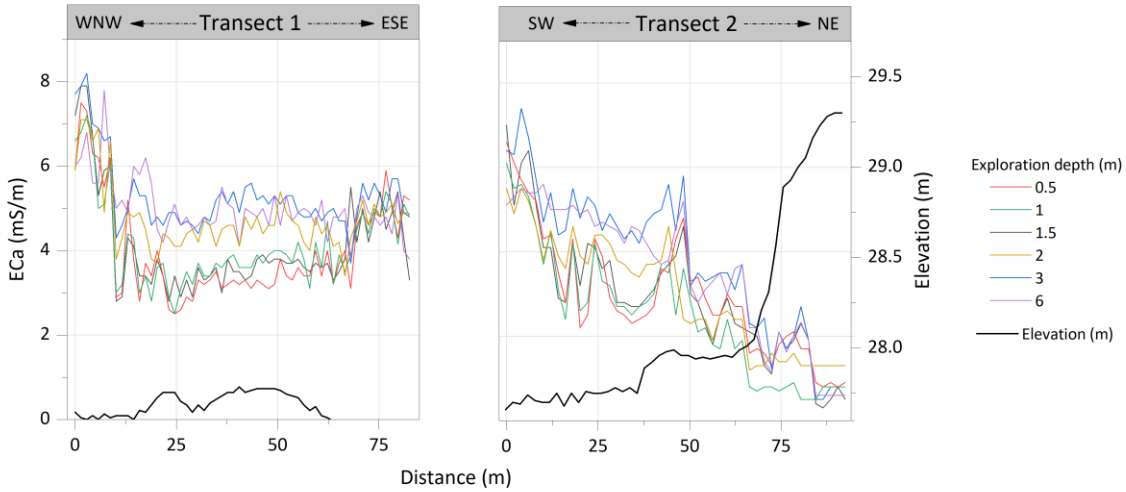

Figure 4.3: Measured apparent soil electrical conductivity (EC_a, mSm^{-1}) along transects 1 and 2 using the Dualem-421S sensor in horizontal coplanar (*Hcon*) and perpendicular coplanar (*Pcon*) at exploration depth 0.5 – 6 m.

4.33 Regression modelling of θ_v using σ

The relationships between σ derived using the inversion *quasi-2D* model, with measured θ_v in each transect, and for the 20 sites are explained in Fig. 4.4. The relationships were good, as indicated by R^2 values. The imaging method for both transects produced similar correlations with θ_v. These relationships allowed the *2D* profiles of θ_v to be modeled using σ. The model performed well (see Fig. 4.5) with θ_v, achieving a correlation of 0.66, and small *RMSE* values of 0.04 $cm^3\ cm^{-3}$. Overall, the predicted θ_v points (n=99) were precise (low *RMSE*) and unbiased (Bias = 0.00 %).

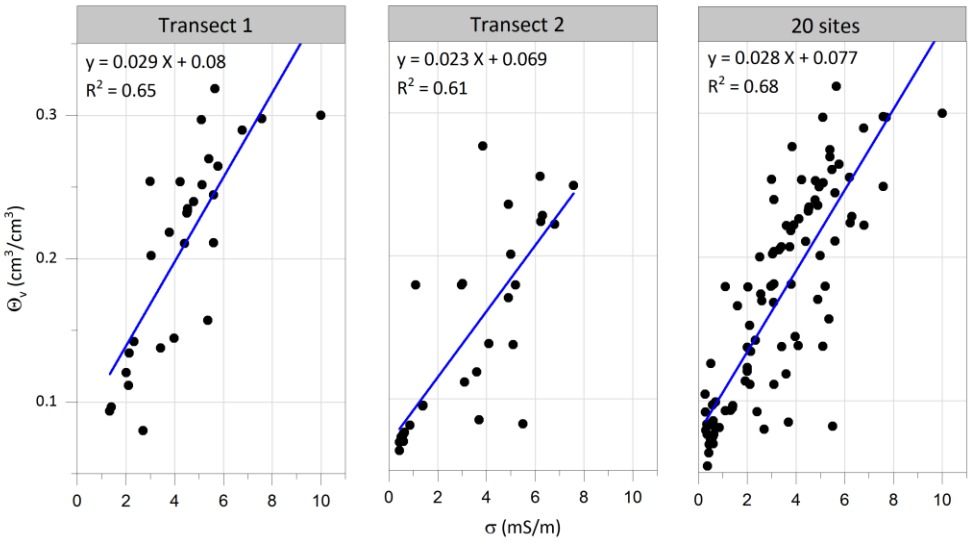

Figure 4.4: The relationships of true electrical conductivity (σ, mSm^{-1}) with volumetric water content (θ_v, $cm^3\ cm^{-3}$) for the two transects and using the available data of 20 sites (99 samples)

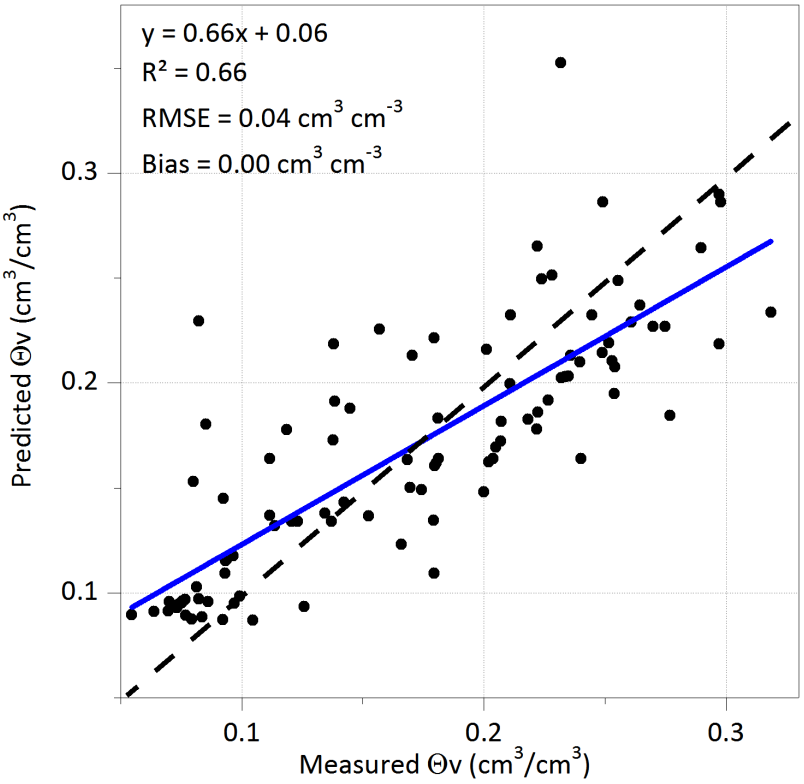

Figure 4.5: Predicted soil water content (θ_v, $cm^3\,cm^{-3}$) derived from true electrical conductivity (σ, mSm^{-1}) versus measured soil water content (θ_v, cm^3cm^{-3}), (n=99).

4.34 *2D* depth profile modeling of predicted σ and θ_v along two transects

Fig. 4.6 shows the *2D* depth profile images for σ and θ_v along two transects. Along transect 1, the θ_v values were typically higher in the topsoil then decreased in the subsoil before increasing again in the deep subsoil. We hypothesise that this pattern reflects the effect of texture on water movement through the soil profile, as was also referred to by Clothier et al. (1977b) and explained in Section 4.35.

A comparison of the measured and predicted top soil θ_v (0 – 0.3 m) at the 20 sites at Zone 1 (0.18 – 0.28 $cm^3\ cm^{-3}$) and Zone 2 (0.22 – 0.30 $cm^3\ cm^{-3}$) with the θ_v values from *AWC* indicate that the topsoils were near field capacity. This is supported by the climate data which showed that on 18 September 2016 (three days before the survey); there was a heavy rainfall event (33.4 mm). Soil θ_v decreased in the subsoil at Zone 1 (0.07 – 0.17 $cm^3\ cm^{-3}$) although this is still likely to be at field capacity (*FC*) (measured *FC* were 0.8 – 0.18 $cm^3\ cm^{-3}$) as the texture is sand at this depth (Allen et al., 1998). In Zone 2, θ_v decreased in the 0.3 – 0.9 m depth (0.12 – 0.25 $cm^3\ cm^{-3}$) and then increased in the 1.2 – 1.5 m depth (0.08 – 0.32 $cm^3\ cm^{-3}$). Considering the topographic elevation, the downward flow of water into lower-lying slope positions could explain differences of σ and θ_v in the topsoil along transect 1. In addition, the locations with higher elevation in transect 2 had less σ and θ_v than lower locations (Fig. 4.6)

The *2-D* depth profile of predicted θ_v along two transects suggests that the two soils zones at the research site may require irrigation at different times and that these differences seem to be related to changes in the depth of the observed sandy layer. If the same magnitude of soil water differences recurs every growing season, due to these intrinsic soil differences, then *VRI* can be managed to take advantage of these differences with a static prescription map even without sensor or using a time-lapse θ_v monitoring approach to monitor the spatiotemporal variations of θ_v and identify inefficiencies in water application rates and use, as was also discussed by Huang et al., 2017a.

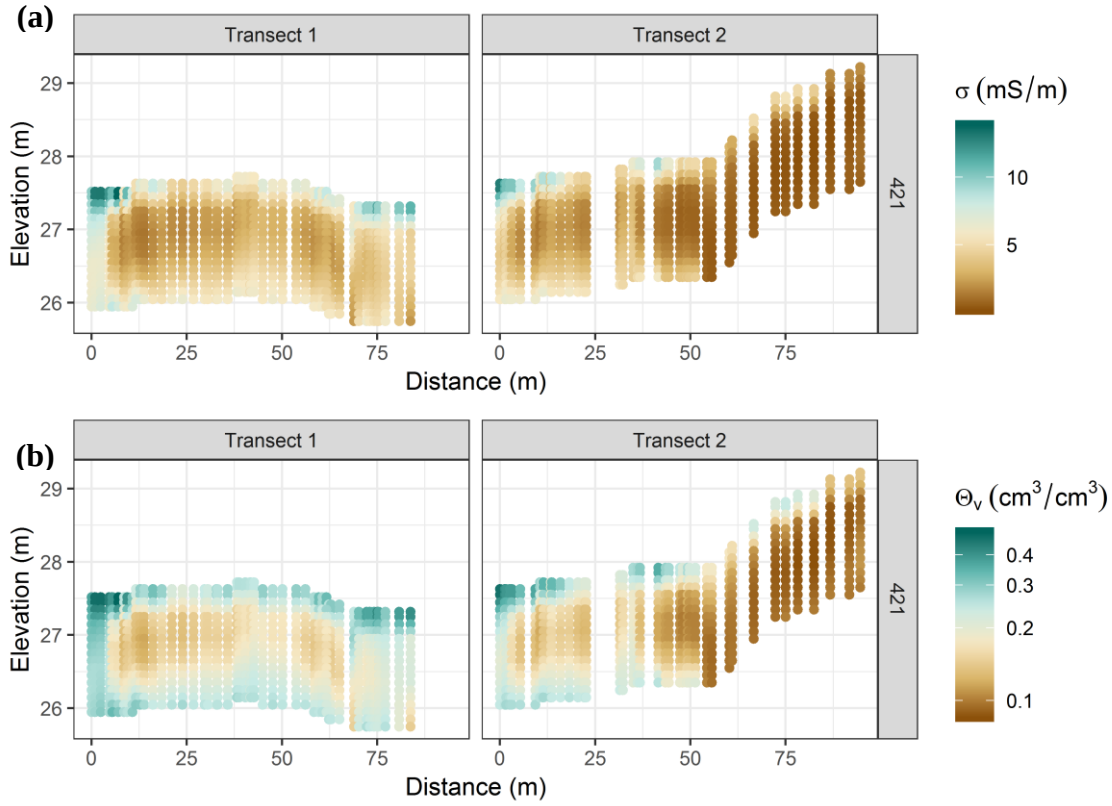

Figure 4.6: a) True electrical conductivity (σ, mSm^{-1}) derived from the *quasi-2D* inversion model for the two transects. P1–P12: positions/locations 1 – 12, and b) volumetric water content (θ_v, $cm^3\ cm^{-3}$) for the two transects as derived from the linear regression models.

4.35 Predicted depth profiles of modeled σ with measured θ_v at specific positions

The soil profiles of these Fluvisols are typically variable. They have formed over the last few 100 years in multiple flood deposits of varying textures and depth over a gravel surface – the texture and depth of each layer depending on the size of the flood event.

Fig. 4.7 shows some examples of the depth profiles of σ and measured θ_v (for positions 6, 9 and 19), with θ_v and σ following similar trends down the soil profile. The θ_v profiles showed different trends with depth below 0.6 m. A comparison of the results presented by Clothier et al., 1977b with the current study demonstrates the ability of the technology developed here to identify this variability in soil texture with depth and an interesting

consequence of this variability for water movement. There were similarities between the θ_v in Zone 1 for profiles both with (i.e. P5, P6, P14 (see, for example, P6 in Fig. 6)) and without (i.e. P10, P11, P19 and P20 (see, for example P19 in Fig. 6)) a gravelly coarse sand layer with the θ_v profiles shown in Clothier et al. (1977b) ((Clothier et al., 1977b); Fig. 8). Clothier et al (1977b) hypothesize that the decreasing and then increasing θ_v with depth is due to the textural break between the soil and the underlying gravel surface which impedes the flow of water into the gravels. This leads to an increase in θ_v in the finer layer above the coarse gravel surface (Clothier et al., 1977b) in some soils, as shown in the P9 trace in Fig. 4.7.

In general, these findings suggest a good relationship exists between EC_a and the soil properties that control θ_v. This relationship can be used to guide the position and depth of placement of soil moisture sensors in the field, to improve the monitoring of the soil moisture profile which in turn informs soil and water management, e.g., for irrigation scheduling.

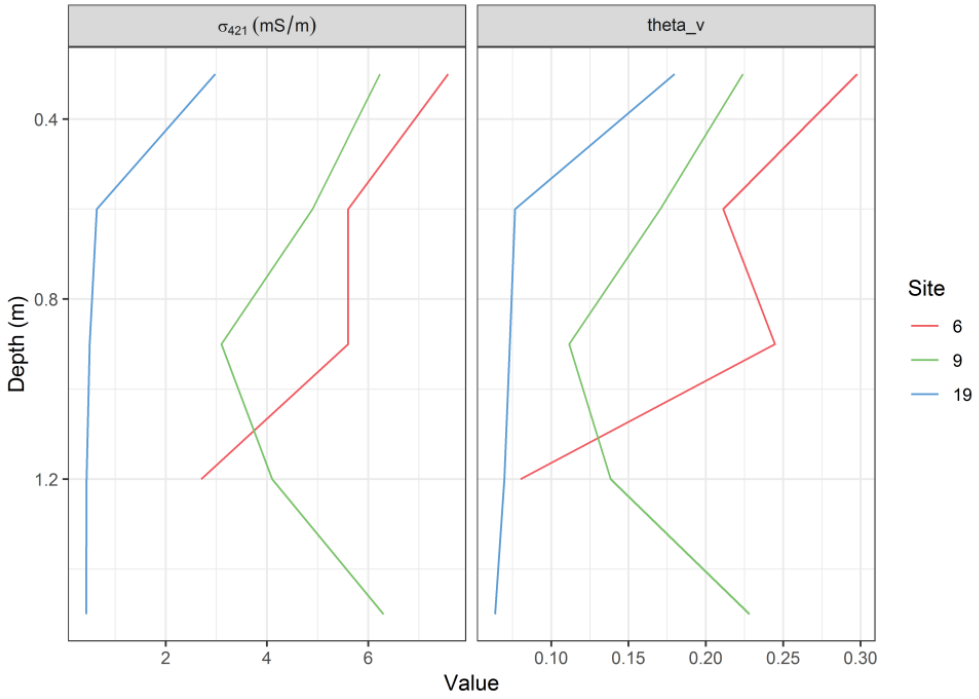

Figure 4.7: True electrical conductivity (σ, mSm^{-1}) using the inversion *quasi-2D* model compared with measured soil water content (θ_v, cm^3cm^{-3}) at specific depths for positions 6, 9 and 19

4.14 Conclusions

The inversion model (EM4soil) has been shown to be a very useful tool for estimating σ continuously down the soil profile using all available coil array data values of EC_a measured by a Dualem-421S sensor during a routine survey. Inversion modeling has also been used to relate σ to measured θ_v values for soil profiles to 1.5m depth, and to predict *2D* profile maps of these soil properties. The predicted θ_v showed a significantly higher correlation and lower biases and errors with the measured θ_v. In this study, the spatial variability of a coarser textured (Zone 1) and intermediate textured (Zone 2) Manawatū soil was characterized. The θ_v depth profile maps indicate the effect of texture and texture transitions on soil wetness. The predicted θ_v profile was able to identify water perching above a gravelly layer in the Manawatū fine sandy loam as described by earlier researchers (Clothier et al., 1977b).

Integration of the *EM* data, which represents soil spatial variability, with soil moisture monitoring (reliable measurement of temporal changes in θ_v), could be used for improving irrigation management by guiding the position and depth placement of soil moisture sensors to best monitor the spatial and temporal variability of soil moisture profiles that typically occurs in alluvial soils.

Future work could be undertaken to predict spatiotemporal changes in θ_v by developing a calibration of variable θ_v and EC_a and generating *quasi-3D* models of σ.

Connecting text to Chapter 5

The ability of electromagnetic (*EM*) technology, as discussed in the previous chapter, to assist in the delineation of precision irrigation management zones requires an accompanying method for dynamic irrigation scheduling to enable variable-rate irrigation (*VRI*). In this chapter, two *VRI* scheduling methods, water balance model and sensor networks, were assessed for a pea and a French bean crop over one season. This chapter was accepted for publication in November 2019 in Agricultural Water Management, https://doi.org/10.1016/j.agwat.2019.105901

Chapter 5

Soil sensing technology improves application of irrigation water

Abstract

Dynamic irrigation scheduling for variable-rate irrigation systems is essential to accurately estimate the spatiotemporal pattern of irrigation water requirement. Real-time, sensor-based and soil-water balance scheduling methods were compared on a trial under a variable-rate centre pivot irrigation system. The soil-water balance scheduling used the FAO56-ET model to calculate daily soil-water deficits and to determine crop water requirements using climate data from a local climate station. The sensor-based scheduling system used a wireless soil moisture sensing network to trigger irrigation when soil water deficit reached a critical value in a web-based user interface. The scheduling was conducted on pea and French bean crop trials under one centre pivot, with two delineated irrigation management zones at Massey University's No.1 Farm, Palmerston North, New Zealand.

The results showed variation between the two scheduling methods where the soil water balance assumed that the soil is well drained. The sensor-based scheduling technique delivered 23–45% less water. As there were no significant crop growth and yield differences between the two approaches, irrigation-water-use efficiency was greater under the sensor-based scheduling regime. Further research is planned to assess the feasibility of including this monitoring system in a precision irrigation control system.

Keywords: Precision irrigation; Variable rate irrigation; Wireless sensor network; Soil moisture sensors; Soil water balance; Irrigation water use efficiency; Water productivity.

5.1 Introduction

Variable-rate irrigation (*VRI*) systems make it possible to spatially vary water application depths across a field in a manner that addresses specific soil, crop, and/or other conditions (e.g. topography; sequential row crop sowing). By optimizing water application rates, *VRI* can meet the site-specific watering needs of plants while improving the environmental outcomes of irrigated cropland (Evans et al., 2013; Daccache et al., 2015). Some *VRI* systems use customized irrigation zones defined on dedicated software. The variable rate program is then loaded into the precision *VRI* controller that directs individual sprinklers through valve nodes (wireless or cable control system). For centre pivots, *VRI* is currently complemented by two techniques: (i) Speed control varies the– fraction of time that the outermost tower is moving, so application depth can be different in each sector of the field (*VRI* Speed Control - One slice is one sector). (ii) Nozzle control varies the fraction of time each sprinkler or bank of sprinklers is turned on, so application depth can be different angularly and radially. Both mechanisms may be integrated for zone control *VRI* (*VRI* Zone Control -One block is one management zone) (Evans et al., 2013).

VRI management zones have been delineated using soil apparent electrical conductivity (EC_a) maps (Corwin & Lesch, 2003). This method is considered to be a rapid, non-destructive, inexpensive, and very reliable way to map soil variability at high spatial resolution (Corwin & Lesch, 2003). The EC_a primarily relates to soil texture and moisture content (*MC*) in non-saline soils, and as these two soil properties relate to the soil water-holding capacity, EC_a surveys can be used to identify irrigation management zones (Hedley & Yule, 2009a; Sudduth et al., 2005b)

In arid regions where irrigation supplies nearly all the crop's water needs, irrigation scheduling is relatively straightforward because crop water demand can be estimated without having to take into account the effects of daily variable precipitation patterns and consequent changes in *MC* of different soil horizons with varying drainage characteristics (Fant et al., 2012). In humid regions such as New Zealand, irrigation is needed as a supplemental source of water for those times when rainfall is insufficient to meet crop water needs.

In these situations, scheduling irrigation can be a greater challenge because it aims to reduce or eliminate crop stress due to drought, as well as avoid excessive watering with the negative environmental impacts of increased drainage and nutrient leaching. Careful scheduling of *VRI* can maximize irrigation water use efficiency (*IWUE*) by determining the exact timing and amount of water needed to replenish the *MC* to a desired level in order to meet crop water demands.

Three categories of scheduling techniques exist: (i) soil water balance (*SWB*) model calculated using meteorological data (Allen et al., 1998); (ii) soil sensor measurements of *MC* (Smith, 2000); and (iii) crop sensor measurements of plant water status (Jones, 2004b).

With the *SWB*-based approach, the soil water deficit (*SWD*) is tracked by accounting for all water additions (inputs) and losses (outputs) from the soil root zone. Major inputs are precipitation and irrigation. Water might also be transported upward by capillary rise from a shallow water table towards the root zone (Allen et al., 1998). Outputs include crop evapotranspiration (ET_c), drainage, and runoff. Irrigation is required when ET_c exceeds the supply of water from both soil water and precipitation or in other words when a critical *SWD* level (in millimeters) has been reached. ET_c is often determined as the product of the reference evapotranspiration (ET_o) and the crop coefficient (K_c) with the ET_o calculated from climatic parameters (Allen et al., 1998). Accurate estimates of K_c and soil hydraulic properties values are essential because inaccuracies in K_c and field capacity values can potentially result in large errors in the estimated *SWD* (Allen et al., 1998).

A standardized version of the Penman and Monteith (*PM*) equation (FAO56, Allen et al., 1998) is the recommended procedure for calculating ET_o and subsequently plant water requirements. Several water balance models refer to this approach, for example, the FAO AquaCrop model (Steduto et al., 2009) and CropWat (Smith, 1992), and it is also included in many farm-system models, e.g. Overseer (Wheeler & Rutherford, 2014) and APSIM (Keating et al., 2003; Probert et al., 1998).

Another major potential source of error in the widely used FAO56 *SWB* method is the uncertainty of drainage characteristics (especially for poorly drained soils): the method assumes that the soil is well drained and that moisture cannot exceed field capacity, with free movement of soil water and other undetected fluxes in and out of the control volume (Fant et al., 2012; Nolz, 2016).

Other models exist that may be more accurate in estimating drainage (Miller & Aarstad, 1972), but these were not evaluated in this study.

The K_c derived from remotely sensed vegetation indices such as the Normalized Difference Vegetation Index (*NDVI*) makes it possible to account for variations in plant growth due to specific growing and weather conditions, and also improved *SWB* irrigation scheduling due to better estimation of water use and more appropriate timing of irrigations (Kullberg et al., 2017). Several studies have tested the potential use of *NDVI* to predict K_c and transpiration at the field scale (Duchemin et al., 2006; Er-Raki et al., 2007; González-Dugo & Mateos, 2008; Hunsaker et al., 2005). These studies concluded that K_c generated from *NDVI* determine ET_c better than a tabulated K_c in terms of representing the actual crop growth conditions and capturing the spatial variability among different fields.

Soil moisture can be directly measured via gravimetric sampling or estimated using a range of instruments (Charlesworth, 2005). The gravimetric method involves collecting a soil sample, weighing the sample before and after oven drying (for 24 hours), and calculating its *MC*. This *MC* is usually expressed as the ratio of the mass of water present in the soil sample to the dry weight of the soil sample (Hillel, 1982). This method, which involves sampling, transporting, and repeated weighing, is laborious and time-consuming. Instruments based on the neutron-probe technique and dielectric methods (time domain reflectometry (*TDR*) and capacitance techniques) estimate the volumetric *MC* (Smith, 2000). These sensors are easy to use and provide highly reproducible data (van Iersel et al., 2009). The neutron-probe and *TDR* methods have been widely employed and are sometimes used as reference methods (Gardner, 1986; Vicente et al., 2003).

Recent innovations in wireless radio frequency technologies and sensors (such as those mentioned above), along with advances in internet technologies, offer excellent opportunities for real-time monitoring of the field soil, crop and environmental conditions. A number of wireless sensor network (*WSN*) with various topologies (e.g. star, mesh-network) have been developed and investigated under irrigation by different researchers in the past decade (Ruiz-Garcia et al., 2009), including centre-pivot irrigation (O'Shaughnessy & Evett, 2008), linear-move irrigation systems (Kim et al., 2008) and *VRI* centre-pivot (Barker et al., 2018; Hedley et al., 2013; Liang et al., 2016).

Research is required to refine decisions support tools for *VRI* systems. Thus, the objectives of this study were to: (i) investigate and compare the impact of two *VRI* scheduling methods – *SWB* model-based and sensor-based – on the quantity of water applied, crop growth, final yield, and *IWUE* for a pea crop and a French bean crop over one season under a *VRI* centre pivot; and (ii) discuss the potential improvement in the model scheduling method by using the *NDVI* derived from ground-based data, because to our knowledge, this is new work that is critically required to support efficient irrigation scheduling.

5. 2 Materials and Methods

5. 21 Study site

The study was conducted at a research site (1.2 ha) in Massey University's No.1 Dairy Farm, near Palmerston North, New Zealand, during the 2017/2018 growing season. The farm is located at 40.22° South latitude and 175.36° East longitude, at an elevation of 37 m above sea level. The field is currently irrigated with an 86-m *VRI* centre-pivot system (i.e. 1 span) containing 31 sprinklers, each with a spray radius of 5 m and a flow rate of 26.3 m^3 h^{-1}. The water is sourced from groundwater in a nearby well. According to the New Zealand Soil Classification (Hewitt, 2010), the soils are Fluvial Recent soils formed in greywacke alluvium, which correspond to Fluvents in the USDA Soil Taxonomy (USDA, 1975).

5. 22 Irrigation management zones

The soil map for this field (Pollok et al., 2003) shows the presence of two soil types: a Manawatū fine sandy loam and a Manawatū silt loam. EC_a maps were used to delineate the field precisely into irrigation management zones. The electromagnetic (*EM*) survey was carried out at 6-m swath widths using a Dualem-1S. EC_a at an exploration depth of 0.5 m was mapped at a 5-m spatial resolution from the *EM* survey using ordinary kriging

in R version 3.4 (R Core Team, 2018) in the gstat package (Pebesma, 2004). The EC_a map was further split into two classes (irrigation management zones) using k-means clustering.

5. 23 Experimental setup

Field peas (cultivar *Massey*, 260 kg ha^{-1}) and French beans (cultivar *Contender*, 75 kg ha^{-1}) were sown on 15 November 2017 and 9 February 2018, respectively. The experiment comprised four plots (20 x 10 m) in each soil zone plus two plots in a non-irrigated corner of the field. The crop management details for the peas and beans are shown in Table 5.1.

Table 5.1: Management operations for the pea and bean trials at the Massey pivot (2017/2018)

Date	Operation
15 November 2017	Weed control: Pre-Empt applied @ 1.7 l ha^{-1}
15 November 2017	Fertiliser: 250 kg ha^{-1} 'Cropmaster 15' applied (nitrogen (15.1%), phosphate (10%), potassium (10%) & sulphate (7.7%))
15 November 2017	Planting: Peas sown @ 260 kg ha^{-1} (cultivar - *Massey*)
23 January 2018	Harvest: Peas
7–8 February 2018	Chisel ploughed and power harrowed
9 February 2018	Fertiliser: 250 kg ha^{-1} 'Cropmaster 15' applied & incorporated
9 February 2018	Planting: Beans sown at 75 kg ha^{-1} (cultivar: *Contender*)
12 April 2018	Harvest: Beans

5. 24 Scheduling treatments

The experiment consisted of two scheduling treatments in each zone, and a non-irrigated area. Each zone had two replicate plots per scheduling treatment. The two irrigation scheduling methods were (i) the *SWB* method and (ii) the sensor-based method. The non-irrigated treatment was in the non-irrigated corner.

For the *SWB* method, a daily time-step water balance model was developed. This model used daily weather data derived from a local climate station (http://cliflo-niwa.niwa.co.nz/), located 50 m from the trial site, to calculate the daily ET_o, ET_c and

SWD values. The daily ET_o was calculated from the *PM* equation (Allen et al., 1998) as in Equation (5.1):

$$ET_o = \frac{0.408 * \Delta * (R_n - G) + \gamma * \frac{900}{T + 273} * u_2 * (e_s - e_a)}{\Delta + \gamma(1 + 0.34 * u_2)} \quad [5.1]$$

Here, ET_o: reference evapotranspiration (mm d^{-1}), R_n: net radiation at the crop surface (MJ m^{-2} d^{-1}), G: soil heat flux density (taken as zero for daily calculations) (MJ m^{-2} d^{-1}), T: mean daily air temperature at 2 m height (ºC), u_2: wind speed at 2 m height (m s^{-1}), e_s: saturation vapour pressure (kPa), e_a: actual vapour pressure (kPa), $e_s - e_a$: saturation vapour deficit (kPa), Δ: slope vapour pressure curve (kPa $ºC^{-1}$), γ: psychrometric constant (kPa $ºC^{-1}$)

The FAO56 ET_o model and a dual crop coefficient method ($K_c = K_s \times K_{cb} + K_e$), which accounts for variations in soil water availability, inducing either stress and soil evaporation, were used to estimate ET_c, Equation (5.2) (Allen et al., 1998):

$$ETc = (K_s \times K_{cb} + K_e) \times ET_o \quad [5.2]$$

where, ET_c is the crop evapotranspiration (mm d^{-1}), K_{cb} is the basal crop coefficient, K_s is water stress coefficient, and K_e is soil evaporation coefficient. K_e and K_s are calculated based on daily water balance computation in the surface soil evaporation layer of measured effective depth ($Z_{e.i}$) and in the root zone ($Z_{r.i}$), respectively, according to Allen et al. (1998).

Crop coefficients (K_c and K_{cb}) vary according to the crop growth stage and are also affected by the climate conditions. The standard tabulated coefficient values (Allen et al., 1998) were modified to reflect local conditions at that time using Equation (5.3). Also, actual readings of crop height and root depth ($Z_{r.i}$) were taken during the growing season to adjust the predictions. In soil data settings, maximum measured rooting depth of 0.4 and 0.3 m for pea and bean, respectively, were used to match up with the sensor estimated *SWD*.

$$K_{cb\ Stage} = K_{cb\ Stage\ (Tab)} + [0.04\ (u_2 - 2) - 0.004(RH_{min} - 45)]\left(\frac{h}{3}\right)^{0.3} \quad [5.3]$$

$K_{c\ Stage\ (Tab)}$ is the standard value for basal crop coefficient according to the FAO56 approach plant height (m) for each growth stage (0.1 m < h <10 m); u_2 is the value for

daily wind speed at 2 m height over grass during the growth stage (m s^{-1}); RH_{min} is the value for daily minimum relative humidity during the growth stage (%); h is the mean plant height during that crop stage (m), and K_c is crop coefficient.

For the sensor-based method, the *MC* was monitored using frequency domain reflectometry probes (SM300- DeltaT, Burwell, UK) and calibrated, for each soil type, against weekly measurements of *MC* made gravimetrically and with a neutron probe (calibration equation was updated weekly). The SM300 probes were installed horizontally for each plot at 4 depths i.e. 0.10, 0.20, 0.30 and 0.40 m (Fig. 5.1 and 5.2). The neutron probes, which were 1 m long, were installed permanently in a vertical position, close to the SM300 sensors (about 1 m distance), and *MC* readings were taken to a depth of 0.80 m in 0.10 m depth increments. To calibrate the SM300 probes: (i) there were four replicate neutron access tubes in each of the four replicate plots in each soil zone for each crop, and (ii) three undisturbed soil sample replicates of known volume (intact cores) were taken close to the access tubes (about 1–3 m distance) at depths of 0.1, 0.20, 0.30, and 0.40 m. The soil volumetric moisture content was determined by multiplying the gravimetric moisture content by the measured bulk density. The SM300 is connected with a *WSN* developed by Ekanayake and Hedley (2018), which provides a direct continuous measurement of the *MC* in near real-time (at one-hour interval) and displays it on a web page (http://lcrmbei.com/index.php/massey/soil-moisture-zoom/).

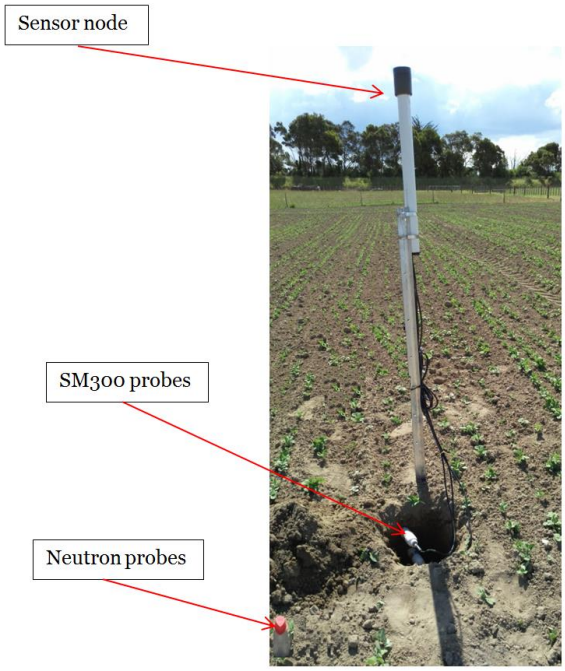

Figure 5.1: Wireless soil moisture sensing system at Massey University No.1 Farm. The system provides a direct continuous measurement of the soil moisture status in a real-time where the data are collected by the sensor node and then relayed to a gateway that collects and transmits the data to a cloud-based database which then extracts, processes and displays it on web pages (http://lcrmbei.com/index.php/massey/soil-moisture-zoom/). The red cap of the neutron probe access tube is shown in the lower left-hand corner of the photo.

5. 25 Scheduling process

Irrigation of the plots was scheduled as follows:

(i) For the *SWB* treatment, daily weather was used to calculate the *SWD* using equation

$$SWD_2 = SWD_1 - IR - P - CR + RO + ET_c + DP \quad [5.4]$$

where, SWD_1 and SWD_2 is beginning and ending total *SWD* (mm), respectively, *IR* is irrigation (mm), *P* is precipitation (mm) *CR* is capillary rise from the groundwater (mm), *RO* is runoff from the soil surface (mm), ET_c is calculated crop water use, or evapotranspiration (mm d^{-1}), and *DP* is deep percolation or drainage out of the root zone (mm).

The initial *SWD* was derived from measured soil moisture content using portable TDR sensor "The MiniTrase (6050X3)" by Equation 5.5. Any excess water in the root zone

(0.4 m for pea and 0.3 m for bean) was assumed to be lost through *DP*. *CR* was assumed to be zero because the water table was more than about 1 m below the bottom of the root zone (Allen et al., 1998). *RO* was assumed to be zero.

(ii) For sensor treatments, data from the calibrated *MC* sensors were used to monitor daily *MC* and calculate *SWD* for each zone, through the entire cropping season. Based on the crop stage, average daily cumulative *SWD* at depths of 0.20, 0.30, and 0.40 m for pea and bean crops were calculated:

$$SWD = (\theta_{\mathrm{FC}} - \theta_{\mathrm{obs}}) * Z_{\mathrm{r,i}} \quad [5.5]$$

where, SWD is daily soil water deficit (mm), θ_{FC} is soil moisture content at field capacity (expressed in mm/100mm), θ_{obs} is soil moisture content (expressed in mm/100mm) at the given layer and $Z_{\mathrm{r,i}}$ is the rooting depth (mm). i is crop stage of 0.20 (initial stage), 0.30 (mid stage) and 0.40 (late stage).

The *MC* sensors were installed 11 and 12 days after planting of pea and French bean crops, respectively, so the first irrigation event before installation of the sensors was based on the *SWB* method for all treatments.

Critical *SWD* values for triggering irrigation and applied irrigation depths (*IR*) are expressed as proportions of the total available water (*TAW*) (Equation 5.6). For each treatment, when allowable deficit (*AD*) level was reached, an irrigation event was scheduled. *AD* levels were determined for both scheduling methods as 0.45 *TAW*, and *IR* was set at 0.75 *AD*. This aims to avoid drainage from irrigation and provide a buffer (25% deficit) in the soil for any rain event. *TAW* is defined as:

$$TAW = 1000\ (\theta_{\mathrm{FC}} - \theta_{\mathrm{WP}})_i * Z_{\mathrm{r,i}} \quad [5.6]$$

where, TAW is the total available soil water in the root zone (mm), θ_{FC} moisture content at field capacity ($m^3\ m^{-3}$), θ_{WP} moisture content at wilting point ($m^3\ m^{-3}$), Z_{r} is the rooting depth (m) (Table 3). The average measured *TAW* in each soil zone was used for irrigation scheduling. A destructive method was used for measuring the maximum effective rooting depth directly at different growth stages. The growth stage days were determined based on days after planting, and linear interpolation for crop parameters (K_{cb}, crop height and $Z_{\mathrm{r.i}}$) were used between stages. For peas, $Z_{\mathrm{r.i}}$= 0.2 (initial stage), 0.3 (mid stage) and 0.4 (late stage); beans $Z_{\mathrm{r.i}}$ = 0.2 (initial stage) and 0.3 (mid and late stages).

5. 26 Assessment of scheduling treatments

Crop assessments (i.e. height, length, number of nodes, flowers, and pods) were conducted manually on a weekly basis until harvest. Three replicates of 25–30 plants were monitored at each time for each plot, to distinguish the impact of irrigation scheduling treatments on crop growth.

To investigate the impact of irrigation treatment on the final harvest yield, the following process was undertaken:

- Cut three 1-m^2 replicates of the aboveground plant material in each plot
- Record number of plants, total biomass weight (fresh biomass)
- Separate pods from vine, count number of pods, record weight (bean's fresh yield)
- Separate seeds from subsample pods and record their weight (pea's fresh yield)
- Dry biomass and yield were calculated on an oven dry-weight basis (70ºC).

To compare the effect of scheduling technique on crop water productivity, the *IWUE* (Howell, 2002) and water productivity (*WP*) were calculated:

$$IWUE = (Y_g - Y_{gd})/IR \quad [5.7]$$

$$WP = Y_g / ET_c \quad [5.8]$$

where *IWUE* is the irrigation water use efficiency (kg m^{-3}), *WP* is the water productivity (kg m^{-3}), Y_g is the irrigated grain yield (g m^{-2}), Y_{gd} is the non-irrigated (rainfed) yield (g m^{-2}), *IR* is the irrigation water applied (mm), and ET_c is the total cumulative crop evapotranspiration (mm).

5. 26 Recalibrating crop coefficient in FAO56 water balance

As K_{cb} derived from *NDVI* measurements reflects the local conditions, the feasibility of directly estimating the K_c and predicting ET_c from sensor readings of *NDVI* was investigated and compared against the calculated K_{cb} values using the FAO56 approach.

A RapidSCAN CS-45 Handheld Crop Sensor (Holland Scientific, Lincoln, NE) was used

to measure the *NDVI* at 1-m intervals along transects 1 m apart in each plot on a weekly basis. The system is equipped with a GPS, so the data were collected and stored for analysing the *NDVI* differences between the plots. Markers were installed in each plot to allow the observations to be made at the same place from one date to another. The average and the standard deviation of *NDVI* were computed, from these measurements.

Collected *NDVI* data were regressed against FAO56 estimated K_{cb} values to predict a K_{cb} curve for the whole season (Taherparvar & Pirmoradian, 2018). The curve was then used to predict daily K_{cb} values (Taherparvar & Pirmoradian, 2018). Furthermore, cross validation was applied to the model.

5. 27 Soil sampling

Soil samples were collected before the growing season, on 15 August 2016, to compare laboratory measurements of available water content (*AWC*) between the two soil zones (Zone 1 and Zone 2). Soil cores were taken from 18 locations (9 for each soil zone) at 0.2-m intervals to a depth of 1 m.

To compare levels of soil nitrate and ammonium between treatments and their impact on crop growth, three replicates of soil samples were taken at 0.15-m intervals to a depth of 0.45 m from each plot at pre-planting and harvest.

5. 28 Laboratory analysis

Laboratory analysis included measurements of (i) *AWC* by draining a proportion of soil volume between pressure potentials of –10 and –1500 kPa (Gardner, 1986; McQueen, 1993), (ii) Mineral nitrogen, ammonium and nitrate (*NH4-N* and *NO3-N*) were extracted with 2 M KCl using a 1:10 soil: extractant ratio and a 1-hour end-over-end shake followed by filtration (Blackmore et al., 1987)

All soil preparation and laboratory analyses were undertaken at the Manaaki Whenua Environmental Chemistry Laboratory, Palmerston North, New Zealand (http://www.landcareresearch.co.nz/resources/laboratories/environmental-chemistry-laboratory).

5. 28 Statistical analysis

The Kolmogorov-Smirnov test of normality (*KS*) was carried out at 5% significance. Analysis-of-variance (*ANOVA*) at P=0.05, Tukey's HSD (data normally distributed) and Bonferroni (*Dunn*) (data non-normal distributed) were conducted to investigate significant differences in measured soil properties and crop measurements.

All the data visualizations and analyses performed in this study were carried out using R (R Core Team, 2018).

5. 3 Results and Discussion

5. 31 Delineating the field into irrigation management zones

The Dualem-1S sensor data were kriged into an EC_a map and classified into two irrigation management zones (Zone 1 and 2, see Figure 5.2, Table 5.2).

The relationships between EC_a values and soil properties (*MC* and cation exchange capacity (*CEC*)) were established for this field site by El-Naggar et al. (2017), who measured linear relationships of EC_a with *MC* and *CEC* (R^2 = 0.66 for *MC* and R^2 = 0.63 for *CEC*). The form of linear regression was: (i) $MC = 0.08 + 0.03\ EC_a$ and (ii) $CEC = 2.86 + 1.09\ EC_a$.

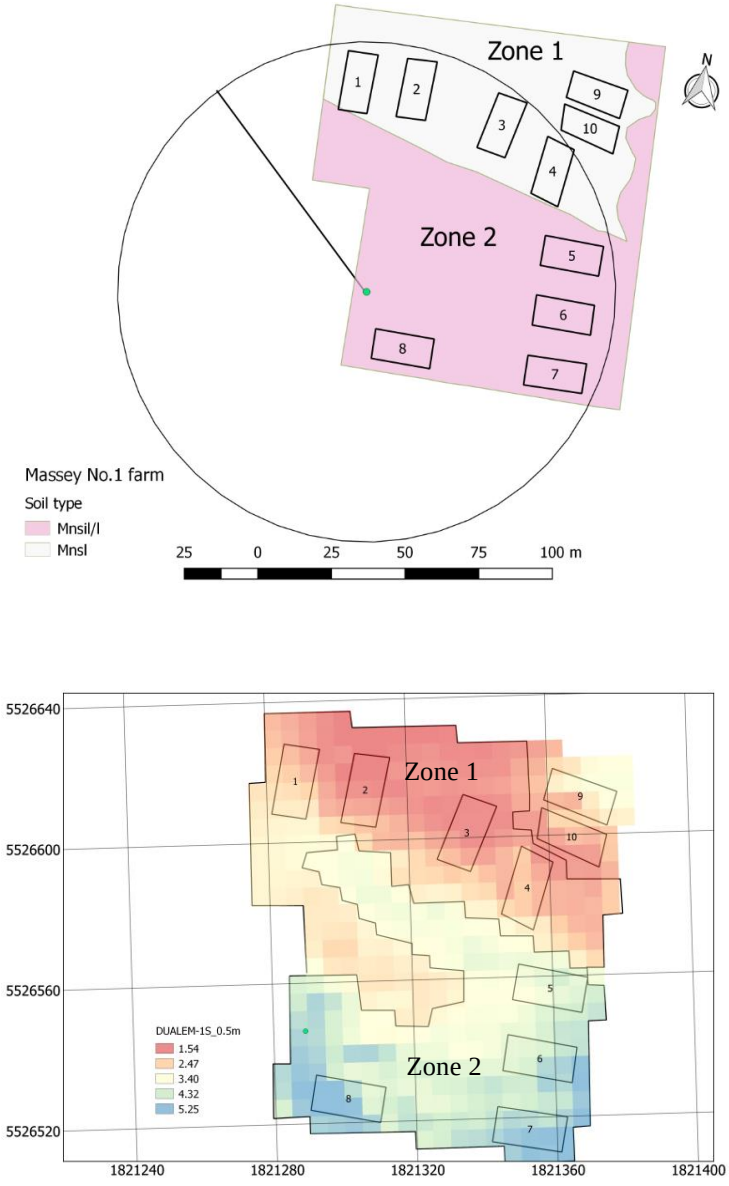

Figure 5.2: Experimental plots in each zone based on the soil types (Zone 1: Manawatū fine sandy loam (0.7 ha), Zone 2: Manawatū silt loam (0.6 ha)) (Pollok et al., 2003) and map of soil apparent electrical conductivity (EC_a, mS m^{-1}) at 0.50 m using a Dualem-1S. *SWB* treatments were in plots 1, 3, 6, and 8, and (ii) Sensor treatments were in plots 2, 4, 5 and 7. The non-irrigated treatment was at non-irrigated corner (plots 9 and 10).

5. 32 Comparison of soil data for the two soil zones

The significance of differences in these properties between the two soil zones was evaluated by both parametric and non-parametric statistical methods. The *KS* test only demonstrated non-normality in the *AWC* of samples at 0.8–1 m. There was no significant

difference in mean *AWC* in the top 0.2 m. At deeper depths (0.2–0.4, 0.4– 0.6, 0.6–0.8, and 0.8–1 m), the mean values of *AWC* were larger in Zone 2 than in Zone 1, with p values < 0.05 (Fig. 5.3). Zone 1 was a coarser textured sandy soil and had a relatively low *AWC* compared with Zone 2. Table 5.2 illustrates the textural distribution and classification of the 18 samples along with the EC_a classes for the 0–0.4 m soil layer. For Zone 1, the sand percentage was always greater than 45%, the clay percentages were always lower than 14%, and the silt percentages ranged between 7 and 38%. For Zone 2, the sand percentage was always less than 42%; the clay percentages were lower than 23%, and the silt percentages ranged between 41 and 65%. These analyses gave weight to the claim that the soil differences between the two soil zones were practically and statistically significant.

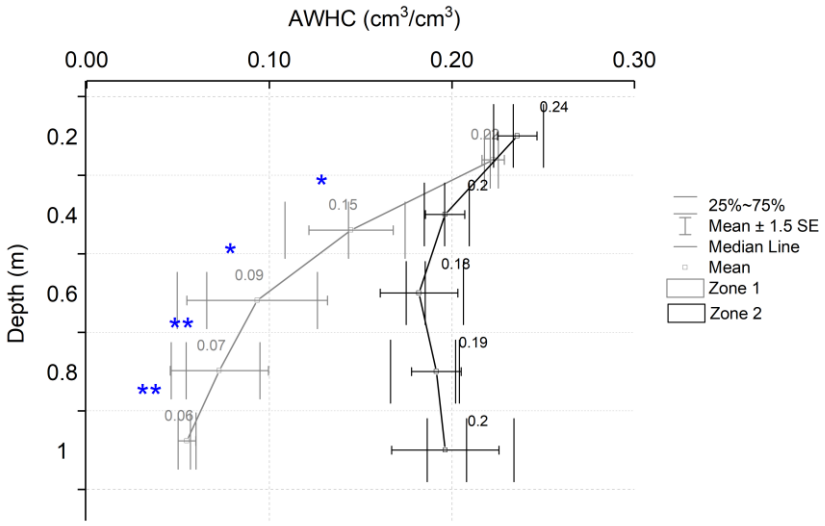

Figure 5.3: Comparing available water content (*AWC*, $cm^3\ cm^{-3}$), measurements between the two soil zones. * The mean difference is significant at the 0.05 level. ** The mean difference is significant at the 0.01 level.

Table 5.2: Soil apparent electrical conductivity (EC_a, mS m^{-1}) classes with particle size distribution (clay (%), silt (%), sand (%) and textural name of the average of 18 samples from the 0–0.5 m soil layer of the two zones.

EC_a class	%clay	%silt	%sand	USDA Texture	NZ Texture
			Zone 1		
Dualem-1S: 1.54–3.40 mS m^{-1}	11.65	23.7	64.65	Sandy clay loam	Sandy loam
			Zone 2		
Dualem-1S: 4.32–5.25 mS m^{-1}	17.85	48.15	34	Silt loam	Loamy silt

5. 33 Irrigation scheduling for the two scheduling treatments in each zone

The details of the *AD* and *IR* values for the two scheduling criteria are given in Table 5.3.

Table 5.3: Scheduling criteria for pea and bean crops, 2017/2018. θ_{FC}: moisture content at Field Capacity; θ_{WP}: moisture content at Wilting Point; *TAW*: total available water; AD: the allowable deficit; Int: initial, M: Mid, L: late.

		Zone 1			**Zone 2**		
		mm/ 0.2m	mm/ 0.3m	mm/ 0.4m	mm/ 0.2m	mm/ 0.3m	mm/0.4 m
Soil characteristics	θ_{FC}	73	97	120	80	113	145
	θ_{WP}	29	37	46	33	46	59
	TAW	44	60	74	47	67	86
Scheduling criteria							
Crop stage		Int	M	L	Int	M	L
AD (mm)		20	27	33	21	30	39
Irrigation (mm)		15	20	25	15	23	29

Sensors were calibrated weekly from neutron probe readings. Fig. 5.4 shows an example of the calibration curves for the sensors over the rooting depth of the crop (0 to 0.4m) against neutron measured volumetric data on 24 January 2018 and 3 April 2018 for pea and bean crops, respectively. Separate calibrations were needed for each soil type. The relationship between the two regression lines for Zone 1 and 2 was significantly different ($p = 0.0312$). The results showed good agreement for *SWD* in the top 0.40 m. An R^2 value of 0.87 and 0.89 with Root Mean Square Errors (*RMSE*) of 1.8 and 1.95 (mm/400mm) were obtained for Zone 1 and Zone 2, respectively. The relationship for *MC* of the top 0.20 m varied with the subsoil below 0.20 – 0.40 m for Zone 1 compared with Zone 2 (Fig. 5.4 and Table 5.4), which was likely due to the variable soil texture and *TAW* below 0.20 m at Zone 1 compared with Zone 2 as observed by El-Naggar et al. (2017). We suggest that the higher scatter in the 0.30 m depth in Zone 1 ($R^2 = 0.74$, *RMSE* = 1.24 (mm/10 mm)) was due to heterogeneity of the soil or poor installation of sensors.

The average Mean Square Errors (*MSE*) for *MC* measurements for the 0 – 0.40 m depth during the crop season in each soil zone is given in Fig. 5.5. The associated standard error of the mean was less for the neutron-probe for both soil zones, due to its ability to integrate over a larger volume of soil and its higher tolerance of the heterogeneity of the soil (not shown). The *MSE* was higher in Zone 2, especially in the control plots for the bean. The error was, in general, less in the Zone 1 plots during the pea trial for both sensors, probably because greater water demand (summer season) helped homogenize soil moisture in the root zones. The soils under this condition retained water over a longer period after each irrigation event, leading to more stable moisture profiles by decreasing the rates of soil moisture loss. Similar findings by Heng et al. (2002) reported that the errors of a capacitance probe and neutron-probe were less under a higher fertility irrigation treatment, because of higher root water extraction giving more homogenized soil moisture. However, the corresponding error at each depth showed rather low *MSE* values especially at 0.10 – 0.20 m depths for both soil zones (not shown). Based on this, to obtain the same level of precision in Zone 2 as observed in Zone 1 more sensors are needed.

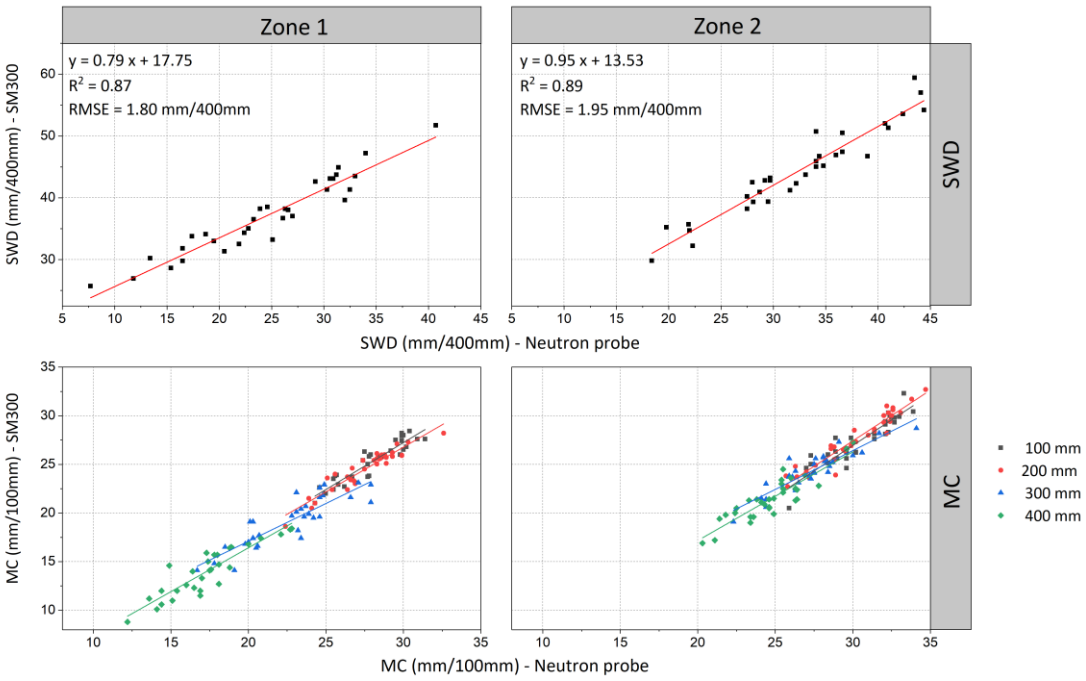

Figure 5.4: The relationship of calibrated total soil water deficit (*SWD*, mm/400mm) and soil moisture content (*MC*, mm/100mm) at 4 depths (100, 200, 300, and 400 mm) measured by frequency domain reflectometry probes (SM300- DeltaT, Burwell, UK) and neutron probes in each soil zone on 24 January 2018 and 3 April 2018 for pea and bean crops, respectively.

Table 5.4: Statistical results (R^2 = coefficient of determination, *MAD* = mean difference, *RMSE* = root mean square error, *MAPE* = mean absolute percentage error, and bias = mean error) for calibrated *MC* at 4 depths (0.10, 0.20, 0.30 and 0.40 m) in each soil zone.

	Zone 1				Zone 2			
Depth (m)	0.10	0.20	0.30	0.40	0.10	0.20	0.30	0.40
R^2	0.86	0.89	0.76	0.82	0.84	0.92	0.81	0.80
MAD	0.69	0.57	0.99	0.93	0.78	0.60	0.76	0.86
RMSE	0.78	0.68	1.24	1.12	0.98	0.77	0.89	1
MAPE	2.74	2.38	5.23	7.03	2.94	2.21	3.16	4.02
Bias	0.12	0	–0.08	–0.31	–0.02	0.09	–0.05	0.03

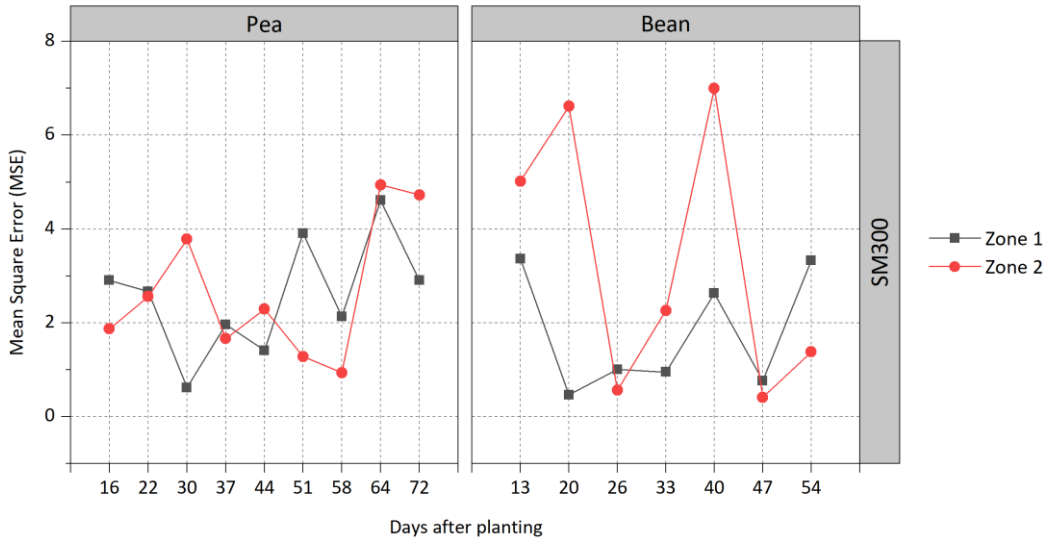

Figure 5.5: The mean square error (*MSE*) performance of calibrated soil water deficit (*SWD*, mm) by soil moisture content sensors (SM300) for the two soil zones for 0–400 mm soil depth.

Irrigation events for each zone under the two scheduling methods for the pea and bean crops are shown in Fig. 5.6 and 5.7.

During the pea trial, the *SWB* method scheduled 6 and 5 irrigation events to Zone 1 and Zone 2, respectively, with a total amount of 110 and 97 mm for Zone 1 and Zone 2, respectively. The sensor method scheduled 5 and 3 for irrigation events to Zone 1 and Zone 2, respectively, with a total amount of 85 and 53 mm for Zone 1 and Zone 2, respectively. Most irrigation occurred in the first part of the season when rainfall was insufficient to meet the crop water demand. Compared with the water balance method, the sensor-based technique reduced withdrawal by 23% of the irrigation water in Zone 1

and 45% in Zone 2. We attributed these observed variations between the two methods to varying features of the soil profiles. Zone 2, with restricted drainage, stayed wetter than predicted by the *SWB* model (Fig. 5.6 and 5.8), which is likely due to the fact that the *SWB* model did not take into account the impact of the layering and 'capillary break' due to the coarse gravels below the subsoil, as described by Clothier et al. (1977a) for this soil type. This leads to an increase in *MC* in the finer layer above the coarse gravel surface that the sensors were able to measure but the *SWB* was unable to account for.

During the bean trial, the rainfall was greater, so less irrigation was required. The *SWB* method scheduled only 2 and 1 irrigation events for Zone 1 and Zone 2, respectively, with a total amount of 35 and 20 mm for Zone 1 and Zone 2, respectively. The sensor method scheduled the same number of irrigation events and the same application depths as the *SWB* method.

Following the bean trial, the sensors identified that the *MC* was above field capacity due to a heavy rainfall event of 75 mm that fell over 3 days. However, if daily rainfall wets the soil above field capacity then the *SWB* model assumes that the total amount of water surplus to field capacity is lost the same day by deep percolation, allowing the soil to return to field capacity (Fant et al., 2012). In reality, the soils at this site did not drain this rapidly. This could also be related to the limitations of laboratory estimates of soil-water limits (i.e. *FC* and *AWC*) used in *SWB*. Ratliff et al. (1983) suggested that laboratory-estimated *MC* limits should be used with caution in *SWB* calculations, and field-measured limits are preferred. Gebregiorgis and Savage (2006); Lukangu et al. (1999) concluded that for approximate estimation of *MC* limits, the laboratory method using undisturbed soil cores yields satisfactory results, but for more critical work, the use of the direct measurement is essential using *MC* or soil-water potential sensors. Ekanayake and Hedley (2018); Salter and Haworth (1961) also found that the sensors and/or field method for estimating *MC* are practical and give more accurate measurements for timing and amount of irrigation.

In general, these results indicate that the timing of the irrigation events varied under the two methods and that the *SWB* method resulted in more water being applied to the pea crop.

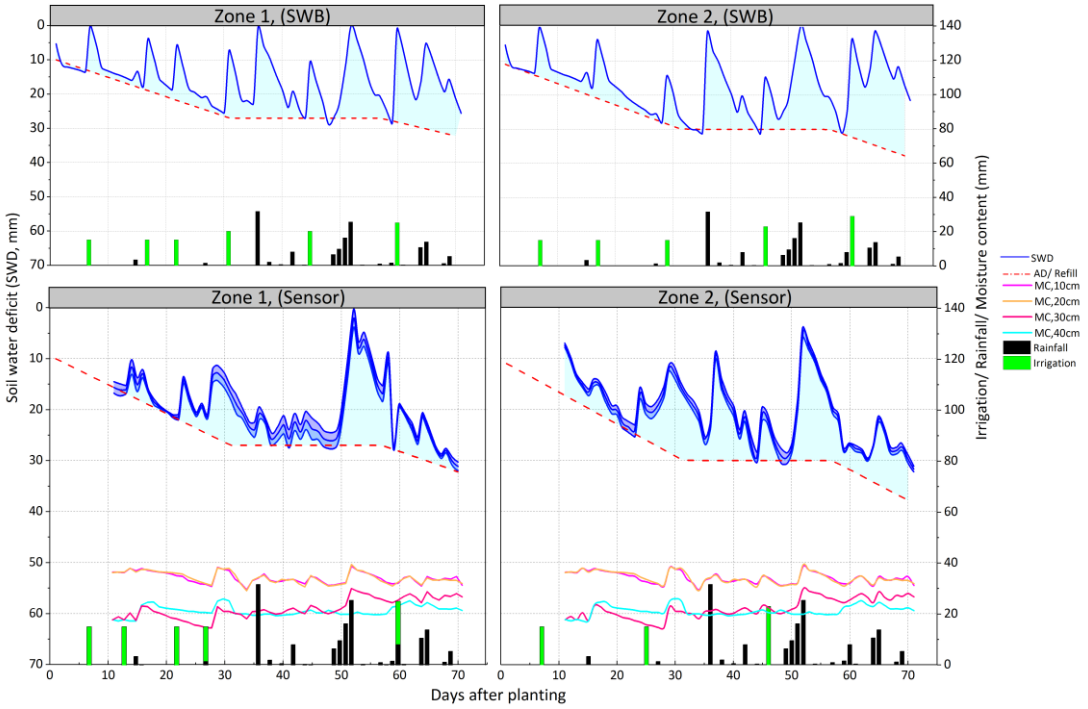

Figure 5.6: Soil water deficit (*SWD*, mm) for the *SWB*-based and Sensor-based scheduling treatments, respectively in each management zone for the pea crop trial. The three blue lines in the Sensor scheduling graphs represent the standard errors of the reported soil moisture content (*MC*) measured by the sensors.

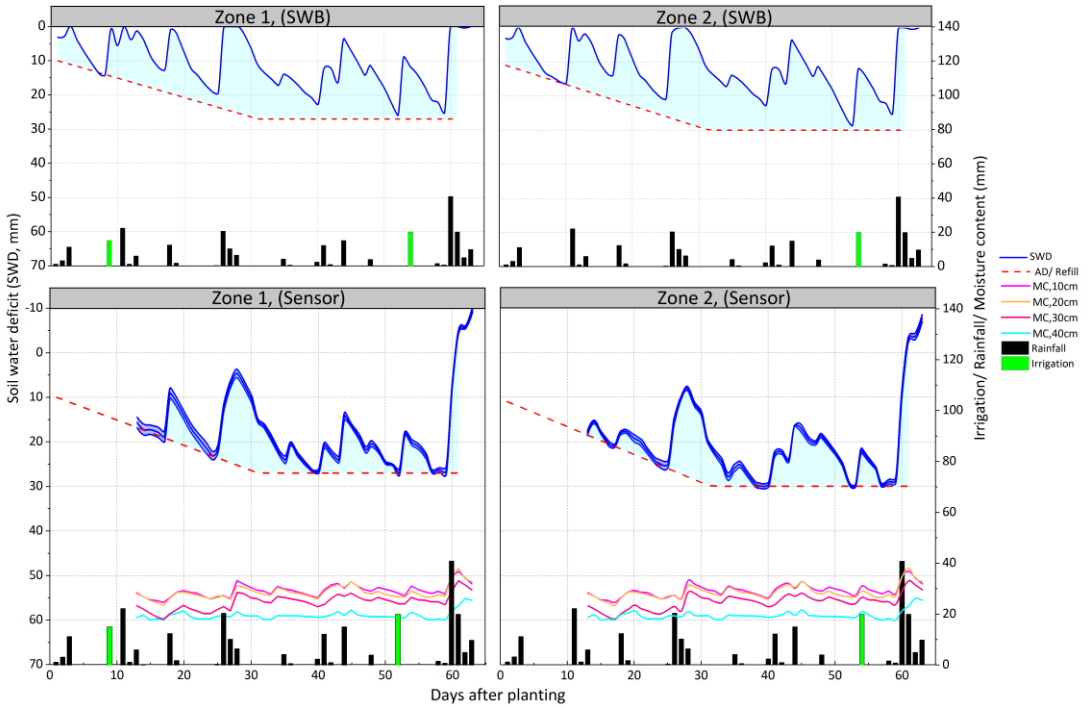

Figure 5.7: Soil water deficit (*SWD*, mm) for *SWB* and Sensor scheduling treatments, respectively in each management zone for bean crop trial. The three blue lines in Sensor scheduling graphs represent the standard errors of the reported soil moisture content (*MC*) measured by the sensors.

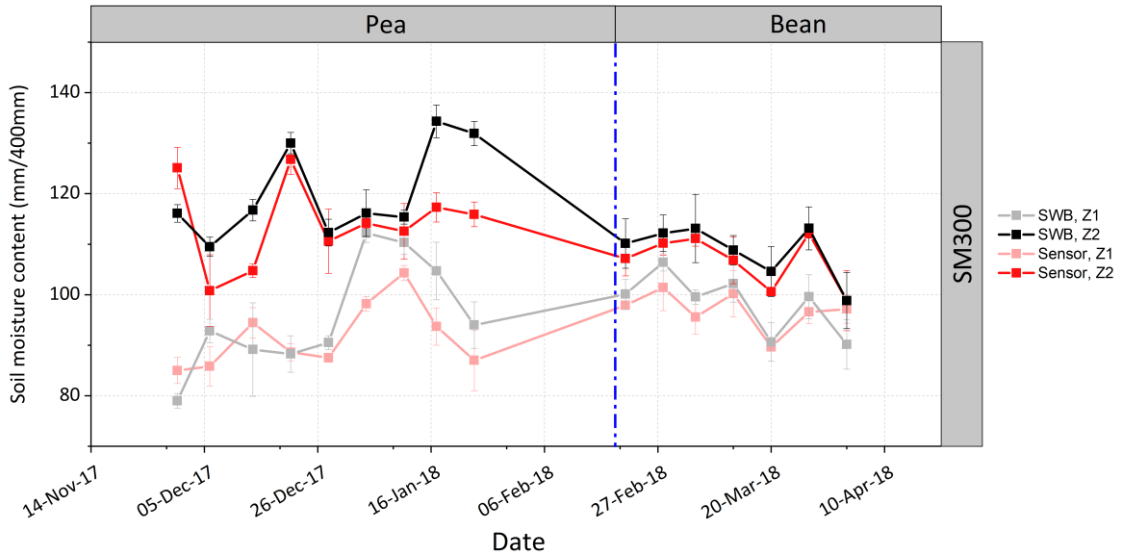

Figure 5.8: Comparing average total soil moisture content (*MC*) in the top 0.40 m obtained using soil moisture neutron-probe for the Sensor and *SWB* schedule treatments in each soil zone. The error bars represent the standard errors of the reported soil moisture content (*MC*) measured by the SM300 sensors.

5. 34 Crop assessment for the two scheduling treatments in each zone

For the pea crop, there was no significant difference in mean crop height, number of pods (see Fig. 5.9), length, number of nodes, and number of flowers (results not included) between the two scheduling treatments. During the pea crop trial, the non-irrigated crop's height and number of pods were significantly less than those observed for the two scheduling treatments. Unsurprisingly, the greater rainfall experienced during the growing of the bean crop resulted in no significant differences in crop height and number of pods between the two scheduling treatments and the non-irrigated treatment.

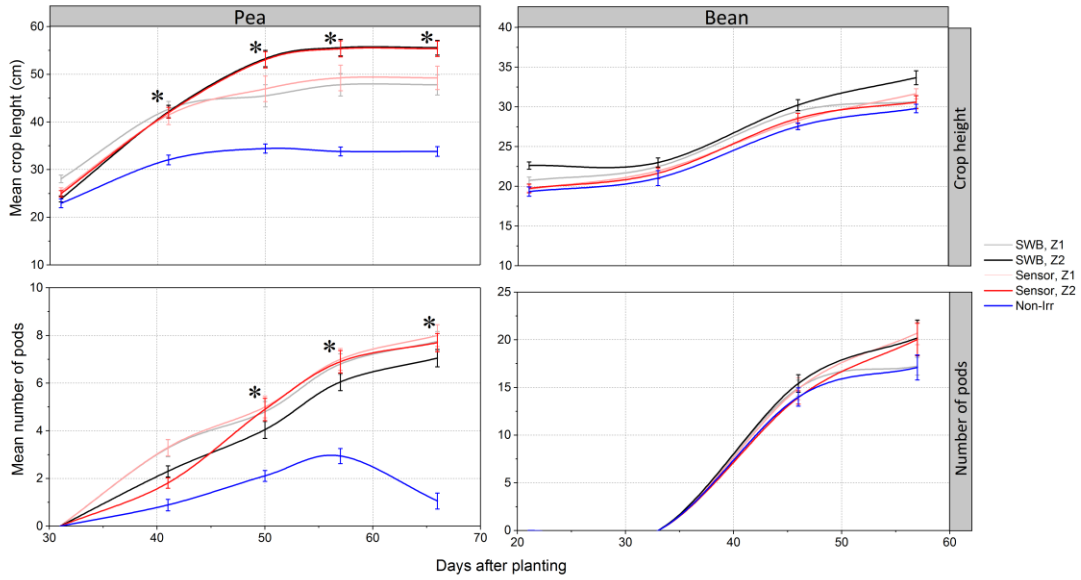

Figure 5.9: Comparing length, and number of pods on five and four measurement dates between the two scheduling treatments (*SWB* and Sensor) in each soil zone for peas and beans, respectively. * The mean difference is significant at the 0.05 level.

The yield and biomass results indicated there were no significant differences (P >0.05) among the scheduling treatments for pea and bean crops (Table 5.5). The mean yields were 2.43 T/ha for the *SWB* treatments (standard deviation 0.01 T ha^{-1}), and 2.33 T ha^{-1} (standard deviation 0.02 T ha^{-1}) for the sensor treatments.

Yield differences in peas were observed between the two irrigation scheduling treatments and the non-irrigated treatment: the yield of the non-irrigated treatment decreased by approximately 80% for the pea crop (Table 5.5).

Table 5.5: Average dry-mass yield, biomass, and irrigation applied for each scheduling method in each zone. * The mean difference is significant at the 0.05 level

Treatment	Irrigation (mm)	Avg. Yield (T ha^{-1})	Avg. Biomass (T ha^{-1})	Irrigation (mm)	Avg. Yield (T ha^{-1})	Avg. Biomass (T ha^{-1})
	Pea			Bean		
SWB, Zone 1	110	2.44	6.35	35	1.10	2.63
Sensor, Zone 1	85	2.31	6.25	35	1.10	2.45
SWB, Zone 2	97	2.41	6.05	20	1.15	2.44
Sensor, Zone 2	53	2.34	6.05	20	1.13	2.34
Non-Irrigated	0	0.46*	1.2*	0	0.87	2.27

5. 35 Irrigation water use efficiency for the two scheduling treatments in each zone

In the pea trial, *IWUE* increased by 0.5 kg m^{-3} for Zone 1 and 1.5 kg m^{-3} for Zone 2 for the Sensor-based treatment compared with the model-based scheduling (Fig. 5.10). In the bean trial, *IWUE* was not significantly different between both scheduling treatments. There were no differences in crop *WP* between Sensor-based and *SWB*-based treatments for either crop.

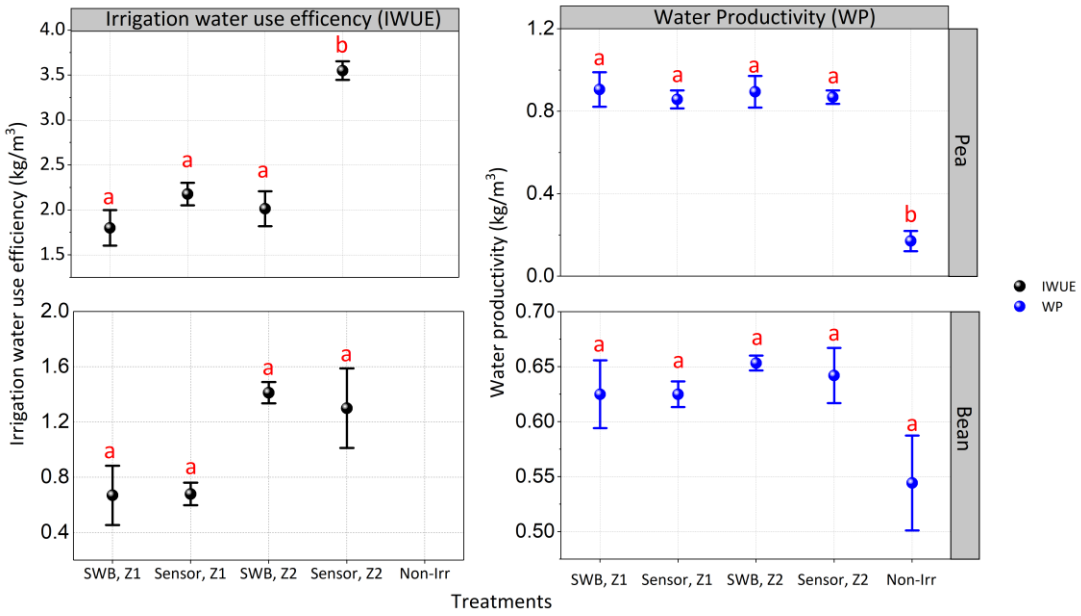

Figure 5.10: Comparing irrigation water use efficiency (*IWUE*, kg m^{-3}) and water productivity (*WP*, kg m^{-3}) for the two scheduling treatments in each zone, and a non-irrigated treatment. The different lowercases indicate the mean difference is significant at the 0.05 level.

5. 36 Soil nitrate content for the two soil zones

All plots received the same adequate amount of *N* fertilizer at the beginning of the season to ensure any yield differences could be related to different irrigation schedules and not to fertility differences.

We also measured the soil *N* content at pre-planting and harvest to check for any impacts of residual N differences. There was no significant difference in the quantities of *NO3-N*

and *NH4-N* in the upper 0.45 m of soil between the treatments at harvest for both crop trials (Table 5.6).

Table 5.6: *ANOVA* and Tukey's HSD test's result (mean ± standard error) for nitrate content (*NO3-N* (mg kg^{-1})) and ammonium content (*NH4-N* (mg kg^{-1})) in the upper 0.45 m of soil at harvest. The same lowercases represent no significant differences of two zones.

Pea 2017/2018					
		SWB, Z1	Sensor, Z1	SWB, Z2	Sensor, Z2
Pre-planting	*NO3N*	26.89 ± 1.97[a]	23.209 ± 5.59[a]	37.31 ± 9.15[a]	30.43 ± 5.98[a]
	NH4N	2.35 ± 0.53[a]	5.79 ± 1.70[a]	7.70 ± 4.37[a]	4.09 ± 0.84[a]
At harvest	*NO3N*	3.74 ± 0.90[a]	3.43 ± 0.50[a]	5.14 ± 0.54[a]	2.91 ± 0.35[a]
	NH4N	5.21 ± 1.52[a]	3.64 ± 1.19[a]	6.44 ± 0.50[a]	6.58 ± 0.65[a]
Beans 2017/2018					
Pre-planting	*NO3N*	31.22 ± 7.38[a]	38.46 ± 4.97[a]	35.28 ± 6.77[a]	36.77 ± 2.20[a]
	NH4N	6.38 ± 4.44[a]	12.55 ± 5.59[a]	2.99 ± 0.57[a]	3.33 ± 0.90[a]
At harvest	*NO3N*	7.74 ± 1.19[a]	12.96 ± 2.26[a]	13.30 ± 2.87[a]	14.66 ± 3.39[a]
	NH4N	1.04 ± 0.10[a]	0.69 ± 0.11[a]	0.83 ± 0.19[a]	0.81 ± 0.12[a]

5. 37 Evaluation of *NDVI* readings to refine FAO56 crop coefficient values.

The results of the regression analysis between FAO56 estimated K_{cb} values and *NDVI* values are provided in Table 5.7. These equations were used to predict more accurate pea and bean K_{cb} and ET_c estimates. The analysis shows that for *NDVI*, the estimated K_{cb} and predicted K_{cb} had the same trend through the growing season (Table 5.7 and Fig. 5.11). The ET_c was calculated by multiplying the K_c values by the value of the ET_o (see Equation 5.2). The estimation of K_{cb} and ET_c using *NDVI* sensing data was essentially significant. The results show high R^2 and adjusted R^2 for the predicted values of K_{cb} for pea and bean 0.87 and 0.92, respectively.

The *NDVI* minimum value was measured at the beginning of the growing season over the dry bare soil and was about 0.16 and 0.14 for the pea and bean crops, respectively. *NDVI* maximum values were 0.80 and 0.72 for the pea and bean crops, respectively. The *NDVI*

increased from crop emergence until maximum values were attained about 50 days after planting and then they began to decrease slightly through to the end of the season (Figure 11). The *NDVI* curves flatten out at mid-season where the *NDVI* saturates with high values of leaf area index when the soil was almost totally covered by the canopy (Duchemin et al., 2006).

The *NDVI* values were slightly higher for the pea irrigation treatments than the bean irrigation treatments, especially during the mid-season, and this is likely due to the dense canopy of the pea crop compared with the bean crop. At times, the heterogeneity of *NDVI* data in crops with low values was visible at high spatial scale resolution imagery, particularly for the non-irrigated treatment (not shown).

K_{cb}–*NDVI* values were interpolated at a daily time step in order to compare them with the continuous series of K_{cb}–FAO56 values for the entire growing season. The result of the comparison is displayed in Fig. 5.11. The K_{cb}–FAO56 average values obtained at three stages (initial, mid-season, and late-season) were 0.15, 1.17, and 1.05, respectively. These values are only slightly different from those given by K_{cb}–*NDVI* ($K_{cb,ini}$ = 0.14, $K_{cb,mid}$ = 1.10, $K_{cb,end}$ = 1.03), which reflect the local conditions.

Overall, the estimated ET_c by *NDVI* did not significantly improve the FAO56 approach. The FAO56 model has mainly been designed to plan irrigation schedules in arid to semi-arid regions. Thus, the model requires a limited set of soil inputs, does not account for any vertical differences in soil moisture, and assumes that the soil moisture cannot exceed field capacity. In order to improve the utility of the model in the widest range of soil types, the model should include a multi-layer soil feature that accounts for slower drainage rates and the associated water storage, especially in temperate regions, when rainfall often occurs during the irrigation season. In some cases, the model should consist of detailed soil, crop, weather and management modules (e.g. APSIM (Keating et al., 2003) and DSSAT (Jones et al., 2003)) that require very accurate and numerous inputs, all of which tend to vary dramatically from one field to another.

Table 5.7: The correlation between calculated (K_{cb}) by FAO56 and crop vegetation index (*NDVI*) for pea and bean.

Crop	Prediction equation	R^2	Adj.R^2	*RMSE*	Signif. prob.
Pea	$K_{cb} = 1.42 \times NDVI + 0.03$	0.87	0.86	0.19	0.0006
Bean	$K_{cb} = 1.66 \times NDVI - 0.005$	0.92	0.91	0.13	0.0002

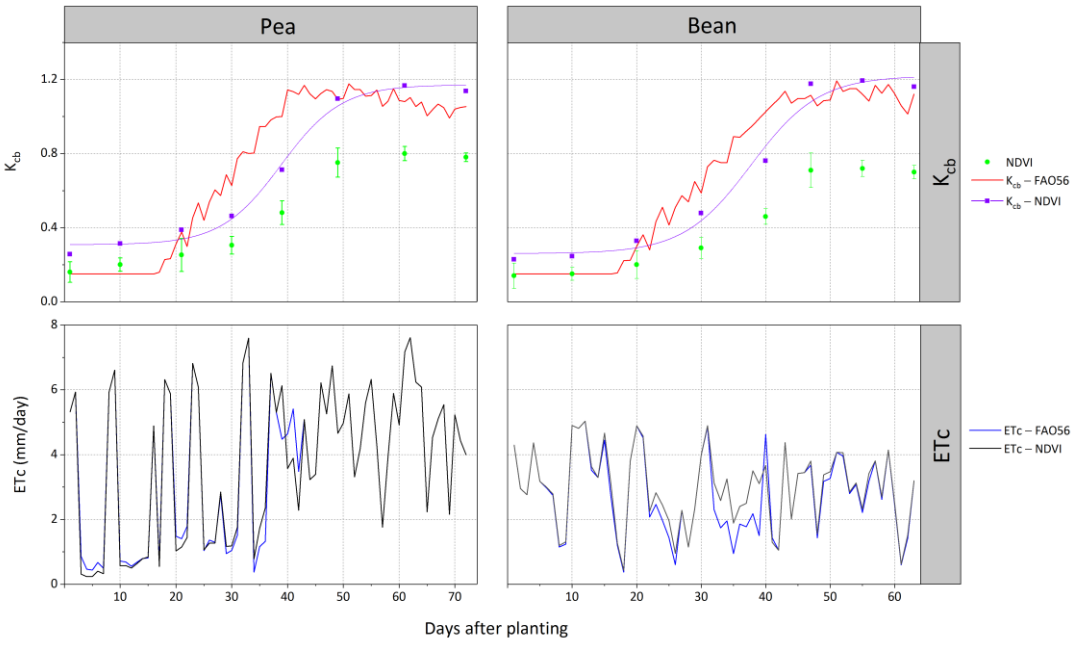

Figure 5.11: Average crop vegetation index (*NDVI*) values measured at the study site. The K_{cb}–*NDVI* and ET_c–*NDVI* values have been obtained from the linear relationships versus K_{cb}–FAO56 and ET_c–FAO56 values for pea and bean.

5. 4 Conclusions

Dynamic irrigation scheduling is required to help farmers meet the site-specific water requirements of plants and reduce the negative environmental impacts of irrigation. *SWB*-based and sensor-based techniques were used to schedule irrigations to pea and bean crops in two delineated irrigation management zones of contrasting soil texture, under a *VRI* system. In addition, a potential improvement of the FAO56 scheduling approach was evaluated by using K_{cb} derived from sensor readings of *NDVI*.

Daily *SWD* was monitored using two contrasting techniques – *SWB*-based modelling and

sensors – and irrigation was triggered when a prescribed *AD* was reached. The *SWB*-based model relied on soil *TAW* and weather data. The sensor-based method, which used a wireless soil moisture sensor network, provided measurements of the actual soil water conditions in the field. The two scheduling methods showed a variation in timing and the quantity of irrigation applied to the pea crop: the *SWB*-based method resulted in more water being applied. The sensor-based technique saved about 23–45% of the irrigation water and produced the same pea yields as the *SWB*-based model.

This difference can be attributed to some of the inherent limitations of a simple *SWB*. In the period following a rain event that wet the soils above field capacity, the *SWB* models predicted a faster drying rate than was actually measured with the soil moisture sensors. This is because the *SWB* model does not account for the restricted drainage that occurs in the Manawatū silt loam soil profile (Zone 2). This restricted drainage is due to the compact nature of the silt loam subsoil as well as the impact of the textural break that occurs between the base of the subsoil and the underlying coarser gravels. The estimated ET_c by K_{cb}–*NDVI* did not significantly improve the FAO56 approach. Crop growth was not significantly different between the two scheduling treatments. Therefore, the *IWUE* for the pea crop was significantly more efficient for the sensor-based technique compared with the *SWB* technique for scheduling irrigation.

Future research could be undertaken to extend the comparison of these two scheduling systems to different crops and for different climatic conditions. In addition, future research is required to investigate the value of including *WSN* monitoring systems into precision irrigation software control systems to increase options for automated adaptive irrigation scheduling.

Connecting text to Chapter 6

The previous chapter includes the development of a method that used crop vegetation index (e.g. *NDVI*) data, collected by a crop sensor, to track crop stage in the field. This information as well as crop height, leaf cover, and biomass are relevant for the assessment of crop stands (e.g. crop yield, the site-specific amount of water, crop water use (Chapter 5) and the development of agricultural water management models (Chapter 7, 8 and 9). In this chapter, a Terrestrial Laser Scanning system method was devised to establish multi crop surface height maps for barley, pea and bean. This chapter was presented in Irrigation New Zealand conference in Alexandra, New Zealand (2018). Conference presentation.

Chapter 6

The use of Terrestrial LiDAR to monitor crop growth

Abstract

Monitoring the spatio-temporal distribution of crop height and biomass is important for crop management in terms of applying irrigation, fertilizer and pesticides. This paper reports the performance of a Terrestrial Laser Scanning (*TLS*) based system for measuring crop height and biomass for barley (*Hordeum vulgare*., cv. 'Carfields CKS1'), pea (*Pisum sativum*., cv. 'Massey') and bean (*Phaseolus vulgaris*., cv. 'Contender') grown under field conditions.

Four *TLS*-surveys were carried in the growing period 2017/2018 to monitor the plant height. The results were analysed using classical statistics and geostatistics by constructing (two-dimensional) maps of canopy surface height with a high resolution of 0.01 m. Spatio-temporal differences of the measurements were obtained within and between subsequent surveys. The results were validated against manually measured plant heights and biomass.

High coefficients of determination (R^2) of the linear regression were achieved between manually measured and *TLS*-derived canopy height (R^2 = o.95, 0.93 and 0.91 for barley, pea and bean, respectively). The method also showed potential to estimate bean biomass (R^2 = 0.70). Overall, the results showed the *TLS* approach has the potential to measure crop height surface with a high spatio-temporal resolution for different crops under variable-rate scheduling of irrigation. This approach can be considered a very promising tool for site-specific management.

Keywords: Precision agriculture; Remote sensing; *LiDAR*; *TLS*; Data acquisition; Spatio-temporal; Crop height; Biomass.

6.1 Introduction

Information about the distribution of crop height and biomass on fine spatial and temporal scales is highly valuable for improving agricultural productivity and efficiency. This in turn can provide a means of improving food supply and of tackling crop production challenges related to climatic change (Lati et al., 2013). Furthermore, if these two parameters are known in real time then expected crop yields can be predicted, and the site-specific crop management of fertilisers, pesticides, and irrigation can be optimised (Ehlert & Dammer, 2006). The literature suggests that peas and barley are sensitive to small amounts of either excessive or limited water availability, and that water stress has the greatest effect on the biomass and grain yield which, in turn, is caused by a decrease in grain number and size (Belford et al., 1980; Greenwood & McNamara, 1987; Jamieson et al., 1995). Hence, precise field data acquisition and real-time monitoring methods are required.

In precision agriculture fields, remote and proximal sensing methods can be used for accurate crop monitoring to improve the relation between in- and outputs (Mulla, 2013). Researchers have reported several techniques for monitoring crop height and biomass. Crop height is measured by rulers, light barriers (Fender et al., 2005), ultrasonic rangefinders (Scotford & Miller, 2003) and radar (Holmes et al., 2004). Crop biomass is measured manually by destructive harvest (Lokhorst & Kasper, 1998), and methods for non-destructive direct biomass determination are not available. Biomass can also be estimated indirectly using other parameters (Tilly et al., 2013). For these methods, canopy or plant height is recorded, and an empirical relationship between height and dry matter is developed (Pittman et al., 2015). Devices such as the rising plate meter (Dougherty et al., 2013; Sanderson et al., 2001), capacitance meter (Sanderson et al., 2001), and meter stick are examples of devices used for physical measurements of biomass estimation. These methods, which requires physical measurements are labour and time intensive. In addition, variations due to growth characteristics and spatial variability can be difficult to accurately represent by physical sample collection which limits the ability to develop a robust estimation model (Pittman et al., 2015).

Besides hyperspectral and optical sensors, the use of the technology of light detection and ranging (*LiDAR*) offers a good opportunity to make non-invasive and non-destructive measurements of canopies to characterize plant growth and to analyze diverse architectural parameters (Friedli et al., 2016; Zhang & Grift, 2012). *LiDAR* measures the distance between the sensor and a target, based on the elapsed time between the emission and return of laser pulses (the time-of-flight method) or based on trigonometry (the optical-probe or light-section methods) so that 3-dimensional (*D*) information of the target can be obtained (Hosoi & Omasa, 2009). *LiDAR* systems can be used in different ways such as by satellites and airborne *LiDAR* systems (*ALS*) for detecting medium-range areas from aircrafts (500-1,000 m) and helicopters (200-300 m) (Woods et al., 2011), or by terrestrial or ground-based *LiDAR* sensors (*TLS*) which are suitable for surveying purposes such as architectural applications, mobile road-mapping systems, the determination of forest inventory parameters and agricultural purposes (Ehlert et al., 2010d). The *TLS* measurements produces point clouds that depict the surface of the visible canopy oriented towards the observing device (Friedli et al., 2016). These point clouds can be further analyzed, as has been done already in the fields of forest ecology and precision agriculture (Friedli et al., 2016).

Li et al. (2015) used *ALS* to measure the crop height of maize fields and found good correlations between the *ALS* data and manual field measurements. In recent studies, unmanned aerial vehicles (*UAV*s) with *LiDAR* laser scanners were used to estimate the height of maize (Anthony et al., 2014). Bendig et al. (2013) successfully used *UAV*-based imaging to generate a crop surface model (*CSM*) for rice. Friedli et al. (2016) used *TLS* to monitor crop growth of maize, soybean, and wheat under field conditions. Crommelinck and Höfle (2016) investigated the requirements in terms of *TLS* sensor resolution for deriving crop height models, aimed at low-cost devices for permanent crop monitoring. For estimating the biomass of small grain cereals like barley, oats, and wheat, Lumme et al. (2008) stated that *TLS* is a promising method. In another study, *TLS* was used to estimate crop density (Hosoi & Omasa, 2009; Saeys et al., 2009), or leaf area index (Gebbers et al., 2011).

To our knowledge, little work has been undertaken to examine the spatial and temporal resolution of *TLS* to map crop growth during one growing season under field conditions.

Therefore, the objectives of this research were to (i) measure precisely the plant height of barley, pea and bean treatments with a *TLS* scanner so as to establish multi-temporal crop surface height maps and compare these heights with manual measurements; and (ii) evaluate the relationship between dry biomass for bean measured via destructive removal and a *TLS*- measured canopy height.

6.2 Materials and Methods

6.21 Study site

The surveys were conducted at two field sites (Fig. 3.1, Chapter 3).

The first experimental field (1.2 ha) is on Massey University's No.1 Farm (latitude 40.22° S, longitude 175.36° E, altitude 37 m) which is located near Palmerston North, Manawatū, New Zealand. Measurements were made at this site during the 2017/2018 growing season. The soil survey map for this field (El-Naggar et al., 2017; Pollok et al., 2003) indicates the presence of two different soil types: a Manawatū fine sandy loam (free draining soil, Zone 1) and a Manawatū silt loam (imperfectly drained soil, Zone 2). Field peas (*Pisum sativum*., cv. 'Massey', 260 kg ha^{-1}) and French beans (*Phaseolus vulgaris*., cv. 'Contender', 75 kg ha^{-1}) were sown on 15 November 2017 and 9 February 2018, respectively. The seed yield was harvested on 23 January 2018 and 12 April 2018 for pea and bean, respectively.

The second experimental field is in Otane, Hawke's Bay, New Zealand (-39. 533°S °N; 176.402°E, altitude 130 m). The existing soil database for this field indicates the presence of soil variability: a Twyford sandy loam (well-drained soil, Zone 1) and a Kaiapo silt loam (poorly drained soil, Zone 2). Barley (*Hordeum vulgare*., cv. 'Carfields CKS1') was sown on 2 August 2017 using 100 kg seed grain/ha and 50 cm row spacing. Grain yield was harvested on 16 January 2018.

At the Manawatū site, both of the soil zones had four replicate plots (20 m x 10 m), along with two non-irrigated plots on the Zone 1 soil type. A variable-rate irrigation (*VRI*)

system was used for irrigating the plots. At the Hawke's Bay site, four plots (20 m x 15 m) were established for each soil zone. During the complete growth period irrigation was applied to both soil zone plots as applications of 15 mm at a fixed interval per stage (7 days) with a total irrigation depth of 150 mm.

6.22 *TLS* scanner

A "Faro Focus 3D X 330" laser scanner (Faro Technologies Inc., Laker Mary, USA) (https://www.faro.com/) was used to assess crop height. The scanner allows the acquisition of point clouds (measurement resolution) up to 70-megapixel color. The scanning range of the device is up to 330 m and the accuracy at 10 m distance is 0.4 mm. The device uses a laser beam at 1550 nm and the "phase shift measurement technology" to detect distances. In this system, infrared laser light is sent out and reflected back to the system. The laser scanner emits a laser beam from a rotating mirror out towards the area being scanned. Then the unit distributes the laser beam at a vertical range of 300° and a horizontal range of 360°. The laser beam is then reflected back to the scanner by objects in its path. The distance to the objects in an area is calculated as well as their relative vertical and horizontal angles. The data is captured and transmitted via WLAN (*WiFi*) for the calculation of precise *3D* renderings (Faro Scene, 2013).

6.23 Data acquisition and field measurements

The crops were scanned on four occasions throughout the season. The scan dates for each crop are shown in Table 1. The *TLS* scanner was mounted on a tripod, at a height of about 1.5 m above ground. To capture all plots, the experiment sites were observed from nine scan positions for barley and seven positions for pea and bean. The crops were always scanned from the same positions. Three common tie points for each scan position were required to enable the merging of the point clouds in the processing of data. Six white spherical targets were distributed between every two scans to allow for the later merging of the single scans from the same point in time but from different positions of a field to a scan point cloud. These targets were fixed on poles (2 m in length for the barley; and 1.5

m in length for pea and bean) placed on the fences between the plots. The positions of the tie points and the spherical targets were georeferenced and remained constant during the season and defined a fixed coordinate system for all measurements.

Manually measured plant heights (25–30 plants) were used to validate the *TLS*-derived results. To investigate the relationship between *TLS* readings and bean biomass, destructive crop sampling was used (three replicate areas within each plot, 1 m in length and 1 m wide). The whole plant samples were taken to the laboratory and oven-dried to constant weight at 70 ^{o}C, which took about three days to obtain the dry matter content.

Table 6.1: Overview of the scanned crops, dates, and measurements per days after planting (*DAP*)

Barley		Pea		Bean	
Date	*DAP*	Date	*DAP*	Date	*DAP*
1-Sep-17	31	4-Dec-17	20	1-Mar-18	21
10-Oct-17	70	15-Dec-17	31	13-Mar-18	33
19-Nov-17	110	29-Dec-17	45	26-Mar-18	46
13-Dec-17	134	6-Jan-18	53	6-Apr-18	57

6.24 Data post-processing

Data post-processing was carried out in the "FARO SCENE" (Faro Technologies Inc., Laker Mary, USA) software which included the registration of the scan positions and merging of the point clouds (User Manual for Scene, 2019). Next, the CloudCompare software (CloudCompare, 2016) was used for filtering and extracting the area of each plot. For the spatial and statistical analyses, the filtered point clouds of the plots were exported as xyz-files (asci format) and later processed with CloudCompare. The point clouds were interpolated with the Nearest Neighbourhood (*NN*) algorithm to receive a raster for each plot with a consistent spatial resolution of 0.01 m. To calculate the plant heights, the point clouds from a reference surface (bare soil) were used to interpolate a Digital Elevation Model (*DEM*). After that, a *CSM* was generated for each plot. Then, the *DEM* was subtracted from each particular *CSM*. By subtracting the sequential *CSM*s, a *CSM* for each plot was generated with a high spatial resolution representing plant height at a specific time in the growing period.

6.25 Data analysis

For the statistical analyses, the plant heights of both measurement methods were averaged for each plot. To compare the impact of the treatments in each crop trial, the Bonferroni (*Dunn*) test, median values, and the probability-values were calculated for both measurement methods.

Regression analyses for *TLS* readings with crop height and biomass were performed to evaluate relationships between measured and estimated values using the open-source software package R 3.5.1 (R Core Team, 2018). The accuracy of estimation models was evaluated on a percent basis by calculating the root mean square error (*RMSE*)

6.3 Results and Discussion

6.31 *TLS* measurements

The *TLS*- derived temporal development of spatial patterns of crop height can be visualised as *2D* maps. For all plots, the variability in plant height within the plot is visible. Figs. 6.1, 6.2 and 6.3 show the maps of eight plots of barley and ten plots for pea and bean. The raster data for each plot has a resolution of 0.01 m.

6.311 Barley

Four repetition plots were selected for each soil zone (Zone 1: 1, 2, 3 and 4; Zone 2: 5, 6, 7 and 8). The lines of the wheel tracks within plots 1, 6, 7 and 8 are detectable. It is clear that the plant height patterns of Zone 2's plots were taller than Zone 1, particularly at the last two sampling dates. The fourth repetition of Zone 2 (plot 8) always had the tallest plant height patterns. Considering that all plots received the same quantity of adequate irrigation and *N* fertiliser during the growing season (see Fig. 6.4) these differences are not easy to explain. The comment about adequate irrigation notwithstanding, perhaps,

these differences are due in some way to the larger water storage capacity of the Zone 2 soil (Zone 1 = 190 mm m^{-1} and Zone 2 = 273 mm m^{-1}). In the third repetition of Zone 2 (plot 7) lower plant height values occur in the north-west corner while the northeast corner was the highest. This variability in this plot might be related to differences in seed germination or soil compaction.

6.312 Peas

Four plots for Zone 1 (plot 1, 2, 3 and 4) and four plots for Zone 2 (plot 5, 6, 7 and 8) are shown in Fig 2. The plants on the irrigated plots were taller than those on the rainfed plots (plot 9 and 10). This is due to no irrigation plus the low rainfall experienced during the growing of the pea crop specifically 30 days after planting (rainfall = 0.3 mm) which reduced crop height and consequently the yield and biomass (see Fig. 6.4). The development of plant height patterns were consistent within the plots during the season.

6.313 Beans

Plots 1 and 6 in Zones 1 and 2, respectively, had the tallest bean plants. After 21 days, taller plants were observed in plot 5. Whereas those patterns were not higher in the later campaigns which contrasted with plot 6. In plot 7, large numbers of weeds were detected at the northern edge of the plot. Poor seed germination was observed in the south part of plot 10 (non-irrigated plot).

The plant heights were slightly higher for the pea irrigation plots than the bean irrigation plots, especially at the last two dates. This is likely due to the dense canopy of the pea crop compared with the bean crop.

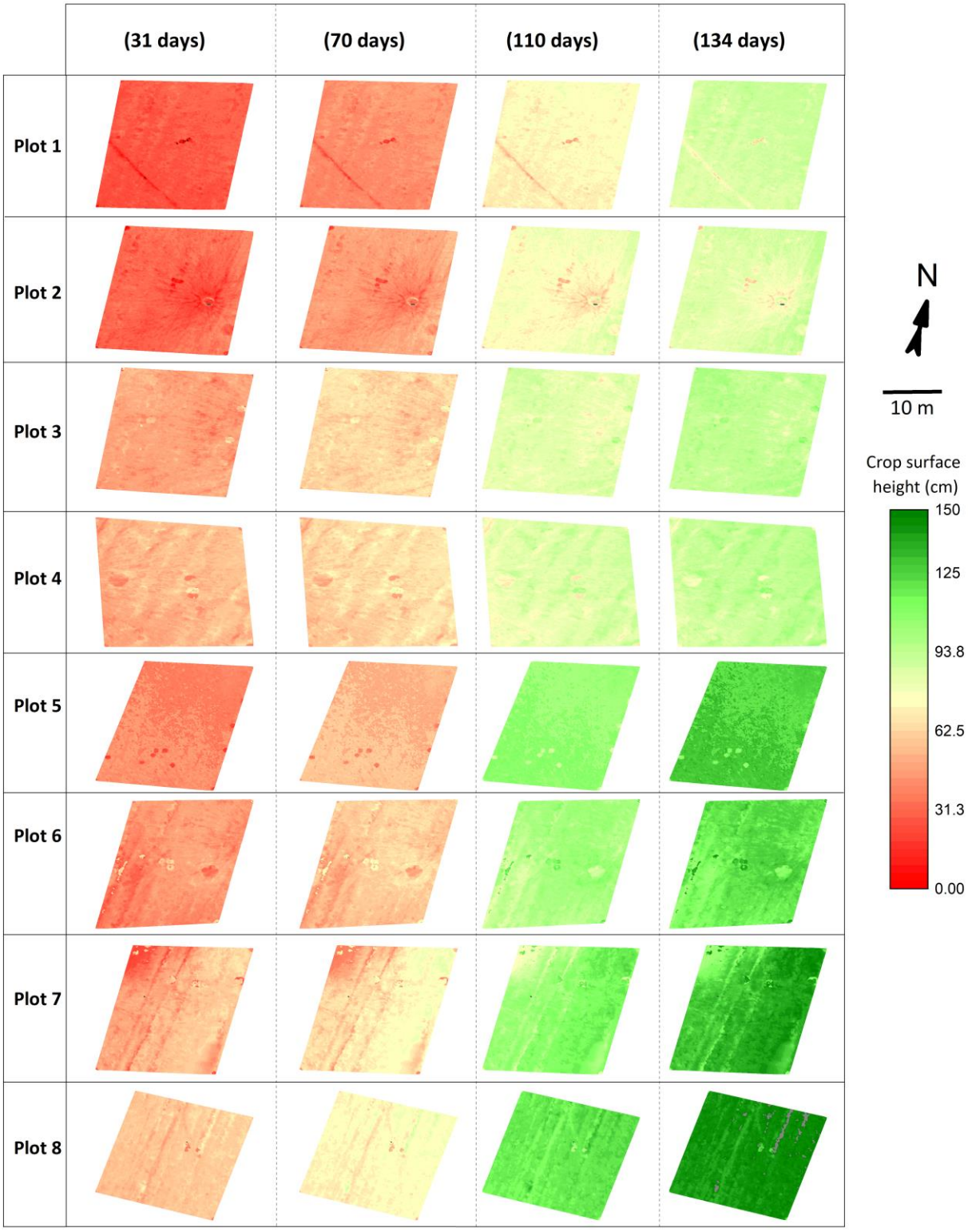

Figure 6.1: Crop surface height for barley trial visualised as maps for each plot on each measurement date after planting.

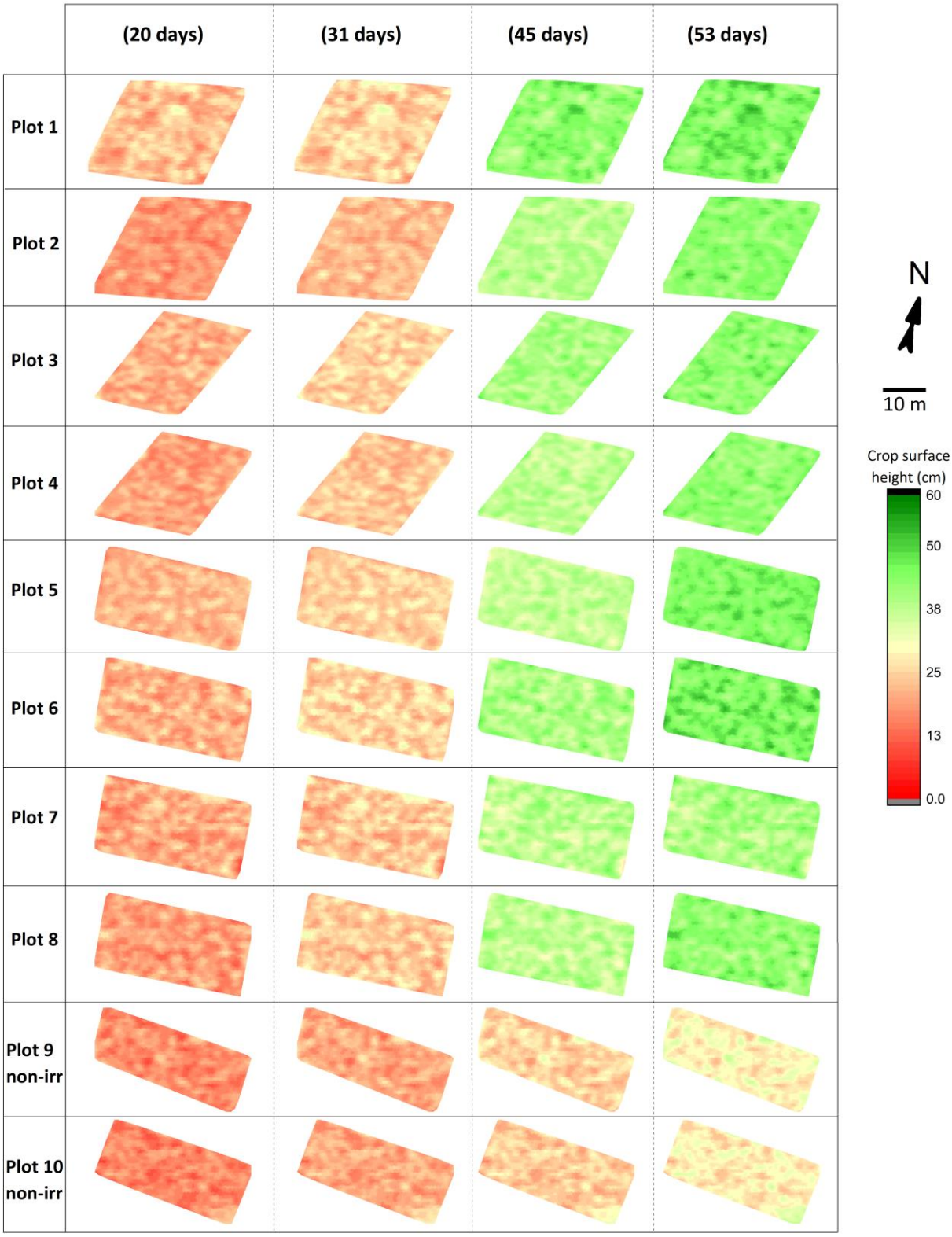

Figure 6.2: Crop surface height for pea trial visualised as maps for each plot on each survey days after planting.

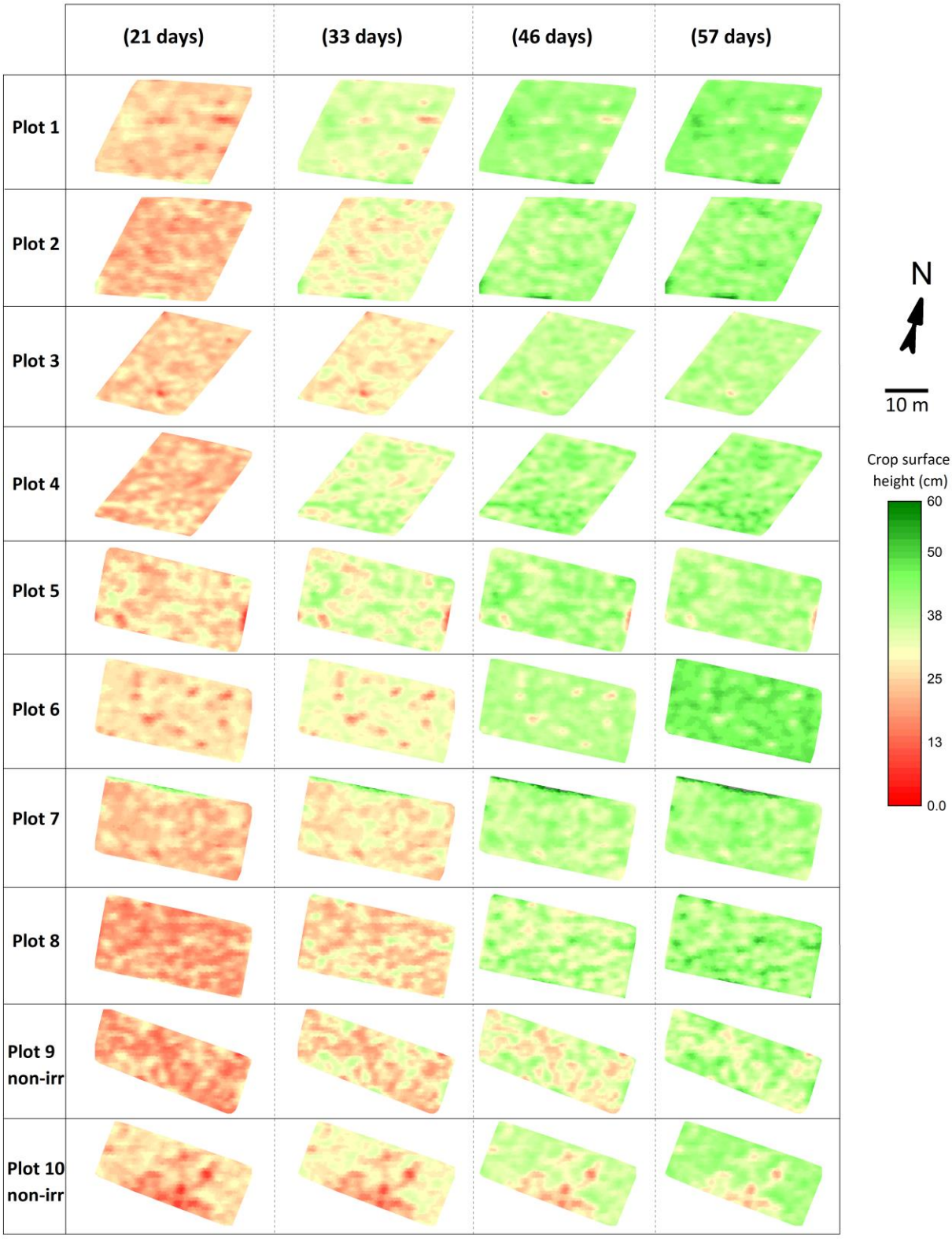

Figure 6.3: Crop surface height for bean trial visualised as maps for each plot on each survey days after planting.

6.32 Manual plant height and biomass measurements

6.321 Barley

In the barley trial, measurements with a tape measure were carried out between 1 September and 13 December 2017. The measurements of barley height started at the stem extension growth stage and finished at the heading growth stage. The *LiDAR* surveys show a continuously increasing plant density and height (Fig. 6.4). The last two measurements resulted in a significant increase ($P < 0.05$) of height for Zone 2 compared to Zone 1 (Fig. 6.4). This can be explained by water stress occurring prior to flowering for Zone 1 which gradually decreased the plant height (Chapter 3, Fig. 3.9) where a soil water deficit at 65-70% total available water (Chapter 3, Fig. 3.4) produced almost 40–60% decrease in plant growth.

6.322 Peas

The green pea crop was surveyed between 4 December 2017 and 6 January 2018. The measurements started at the bloom crop growth stage and finished at the flowering stage. The growth was clearly detected by an increase of mean crop height as assessed by both the *TLS* values and yield cuts. No significant difference ($P > 0.05$) in crop height was observed between the two zones (Fig. 6.4). The rainfed crop's height was significantly less than those observed for the two irrigated zones. On days 45 and 53 after planting, the growth rate for irrigated plots was nearly twice as large as it was at the first two measurement dates. This difference in growth rate can probably be related to the characteristics of the genotype or due to the increase in air temperature in December compared to November.

6.323 Beans

The French beans were monitored from 1 March to 6 April 2018 i.e. from the trifoliolate stage to the beginning of flowering. A continuous increase of plant height and biomass

density was detected. The results showed no significant differences (P >0.05) in crop height and biomass between the two zones or between the irrigated and the rainfed plots (Fig. 6.4). The latter observation is due to the greater rainfall experienced during the growing of the bean crop. For the period from the second to the third measurement, the increase in canopy height was not large for both methods—according to the *TLS* and manual reference measurements— between 0.2 and 0.4 m.

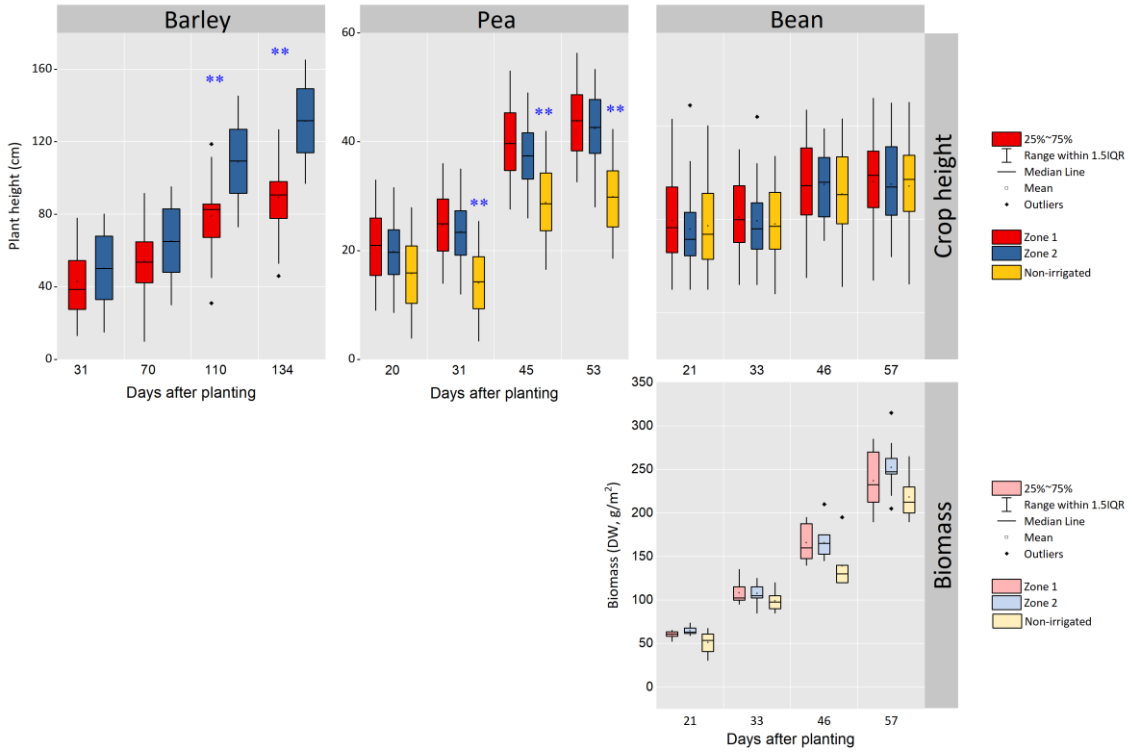

Figure 6.4: Mean manual plant height and biomass measurements for each crop on each campaign days after planting. ** The mean difference is significant at the 0.01 level.

6.33 Relations between manually and *TLS*-derived canopy height and biomass

Coefficients of determination (R^2) and the *RMSE* for crop height and biomass relationships are compiled in Figs. 6.5 and 6.6. The results of the regression analysis were performed based on four measurement dates for each crop trial.

Additionally, the mean plant height was calculated for each date for both measurement methods to execute correlation and regression analysis (Table 6.2).

6.331 Barley

The *TLS*-estimated height measurements were well correlated (R^2 = 0.95) to physically-measured canopy height using all the measurements (Fig. 6.5). The R^2 reached highest values for the last measurement date. At this date, the canopies of the barley plots reached the closure stage. Thus, most of the scan points were located on top of the canopy. In agreement with Friedli et al. (2016) who reported that the highest value of R^2 was obtained when the canopies of the wheat crop were denser and the laser beam could not penetrate very deep into the canopies.

6.332 Peas

The R^2 increased from 0.76 for the first date to 0.84 for the second date (Table 6.2) then decreased to 0.80 and 0.70 for the second and third date, respectively. Using the three dates combined in a regression, the relationship reflects higher coefficients of determination (R^2 = 0.93) (Fig. 6.5).

6.333 Beans

The value of R^2 between *TLS*-measurements and physically- measured canopy height was 0.90 (Fig. 6.5). The R^2 was comparable for the first (R^2 = 0.76), the second date (R^2 = 0.70) and the third date (R^2 = 0.71) but was higher (R^2 = 0.80) for the fourth date (Table 6.2).

Furthermore, a good correlation between *TLS*- measurements and dry biomass was achieved (R^2 = 0.70) and the linear regression shows the dependence of biomass on plant height (Fig. 6.6).

Overall, the results of the study show the ability of *TLS* to achieve canopy height maps with a high spatial resolution of up to 0.01 m. The *TLS* approach, therefore, can be considered as a valuable tool to measure the growth in canopy height of different crops under field conditions. The high correlation observed between the manually measured and the *TLS*-derived canopy heights of barley, pea and bean demonstrates the high accuracy of this applied method under these experimental sites.

Table 6.2: The correlation between manually measured and *TLS*-derived canopy height for each crop on each measurement date after planting. *DAP* is the days after planting.

Barley			Pea			Bean		
DAP	R^2	*RMSE*	*DAP*	R^2	*RMSE*	*DAP*	R^2	*RMSE*
31	0.75	4.59	20	0.76	1.07	21	0.76	1.31
70	0.82	3.43	31	0.84	0.78	33	0.70	1.95
110	0.85	7.00	45	0.80	2.91	46	0.71	1.86
134	0.97	2.88	53	0.78	3.43	57	0.80	1.64

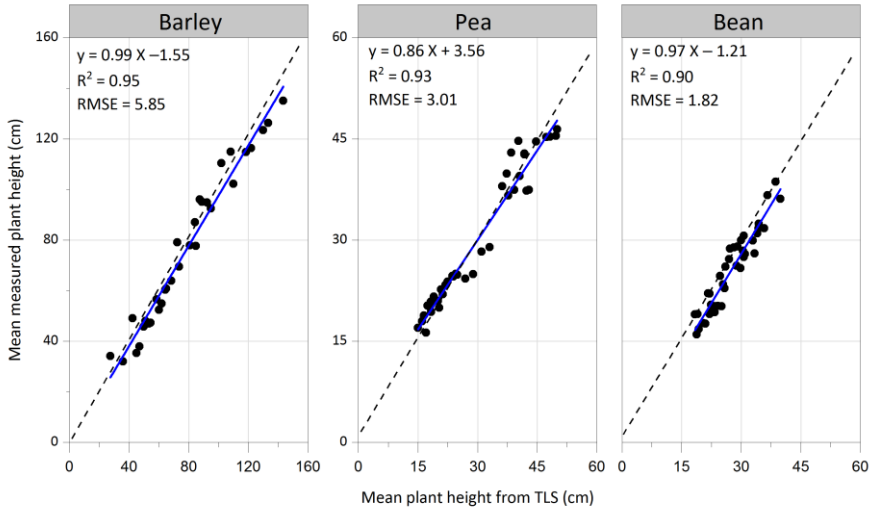

Figure 6.5: Regression of the mean *TLS*-derived and manually measured plant heights (n = 32 for barley and 40 for pea and bean).

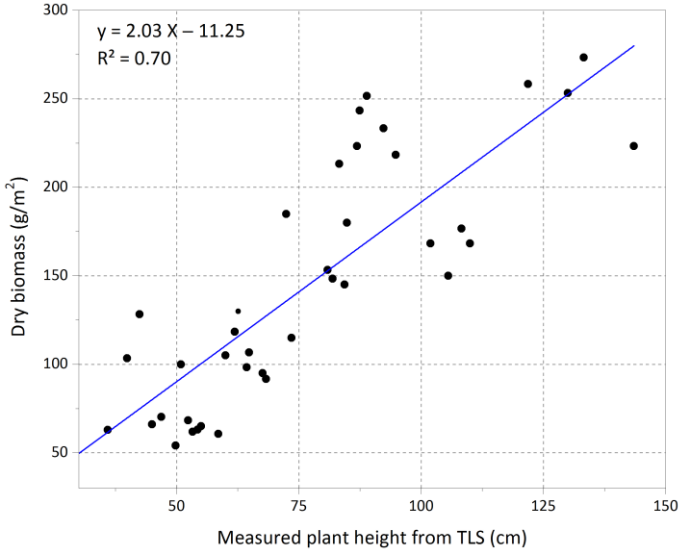

Figure 6.6: Regression of the mean *TLS*-derived plant height and the dry biomass for bean (n = 40).

6.4 Conclusions

The *TLS* based system was used to monitor precisely the spatio-temporal differences of the height of barley, pea and bean crops on four occasion during the 2017/2018 growing season. The excellent correlation coefficients (R^2) of o.95, 0.93 and 0.91 found for the *TLS* system and manual measurements of the height of barley, pea, and bean, respectively, as well as the small differences between the mean crop height-derived and manually measured plant heights show the ability of *TLS* to monitor plant height. The good correlation (R^2 = 0.70) between plant height and dry biomass confirms the applicability of plant height as a predictor for estimating the actual biomass for the bean. The results show the applicability of *TLS* to produce a *2D* map of canopy surface height with a high resolution of 0.01 m

Future research is needed to investigate the applicability of the *TLS* method for estimating crop height to other growth parameters such as biomass and leaf area index etc. for a range of crops and to explore how this method can be utilized in crop management.

Connecting text to Chapter 7

The previous chapter described a new method for spatially tracking crop growth in a field. This chapter expands on this by integrating crop sensing methods (vegetation index, canopy surface temperature, crop growth) to measure accurately the daily crop water use and importantly to capture the spatial characteristics among different fields. In this chapter, crop sensor data is used to calibrate the FAO56 algorithm to estimate daily crop evapotranspiration (ET_c) from barley, pea and bean crops. The potential benefits of calibrating a model with in-field sensor data are detecting the spatio-temporal differences in ET_c and identifying the irrigation water demand which may vary over relatively small distances. This chapter was presented in Irrigation New Zealand conference in Alexandra, New Zealand (2018). Conference presentation.

Chapter 7

Using field-level proximal sensing data to improve crop evapotranspiration estimates

Abstract

In this study, proximal sensing was used to modify the FAO-56 Penman-Monteith algorithm to provide a site-specific estimate of crop evapotranspiration. This was carried out for barley, pea and bean crops managed within two irrigation management zones (Zone 1: sandy loam and Zone 2: silt loam) under variable-rate irrigation systems in New Zealand.

Daily crop evapotranspiration estimates were calculated using data from a weather station situated at the field site combined with in-field crop sensing data (spectral reflectance, canopy temperature). In addition, soil moisture data was used with a soil water balance model to compare estimations of daily crop evapotranspiration with those estimated using the crop sensing method.

The results indicated that variable crop responses to different irrigation strategies and soil types provided a good opportunity to quantify different levels of spectral reflectance, canopy temperature and consequently the estimation of crop water use. The statistical comparisons revealed that the modified FAO-56 Penman-Monteith (*MPM*) using crop sensor data compared well with the more conventional soil water balance approach using soil moisture data (*SWB*) (R^2 = 0.70, 0.83, 0.91 for barley, pea and bean, respectively).

Overall, the results from this study indicated that crop sensing approaches combined with the FAO-56 Penman-Monteith model have potential to provide a more easily determined site-specific field estimation of crop evapotranspiration than other methods, and it can take into consideration the spatial variability of crop growth in a field.

Keywords: Field-level remote sensing; crop evapotranspiration; FAO-56 Penman–Monteith; surface temperature; crop vegetation index; variable rate irrigation.

7.1 Introduction

Agriculture is the most important economic activity in New Zealand. Irrigation is the largest user (78%) of allocated freshwater, followed by industrial and domestic use (Booker et al., 2016). Therefore, developing new water management strategies is essential to use water more efficiently. To achieve that, it is necessary that farmers trial and adopt relevant new technologies for estimating crop water supply and demand more accurately (Reyes-González et al., 2018).

Reliable estimates of evapotranspiration (*ET*) assist attempts to improve water use efficiency (*WUE*). *ET* includes water evaporation from land and water surfaces plus transpiration by vegetation (Gowda et al., 2008). The actual estimation and calculation of *ET* is of vital importance in water resource management and determination of irrigation demand (Hoedjes et al., 2008; Papadavid et al., 2011). Different *ET* methods computed from weather data exist: (a) temperature models (Doorenbos & Pruitt, 1977), (b) radiation models (Doorenbos & Pruitt, 1977; Hargreaves & Samani, 1985; Priestley & Taylor, 1972), and (c) combination models such as Penman-Monteith (*PM*) (Allen et al., 1998). Due to the differences in assumptions, data requirements, and climatic conditions for which these *ET* models were developed, they may result in inconsistent values (Lu et al., 2005). Thus, a number of studies have attempted to validate *ET* models for the different climatic and agricultural conditions.

For crop-specific evapotranspiration (ET_c), *ET* needs to be adapted by crop coefficient (K_c) values. Actual ET_c is generally estimated by multiplying the *ET* by pre-determined K_c, which is dependent on many factors, including planting date, irrigation regimes and management (Djaman & Irmak, 2012). The K_c includes three parameters: a transpiration coefficient or basal crop coefficient (K_{cb}), the evaporative component of the bare soil fraction (K_e) (Wright, 1982), and the water stress coefficient (K_s), which is related to the soil water content (*SWC*) through the water balance in the root-soil layer. In this framework, the K_{cb} is defined as the ratio between ET_c and *ET* in the absence of water stress. ET_c can be estimated or measured using different methods, for example, weighing

lysimeters (Jia et al., 2006; Williams & Ayars, 2005) evaporation pan, soil water balance (*SWB-PM*) (Allen et al., 1998; Senay et al., 2011; Xu & Singh, 2005), atmometer (*ET* gages) (Chen & Robinson, 2009), Bowen Ratio Energy Balance System (*BREBS*) (Kabenge et al., 2013), and Eddy Covariance (*EC*) (Schume et al., 2005; Scott, 2010; Wilson et al., 2001). The most accurate methods for this estimation use lysimeter measurements (Xu et al., 2013) or mathematical models, such as the *PM* equation and iterative methods (Widmoser, 2009). However, lysimeter measurements are relatively difficult, expensive, and time-consuming (Irmak et al., 2003). The inaccuracies of K_c in the FAO56 *PM* equation can potentially result in significant errors in the estimated ET_c (Allen et al., 1998).

In recent years, remote sensing (*RS*) data have been widely used in the assessment of ET_c and crop water stress to obtain accurate spatial information. *RS* imagery from cameras onboard satellites, aerial platforms, airplanes or ground-based systems has been recognized as an exceptional tool to produce spatial information about ET_c (Calera et al., 2017). Numerous studies have been conducted to estimate ET_c based on *RS*. Three main *RS* approaches for ET_c estimation have been applied: (a) based on surface energy balance (*EB*), (b) reflectance-based crop coefficient (reflectance-based K_{cb}) and (c) by directly applying *RS*-based parameters into the *PM* equation (Calera et al., 2017). The first approach is based on the rationale that ET_c is a change of the state of water using available energy in the environment for vaporization (Su et al., 2005). The *RS* based *EB* models convert satellite sensed radiances into land surface characteristics such as albedo, leaf area index, vegetation indices, surface emissivity and canopy surface temperature (T_c) to estimate ET_c as a ‘‘residual’’ of the land surface *EB* equation. In the second and third approaches, red (*R*) and near-infrared (*NIR*) reflectance measurements are used to compute a vegetation index such as Normalised Difference Vegetation Index (*NDVI)* (Rouse et al., 1974) and the vegetation index is then used in place of calendar days or heat units to drive or scale the K_{cb}. *ET* is then computed using local meteorological measurements of incoming solar radiation, air temperature (T_a), relative humidity or dew temperature, and wind speed. K_c generated from vegetation indices determine ET_c better than a tabulated K_c because it represents the actual crop growth conditions and capture the spatial variability among different fields (Kullberg et al., 2017).

Also, a reflectance-based K_c method has been studied (Hunsaker et al., 2005; Reginato & Howe, 1985). Furthermore, K_c has been related to vegetation indices such as *PVI* (Heilman et al., 1982), *NDVI* (Bausch & Neale, 1987; Neale et al., 1990), and *SAVI* (Bausch, 1993). D'urso and Santini (1996) attempted to derive the K_c analytically from *RS* estimated albedo, surface roughness, and aerodynamic resistance. This method does not require knowledge of the crop development stage.

In New Zealand, Brown (pers. comm., September 21, 2018) has developed a method for using T_c measurements in an extended version of the Priestley and Taylor (*PT*) *ET* model that allows more accurate assessment of the ET_c, even as the soil dries. The calculations use data from a standard automatic weather station together with radiometric measurements of T_c. The measurements could be made from sensors mounted in the field or a drone carrying the appropriate sensors, including GPS spatial data, so that variation within a crop could be identified and the information used to inform variable-irrigation applications (*VRI*).

The objectives of the present study were to: (i) modify *PM* with in-field crop sensing of *NDVI* and T_c (*MPM*) (ii) compare daily estimation of ET_c by *PM* with those of *MPM* for barley, pea and bean crops, (iii) compare both *PM* and *MPM* with a soil water balance model informed by in field soil moisture monitoring (*SWB*) and (iv) investigate the impact of soil variability and *VRI* on ET_c and *WUE*.

7.2 Materials and Methods

7.21 Study sites and experimental setup

The study was carried out at two experimental sites in Manawatū and Hawke's Bay, New Zealand as a part of a study investigating the efficient irrigation scheduling techniques in these areas. The sites are characterized by humid climatic conditions. The 10-year normal mean temperature is 13.3 and 14.3 ^{o}C and with mean annual precipitation of 980 and 679 mm for Manawatū and Hawke's Bay, respectively (*NIWA*) (www.niwa.co.nz). The

soils at the two sites were classified as Fluvial Recent soils formed in greywacke alluvium and alluvial soils, respectively. At each site the trial sites established two different soil zones (Table 7.1).

The Manawatū site (1.2 ha) was at Massey University No.1 Farm, Palmerston North, New Zealand (latitude 40.22° S, longitude 175.36° E, altitude 37 m). It was sown with field peas (*Pisum sativum*., cv. 'Massey', 260 kg ha^{-1}) followed by French beans (*Phaseolus vulgaris*., cv. 'Contender', 75 kg ha^{-1}) on 15 November 2017 and 9 February 2018, respectively. The seed yield was assessed by harvest on 23 January 2018 and 12 April 2018 for pea and bean, respectively. The experiment consisted of two soil management zone treatments, where irrigation was tailored to the demands of the crop that varied due to soil textural and drainage differences between the two soil management zones. Each zone had two replicate plots (20 x 10 m) where measurements were made. The irrigation scheduling was based on the *SWB* approach (following the *PM* approach of FAO56) using a *VRI* system.

The Hawke's Bay site was on a commercial mixed cropping farm (-39. 533°S °N; 176.402°E, altitude 130 m). This site was planted with barley (*Hordeum vulgare*., cv. 'Carfields CKS1') on 2 August 2017. 168 days after planting, the crop was harvested on 16 January 2018. Four replicate plots (20 x 15 m) were established in each of two soil zones. Irrigation was applied uniformly for both soil zones at approximate applications of 15 mm per week with a total irrigation depth of 150 mm applied over the whole season.

Table 7.1: Physical properties of the soil (0 – 1m)

Properties	Manawatū site		Hawke's Bay site	
	Soil zones (soil type name)			
	Manawatū fine sandy loam	Manawatū silt loam	Twyford sandy loam	Kaiapo silt loam
	Zone 1	Zone 2	Zone 1	Zone 2
Available water content (*AWC*, mm m^{-1})	123	203	190	273
Bulk density (g m^{-3})	1.41	1.30	1.28	1.17
Sand (%)	80.6	44.9	47.3	1.3
Silt (%)	12.7	40.6	40	70.8
Clay (%)	6.7	14.5	12.8	28

7.22 Field measurements

Daily weather data, which included T_a, relative humidity, incoming solar radiation, wind speed at 2 m high, vapour pressure, and precipitation were recorded by weather stations located at the two sites. For the Manawatū site, a CliFlo climate station (http://cliflo-niwa.niwa.co.nz/) 50 m from the trial site was used. For the Hawke's Bay site, Te Aute Drumpeel Rd climate station situated adjacent to the site was used.

The *SWC* levels were recorded daily for the 0–0.10, 0.10–0.20, 0.20–0.30 and 0.30–0.40 m soil depths for the field sites using frequency domain reflectometry probes (SM300-DeltaT, Burwell, UK) connected with a wireless sensor network (*WSN)* developed by Ekanayake and Hedley (2018). The soil moisture monitoring equipment was installed into the centre of each treatment plot for all three crop trials. Soil sensor calibration was performed for each soil type during the course of the experiment against weekly measurements of *SWC* made gravimetrically and with a neutron probe. The neutron probes, which were 1 m long, were installed permanently in a vertical position, close to the SM300 sensors (about 1 m distance), and *SWC* readings were taken to a depth of 0.80 m in 0.10 m depth increments. To calibrate the SM300 probes: (i) there were four

replicates neutron access tubes in each of the four replicate plots in each soil zone for each crop, and (ii) three undisturbed soil sample replicates of known volume (intact cores) were taken close to the access tubes (about 1–3 m distance) at depths of 0.1, 0.20, 0.30, and 0.40 m to measure volumetric soil water content. The soil volumetric water content was determined by multiplying the gravimetric water content by the measured bulk density.

A RapidSCAN CS-45 Handheld Crop Sensor (Holland Scientific, Lincoln, NE) was used to measure the *NDVI* at 1–m intervals along transects 1-m apart in each plot on a weekly basis. The system is equipped with *GPS* so the data was collected and stored for analysing *NDVI* differences between the plots. Markers were installed in each plot to allow the observations to be made at the same place from one date to another. The average and the standard deviation of *NDVI* were computed, from these measurements. Daily *NDVI* values were determined by using linear interpolation between the weekly collected *NDVI* data.

The crop height was measured using Terrestrial Laser Scanning, validated with manual measurements, during the growing season to adjust the predictions. For details see Chapter 6. A destructive method was used for measuring the maximum effective rooting depth directly at different growth stages. Linear interpolation for measured crop height and root depth was used during the growing season.

The T_c was continuously measured with non-contact thermal infrared radiometers (*IRT*) (Apogee Instruments, Inc., model SI-400). The radiometers were installed about 1 m above ground level and directed vertically down at the plant with a zenith angle of 0^o, thus the area of the field of view was 1.2 m^2. Real-time T_c measurements were recorded every one hour during most of the season using a *WSN* developed by Ekanayake and Hedley (2018) for all plots. The measurements were made for each plot and averaged to get a single value for each treatment.

7.22 Crop Evapotranspiration estimation models

7.221 FAO-56 Penman Monteith estimation of ETc (PM)

The standard daily *ET* estimated using the *PM* equation is expressed as in Equation 7.1. The FAO-56 *PM* is a hypothetical grass reference-based model that has the following characteristics: mean height of vegetation h = 0.12 m, measurement of temperature, humidity, and wind speed at the height of 2 m, latent heat transfer λ = 2.45 MJkg^{-1}, bulk surface resistance 70 sm^{-1}, and albedo = 0.23. The final form of the FAO 56 *PM* equation for a daily time-step is defined in Equation (7.1) (Allen et al., 1998).

$$ET = \frac{0.408 * \Delta * (R_{\mathrm{n}} - G) + \gamma * \frac{900}{T + 273} * u_2 * (e_{\mathrm{s}} - e_{\mathrm{a}})}{\Delta + \gamma(1 + 0.34 * u_2)} \qquad [7.1]$$

Here, ET: reference evapotranspiration (mm d^{-1}), R_n: net radiation at the crop surface (MJ m^{-2} d^{-1}), G: soil heat flux density (taken as zero for daily calculations) (MJ m^{-2} d^{-1}), T: mean daily air temperature at 2 m height (ºC), u_2: wind speed at 2 m height (m s^{-1}), e_{s}: saturation vapour pressure (kPa), e_{a}: actual vapour pressure (kPa), $e_{\mathrm{s}} - e_{\mathrm{a}}$: saturation vapour deficit (kPa), Δ: slope vapour pressure curve (kPa ºC^{-1}), γ: psychrometric constant (kPa ºC^{-1}).The FAO-56 ET_{o} model and a dual crop-coefficient method ($K_{\mathrm{c}} = K_{\mathrm{s}} * \mathrm{K_{cb}} + K_{\mathrm{e}}$) which accounts for variations in soil water availability, inducing either stress and soil evaporation were used to estimate ET_{c}, Equation (7.2) (Allen et al., 1998).

$$ET_{\mathrm{c}} = (K_{\mathrm{s}} * \mathrm{K_{cb}} + K_{\mathrm{e}}) * ET \qquad [7.2]$$

Here, ET_{c} is the crop evapotranspiration (mm d^{-1}), K_{cb} is the basal crop coefficient, K_s is water stress coefficient, and K_{e} is the soil evaporation coefficient. The K_{e} and K_{s} are calculated based on daily water balance computation in the surface soil evaporation layer of effective depth ($Z_{\mathrm{e.i}}$) and in the root zone ($Z_{\mathrm{r.i}}$), respectively, according to Allen et al. (1998).

7.222 Modified FAO-56 Penman Monteith estimation of ETc (MPM)

In the modified daily *ET* estimation method (*MPM)*, R_n, *G*, and K_{cb} were derived from the remotely-sensed data following the method of Brown (pers. comm.). Net radiation (R_n) was calculated as a function of measured solar radiation (R_s), T_c, surface albedo, and *NDVI*.

An empirical relationship for *G*, depending on R_s and T_a was used.

$$G = -c + dR_s * (1 - K_c) + hT_a \quad [7.3]$$

Where *G* the ground heat flux density (MJ m^{-2} day^{-1}), *c* is 0.71 MJ m^{-2} day^{-1}, *d* is 0.21, R_s: solar radiation (MJ m^{-2} day^{-1}), K_c: cover factor (dimensionless), T_a: daily air temperature (ºC) and *h* is 0.07 MJ m^{-2} °C^{-1} day^{-1}.

The *fPAR* of radiation interception was calculated from *NDVI* measurements using a relationship derived from measurements in an earlier experiment (Equation 7.4). It is widely acknowledged that *fPAR* is a major determinant of the basal crop coefficient (K_{cb}) (Bellvert et al., 2018; Marsal et al., 2014; Picón-Toro et al., 2012). In this study, K_{cb} was empirically derived using the K_{cb} function from Brown (pers. comm.). The growth stage days were determined based on days after planting, and linear interpolation for crop parameters (K_{cb}, crop height and $Z_{r.i}$) were used between stages.

$$fPAR = (NDVI - 0.1)/(0.9 - 0.1) \quad [7.4]$$

$$K_{cb,fPAR} = Min\ (1, 0.3 + 1.6 * fPAR) \quad [7.5]$$

The modified ET_c was calculated from:

$$ET_c - MPM\ = (K_s * K_{cb,fPAR} + K_e) * ET \quad [7.6]$$

7.23 Assessment of the two ET_c models

The daily ET_c calculated using the *SWB* budget approach (see Equation 7.7) was used to evaluate the predictive power of the two ET_c models of *PM* and *MPM* for each crop trial. The latter *SWB* approach as described by Evett et al. (2012) and Koksal et al. (2019) is based on measurement of rainfall, irrigation water, and soil water content in the rooting zone and assumed no drainage.

$$ET_{ci} = P_i + I_i \pm \Delta SWC_i + RO_i \quad [7.7]$$

Here, ET_c is crop evapotranspiration (mm d^{-1}), *P* is precipitation (mm), *I* is the irrigation water applied (mm), Δ *SWC* is the soil moisture content difference between two consecutive measurements using a neutron moisture meter (mm), *RO* is the runoff (mm), and *i* is the day of calculation. *RO* was assumed to be zero.

7.24 Yield and Water use efficiency

Crop yield was measured in the replicated plots for each crop trial at crop maturity. In the pea and bean trials, seed yield and aboveground plant material were measured by harvesting an area of 1 m^2 (three replicates/plot). Seed weights were measured on subsamples from this harvest. The dry yield was estimated on an oven dry-weight basis (70ºC). In the barley trial, the crop yield was determined from a yield map provided by the farmer. The map was derived from data collected by a yield monitor positioned on the harvester. The yield map was imported into Trimble Ag Software to load and analyse the performance of the plots.

The *WUE*, here referenced to crop water-use, was calculated by dividing the crop yields for each zone treatment by the total cumulative ET_c for that treatment (Howell, 2001).

7.25 Statistical analysis

Statistical measures were used to compare the two estimation methods for daily ET_c (*PM* and *MPM*) against *SWB* budget approach. The statistical measures include coefficient of determination (R^2), mean bias error and root mean square error (*RMSE*), referring to Liu et al. (2012).

$$RMSE = \sqrt{\sum_{k=0}^{n} \frac{(Pi-Oi)^2}{n}} \quad [7.8]$$

$$MAE = n^{-1}\sqrt{\sum_{1}^{n}(Pi = Oi)} \quad [7.9]$$

Here, n = number of observations, Pi = estimated ET_c by the modified model, Oi = *SWB*–estimated ET_c (actual).

Analysis-of-variance (*ANOVA*) at P=0.05, Tukey's HSD (data normally distributed) and Bonferroni (*Dunn*) (data non-normal distributed) were conducted to investigate significant differences in measured yields and *WUE* between the two soil zone treatments. Statistics were carried out using R version 3.5.1 (R Core Team, 2018).

7.3 Results and Discussion

7.31 Weather data

Trends and magnitudes of climate variables, including *PM–ET* (mm day^{-1}) and rainfall for barley, pea, and bean growing seasons during the study period are presented in Fig. 7.1.

The lengths of barley, pea and bean growing seasons in 2017/2018 were 169 and 72 and 63 days, respectively. The bean crop was planted after the peas were harvested and grown between the dates 9 February 2018 to 12 April. The bean growing season was wet with a total precipitation of 209 mm occurring during their period of growth. Seasonal rainfall and mean temperature were 120 mm and 19 °C for peas, and 199.4 mm and 13.8 °C for

barley, respectively. Total rainfall from 15 November 2017 (1 day after planting (*DAP*)) to 18 December 2017 (34 *DAP*) was 5 mm (5% of the seasonal amount) in pea trial. Total rainfall from 30 October 2017 (90 *DAP*) to 4 January 2018 (156 *DAP*) was 33.6 mm (16.8% of the seasonal amount) in barley trial. This situation affected the crop water requirements during the growing season.

Daily *ET* values, which reflect the climatic conditions of the crop growing season periods, fluctuated between 0.5–6.1 mm day^{-1} for the barley and between 1.6–6.9 mm day^{-1} for the peas, and between 0.5–4.9 mm day^{-1} for the beans, whereas total cumulative *ET* values were 495, 318.1, and 186.3 mm/season for barley, pea and bean, respectively. The relatively higher *ET* for the pea growing season was due to lower precipitation, higher air temperature and solar radiation (mean solar radiation = 16.8, 23.5, 14.9 MJ m^{-2} for barley, pea and bean, respectively).

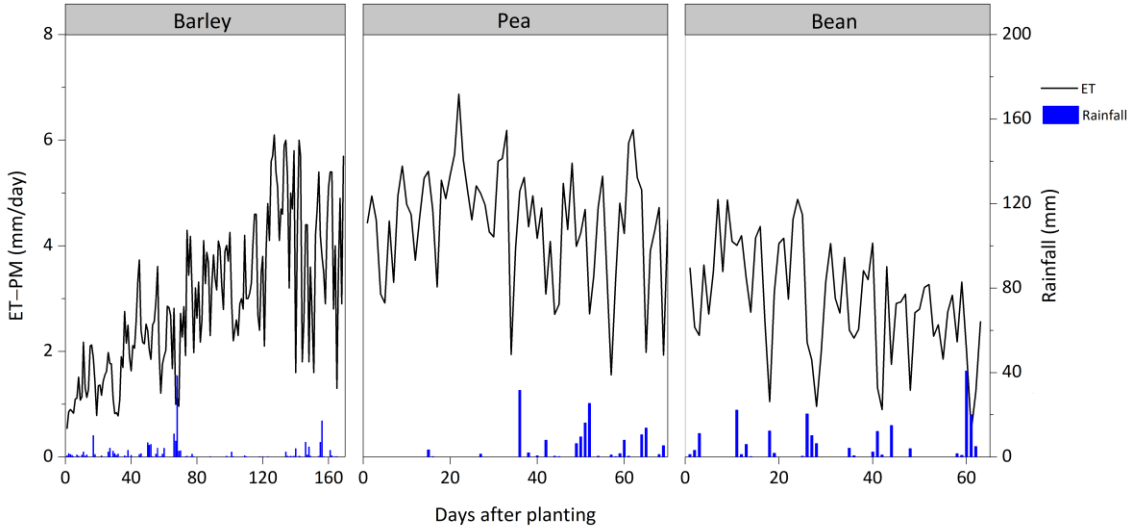

Figure 7.1: Seasonal trends of Penman Monteith evapotranspiration (*ET*, mm day^{-1}) and rainfall (mm) during the growing season for barley, pea and bean crop.

7.32 Field-level remote sensing data

The trends and magnitude in the measured T_c and estimated *fPAR* values for barley, pea and bean crop with the irrigation management zone treatments are presented in Fig. 7.2.

7.321 Tc

During the barley trial, greater T_c values were associated with Zone 1 plots (sandy loam, smaller *AWC* see Table 7.1) compared with Zone 2 plots (silt loam, larger *AWC* see Table 7.1). In general, as the soil dries out T_c values increased with this water stress – T_c being affected by a lower canopy cover percentage and stomatal closure as reported in the literature (Blonquist et al., 2009). The lowest T_c values were measured for the surface of Zone 2 treatment plots after 90 *DAP* due to enough transpiration from leaves and evaporation from soil surfaces. Measured T_c values varied between nearly 11.2 and 34.5 ^oC for Zone 1 and from 8.5 and 29.3 ^oC for Zone 2.

During the pea trial, T_c values fluctuated between 14.3 and 33.4^oC for Zone 1 (smallest *AWC*) and from 12.3 and 30.4^oC for Zone 2 (largest *AWC*). In the early part of the growing season, T_c values measured for Zone 1 plots were slightly higher than Zone 2 plots which is consistent with irrigation demand levels.

During the bean trial, with adequate rainfall for the majority of the season, T_c values for the different treatment plots did not differ from each other as there was not much difference in the irrigation applied and *NDVI* values for the two treatments. As the *fPAR* and *NDVI* started diverging from each other as a result of irrigation applied, lower T_c values relate to greater *NDVI* values (Köksal et al., 2019). In general, T_c varied from ~ 6 during the early part of the season to ~ 21 during the late-season. As expected, the T_c values during the wetter bean growing season were smaller than for the pea crop.

7.322 fPAR

The relevant canopy biophysical parameters involved in canopy transpiration can be described by the *NDVI* and *fPAR* (Bellvert et al., 2018; Rocha et al., 2012). In general, *NDVI* values at the initial stage were low around 0.08 – 0.20 in initial phase. Then the *NDVI* values increase as the crop develops reaching its maximum value (~ 0.8 – 0.90) at mid-season stage followed by plateau from late (Fig. 7.2).

During the barley trial, the *fPAR* value moves from a minimum of ~ 0.08 to a maximum of 0.89 and 0.94 for Zone 1 and 2, respectively on the date of 111 *DAP*. The decrease in the *NDVI* and *fPAR* at the end of season was more notable in the barley trial probably because of senescence of the cover crop (Bellvert et al., 2018), while the *NDVI* and *fPAR* in the pea and bean remained quite constant until the end of the season. Although a somewhat similar trend was observed in Zone 1 and 2 for barley, the Zone 1 plots' data showed consistently less *NDVI* and *fPAR* values after 90 *DAP* due to the water stress. The average *fPAR* for Zone 1 plots reached to 0.65 and 0.76 for Zone 2 treatments.

Slight differences in seasonal patterns were observed between the pea and bean crops. These differences can be explained by differences in the fraction of ground cover. Maximum *fPAR* values were 0.89 (46 *DAP*) and 0.85 (55 *DAP*) for pea and bean, respectively.

During the pea trial, although trends in measured *fPAR* for both treatments did not significantly differ, larger *fPAR* values were associated with highly vegetated conditions in the early part of the season (Zone 1 treatment), followed by Zone 2. Values of *fPAR* ranged from 0.13 and 0.89 for Zone 1 plots and from 0.13 and 0.86 for Zone 2 plots.

During the bean trial, since there was greater rainfall during the growing season, magnitudes of *fPAR* were not significantly different between the two-zone treatments during the first half of the growing season. However, *fPAR* values in Zone 2 plots varied (not significantly) from the Zone 1 treatments later in the season.

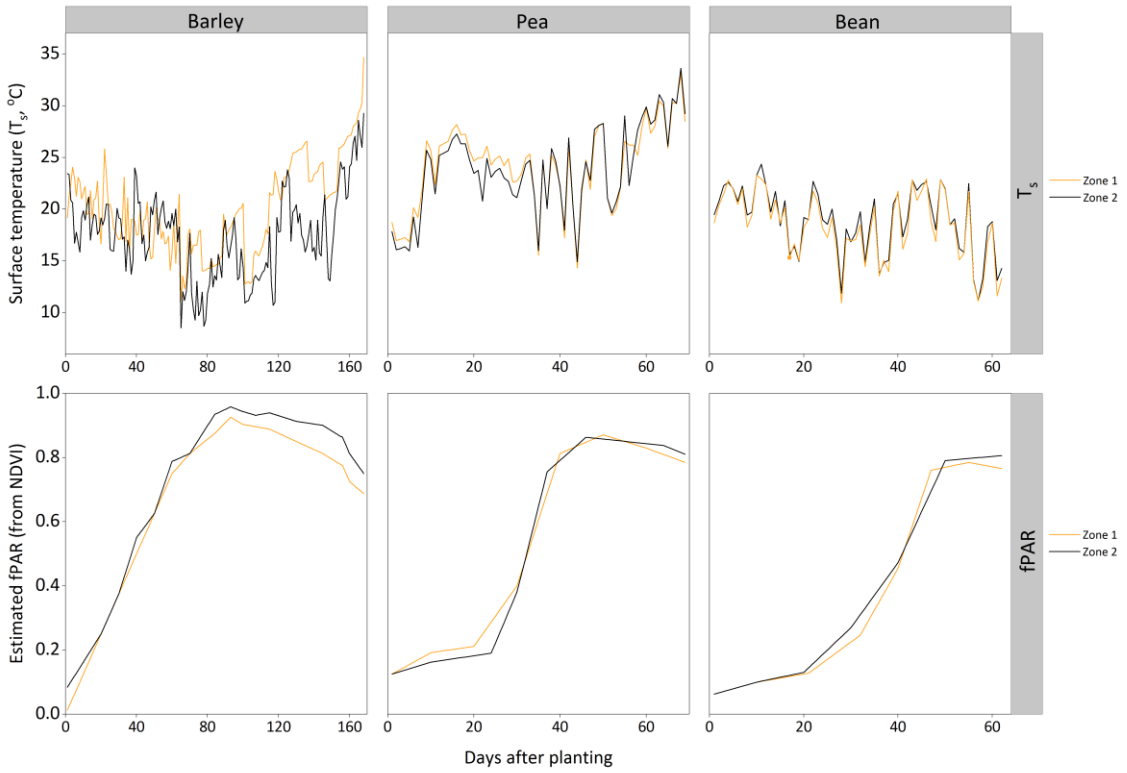

Figure 7.2: Surface canopy temperature (T_c, °C), and the estimated fraction of radiation intercepted by the crop (*fPAR*), values for each zone treatment in each crop trial.

7.33 Evaluating the two ET_c methods

The relationships between the *PM* and *MPM* estimation of daily ET_c with daily ET_c–*SWB* of barley, pea and bean are presented in Fig. 7.3.

The statistical criteria of validation for estimating ET_c using the *SWB* approach and the two ET_c models are shown in Table 7.2.

Performance statistics of ET_c values for *MPM* and *SWB* were better than for daily values of *PM* and *SWB*. In the barley trial, the R^2 was 0.70 and 0.66 ($P<0.05$) for *MPM* and *PM*, respectively with *RMSE* equals 0.70 mm day^{-1} and 0.92 mm day^{-1} for *MPM* and *PM*, respectively. Strong relationships were observed for the pea and bean growing seasons, with R^2 values of 0.83 and 0.73 ($P<0.05$) for *MPM* and *PM* for pea, whereas, for bean R^2 values were 0.91 and 0.71 ($P<0.05$) for *MPM* and *PM*, respectively.

Cumulative ET_c–*MPM*, ET_c–*PM* and ET_c–*SWB* values of each irrigation management zone treatment were calculated for each crop trial (Fig. 7.4).

In the barley trial, cumulative ET_c values for *PM* were greater than cumulative ET_c values for *MPM*. The *PM*–algorithm yielded higher cumulative ET_c values than estimated values by *SWB* (18% to 22%), and this over estimation reached nearly 65 mm.

During the complete growth period (15 November 2017 until 25 January 2018) of the pea trial, the cumulative ET_c–*MPM* was 118.87 and 114.81 for Zone 1 and Zone 2, respectively whereas ET_c–*PM* was 116.20 and 126.88 for Zone 1 and Zone 2, respectively which underestimated (-) and overestimated by – 7%, – 8%, – 9% and 1.6%, respectively compared with ET_c–*SWB*.

In the bean trial, the differences between cumulative ET_c values were very low (– 6.5%, – 6.4%, 3.1% and 6.4% for ET_c–*MPM* and ET_c–*PM*, respectively compared with ET_c–*SWB*) where they slowly increased with crop age and transpiration.

Overall, The *MPM* was more sensitive to the crop as it directly senses crop stress (radiometer-temperature) and crop stage (*NDVI*) as also referred to by Köksal et al. (2019).

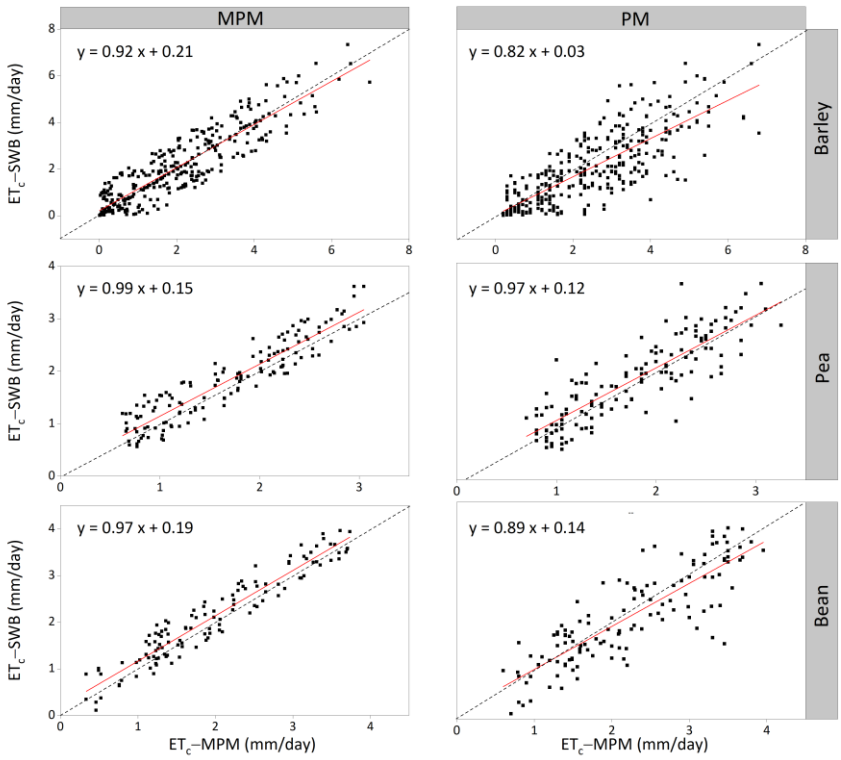

Figure 7.3: Scatter plots of daily estimated crop evapotranspiration (ET_c, mm d^{-1}) using Penman–Monteith (ET_c–*PM*) and modified Penman–Monteith (ET_c–*MPM*) algorithms against estimated values by soil water budget (ET_c–*SWB*) for each crop trial. The red line shows the ordinary least squares linear regression fits. In broken black is the 1-to-1 line.

Table 7.2: Relationship of predicted values of ET_c estimated by Penman-Monteith (*PM*) and modified Penman-Monteith (*MPM*) to those estimated by soil water budget (*SWB*) approach.

	MPM			*PM*		
	Barley	Pea	Bean	Barley	Pea	Bean
R^2	0.70	0.83	0.91	0.66	0.73	0.71
RMSE	0.70	0.29	0.28	0.92	0.39	0.50
Bias	0.01	0.01	0.03	0	0	0.02

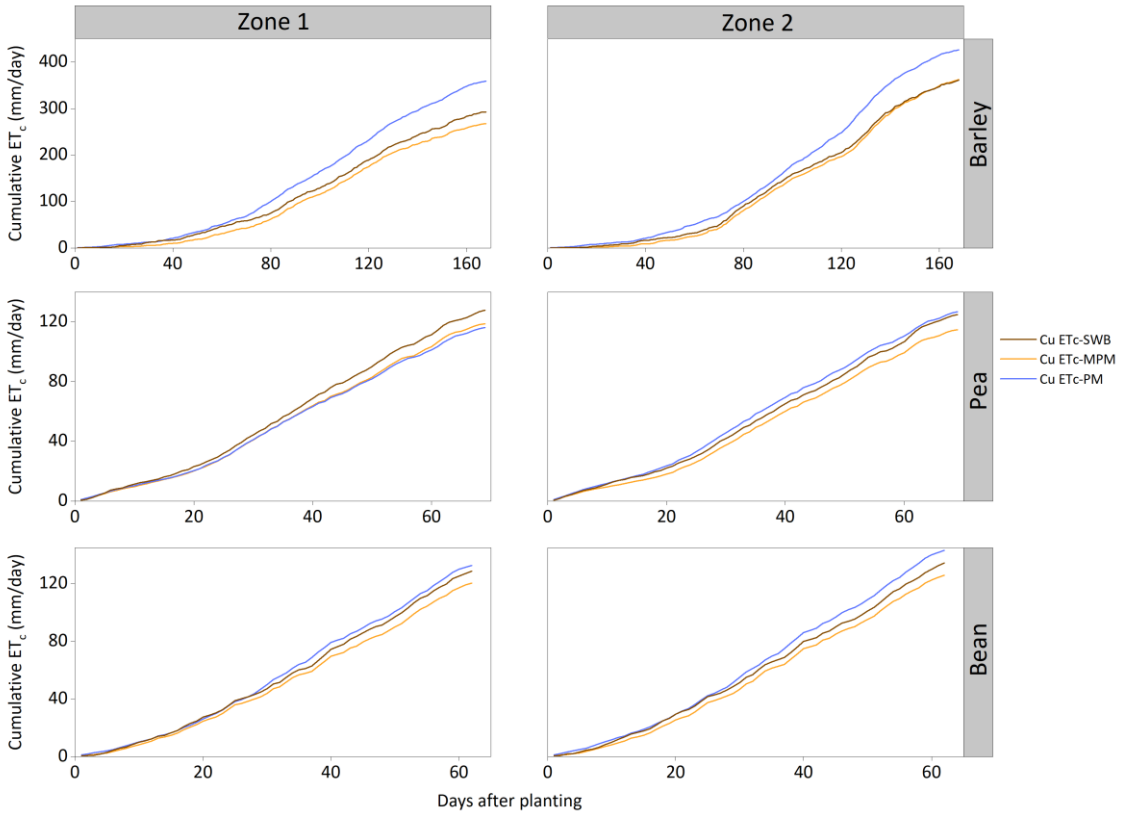

Figure 7.4: Comparison of estimated cumulative crop evapotranspiration (ET_c, mm d^{-1}) between different models for each zone treatment in each crop trial.

7.34 Comparison of ET_c between the two zones treatment

Fig. 7.5 shows seasonal ET_c values for the different irrigation zone treatments derived using the *MPM* method for barley, pea, and bean. The results show fluctuations of daily ET_c throughout the crop season with respect to irrigation and rainfall for each treatment separately.

7.341 Barley trial

The ET_c increased gradually from mid-October to end-October (73 to 90 days after planting (*DAP*)), when maximum values of ~ 5 and 4.5 mm day^{-1} were achieved. After end-October, the ET_c dropped slightly until early December (123 *DAP*). After that, the ET_c of Zone 1 dropped progressively until the end of the season. The decrease in ET_c corresponded with the water stress period for Zone 1 treatment where the irrigation application at a fixed interval (15 mm/week) wasn't enough to meet the crop water demand for barley in Zone 1 whereas ET_c was much higher in Zone 2, suggesting more vigorous growth. During that period, transpiration declined to minimum values of 2.8 mm day^{-1} in Zone 1 compared to Zone 2.

7.342 Pea trial

During the pea trial most irrigation occurred in the first part of the season when rainfall was insufficient to meet crop water use. Irrigation was applied 6 and 5 times to the Zone 1 and 2 plots, respectively. Average allowable deficit level was 45% of plant available water (*PAW*) (Allen et al., 1998). The ET_c was very low (0.6 mm day^{-1} to 1.5 mm day^{-1}) in early growth period during 15 November – 7 December). Then, it increased with crop age due to canopy development and the consumption rate was a maximum of 3 mm day^{-1} on 12 December (27 *DAP*). The ET_c trend for Zone 1 treatment was higher than Zone 2 in the first part of the season and this might be caused by the irrigation water applied during this period (60 mm for Zone 1 and 30 mm for Zone 2). The difference between water used through ET_c and that applied through irrigation and rainfall accounted for 111.13 and 102.19 mm for Zone 1 and 2, respectively, which corresponds to the amount of water provided from soil storage for the growing season.

7.343 Bean trial

The total length of the growing season was similar in bean (63 days) and pea (70 days); however, rainfall patterns deviated between the two seasons, with the total rainfall for the bean growing season (209 mm) more than that for the pea growing season (120 mm).

Moreover, the rainfall was uniform during the bean growing season (Fig. 7.5). Due to these conditions, total irrigation varied significantly between the two experimental seasons. The irrigation events were scheduled only twice and once for Zone 1 and Zone 2, respectively, with a total amount of 35 and 20 mm for Zone 1 and Zone 2, respectively. The ET_c in Zone 1 followed the same trend as Zone 2, and ET_c for bean was slightly higher than for pea (Fig. 7.5). Maximum values reached to ~ 3.6 mm day^{-1}.

Overall, these results indicate that the ET_c trend patterns are strongly influenced by the specific weather conditions and confirm the requirement of site-specific ET_c considering soil types and remarkable seasonality in precipitation during the growing seasons in the study area.

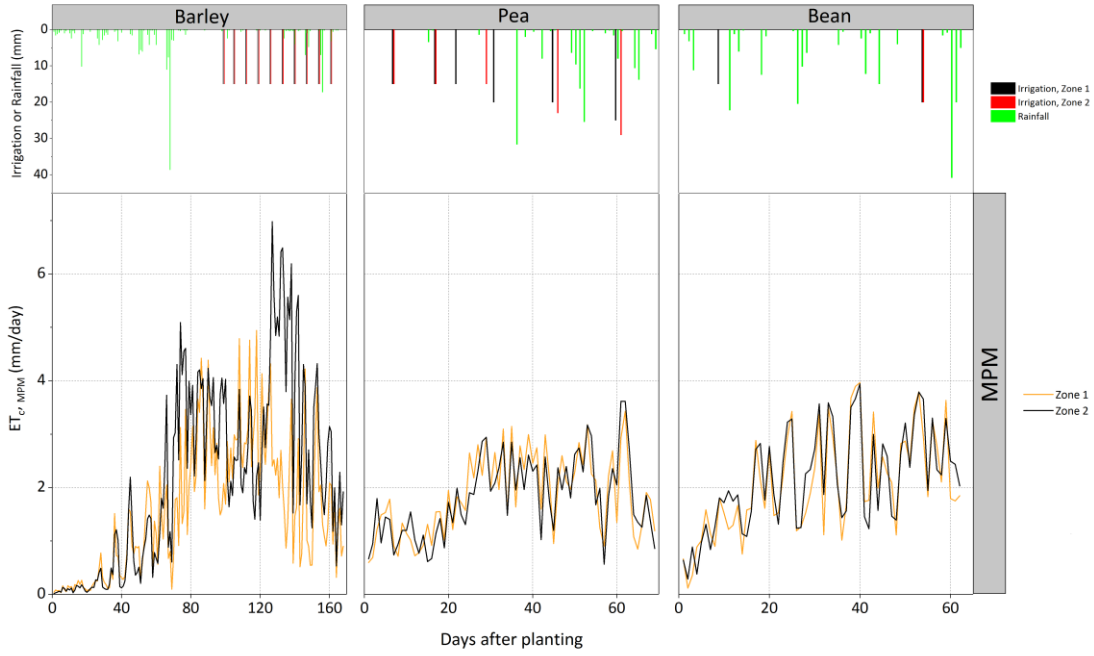

Figure 7.5: Applied amount of irrigation water, amount of rainfall and comparison of daily estimated crop evapotranspiration (ET_c, mm d^{-1}) using modified FAO-56 Penman-Monteith (*MPM*) between the zones treatment for each crop trial.

7.35 Yield and efficiency

Yield, ET_c, and *WUE* for the two soil zone treatments for each crop trial as well as the results of *ANOVA* tests are given in Table 7.3.

Total yields for barley ranged from 4 t ha^{-1} and 10.3 t ha^{-1} for Zone 1 and Zone 2,

respectively, representing significant differences in yield-values between treatments at a 95% confidence level. In the barley trial, *WUE* values for Zone 1 (1.5 kg m^{-3}) were lower than Zone 2 (2.84 kg m^{-3}). This is attributable to differences in ET_c and yield values related to soil variability, atmospheric conditions, and irrigation applications. The relationship between barley yield and water stress observed in the present study is in line with the findings of previous studies by González et al. (1999); Jamieson et al. (1995); Samarah (2005), who reported water stress to significantly affect barley grain yield.

For the pea and bean crops, yield results indicated there were no significant differences (P >0.05) among the two soil zone treatments (Table 7.3). The mean yields were 2.44 and 2.41 t ha^{-1} for the pea treatments (standard deviation 0.01 t ha^{-1}), and 1.10 and 1.15 t ha^{-1} (standard deviation 0.02 t ha^{-1}) for the bean treatments. *WUE* was not significantly different between both soil zone treatments for pea and bean crop.

The *WUE* were 2.05 and 2.09 kg m^{-3} for the pea treatments and 0.91 and 0.91 kg m^{-3} for the bean treatments.

Table 7.3: Barley, pea and bean yield, crop evapotranspiration (ET_c) estimated by modified FAO-56 Penman-Monteith (*MPM*) model and water use efficiency (*WUE*) under two soil management zones. * indicate significant differences (P < 0.05) between treatments for each crop trial.

	Barley			Pea			Bean		
	Yield	ET_c	*WUE*	Yield	ET_c	*WUE*	Yield	ET_c	*WUE*
	T	mm	kg	T	mm	kg	T	mm	kg
	ha^{-1}	d^{-1}	m^{-3}	ha^{-1}	d^{-1}	m^{-3}	ha^{-1}	d^{-1}	m^{-3}
Zone 1	4*	268.2	1.5*	2.4	118.9	2.01	1.1	120.5	0.91
Zone 2	10.3*	362.8	2.8*	2.4	114.8	2.01	1.2	125.8	0.95

7.4 Conclusions

This study evaluated the performance of *PM* and *MPM* estimation of ET_c of barley, pea, and bean grown under two irrigation management zones against ET_c calculated by a *SWB* equation. The ET_c–*MPM* was calculated using data from a site-specific weather data with measurements of T_c and surface reflectance in visible and near-infrared wavelengths (*NDVI*). The ET_c–*SWB* was estimated from the water balance using the soil moisture

measurements and inputs of irrigation and rainfall and assumed no drainage.

The results revealed that the barley crop (Zone 1) was sensitive to insufficient water, as determined by the use of crop sensing for direct estimation of physiological responses. Such measurements offer significant opportunity to detect the crop response to irrigation and soil variability impact. This is because when the water stress became more severe in the coarser textured soil (Zone 1), the T_c increased and *NDVI* decreased, and then ET_c decreased.

Our trials indicate that the ET_c–*MPM* model is applicable for three quite different crops, showing a high linear correlation near the 1:1 line and yielding a high R^2 (0.79, 0.83, 0.91) and a low *RMSE* (0.70, 0.29, 0.28 mm day^{-1}) between *SWB*-estimated and *MPM*-modelled daily ET_c for barley, pea and bean, respectively. The surface reflectance data could be used in a practical way to estimate the K_{cb} in spatially heterogeneous crops based on empirical equations with biophysical parameters such as *fPAR*.

The *WUE* values, referenced between yield and ET_c, were highest (2.8 kg m^{-3}) for the Zone 2 treatment in barley and lowest (1.5 kg m^{-3}) for the Zone 2 irrigation treatment. The *WUE* values for pea, ranged between 2.05 and 2.09 kg m^{-3} for Zone 1 and 2, respectively and 0.91 kg m^{-3} in bean, indicated *VRI* to be a reliable water management system to improve the *WUE*.

Future work is needed with different crops under different climatic conditions for a thorough evaluation of the application of ET_c–*MPM* model with remotely sensed data at field scales.

Connecting text to Chapter 8

The previous chapters have presented new methods for mapping and monitoring soil and crop at high resolution to inform precision irrigation management. In Chapter 4 a field method for monitoring soil variability spatially and with depth was provided then Chapter 5 presented and compared accurate methods for managing this variability by estimating irrigation water demand based on real-time soil moisture monitoring. In Chapter 6 a new crop sensing method with *LiDAR* sensor was used to assess crop height and biomass at high spatio-temporal resolution. In Chapter 7 a crop sensing approach was tested for estimating daily crop evapotranspiration (ET_c) by integrating the remote sensing measurements (i.e. *NDVI* and canopy surface temperature (T_c)) with a FAO-56 Penman-Monteith (*PM*) algorithm. All these sensing methods are required in precision irrigation control systems for effective and timely application of the information that they provide. Therefore, the main objective of this chapter was to test a model-based decision support software system to efficiently manage water to variable soils, multiple crops, and to compare its outputs with real-time sensing measurements. Also, the trial discussed the options for including real-time sensing data into *VRI* software control systems. This chapter was presented in conference proceedings:

(i) Irrigation New Zealand conference in Alexandra, New Zealand (2018). Conference presentation.

(ii) New Zealand Society of Soil Science& Soil Science Australia (NZASSS) conference in Napier, New Zealand (2018). Conference presentation.

Chapter 8

A decision support system for variable-rate irrigation in New Zealand

Abstract

A model-based decision support software system for variable-rate irrigation that automates irrigation scheduling to variable soils and multiple crops was tested. The system is incorporated into a web-based irrigation scheduling tool to predict irrigation timing using soil and crop information, a virtual weather model, and applied irrigation inputs to a soil water balance model.

The system, termed *VRI–DSS*, was evaluated in a commercial field irrigated by a variable-rate irrigation centre pivot for maize and sweetcorn crops planted in two soil management zones under the grower's operation. The evaluation process involved a comparison between outputs created by *VRI–DSS* using its default parameters (Scenario-virtual) and outputs simulated with local data (Scenario-local).

The results indicate that the *VRI-DSS* performed well, and its virtual weather model provided an accurate estimation of evapotranspiration (R^2= 0.79, bias= –0.19 mm d^{-1}, *MSE*= 0.28 mm d^{-1} and *RMSE*= 0.53 mm d^{-1}), except for some larger rainfall events when it overestimated total rainfall by +12%. Water use efficiency varied considerably for the two soil management zones, providing evidence for the benefits of variable rate irrigation at this site. The two zones produced similar yields but required different irrigation schedules, the finer textured soil zone having higher water use efficiencies than the coarser textured soil zones.

Overall, the evaluation revealed that *VRI–DSS* with accurate climate data provides a practical tool to estimate the needs of irrigation for maize and sweet corn. It showed

potential as an effective *VRI* control system for complex soil-crop combinations that might occur under any one irrigation system. Further testing is required with other crops and soil types and with site-specific rainfall data to validate this decision software system.

Keywords: Irrigation scheduling; *VRI–DSS*; Dynamic decision support system; Soil water balance; *VFM* climate models; Water stress; *VRI* centre pivot.

8.1 Introduction

Worldwide, irrigation uses about 70% of available freshwater resources (FAO, 2015). In New Zealand, irrigation accounts for 78% by total water allocated (Booker et al., 2016). Some important agricultural areas on New Zealand's east coast, located in the rain shadow of the Southern Alps, and parts of Hawke's Bay, are already facing limitations associated with a shortage of available water (Dark et al., 2017).

The challenge for the agricultural sector is to maximize the economic return per unit of water used. This will involve more proper water allocation mechanisms (De Fraiture et al., 2007; Molden et al., 2007) such as appropriate methods to observe, measure, and respond to field and crop conditions.

Variable-rate irrigation (*VRI*) systems precisely match water application with crop requirements, and they are especially useful where there are variations in soil, landscape, and plant performance (Evans et al., 2013). However, the success of *VRI* equipment relies on well-informed irrigation scheduling. Specifically, *VRI* requires correct irrigation timing and placement in order to maximise production and minimise adverse environmental impacts. Hedley and Yule (2009a) reported that *VRI* scheduling can save approximately 25% of the water applied compared with the uniform application of irrigation.

Irrigation scheduling decision support systems (*DSS*) provide advice on when and how much to irrigate. Many *DSS* have been developed to enhance irrigated crop management within a single field or several fields to maximize total yield over the area (Rinaldi & He, 2014). Here we define a *DSS* as an interactive, computational system that involves the

formulation and integration of three main components: a database; an administrator model; and a graphical user interface. In addition, a *DSS* should be able to incorporate the decision maker's own insights (Rinaldi & He, 2014).

Numerous *DSS* have been developed in the last decade (Rinaldi & He, 2014). Smith (1992) developed an empirical *DSS* (CropWat). The model, which considers climate, soil, and crop data, is based on the FAO Irrigation and Drainage Papers No. 56 "Crop evapotranspiration" and No. 33 "Yield response to water," and uses the Penman-Monteith equation and respective crop coefficients to calculate crop evapotranspiration (ET_c) rates.

Steduto et al. (2009) developed a *DSS* (AquaCrop) based on FAO Irrigation and Drainage Paper No. 33 "Yield Response to Water" (Doorenbos & Kassam, 1979). The model is used for developing a seasonal irrigation schedule for a specific crop and field, identifying the date of the next irrigation, determining seasonal water requirements, and developing water production functions and using them in economic decision tools. In China, Zhang and Feng (2009) developed an irrigation *DSS* (CropIrri) to operate the optimal allocation of water resources in irrigation districts. The CropIrri system was designed for dryland crops (wheat, maize, and soybean).

In Australia, the IrriSatSMS *DSS* model was developed. It uses satellite-derived crop coefficients in a daily water balance approach (Car et al., 2012). This *DSS* does not inform specifically when or how much to irrigate but instead suggests a fixed amount on any given day, to return soil water deficit (*SWD*) to zero. The *DSS* HydroLOGIC was also designed in Australia (Richards et al., 2008), mainly to evaluate the consequences of several irrigation strategies and to explore options to optimize yield and water use efficiency (*WUE*) in cotton at field level.

In New Zealand, the Foundation for Arable Research (*FAR*) and Plant and Food Research developed the *DSS* AquaTRAC™. The system estimates crop water demands using a soil water balance (*SWB*) model with inputs related to crop type, soil type, weather, and irrigation to date.

Most of the current *DSS*s mentioned above were developed to output a single recommendation for when and how much irrigation to apply to optimise yield for any one crop. However, a dynamic *DSS* has recently been developed in a Geographic Information System (*GIS*) framework to be integrated with a *VRI* system to account for within-field

variability of soils, which often results in the delineation of soil management zones (http://www.myfieldnet.com/fieldnet-advisor). This *DSS* also manages multiple crops under one *VRI* system to give farmers the immediate ability both to activate or modify their irrigation decisions (e.g. irrigation depth). This type of system is required to improve *WUE*, e.g. (O'Shaughnessy & Evett, 2010; Vellidis et al., 2008). The *DSS* should incorporate up-to-date information on weather and crop demand predictions and irrigation scheduling options. The benefit of virtual climate forecast models (*VFM*) for irrigation scheduling *DSS* and crop production has been demonstrated by several authors (Gowing & Ejieji, 2001; Wang & Cai, 2009).

The *VFM* (e.g. *GDAS*, *GEFS*, *CFS*; (Saha et al., 2010; Yuan et al., 2011) uses a global numerical weather prediction system to generate either short-term weather forecasts or longer-term climate predictions in different countries worldwide. It uses current weather observations relayed from weather satellites and/or other observing systems as inputs. The weather observations serve as input to the numerical computer models through a process known as data assimilation to produce outputs of temperature, precipitation, and other meteorological elements from the oceans to the top of the atmosphere.

The objective of this study was, therefore, to determine whether a dynamic model-based and spatially structured *DSS* for variable-rate irrigation systems (*VRI–DSS*) can be reliably used as a scheduling tool for farmers in New Zealand.

To do this we aimed to evaluate the ability of the *VRI–DSS* to predict the critical *SWD* at which irrigation is simultaneously scheduled to two crops in two soil management zones under one system.

An additional objective was to quantify differences in *VRI-DSS* outputs of soil moisture deficit against those predicted by local climate and moisture data inputs.

8.2 Materials and Methods

8.21 Study area

The study area is a 101-ha commercially farmed field (39. 533° S; 176.402°E). The climate is humid, and the annual rainfall is about 679 mm (www.niwa.co.nz). Irrigation is needed to supplement rainfall in summer to meet crop water needs. The field is currently irrigated by a 580-m long *VRI* centre pivot system that applies water pumped from a nearby groundwater well. The weekly allocations described in Table 8.1 are typically related to the maximum volumes used during a dry summer. The total weekly allocation is 31,700 m^3 per week. The crops irrigated by this system in the 2017/2018 growing season are listed in Table 8.2.

Table 8.1: Consented fresh water takes and water allocation at the field site.

Weekly water allocation (m^3/week)	Centre pivot area (ha)	Average application depth (mm d^{-1})	Pivot rotation time (days)	Max. irrigation depth (mm)
31,700	102	4.5	2.5	25

Table 8.2: Area, cultivation and harvest date of 2017/2018 crop year at the study site.

Crop	Area (ha)	Cultivation date	Harvest Date
Squash	4.36	27 January 2017	16 May 2017
Peas	21.18	5 July 2017	12 September 2017
Spring Barley	8.08	2 August 2017	17 January 2018
Baby Carrots	6.36	15 September 2017	23 December 2017
Maize	23.46	18 October 2017	15 March 2018
Sweet Corn	37.56	30 November 2017	29 March 2018

8.22 Irrigation management zones

The soils at the study site have formed on an alluvial surface. An electromagnetic (*EM*) sensor survey was carried out at 12-m-swath widths using a Dualem-1S with an exploration depth of 0.5 m to measure their apparent electrical conductivity (EC_a), which is a surrogate measurement of soil texture and moisture in non-saline soils (e.g. Doolittle and Brevik (2014). The EC_a map was produced from the *EM* survey at a 5-m spatial resolution using ordinary kriging in R version 3.4 (R Core Team, 2018) using the gstat package (Pebesma, 2004). The EC_a map was further split into two classes (irrigation management zones) using k-means clustering. This supported a conventional soil survey that ground-truthed the *EM* map and described the observed soil profile differences at a scale of 1:10,000.

8.23 Experimental setup

Maize (*Zea mays*., cv. 'P1253') and sweetcorn (*Zea mays* L., cv. 'GSS8357') were planted with a row spacing of 0.76 m into parts of the study area. To take measurements and observations of the soil and crop to evaluate the performance of *VRI–DSS*, four replicated plots (20 × 15 m) were established in each soil zone for each crop. All plots had the same fertilizer management during the crop season, and the farmer scheduled irrigation for the plots and the rest of the field using *VRI–DSS*. Four replicated neutron access tubes were installed into each of the four replicate plots in each soil zone for each crop (see Fig. 8.2). The *SWD* was determined by subtracting the average soil moisture content (*SMC)* of the four neutron-probe measurements from the field capacity value for that soil (Lenka et al., 2009). The *SMC* measurements started 58 and 15 days after cultivation for maize and sweetcorn, respectively. Local climate data were collected from a climate station situated on the farm.

During the experimental trials, *VRI–DSS* recommended irrigation amounts for each crop that can immediately be put into action, modified or declined by farmer decision. The *VRI–DSS* model was then automatically updated according to farmer decision and

reported any potential yield reduction with recommendations for the next irrigation event. Irrigation timing was based on the critical *SWD* (0.4 total available water (*TAW*)) for each treatment (i.e. soil-crop combination) with a maximum irrigation amount set at 25 mm (Table 8.1).

8.24 Soil sampling

Soil cores were extracted from 6 locations (3 for each soil zone) at 0.2-m intervals to a depth of 1 m to estimate available water content (*AWC*, cm^3 cm^{-3}), saturated hydraulic conductivity (K_{sat}, mm hr^{-1}), cation exchange capacity (*CEC*, meq/100g), and soil organic carbon (*C*, %).

Three replicate soil samples were also collected from each plot at harvest at 0.15-m intervals to a depth of 0.45 m to estimate mineral nitrogen, which is the plant available fraction of the total nitrogen in the soil profile.

8.25 Lab analysis

Laboratory analysis included measurements of (i) *AWC* by draining a proportion of collected intact soil cores between pressure potentials of –10 and –1500 kPa (Gardner, 1986; McQueen, 1993), (ii) K_{sat} was determined by measuring the flow of draining water maintained under a head of 10 mm (Clothier & White, 1981; Klute & Dirksen, 1986), (iii) *CEC* was determined by the 1 M ammonium acetate (pH 7) method (Blackmore et al., 1987), (iv) total *C* was measured using a Leco TruMac which utilises the Dumas dry combustion principle (Leco, 2003), and (v) Mineral nitrogen (*NH4-N* and *NO3-N*); ammonium and nitrate were extracted with 2M KCl using a 1:10 soil: extractant ratio and a 1 hour end-over-end shake followed by filtration (Blackmore et al., 1987) and then quantified using a QuikChem 8500 flow injection analyser.

All soil preparation and laboratory analyses were undertaken at the Manaaki Whenua Environmental Chemistry Laboratory, Palmerston North, New Zealand. (http://www.landcareresearch.co.nz/resources/laboratories/environmental-chemistry-laboratory)

8.26 Operation of the *VRI–DSS* software

The *VRI–DSS* is a single integrated platform designed to schedule and control *VRI* sprinkler irrigation systems (http://www.myfieldnet.com/fieldnet-advisor). It automatically generates prescription maps that are dynamically optimized on a daily basis using a *SWB* modelling approach. The *SWB* approach is a recommended and commonly used method for tracking crop water needs and irrigation scheduling (Allen et al., 1998). It is based on the conservation of mass, which states that the change in soil water storage (ΔS) of the root zone of a crop is equal to the difference between the amount of water added to the root zone (Q_i), and the amount of water lost or withdrawn (Q_o) (Hillel, 1998) in a given time interval as in Equation (8.1). The *SWD* is tracked by accounting for all water additions (precipitation, irrigation, and capillary rise) and subtractions (crop evapotranspiration, surface runoff, and drainage) from the soil root zone (Allen et al., 1998) as in Equation (8.2). Irrigation is required when a critical *SWD* level of the root zone (in millimeters) has been reached.

$$\Delta S = Q_i - Q_o \qquad [8.1]$$

$$SWD_2 = SWD_1 - IR - R - CR + RO + ET_c + DP \qquad [8.2]$$

where SWD_1 and SWD_2: daily beginning and ending total available root zone soil water deficit (mm), respectively, *IR*: irrigation (mm), *R*: precipitation (mm), *CR*: capillary rise (only relevant where the water table is within 2–3 metres of the soil surface), ET_c: calculated crop water use, or evapotranspiration (mm d^{-1}), *DP*: deep percolation or drainage out of the root zone (mm) and *RO* is surface runoff.

The initial depletion was measured and updated to the *VRI–DSS* model at the beginning of the season. *RO* was assumed to be negligible as the field was almost flat and irrigation was observed to easily infiltrate into the soil. *CR* was also assumed to be zero as the water table was > 1 m below the bottom of the root zone (Allen et al., 1998).

VRI–DSS uses a global *VFM* (e.g. explained by Dueben and Bauer (2018); Yuan et al. (2011)) to predict daily potential evapotranspiration (ET_o) values. The ET_o model and locally calibrated crop coefficient (K_c) function values were used to estimate ET_c, *SWD*

and irrigation schedules.

The average measured *TAW* (mm) values of 190 mm and 273 mm for Zone 1, and Zone 2, respectively, were used for *VRI–DSS* irrigation scheduling.

Irrigation was triggered when the *SWD* was equal to an average fraction of 0.4 *TAW*. The constant values for the irrigation trigger (critical soil moisture deficit) for each specific growing period were at 0.14, 0.44 and 0.6 *TAW* for initial, mid and late crop stage, respectively. Linear interpolation for crop parameters (K_c and rooting depth) and irrigation trigger values were used between growth stages. The measured effective rooting depths during the growing season were used, reaching a maximum value of 1 and 0.8 m for maize and sweetcorn, respectively.

Following McMaster and Wilhelm (1997), *VRI–DSS* determines the growth stage of the crop using growing degree day units (*GDD*s) after emergence in preference to the number of days after emergence.

$$GDD = \frac{T_{max} + T_{min}}{2} - T_{base} \qquad [8.3]$$

Where T_{max} and T_{min} are daily maximum and minimum air temperature, T_{base} is the base temperature (°C) below which crop growth ceases; and it ranges from 0 to 10 °C. T_{base} varies among crop species and likely varies with growth stage.

Fig. 8.1 shows the *VRI–DSS* procedures and structure for scheduling irrigation at the trial site. A soil map of the irrigated area and information for the different crops (crop type, hybrid, planting date) is loaded into *VRI–DSS* platform, which then uses all this information along with the *VFM* data to generate an optimized irrigation recommendation and daily *VRI* prescription maps. In turn, these maps are actioned by software control. *VRI–DSS* also estimates the amount of yield that would be lost due to daily water stress, which varies based on the crop's development stage and the severity of the stress (Steduto et al. (2012).

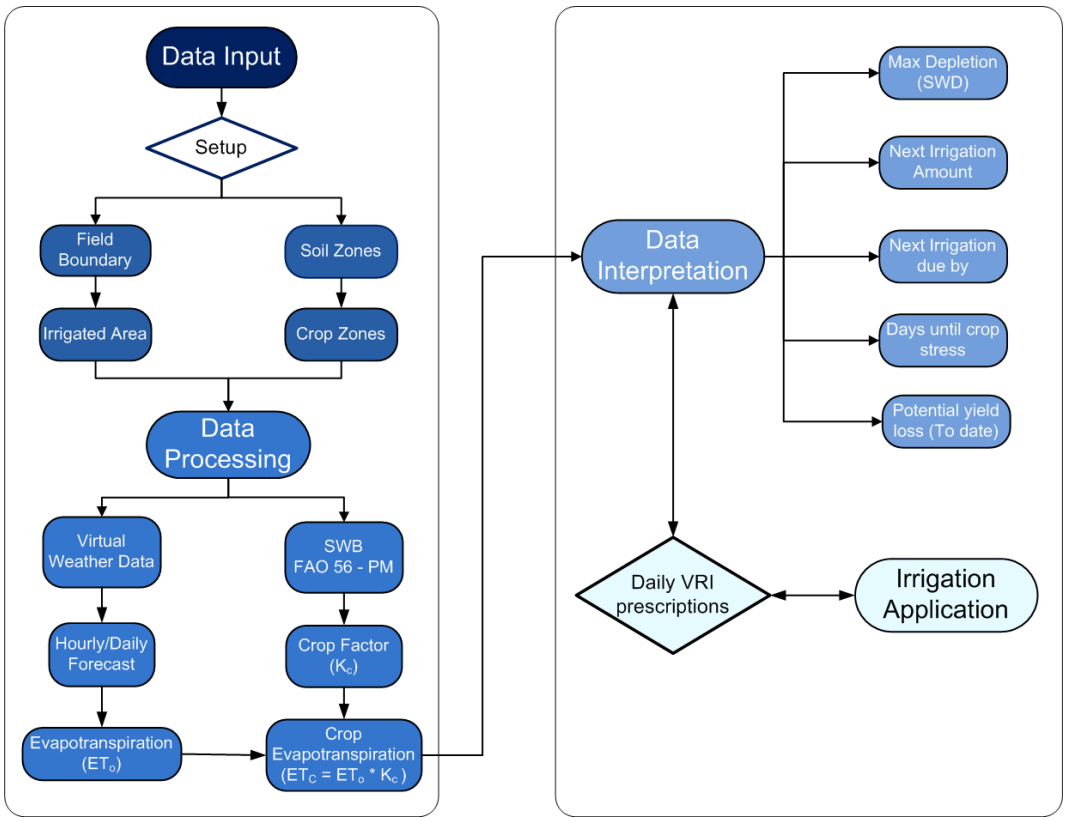

Figure 8.1: Schematic of the *VRI–DSS* for irrigating maize and sweetcorn crops.

8.27 Yield assessment

Grain yield was measured in order to calculate the *WUE* for the different soil-crop treatments. The crop yields were assessed in each plot (Fig. 8.2) by harvesting the plants in a 5-m length of two adjacent rows. This process was repeated four times on each plot. The number of plants was counted, and the weight of the cobs and grain was measured (fresh yield). Yield is reported on an oven dry-weight basis (70ºC).

The water use efficiency (*WUE*) was estimated as the kilograms of crop yield per m^3 of water (rainfall plus irrigation) applied (kg m^{-3}) as described by (Gregory, 2004):

$$WUE = \frac{Y}{IR + R} \qquad [8.4]$$

Where Y: Yield per unit area (g/m^2), $IR + R$: Water used to produce that yield per unit area (mm).

8.28 Statistical Analysis

ANOVA and Tukey's honestly significant difference (*HSD*) test were conducted to investigate any significant differences of measured soil properties (*AWC*, K_{sat}, *CEC*, *C* and Mineral nitrogen), grain yield, and *WUE* data between the two soil management zones. The Kolmogorov-Smirnov test of normality (*KS*) was carried out. All significant differences were evaluated at the 0.05 level. Data analyses performed in this study were carried out using the 'stats' package in R version 3.4 (R Core Team, 2018). Linear regression relationships with performance indicators: coefficient of determination (R^2), bias, mean absolute deviation (*MSE*), and root mean square error (*RMSE*) (Cohen Liechti et al., 2012; Moazami et al., 2013) were applied to compare outputs (temperature, solar radiation, humidity, ET_o and ET_c) from the *VRI–DSS* against on-farm measurement data.

8.3 Results and Discussion

8.31 Delineating the field into irrigation management zones

The soil survey map for the field site showed two different soil types: a Twyford sandy loam and a Kaiapo silt loam (Fig. 8.2), which correspond to Fluvisols and Gleyic Fluvisols in the FAO World Soil Reference Base (Michéli et al., 2006), respectively. The Twyford sandy loam is distinguished by the presence of coarse, relatively un-cohesive sands throughout the profile, and topsoil with a sandy loam texture. It is excessively well-drained soil. The Kaiapo silt loams have a finer texture, which contributes to relatively slow internal drainage. It is classified as a poorly drained soil. There was an agreement between field observations and EC_a patterns (Fig. 8.2). Based on this information, the field was delineated into two irrigation management zones (Zone 1 and 2).

Comparison of soil properties (*AWC*, K_{sat}, *CEC*, and *C*) between the two soil zones for the soil profile from 0 to 1 m are shown in Fig. 8.3. The statistical analysis showed that there is a significant difference (p values < 0.05) in mean *AWC* and *CEC* between the

two soil zones. The *C* values were small and not significantly different in the top 0.2 m (p values > 0.05). These analyses support the claim that Zone 1 has a significantly coarser texture (sandy loam soil) and lower *AWC*, *CEC* and higher K_{sat} compared with Zone 2 (silt loam soil).

The soil survey map and site-specific measurements suggest that the variability in *AWC* and K_{sat} across the field is sufficiently large to warrant the use of *VRI*. This variability is mostly explained by the large differences in texture between the soils in the two zones described above.

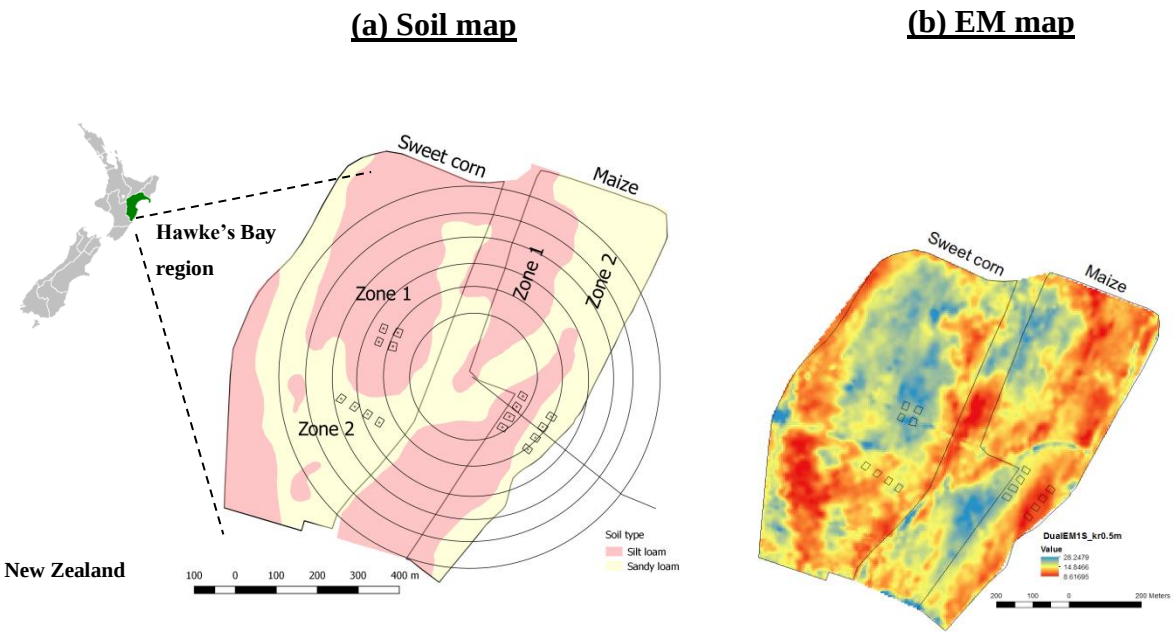

Figure 8.2: (a) soil survey map (Manderson map "unpublished") and experimental plots (Otane, Hawke's Bay, New Zealand) for two soil management zones defined for maize and sweetcorn crops. Zone 1: sandy loam, Zone 2: silt loam. Sweetcorn area: 37.56 ha, Maize area: 23.46 ha. (b) Delineated irrigation management zones based on the electric conductivity (EC_a, mS m^{-1}).

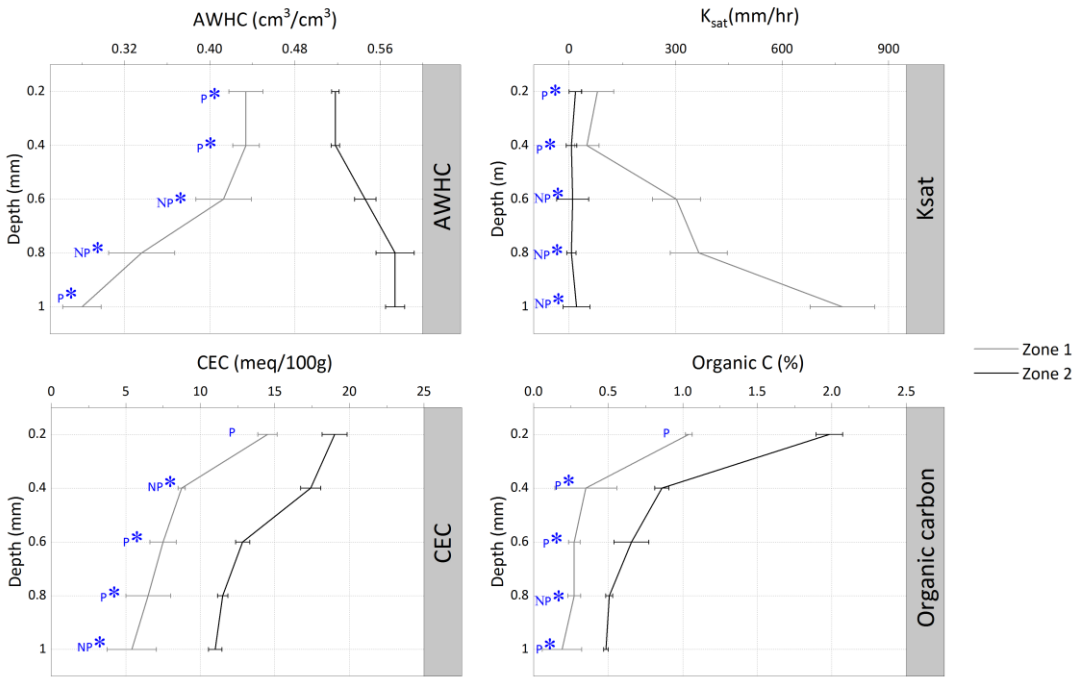

Figure 8.3: Comparing available water content (*AWC*, $cm^3\ cm^{-3}$), saturated hydraulic conductivity (K_{sat}), cation exchange capacity (*CEC*) and organic carbon (*C*, %) measurements between the two soil zones. *P*= parametric test. *NP* = non-parametric test. * The mean difference is significant at the 0.05 level.

8.32 Evaluating the *VRI-DSS* System

The following section provides a comparison of the default *VRI-DSS* outputs (Scenario-virtual) with simulated *VRI-DSS* outputs using local data (Scenario-local).

8.321 Validation of virtual climate data

To assess the potential impact of climate data on estimates of crop water use, the virtually predicted daily climate data (*VRI–DSS*) were compared with climate data measured on farm (Fig. 8.4). The average daily ET_o predicted by *VRI–DSS* showed a significantly high correlation and low biases and error with the observed local data (R^2= 0.79, bias= –0.19 mm d^{-1}, *MSE*= 0.28 mm d^{-1} and *RMSE*= 0.53 mm d^{-1}).

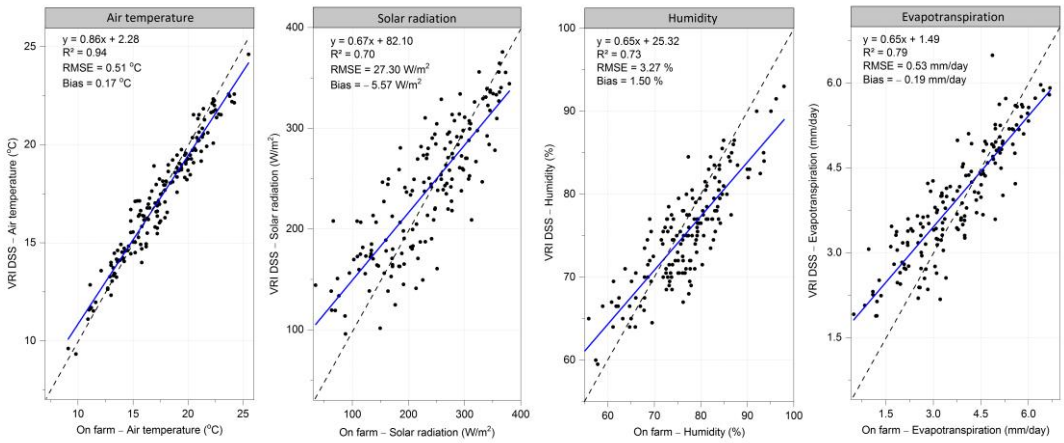

Figure 8.4: The relationships of daily measured air temperature (°C), solar radiation (W m^{-2}), humidity (%), and reference evapotranspiration (ET_o, mm) at farm site with estimated values by *VRI–DSS*'s virtual weather model (*VFM*).

The total amount of rainfall during the period of these trials was overpredicted by the virtual forecast model (*VFM*) in *VRI-DSS* by 12% (28 mm) compared with the local measurement (228 mm compared with 200 mm). This was mainly due to three large rainfall events. The largest discrepancies of virtually predicted rainfall were 15–25 mm, occurring after 85–87, 132, and 142 days planting, respectively. This illustrates the challenge of reliably predicting rainfall for a small area using climate models (Austin, 1987; Gebrechorkos et al., 2018; Rico-Ramirez et al., 2007; Schmidt et al., 2009) and is accentuated in areas such as New Zealand where the topography is complex and characterized by multiple and regionally variable rainfall regimes (Schmidt et al., 2009). On-going refinements to the *VFM* software component are occurring to reduce discrepancies between predicted and actual rainfall data.

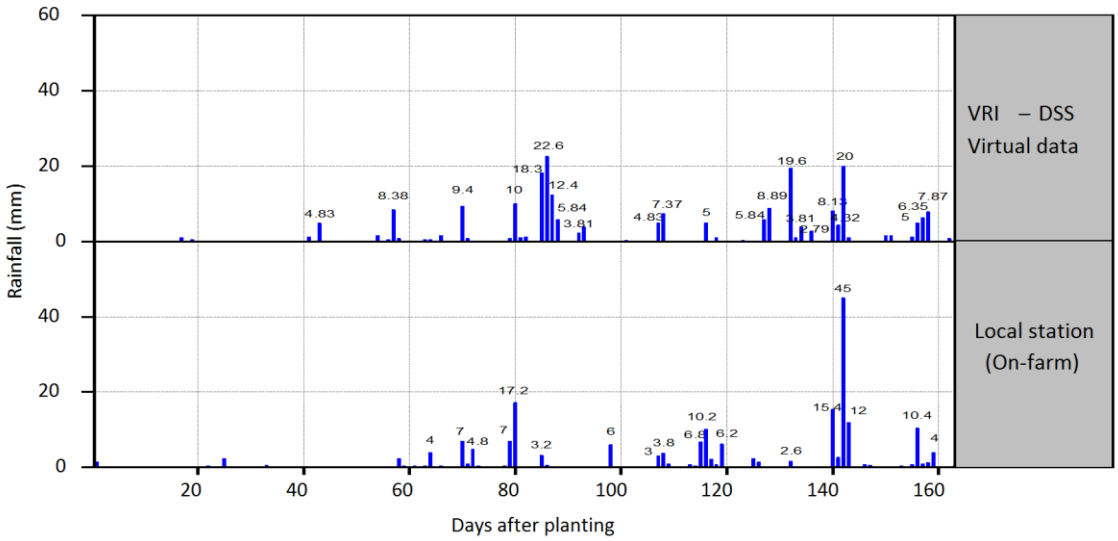

Figure 8.5: Comparisons of daily rainfall (mm) events, estimated by *VRI–DSS*'s virtual model (*VFM*) and recorded by on-farm climate station.

8.322 Comparison of irrigation scheduling for two scenarios

We compared the irrigation schedules generated by *VRI–DSS* using virtual climate data (Scenario-virtual) with the schedule simulated with on-farm climate data (Scenario-local) (Figs 8.6 and 8.7); and the virtually predicted *SWD* against the *SWD* estimated using the *SMC* measured by a neutron-probe (Fig. 8.8). Figs. 8.6 and 8.7 show that the recommended irrigations of *VRI–DSS*'s scenarios and the actual irrigation applied by the farmer.

During the maize trial, Scenario-virtual scheduled 9 and 7 irrigations events for Zone 1 and Zone 2, respectively, with a total amount of 225 and 170 mm for Zone 1 and Zone 2, respectively. Scenario-local scheduled 13 and 10 irrigations events for Zone 1 and Zone 2, respectively with a total amount of 280 and 210 mm for Zone 1 and Zone 2, respectively. During the sweetcorn trial, Scenario-virtual scheduled 3 and 2 irrigation events for Zone 1 and Zone 2, respectively with a total amount of 100 and 75 mm for Zone 1 and Zone 2, respectively. Scenario-local scheduled 7 and 6 irrigation events for Zone 1 and Zone 2, respectively with a total amount of 145 and 120 mm for Zone 1 and Zone 2, respectively.

Therefore, Scenario-virtual scheduled less irrigation than Scenario-local (Table 8.3), and we hypothesise that this is largely due to the overpredicted rainfall 80 – 87 days after planting (Fig. 8.5).

Water-allocation restrictions and operational constraints of the system caused some actual amounts applied by the farmer to differ from amounts recommended by *VRI-DSS* for the maize crop (Figs. 8.6 and 8.7 and Table 8.3).

Note the centre pivot was also managing irrigation to barley and carrot crops (Table 8.1) during the first 60 days of our trials. Insufficient water allocation from the regional council causes the farmer to reduce recommended irrigation to the maize and sweetcorn crops.

In addition, due to the operational constraints of the 580-m long pivot, there was a delay in applied irrigation of one–two days from the recommended time. It takes approximately 60 h for the pivot to complete one full circle applying 4.5 mm of water. Because *AWC* is relatively small in Zone 1, the delay in applied irrigation results in the *SWD* increasing rapidly and the crop experiencing water stress. Given the time it took to complete an irrigation event, it appears the irrigation trigger for Zone 1 could have been lower (e.g. 0.30 *TAW*). In dry seasons and/or periods of reduced access to water resources (allocation restrictions), the *VRI-DSS* for long centre-pivot irrigation systems may need to be adapted to practice deficit irrigation– a strategy which maintains the soil profile in a drier condition, as described by (Liang et al., 2016; Vellidis et al., 2016).

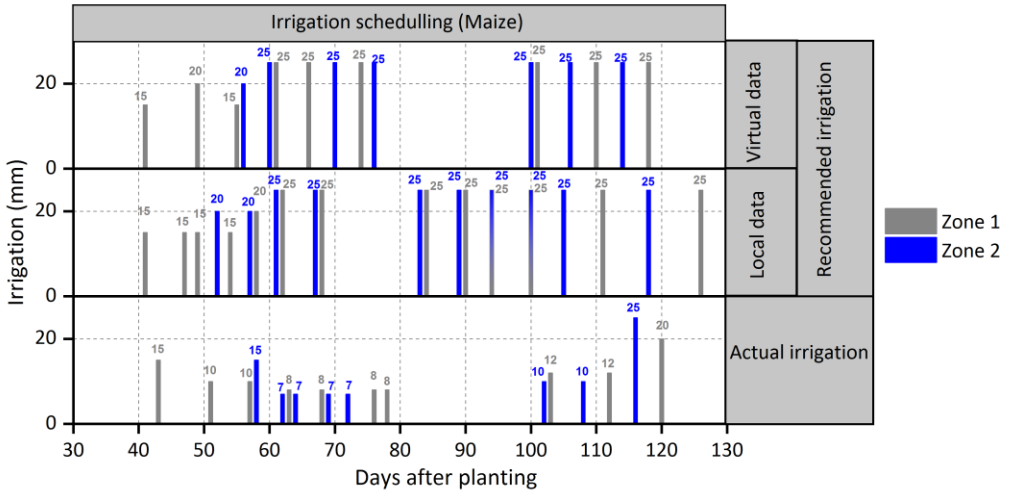

Figure 8.6: Comparing the irrigation recommendations of *VRI–DSS*'s scenarios and actual irrigation applied by the farmer for maize.

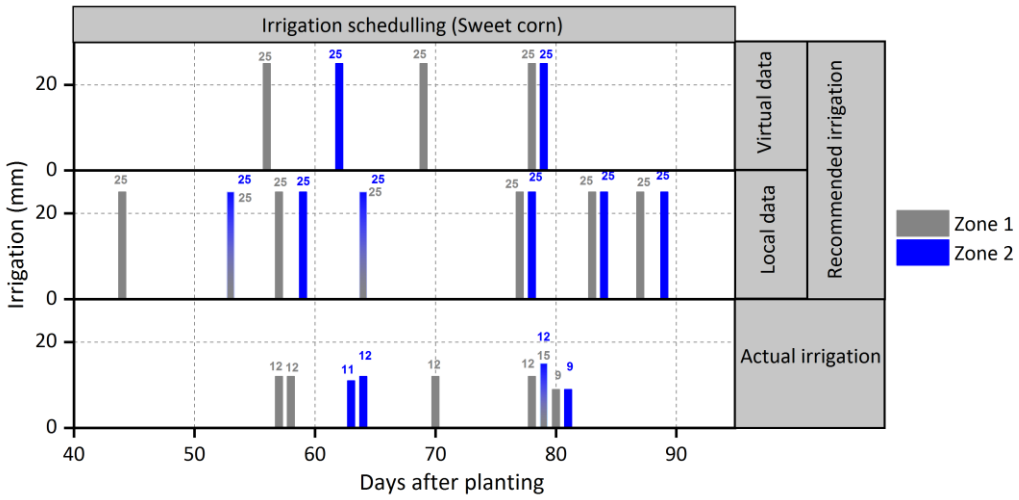

Figure 8.7: Comparing the irrigation recommendations of *VRI–DSS*'s scenarios and actual irrigation applied by the farmer for sweet corn.

Table 8.3: Amounts (mm) of irrigation water applied for the *VRI–DSS*'s scenarios and actual irrigation applied by the farmer for sweet corn

	Maize			Sweet corn		
	Scenario-virtual	Scenario-local	Actual irrigation	Scenario-virtual	Scenario-local	Actual irrigation
Zone 1	225	280	131	100	145	82
Zone 2	170	210	95	75	120	54

8.323 Comparison of crop evapotranspiration for two scenarios

The daily estimated ET_c for each zone for Scenario-virtual compared with Scenario-local using actual irrigation is shown in Figure 8.

The estimated ET_c appears to increase as the rainfall or irrigation level increased, suggesting that evapotranspiration had not been occurring at its potential rate. Daily estimated ET_c was similar for the two scenarios for the first 80 days after planting and after that, Scenario-local had less estimated ET_c than Scenario-virtual due to lower rainfall impact until 128 days after planting. The rainfall had a significant effect on ET_c calculations and the *VRI–DSS*'s scenarios correlation for maize crop. The cumulative estimated ET_c did not differ significantly between the two scenarios for the sweet corn

crop (325.6 and 332.3 mm for Scenario-virtual and 301.4 and 316.7 mm for Scenario-local) and this is because the period of water deficit was not significant between both scenarios (Figs. 8.7, 8.8, and 8.9). In contrast, there was a large difference between cumulative estimated ET_c for the maize crop and Scenario-local (384.4 and 415.3 mm for Scenario-virtual and 345.4 and 374.6 mm for Scenario-local) due to the long stress period compared with Scenario-virtual (Figs. 8.7, 8.8 and 8.9).

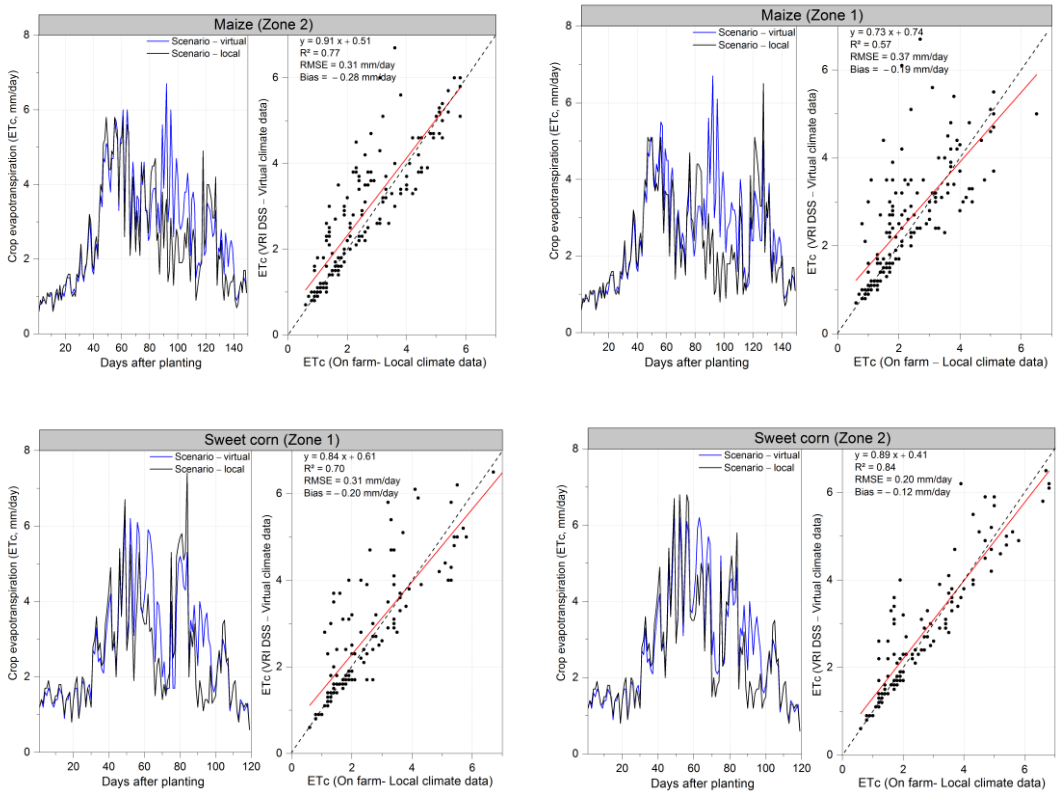

Figure 8.8: Comparisons of daily estimated crop evapotranspiration (ET_c) in each zone for Scenario-virtual with Scenario-local using actual irrigation.

8.324 Comparison of soil water deficit for two scenarios

Fig. 8.9 show the progression of *SWD* estimated by *VRI–DSS* using actual irrigation compared with *SWD* calculated using the neutron-probe soil moisture data through the growing season.

The overestimation of rainfall in Scenario-virtual (52 mm for virtual data and 3 mm for on-farm data) after 80–87 days of planting (Fig. 8.5) indicated that the *SWD* was less than the actual allowable amount, while Scenario-local showed the soil was drier.

The maize crop initially went into stress (*SWD* > crop stress threshold) after 53 and 90 days of planting for Zone 1 and Zone 2, respectively, in both scenarios. After 118 and 125 days of planting, the rainfall and irrigation were enough to indicate non-water-stress conditions for Scenario-local and virtual.

In Scenario-virtual, sweetcorn was considered non-water stressed for both zones during the whole season. Scenario-local indicated that short water-stress conditions started between 60 and 80 days after planting for Zone 1 and Zone 2, respectively.

The *SWD* in Scenario-local and the measured *SWD* showed very similar trends in each zone during the growing season for each crop trial. This indicates that *VRI–DSS* was able to track the *SWD* accurately when using local climate data.

The above results indicate that the *VRI–DSS* model with local climate data was predicting *SWD* well enough to be used for making *VRI* irrigation scheduling decisions. The *VRI–DSS* – sweetcorn model provided the depth of irrigation water needed to bring the *SWD* above the irrigation trigger, taking into account a maximum irrigation amount of 25 mm (Figs. 8.6, 8.7, and 8.9). For the sandy loam soil (Zone 1), soil water depletion was relatively rapid, and irrigation quantity was more. When the soil texture became finer (i.e. Zone 2), *SWD* was slowed down, and the irrigation requirement was less.

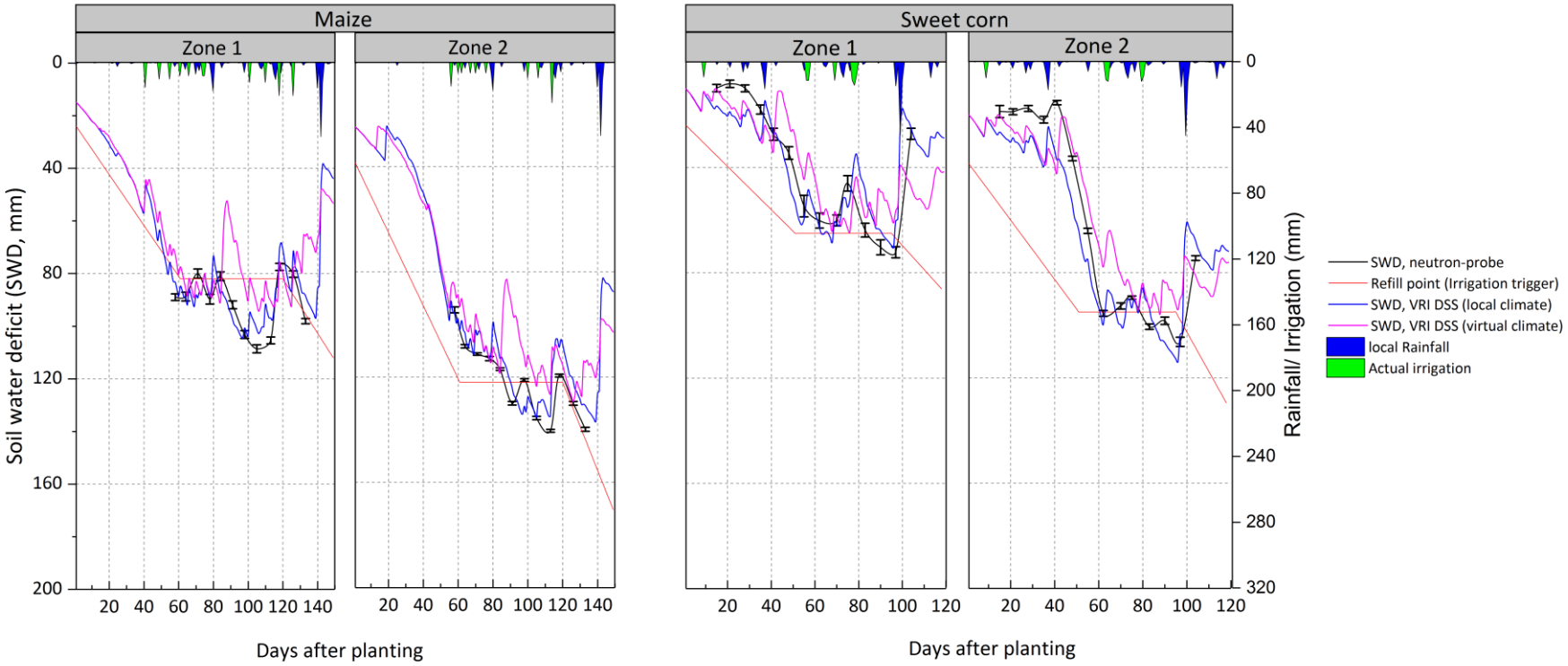

Figure 8.9: Estimated soil water deficit (*SWD*, mm) for *VRI–DSS* (virtual climate and local climate data) with actual irrigation versus average *SWD* measured by neutron-probes in each management zone for maize and sweet corn crop. The *SWD* measured by neutron-probes was determined by subtracting the neutron probe volumetric soil moisture measurement from field capacity for each depth increment.

8.33 Soil nitrate content for the two soil zones

There was no significant difference in *NO3-N* and *NH4-N* levels in the upper 45 cm of soil at harvest, despite some evidence for higher soil nitrate content in Zone 2 than Zone 1 (Table 8.4) for both crop trials. Therefore, we can conclude that *N* fertility was not a contributing factor and moisture differences played a major impact on crop growth and yield for this experimental trial.

Table 8.4: ANOVA and Tukey's HSD test's result (mean ± standard error) for nitrate content *(NO3-N* (mg kg^{-1})) and ammonium content (*NH4-N* (mg kg^{-1})) in the upper 45 cm of soil at harvest. *P* = parametric test. The same lowercases represent no significant differences between the two zones.

	Zone 1	Zone 2
	Maize	
NO3N^{P}	14.3 ± 4.0 ^{a}	20.7 ± 2.6 ^{a}
NH4N^{P}	1.0 ± 0.2 ^{a}	0.5 ± 0.2 ^{a}
	Sweet corn	
NO3N^{P}	14.0 ± 5.4 ^{a}	25.9 ± 6.7 ^{a}
NH4N^{P}	0.4 ± 0.1 ^{a}	0.8 ± 0.1 ^{a}

8.34 Yield assessment and water use efficiency for the two soil zones

The actual yield difference between Zone 1 and Zone 2 for both crop trials is shown in Table 8.5. The responses of yield to water stress level were different between the two zones. Maize yield for Zone 1 = 1180.35 g m^{-2} (11.80 T ha^{-1}) was lower than Zone 2 = 1355.17 g m^{-2} (13.55 T ha^{-1}), and significantly different. The sweetcorn yield was consistent = 1385.62 and 1408.20 g m^{-2} (37.5 and 38.5 T ha^{-1}) for Zone 1 and Zone 2, respectively. This could be attributed to the non-significant difference in water-stress conditions (short period) for sweetcorn zones (Fig. 8.9).

Actual water applied to the *VRI–DSS*, Zone 2 treatment was 27% and 34% less than the Zone 1 treatment for maize and sweetcorn, respectively. The *WUE* equals the amount of

grain produced by irrigation water divided by the amount of irrigation water applied. The *VRI–DSS*, Zone 2 treatment had the highest *WUE* because of the less irrigation water applied. This result showed the *VRI–DSS* management was able to use irrigation water more efficiently.

Table 8.5: Average dry-mass yield and water use efficiency (*WUE*) (mean ± standard deviation) in each zone. * The mean difference is significant at the 0.05 level. Same letters indicate *P* > 0.05 (not significantly different).

Treatment	Avg. Yield ($T\ ha^{-1}$)	*WUE* ($kg\ m^{-3}$)	Avg. Yield ($T\ ha^{-1}$)	*WUE* ($kg\ m^{-3}$)
	Maize		Sweetcorn	
Zone 1	11.80 ± 0.59 [a]	9 [a]	13.86 ± 0.23 [a]	16.90 [a]
Zone 2	13.55 ± 0.09 [b]	14.26 [b]	14.08 ± 0.30 [a]	26.07 [b]

8.4 Conclusions

A model-based *VRI–DSS* system was evaluated for maize and sweetcorn crops using local field measurements at a commercial farm in New Zealand.

The case study showed that the *VFM* used for this study provided an adequate prediction of evapotranspiration and overestimate prediction of local rainfall (+12%). This is expected as rainfall events are very sporadic, with large local variations in the temperate, maritime climate conditions of New Zealand, and means that on-going improvements to the *VFM* are occurring and are a focus to improve overall recommendations. Therefore, due to variations in rainfall data, *VRI–DSS* underestimated *SWD* and ET_c. However, when local data was used with *VRI–DSS* to simulate results the *SWD* had very similar trends with that derived from measured *SMC* data. Soil water increase was comparable to applied irrigation in each soil zone for the maize and sweetcorn crop trials, indicating effective use of irrigation by the plant. The soil water was extracted from the whole soil profile in each zone for both crop trials to meet the crop water demand and surface soil evaporation. *WUE* for maize and sweetcorn under variable irrigation rates were improved by the *VRI* irrigation strategy. Maximum values of *WUE* occurred at the Zone 2 treatments, which had a high capacity for water storage. The use of *VRI–DSS* system-based irrigation scheduling allowed two-thirds of the irrigation water to be saved for the

high *AWC* soil (Zone 2) with the same yields as the low *AWC* soil (Zone 1) under these experimental, soil, crop. and climatic conditions.

Further research is required to use *VRI–DSS* with local weather stations and for a greater variety of crops and soil conditions at different sites. In addition, further research is required to investigate the potential integration of the site-specific sensed data presented in Chapters 5, 6 and 7 to refine the *VRI* control software and make it more sensitive to spatial and temporal variability of field conditions.

Connecting text to Chapter 9

This thesis has presented new sensing and modelling approaches that can be used to inform irrigation scheduling at high spatial and temporal resolution. Chapter 9 investigates in more detail the appropriate timing to initiate irrigation based on soil moisture status. It compares two different soil moisture status thresholds for irrigation timing together with their respective water use efficiency performance indicators. The trial used two soil water content thresholds to adjust irrigation timing to field grown spring wheat. It also tests a new version of the *VRI–DSS* software, adapted to receive local rainfall data, based on recommendations from Chapter 8.

Chapter 9

Response of spring wheat (*Triticum aestivum* L., cv. 'Sensas') to soil type and soil moisture status thresholds

Abstract

A model-based decision support software system (*VRI–DSS*) that automates irrigation scheduling was used to schedule irrigation to spring wheat (*Triticum aestivum* L., cv. 'Sensas') using a *VRI* system. This experiment was conducted (1) to evaluate the *VRI–DSS*–Wheat model for scheduling irrigation, and (2) to compare the effects of varying irrigation thresholds on spring wheat grain quality, yield, dry matter, soil water uptake, irrigation water use efficiency (*IWUE*) and crop water productivity (*WP*). Two irrigation threshold treatments at 40% and 60% *AWC* and a rainfed treatment were applied to the spring wheat growing in two different soil types; a sandy loam (Zone 1) and a silt loam (Zone 2) at Massey University's No.1 Farm, Palmerston North, New Zealand.

The results indicated that the crop evapotranspiration rates estimated by the *VRI–DSS*–Wheat model data were similar to the values measured near the study site (R^2= 0.91, *RMSE*= 0.22 mm d^{-1}, and bias= 0.21 mm d^{-1}). The plant height, grain yield, 1000-grain weight, percentage of dressing loss, grain density and total biomass variables were not significantly affected by soil type or by varying the irrigation schedule. Soil-water uptake pattern was affected mainly by the soil type, rather than irrigation. The soil water uptake decreased with soil depth for Zone 1 treatments. The soil water was uniformly taken up from all soil layers for Zone 2 treatments. The 60% irrigated treatments were very comparable to the 40% treatments in terms of *IWUE* and were therefore both applicable *VRI* strategies for increasing *WP* for spring wheat while using 40% less irrigation water due to the soil type effect.

Keywords: Water use efficiency, Irrigation water use efficiency, Variable rate irrigation, Irrigation schedule threshold, Decision support software system, Soil water balance.

9.1 Introduction

The concerns over water availability and water quality increasingly require irrigated agriculture to manage water resources more efficiently. The competition for existing freshwater supplies will require a paradigm shift from maximizing productivity per unit of land area to maximizing productivity per unit of water consumed (Evans & Sadler, 2008), reducing the total amount of water used for irrigation across landscapes (Grafton et al., 2018).

Precision irrigation equipment such as variable rate irrigation (*VRI*) has the potential to minimise the amount of irrigation needed to achieve a desirable yield (Perea et al., 2018). With *VRI*, the application depth, intensity, and timing, as well as the spatial extent of each soil management zone, can now be controlled at levels of precision that had previously been impossible in the large fields of modern agriculture (Evans et al., 2013; Daccache et al., 2015). The *VRI* system is necessary in humid areas such as New Zealand to reduce the risk of excessive irrigation and eliminate many associated problems, where excessive water can increase nitrogen (*N*) losses due to accelerated leaching and/or denitrification. In other words, irrigation scheduling is a critical element in reducing deep percolation and improving water quality downstream.

Several researchers have reported on the main approaches to irrigation scheduling in soils and the available techniques available over the years. A range of reviews has concentrated on measuring soil moisture content (*SMC*) (e.g. Bittelli (2011); Dane and Topp (2002), physiological measurements (e.g. Cifre et al. (2005); Jones (2004a) or water balance calculations (e.g. Allen et al. (1998). The sensor-based approach has typically scheduled irrigation events on the basis of *SWC* status, whether using direct *SMC* measurements with capacitance devices, neutron-probes or TDR-type sensors (Topp & Davis, 1985), tensiometers (Smajstrla & Harrison, 1998).

Best-practice irrigation scheduling requires accurate threshold values for individual crops and soil types (Thompson et al., 2007). These threshold values for scheduling are often expressed as a percentage of soil available water content (*AWC*). A range of *AWC* threshold values (25-70%) has been investigated by many researchers in order to obtain maximum crop yield, and/or water use efficiency (*WUE*) (Allen et al., 1998; Coolong et al., 2012; Yadav et al., 2018). *AWC* threshold values require site-specific assessment as there is considerable uncertainty when fixed values for irrigation scheduling are used (Girona et al., 2002).

The quality and yield response of spring wheat to irrigation is very dependent on how the irrigation is scheduled. The timing and amount of irrigation required by wheat varies with soil type and season (Kang et al., 2002). Kang et al. (2002) concluded that the grain yield response to irrigation varied considerably between seasons due to differences in soil moisture contents and irrigation scheduling. Al-Kaisi et al. (1997) and Xue et al. (2003) reported that the grain yield of wheat was significantly increased with increasing irrigation frequency. Yadav et al. (2018) found that when different quantities of irrigation were used at different growth stages, there was no significant difference in plant height, spikes m^{-2}, grains per spikes, spike length, grain yield and total biomass variables while 1000 grain weight, and harvest index were significantly affected. Khan et al. (2007) reported no difference in yield and yield components when the crop was irrigated according to the full evaporation and half pan evaporation. In contrast to these results, Salunkhe et al. (2014) found significant yield difference between different irrigation scheduling regimes. Khan et al. (2007) also concluded that there was a significant effect of irrigation intervals on grain yield, number of grains per spike, grain weight per spike, and number of tillers per plant.

To increase both the feasibility and acceptance of *VRI* systems, research is required to develop *VRI* decision support systems (*DSSs*) including the *AWC* thresholds at which water should be applied to crops to improve irrigation water use efficiency (*IWUE*) and yield. Numerous *DSSs* have been developed in the most intensive agricultural areas in the world to enhance irrigated crop management within a single field or over several fields to maximize total yield over the area (Rinaldi & He, 2014). The *DSS* generally provides a daily or seasonal irrigation schedule for a specific crop and field, determines the date of

the next irrigation and the seasonal water requirements, develops water production functions, and uses them in economic decision support tools. Most *DSSs* estimate the crop water needs on the basis of (i) a water balance which uses local climate, soil, and crop data (e.g. CropWat (Smith, 1992), AquaCrop (Steduto et al., 2009), CropIrri (Zhang & Feng, 2009), and PlanteInfo Irrigation manager (Thysen & Detlefsen, 2006)), (ii) wireless sensor networks (e.g. Barker et al. (2018); Hedley et al. (2013); Kim et al. (2008); Liang et al. (2016); O'Shaughnessy and Evett (2008)), and recently (iii) satellite-derived image data (e.g. IrriSatSMS (Car et al., 2012), CubeSat-based satellite systems (Aragon et al., 2018)

To our knowledge, no study has been conducted to determine the effects of *AWC* threshold for scheduling irrigation to spring wheat on different soil types in New Zealand. In this study, our objectives were (i) to evaluate a *VRI–DSS* system in a research field irrigated by a *VRI* centre pivot system and planted to spring wheat, and (ii) to investigate the relationship between soil type and irrigation schedule threshold for spring wheat.

9.2 Materials and Methods

9.21 Study site

The experiment was conducted during the 2018/2019 growing season under a 4-ha *VRI* centre-pivot system on Massey University's No.1 Dairy Farm, near Palmerston North, New Zealand (40°22'56.28"S, 175°36'24.72"E, elevation 37 m). The site is located on New Zealand's west coast and has an annual mean rainfall of 980 mm and a mean temperature of 13.3 °C (NIWA, 2018) (www.niwa.co.nz). The soils were formed in greywacke alluvium, and are classified as a Fluvial Recent (Hewitt, 2010). A soil survey of this field site indicated two different soil types: a Manawatū fine sandy loam (Zone 1) and a Manawatū silt loam (Zone 2) (Pollok et al., 2003) (Fig. 9.1). The physical characteristics of the soils are given in Table 9.1 (El-Naggar et al., 2017).

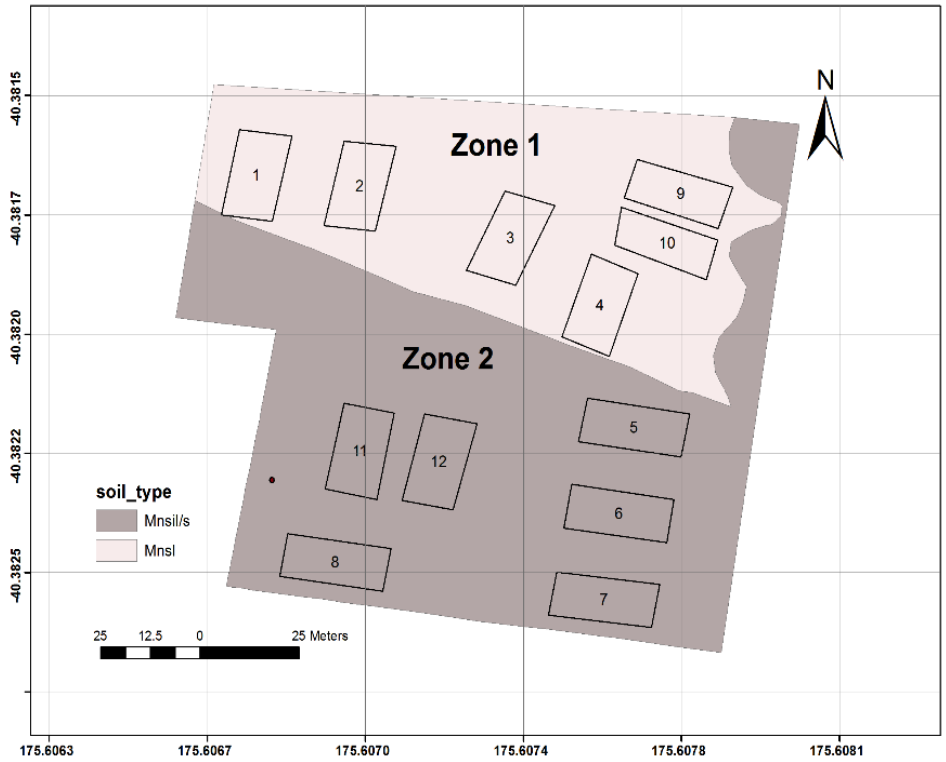

Figure 9.1: Soil map and the experimental plots in each zone based on the soil types (Zone 1, *Mnsl*: Manawatū fine sandy loam (0.7 ha), Zone 2, *Mnsil*: Manawatū silt loam (0.6 ha)) (Pollok et al., 2003)

Table 9.1: Physical properties of the soil (0 – 1 m)

Properties	Soil types/ zones	
	Zone 1 (sandy loam)	Zone 2 (silt loam)
Available water content (mm m^{-1})	123	203
Bulk density (g cm^{-3})	1.41	1.30
Sand (%)	80.6	44.9
Silt (%)	12.7	40.6
Clay (%)	6.7	14.5

9.22 Experimental design and irrigation treatments

The experiment consisted of two irrigation treatments - corresponding to irrigation at thresholds of 40% and 60% *AWC* - and a rainfed treatment. The plots had dimensions of 20 m x 10 m. All treatments were replicated two times in a randomized complete block design (Fig. 9.1 and Table 9.2). At each irrigation event, 25 mm of water was applied each time the soil water in the root zone was depleted by about 40% or 60% of the *AWC* for the two treatments.

Spring wheat (*Triticum aestivum* L., cv. 'Sensas') was planted on 17th November 2018 at a row spacing of 20 cm and a rate of 260 kg. ha^{-1}. The plants emerged on November 25, 2018 and were harvested on February 28, 2019. All treatments were fertilized equally (260 N kg ha^{-1}).

Irrigation water was applied by an 86-m *VRI* centre pivot system (1 span, 31 sprinklers, spray radius of 5 m and a flow rate of 26.3 m^3 h^{-1}) using the *VRI–DSS* scheduling program. All treatments received the same depth of water from spring rainfall at the beginning of the crop trial until the midpoint of the season, bringing the *SWC* to field capacity for all treatments and providing adequate and uniform soil moisture for planting, crop germination and establishment.

Table 9.2: Experimental design and irrigation treatments

	Treatments (% *AWC*)					
Zone	Zone 1			Zone 2		
Treatments	I_{40}_Z1	I_{60}_Z1	Rainfed_Z1	I_{40}_Z2	I_{60}_Z2	Rainfed_Z2
% *AWC*	40	60	-	40	60	-
Replicated plots	2 and 4	1 and 3	9 and 10	5 and 7	6 and 8	11 and 12

9.23 *VRI–DSS* scheduling program

The *VRI–DSS* is a single, integrated platform designed to schedule and control *VRI* centre pivot and lateral sprinkler irrigation systems. It automatically generates *VRI* prescription maps that are dynamically optimized daily using a water balance modelling approach (http://www.myfieldnet.com/fieldnet-advisor)

The *VRI–DSS* is using a virtual global weather forecast model (as explained by Das et al., 2010; Dobbs et al., 2003) to predict daily evapotranspiration (ET_o) values. The virtual model joins up different weather forecast models of up-to-date information to identify which one works best for different locations. The model contains hourly weather forecast data for 4-day and 14-day periods with a forecast of maximum crop water needs. The forecast information is (i) rainfall amounts; (ii) minimum and maximum temperatures; (iii) cloudiness; (iv) wind speed; (v) solar radiation, and (vi) relative humidity. The model calculates the daily reference evapotranspiration (ET_o), using day-to-day weather

forecasts based on the Penman-Monteith (*PM*- ET_o) model. The *PM*- ET_o model and the FAO-56 crop coefficient function (Allen et al., 1998) are used to estimate the crop evapotranspiration (ET_c) and then the daily soil water balance model (Allen et al., 1998) is used to calculate the soil water deficit (*SWD)* and schedule irrigation. Following a method similar to that described by McMaster and Wilhelm (1997), *VRI–DSS* uses growing degree day units after emergence, in preference to the number of days after emergence, to determine the growth stage. As it is a challenge for climate models to detect rainfall for a small area in New Zealand (Schmidt et al., 2009), the accumulated daily rainfall data were obtained from a rain gauge located at the study site and automatically updated in the *VRI–DSS* system. This refinement was added as a potential improvement for *VRI–DSS* after, and as a result of, our trial results in Chapter 8.

The constant values for the irrigation trigger (critical soil moisture deficit) for the 40% *AWC* in each specific growing period were at 0.11, 0.40 and 0.70 total available water (*TAW*) for initial, mid and late crop stage, respectively. The constant values for the irrigation trigger (critical *SWD*) for the 60% *AWC* in each specific growing period were at 0.11, 0.60 and 0.93 *TAW* for initial, mid and late crop stage, respectively.

Linear interpolation for crop parameters (K_c and rooting depth) and irrigation trigger values were used between growth stages. The measured effective rooting depths during the growing season were used.

The soil map of the study site (Fig. 9.1 and Table 9.1) and information for spring wheat crop (crop type, hybrid, planting date) was loaded into the *VRI–DSS* platform, and all this information along with the virtual weather data and rain gauge data were used to simulate the water balance under spring wheat and generate daily *VRI* prescription maps. In turn, these maps were actioned manually using the software control.

9.23 Measurements

Meteorological data, including daily air temperature, wind speed, relative humidity, rainfall, solar radiation, and ET_o were collected from the Palmerston North CliFlo climate station (http://cliflo-niwa.niwa.co.nz/) (lat. -40°22′55″S, long. 175°36′32″E and 21 m elevation, located 0.2 km from the trial site) and used to assess the predictive power of

the virtual weather data predicted by *VRI–DSS*.

The *SMC* was measured at 0.1 m depth intervals to 0.8 m in all irrigation treatments using a neutron-probe. Measurements were recorded once each week. The *SWD* was determined by subtracting the mean of neutron meter measurements of *SMC* from the *AWC* (Lenka et al., 2009). *AWC* values are reported in Table 9.1.

The length of 60 plants was measured manually at harvest for each plot to distinguish the impact of treatments on final crop height. The impact of treatments on the harvest grain yield was determined by weighing the grain harvested from each plot using a plot harvester (Fig. 9.2).

Figure 9.2 Yield measurement using a plot harvester at the field site.

Yield data were adjusted to 14% moisture content. Whole plot samples were weighed, and a sub-sample from each plot was collected and dried at 70° C for four days to determine grain moisture concentration. Yields were reported as dry grain yields. Also, the following wheat quality parameters were assessed:

- Mass of plant (total biomass) in g m^{-2} (three replicates with a dimension of 1 m^2)
- After discard seeds that removed by cleaning/grading, the percentage of dressing loss and seed size (triplicate 500 g sub-sample) was measured by weighing 1000 grains, known as the 1000-grain weight.
- Grain density (kg hL^{-1}) or Hectolitre weight was obtained with a Shopper chondrometer equipped with a 250 ml cylinder.

The *IWUE* was calculated as the ratio between total yields (marketable yield) harvested (kg) and the total volume of irrigation applied (m^3). The *WP* was calculated by dividing the mean plot yield by the total water applied (irrigation + rainfall).

Three replicates of soil samples were collected at 0.15-m intervals to a depth of 0.45 m from each plot at harvest for a comparison of the levels of soil nitrate and ammonium between treatments and their impact on crop growth. Laboratory analysis included measurements of mineral nitrogen (*NH4-N* and *NO3-N*); ammonium and nitrate were extracted with 2 M KCl using a 1:10 soil: extractant ratio and a 1-hour end-over-end shake followed by filtration (Blackmore et al., 1987) and then quantified using a QuikChem 8500 flow injection analyser.

9.24 Statistical Analysis

To evaluate the *VRI–DSS* model, the outputs created by the model (temperature, wind, solar radiation, humidity and ET_c) were calibrated and validated against the field experimental data using coefficient of determination (R^2), bias, and root mean square error (*RMSE*) (Cohen Liechti et al., 2012; Moazami et al., 2013).

Biomass, yield, and yield components data were statistically analyzed for the treatment effects and year using analysis of variance (*ANOVA*). Means were separated by calculating the least significant difference (*LSD*) in R version 3.5.1 (R Core Team, 2018). All significant differences were evaluated at the 0.05 level.

9.3 Results and Discussion

9.31 *VRI–DSS* model evaluation

The model validation showed that the predicted weather data, using rainfall data from the trial area, agreed closely with the measured data across the crop season. The average predicted air temperature showed a significantly high correlation and lower biases and

errors (R^2= 0.87, *RMSE*= 0.83 ºC, and bias= 0.63ºC) (Fig. 9.3a). The simulated wind speed values were generally higher than the measured speeds (R^2, *RMSE*, and bias values of 0.79, 0.52 m s^{-1} and – 0.46) especially during the beginning and later growth stages (Fig. 9.3b). The predicted solar radiation values were closer to the measured data (Fig. 3c): the overall R^2, *RMSE*, and bias values were 0.90, 4.33 w m^{-2} and 2.12 w m^{-2}, respectively.

The ET_c predicted by *VRI-DSS* agreed closely with ET_c calculated using measured data (Fig. 9.3e): the corresponding R^2, *RMSE*, and bias values for predicted ET_c were 0.91, 0.22 mm d^{-1}, and 0.21 mm d^{-1}, respectively. These results are comparable with previous simulation study (Chapter 8) by *VRI–DSS* model with *RMSE* values of 0.17 ºC, – 27.30 w m^{-2}, 3.27 % and 0.53 mm for air temperature, solar radiation, humidity and ET_c at farm site in Hawke's Bay region in New Zealand, but improved by the use of local rainfall data instead of rainfall predicted by a global model.

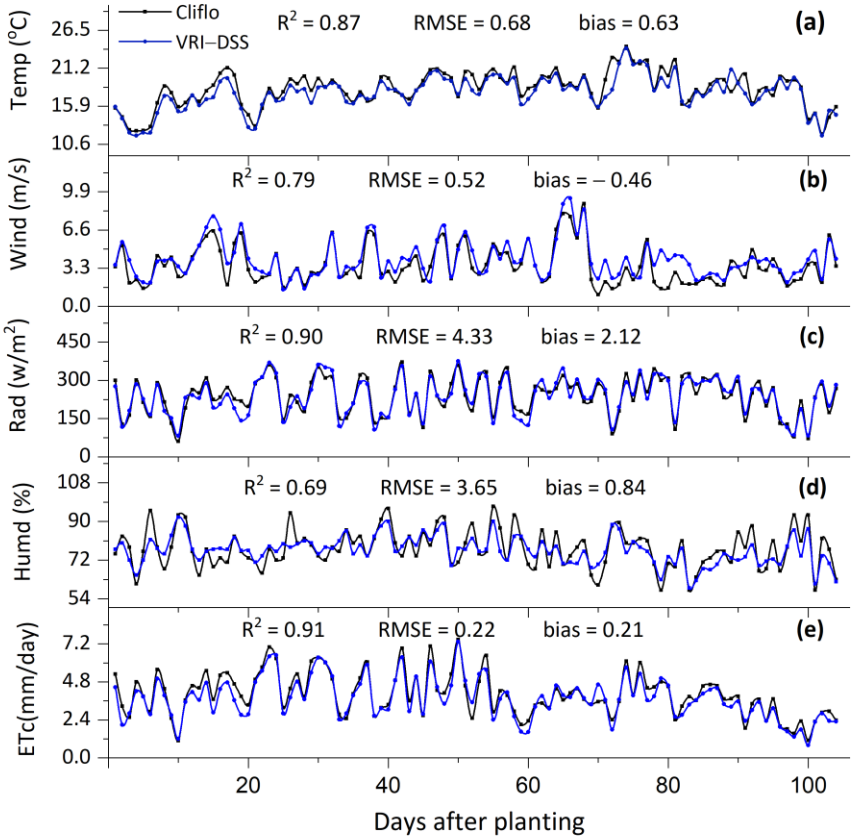

Figure 9.3: Comparisons between (a) average air temperature (Temp, °C), (b) wind speed (Wind, m s^{-1}), (c) solar radiation (Rad, w m^{-2}), (d) Humidity (Humd, %), and (e) daily crop evapotranspiration (ET_c, mm d^{-1}) estimated by *VRI–DSS*–Spring wheat model and measured values from Palmerston North CliFlo climate station (http://cliflo-niwa.niwa.co.nz/) for the wheat trial (17Nov2018 to 28Feb2019).

9.32 Irrigation application and soil water uptake for each treatment

The *SMC* was often wetter than field capacity because of excessive precipitation from the beginning of the crop trial until the midpoint of the season i.e. from approximately 6 to 41 days after planting (stage 7, fully extended to stage 8, flag leaf emerged). After the mid-point of the season, less rainfall meant that irrigation was required until the grain maturity stage (see Fig. 9.4). The total number of irrigations during the experiment were 5, 3, 3 and 1 for I_{40}_Z1, I_{60}_Z1, I_{40}_Z2, and I_{60}_Z2, respectively. Accumulated irrigation water amounts for the treatments I_{40}_Z1, I_{60}_Z1, I_{40}_Z2, and I_{60}_Z2 were 125, 75, 75 and 25 mm, respectively (Fig. 9.4). The *SWD* showed differences by soil layer and irrigation application (Fig. 9.4 and 9.5). The greatest *SWD* occurred under the rainfed treatments, and the rainfed_Z1 extracted the least soil water in the root zone.

Plant water uptake in Zone 1 was mostly from the two surface soil layers (0 – 0.2 m and 0.2 – 0.4 m) (Table 9.3) whereas water uptake in Zone 2 was more uniform down the profile (Table 9.3). The rainfed treatments experienced the greatest *SWD* up to near wilting point at late season (85% and 76% of *AWC* for Zone 1 and Zone 2, respectively). Considering the wheat root zone of 0.7 – 1 m (Allen et al., 1998; Fan et al., 2016) only the rainfed_Z1 treatment exhibited a high rate of water stress (Fig. 9.4).

Under Zone 1 irrigated treatments (Fig. 9.5a, b, and c), the topsoil layer (0 – 0.2 m) was the most depleted during the growing season. The largest *SWD* of the topsoil (0 – 0.2 m) was about 33 mm (28% of *AWC*) for I_{40}_Z1 and 38 mm (33% of *AWC*) for I_{60}_Z1 at 88 days after planting (stage 15, hard dough to stage 16, ripe (kernel hard)). The decrease in soil water extraction from the 0.4 – 0.6 m and 0.6 – 0.8 m layers could have been caused by low capacity for water storage in the sand as observed by El-Naggar et al. (2017) so that fewer roots will grow down through them. The *SMC* was relatively stable at field capacity in the 0.4 – 0.6 m and 0.6 – 0.8 m soil layers for I_{60}_Z1 and rainfed_Z1 treatments while it was above field capacity in the 0.4 – 0.8 m layer after the first irrigation event for I_{40}_Z1 (57 days after planting). Similar to the rainfed_Z1 treatment, less water was depleted from the deeper layers by root uptake and evaporation.

Under Zone 2 irrigated treatments (Fig. 9.5d, e, and f), water use was uniformly partitioned between the soil layers (0 – 0.8 m) and this due to the greater root depth allows water extraction from all soil layers (Wasson et al., 2014). This agrees with Joffre et al. (2001) who observed that when heavier textured soil layers lose water by transpiration, the water potential reduces, and the extraction moves toward deeper layers. The largest *SWD* of the topsoil (0 – 0.2 m) was about 25 mm (14% of *AWC*) for I_{40}_Z2 at 88 days after planting and 39 mm (23% of *AWC*) for I_{60}_Z2 at 94 days after planting (stage 16, Ripe (Kernel Hard)). Similar to the rainfed _Z2, water depleted uniformly between the soil layers and the largest *SWD* was in the topsoil (0 – 0.2 m and 0.2 – 0.4 m).

Overall, the greatest water uptake due to both soil evaporation and plant transpiration through roots was from the top layers (0 – 0.4 m) for Zone 1 and from the whole soil profile (0 – 0.8 m) for Zone 2. The I_{40}_Z1 treatment was the highest irrigated treatment, and the 0.6 – 0.8 m soil layer was always its maximum *AWC*.

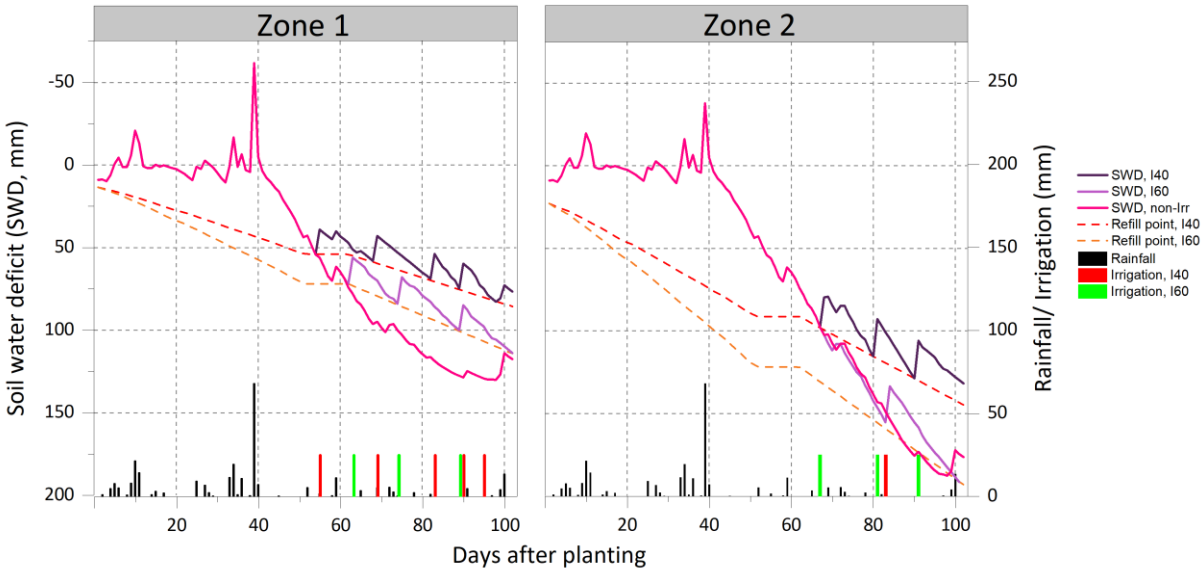

Figure 9.4: Soil water deficit (*SWD*) for each soil zone estimated by *VRI–DSS* and irrigation application under different irrigation treatments: (a) I40, (b) I60, (c) rainfed

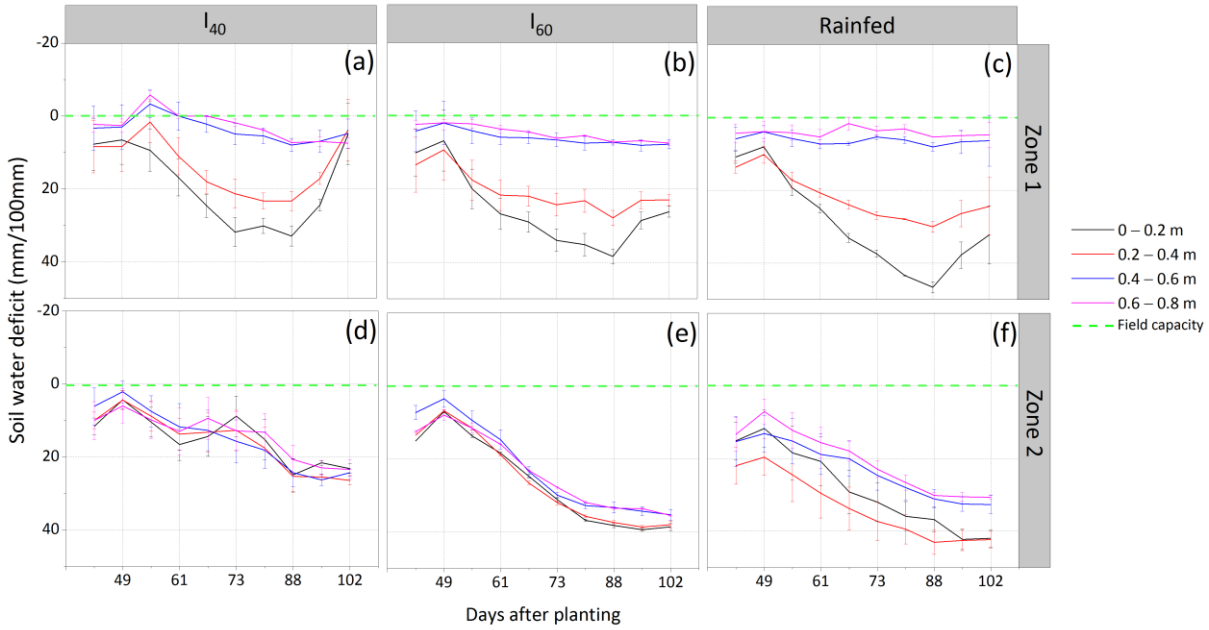

Figure 9.5: Average soil water deficit at different depths (0 – 0.8 m) as calculated using the neutron probe data from each irrigation treatment: (a) I_{40}_Z1, (b) I_{60}_Z1, (c) rainfed_Z1 (d) I_{40}_Z2 (e) I_{60}_Z2, and (f) rainfed _Z2 during the spring wheat growing season.

Table 9.3: The fraction of total soil profile water deficit (*SWD*) per depth calculated from neutron-probe measurements under the irrigation and rainfed treatments in each soil zone

	fraction Total SWD			
Depth (m)	0-20	20-40	40-60	60-80
I_{40}_Z1	0.48	0.34	0.11	0.07
I_{60}_Z1	0.45	0.36	0.10	0.08
rainfed_Z1	0.55	0.36	0.04	0.05
I_{40}_Z2	0.25	0.26	0.25	0.24
I_{60}_Z2	0.27	0.26	0.23	0.24
rainfed _Z2	0.31	0.34	0.20	0.14

9.33 Wheat crop assessment for each treatment

The effects of soil type and irrigation thresholds of 40 and 60% *AWC* on final plant height, grain yield, and total biomass were evaluated. The results are summarized in Table 9.4. I_{40}_Z1, I_{60}_Z1, I_{40}_Z2, and I_{60}_Z2 produced a marketable yield of 4.8, 4.7, 6.5 and 5.4 T ha^{-1} against applied water depth of 125, 75, 50 and 25 mm, respectively. There was no

significant difference in grain yield between the irrigation treatments at the 0.05 probability level using *ANOVA* and Tukey's HSD tests. Marketable yields from rainfed treatments had a significantly lower value ($P < 0.05$) than the irrigated treatments. In comparison with average of the irrigation treatments, the yield reduction percentages in rainfed_Z1 and rainfed_Z2 were 55 and 38%, respectively.

There were no significant differences in the plant height, biomass, 1000-grain wt and grain density observed amongst the different irrigation treatments. Rainfed treatments resulted in biomass reductions compared to those with irrigated treatments. In general, the percentage of seeds dressings was slightly lower with increasing irrigation water amounts. Dressing loss under rainfed_Z1 treatments were significantly different, while I_{40}_Z1, I_{60}_Z1, I_{40}_Z2, I_{60}_Z2, and rainfed_Z2 treatments showed no significant differences.

The results indicated that while yield was maximized in I_{40}_Z1 and I_{40}_Z2, the slightly lower yields in the I_{60}_Z1 and I_{60}_Z2 were similar with approximately 40% less water used to achieve those yields. Although less irrigation water was applied for Zone 2 treatments in comparison to Zone 1 treatments, the greater root depth allows increased water uptake and higher yields for Zone 2 which agree with Gao et al. (2016); Lilley and Kirkegaard (2011); Lynch (2013) who reported the deep rooting is a useful trait and likely to be associated with better exploration of surface layers and water or nutrient uptake. Similar findings by Wasson et al. (2014) showed that the soil type had the greatest effect on the distribution of roots with depth for the wheat crop, with one of the soils encouraging a much greater root length density.

Table 9.4: Statistical analysis of wheat quality parameters as influenced by each treatment. Means followed by the same letter are not significant ($p<0.05$)

Treatments	Plant height (cm)	Yield (T ha^{-1})	Biomass (T ha^{-1})	1000- grain wt (g)	Dressing loss (%)	Grain density $Kglha^{-1}$
I_{40}_Z1	81.9^{a}	4.8^{a}	9.2^{a}	39.3^{a}	0.9^{a}	82.2^{a}
I_{60}_Z1	80.2^{a}	4.7^{a}	8.9^{a}	38.7^{a}	1.1^{a}	80.5^{a}
I_{40}_Z2	83.5^{a}	6.5^{a}	10.1^{a}	40.5^{a}	0.9^{a}	81.4^{a}
I_{60}_Z2	83.9^{a}	5.4^{a}	10^{a}	38.2^{a}	1.3^{a}	80.6^{a}
rainfed _Z1	75.1^{b}	2.4^{b}	6.2^{b}	30^{b}	2.6^{b}	77.1^{b}
rainfed _Z2	77.6^{b}	3.7^{b}	7.8^{b}	37.5^{a}	1.4^{a}	79.9^{a}

9.34 Irrigation water use Efficiency (*IWUE*) and Water productivity (*WP*)

The greatest amount of irrigation water was applied to Zone 1 at 125 and 75 mm for I_{40}_Z1 and I_{60}_Z1 treatments, respectively. The *IWUE* and *WP* values varied depending on the treatment and the soil type (Table 9.5). The *IWUE* was 3.8 and 6.3 kg m^{-3} for I_{40}_Z1 and I_{60}_Z1, and 8.7 to 21.6 kg m^{-3} for I_{40}_Z2 and I_{60}_Z2, respectively. The *WP* values were 1.3 and 1.2 kg m^{-3} in Zone 1 treatments and 1.6 kg m^{-3} in Zone 2 treatments. The rainfed_Z1 treatment had the lowest *WP* in both soil zones. In comparison to I_{40}_Z1, less water (40 to 80%) was used by I_{60}_Z1 and I_{60}_Z2, respectively.

Generally, both *IWUE* and *WP* increased as the irrigation threshold increased. This was due to the fact that although less irrigation was applied to the 60% *AWC* treatment, this did not result in a significant decrease in grain yield. The findings in Table 9.4 and 9.5 indicate that the highest irrigation volume does not necessarily result in higher yields and the highest *IWUE* (Sezen et al., 2006) which agrees with (Howell, 2001) who reported that the highest *IWUE* with less irrigation, implying full use of the applied water and perhaps a tendency to promote deeper soil water uptake to make better use of both the stored soil water and the growing seasons rainfall. The highest *IWUE* and water-saving were obtained with *AWC* threshold of 60% in both soil zones because much of the water consumption was to meet ET_c needs, and the effect of soil texture on water retention (Clothier et al., 1977a; El-Naggar et al., 2017) and water uptake in Zone 2 enhanced yield.

Overall, varying the irrigation between the two soil zones with a *VRI* system and a threshold of 60% *AWC* was a viable strategy for scheduling irrigation to spring wheat at this site under the weather conditions experienced here. The effects of *AWC* thresholds investigated in this study showed the importance of determining this value under different soil types and its practical use in irrigation scheduling.

Table 9.5: Irrigation water amount, irrigation water use efficiency (*IWUE*) and water productivity (*WP*) for each treatment. The same lower cases represent no significant differences of the treatments.

Treatments	Water use (mm)	Water-saving (%)	IWUE (kg m^{-3})	WP (kg m^{-3})
I_{40}_Z1	125	-	3.8 [c]	1.1 [b]
I_{60}_Z1	75	40	6.3 [b]	1.2 [b]
I_{40}_Z2	75	40	8.7 [b]	1.6 [a]
I_{60}_Z2	25	80	21.6 [a]	1.6 [a]
rainfed _Z1	0	0	0	0.8 [c]
rainfed _Z2	0	0	0	1.2 [b]

9.35 Soil nitrate content for the two soil zones

All plots received the same adequate amount of *N* fertilizer (260 N kg ha^{-1}) at the beginning of the season to ensure any yield differences could be related to different irrigation schedules and not to fertility differences. We also measured the soil *N* content at harvest to check for any impacts of residual *N* differences. There was no significant difference in the quantities of *NO3-N* and *NH4-N* in the upper 45 cm of soil between the treatments at harvest for both crop trials (Table 9.6).

Table 9.6: *ANOVA* and Tukey's HSD test's result for mean (standard error) nitrate content (*NO3-N* (mg kg^{-1})) and ammonium content (*NH4-N* (mg kg^{-1})) in the upper 45 cm of soil at harvest. Means followed by the same letter are not significant ($p<0.05$).

Treatments	NO3N	NH4N
I_{40}_Z1	5.9 (1.8)[a]	1.1 (0.6)[a]
I_{60}_Z1	5.5 (1.2)[a]	1.3 (0.4)[a]
I_{40}_Z1	6.7 (0.9)[a]	2.5 (0.1)[a]
I_{60}_Z1	5.9 (1.2)[a]	0.5 (0.0)[a]
rainfed _Z1	5.5 (1.8)[a]	0.4 (1.1)[a]
rainfed _Z2	4.8 (1.3)[a]	0.2 (0.2)[a]

9.4 Conclusions

An irrigation scheduling program "*VRI–DSS*–Wheat model" has been tested and used to quantify the impact of soil type and irrigation threshold strategies on a spring wheat crop grown under variable irrigation application. Results showed that, with the use of measured rainfall, the *VRI–DSS*–Wheat model was able to simulate the spring wheat water balance very well. The greatest depths of irrigation water were applied to Zone 1 at 125 and 75 mm for 40 and 60% *AWC* treatments, respectively. The amount of irrigation water applied to Zone 2 were 75 and 25 for 40 and 60% *AWC* treatments, respectively. There weren't significant differences in biomass, yield and yield components between the two irrigation strategies. Soil type impacted the soil water uptake pattern, which decreased markedly with depth for the coarser textured soil (Zone 1) but was uniform with depth for the intermediate texture soil (Zone 2). The *IWUE* and *WP* for spring wheat under variable irrigation rates were affected by soil type and *VRI* irrigation strategies.

Maximum values of *IWUE* and *WP* occurred at the treatments for which the irrigation threshold strategies were 60% *AWC*. The I_{60}_Z2 resulted in the largest *IWUE* of 21.6 kg m^{-3}. Water saving was about 40% under this experimental, soil and crop, and climatic conditions.

Future research should be conducted to evaluate the *VRI* irrigation strategy with different *AWC* threshold values (30–70%) with other crops, soil types, and climate conditions to obtain maximum crop yield and *WUE*.

Chapter 10

Overall summary and conclusions

10.1 Summary and Conclusions

Irrigated cropping systems depend on the use of water resources. With depleting global freshwater resources, it is essential to develop precise methods for estimating soil water supply and crop water demand so as to inform the scheduling of precision irrigation (*PI*). Frequently, variations in water availability across a field due to different soil types or crop water needs require site-specific irrigation management to achieve optimum yields and improve irrigation water use efficiency (*IWUE*). In this context, this study developed new sensing technology methods to deliver high resolution spatio-temporal information to support variable-rate irrigation (*VRI*) scheduling.

Therefore, in Chapter 3 this study established two sites to investigate the impact of short-range soil variability on crop growth. The first site is (i) a 4-ha experimental plot irrigated by a *VRI* pivot at Massey University, Palmerston North, Manawatū, and the second site is (ii) a 102-ha field irrigated by a *VRI* pivot on a commercial farm near Otane, Hawkes Bay. An irrigated pea crop trial at the Manawatū site evaluated the different responses of the crop to waterlogging in an imperfectly drained soil zone adjacent to a well-drained soil. Waterlogging in the imperfectly drained soil resulted in a substantial reduction in pea crop growth and yield at harvest, with an average of 1.75 T ha^{-1} compared with 4.15 T ha^{-1} in the free draining soil. Assuming the value of fresh peas is $400 per tonne this crop yield reduction equates to a financial loss of $960/ha. This difference provides some evidence for the importance of varying irrigation amounts to two soil zones of contrasting drainage characteristics. In the barley trial, undertaken on the Hawkes Bay commercial farm, the amount of irrigation applied at a fixed interval (15 mm/7 days) was insufficient to fully restore plant available water for barley on the free draining sandy soil. The observed barley growth and yield was reduced (P *level* < 0.01) compared to the imperfectly drained silty soil. A novel crop water stress index (*CWSI*) for pea and barley

crops was also developed in these trials using in-field radiometer measurements. The highest *CWSI* values of 0.6 (Manawatū site) and 1.7 (Hawkes Bay site) were obtained in the free draining soils. These pea and barley trials provided evidence of the effects of soil-climate combinations at very small scales (i.e., within fields) on crop growth, supporting the need for precision irrigation methods.

Given the results of Chapter 3, the study in Chapter 4 developed a *quasi-2D* inversion algorithm field method using electromagnetic induction (*EMI*) data for identifying soil spatial variability, both across the field (resolution 6 m) and with depth (resolution < 0.15 m to 1.5 m). The *quasi-2D* algorithm is developed to invert the apparent electrical conductivity (EC_a) data at low induction numbers to generate a model of volumetric moisture content (θ_v) at specific depths and produce two-dimensional (*2D*) images of the soil profile. The predicted θ_v showed a significantly high correlation and low biases and errors with the measured θ_v (R^2 = 0.66, *bias* = 0.00 $cm^3\ cm^{-3}$, *RMSE* = 0.04 $cm^3\ cm^{-3}$). The θ_v depth profile maps indicate the effects of texture and texture transitions on soil wetness. The predicted θ_v profile was able to identify water perching above a gravelly layer in the Manawatū fine sandy loam as described by earlier researchers (Clothier et al., 1977). This research provides an improved method to identify and map, spatially and with depth, the soil properties that influence irrigation scheduling decisions at precision scales. The 'multi soil layer' outputs developed by this method could improve the ability of water dynamic models to account for drainage characteristics and associated water storage at fine scales.

In Chapter 5, this study investigated and compared accurate methods for estimating irrigation water demand for a pea crop followed by a French bean crop over one season under a *VRI* centre pivot. Methods developed in the EC_a imaging study (Chapter 4) were used to delineate soil zones and guide placement of soil moisture sensors (Chapter 5). The irrigation scheduling methods were based on real-time soil moisture monitoring (*Sensor-based*) and the FAO-56 water balance model (*SWB*). In addition, the local crop coefficient (K_{cb}) derived from ground-based normalized difference vegetation index (*NDVI*) measurements were assessed for their ability to improve the *SWB* predictions of crop evapotranspiration (ET_c) and soil water deficit (*SWD*). The *SWB* model predicted a faster drying rate than was actually measured with the soil moisture sensors. The *Sensor*-based technique saved about 23–45% of the irrigation water and produced the same pea

yields as the *SWB*-based model. The 23–45% water saving using real-time soil moisture monitoring of a pea crop equates to 25–44 mm water saved. Assuming that the cost of irrigation water applied is $2/mm/ha (https://www.irrigationnz.co.nz), this would equate to a $50 - $88/ha cost saving on irrigation. The ET_c estimated using the *NDVI* values did not significantly improve the FAO 56 approach. In the bean trial, due to sufficient rain during the growing season, *IWUE* was not significantly different between the scheduling treatments. These trials provide evidence to support the benefits of site-specific soil moisture monitoring to inform precision irrigation decisions under a *VRI* system.

Given the model results of Chapter 5, The study developed a novel sensing method for high resolution mapping of crop height (0.01 m accuracy) to inform spatial *VRI* scheduling tools and models. Terrestrial Laser Scanning (*TLS*) was used to assess the height and biomass of barley, pea and bean crops at high spatio-temporal resolution. Four campaigns were carried out periodically with the *TLS* scanner throughout the season to map vegetative growth. *2D* mapping of canopy surface height with a high resolution of 0.01 m was obtained from the *TLS*-derived results. Linear regression between manually measured and *TLS*-derived canopy height showed excellent correlation (R^2 = 0.95, 0.93 and 0.91 for barley, pea, and bean, respectively). Furthermore, a good correlation between *TLS*- measurements and dry biomass was achieved (R^2 = 0.70) and the linear regression showed the dependence of biomass on plant height. The *TLS* multi-temporal, crop height maps were used to improve crop coefficient and ET_c estimates for the *SWB* model in Chapter 7. This research has developed a new method which has significant potential for improved high resolution (in time and space) monitoring of crop growth (height, biomass) which could critically improve model-based prescription maps that underpin *VRI* scheduling decisions.

Chapter 7 presented field data that tested a new crop sensing approach (modified Penman-Monteith algorithm, *MPM*) to estimate daily ET_c by integrating remote sensing measurements (*NDVI* and canopy surface temperature (T_c)) with an FAO-56 Penman-Monteith (*PM*) algorithm. The new ET_c algorithm was used to estimate ET_c of barley, pea and bean plots managed with two different irrigation treatments. The ET_c –*SWB* was calculated from the water balance using the θ_v measurements and inputs of irrigation and rainfall and assumed no drainage. This was then used to compare estimations of daily ET_c with those estimated using the two algorithms (*PM* and *MPM*). The results indicated that

the barley crop was sensitive to restricted water, and the physiological responses were determined through remote sensing data. The *MPM* method outperformed the classic FAO-56 *PM* (*MPM*: R^2 = 0.81 and *RMSE* = 0.42 mm day^{-1}; *PM*: R^2 = 0.70 and *RMSE* = 0.60 mm day^{-1}). This study evaluated a new approach that estimates daily crop water use using site specific crop sensor data and shows that it gives very good agreement with more conventional approaches that parameterise ET_c models with climate data and lookup tables for crop growth. It therefore has the potential to use crop sensors to monitor varying site-specific crop growth differences, that would otherwise be missed by more conventional modelling approaches.

In Chapter 8, this study then went on to report on which of the sensing methods investigated and developed in this research study could best inform the model-based approach. A model-based decision support software system (*VRI–DSS*) that automates irrigation scheduling to variable soils and multiple crops was evaluated. The *VRI–DSS* uses a virtual climate forecast models (*VFM*) to predict daily *ET* with a *SWB* model. Data from the soil zones and maize, sweet corn and wheat were utilized to calibrate and validate the model at the Hawkes Bay commercial farm study site. In addition, the differences in the outputs of the *VRI-DSS* were investigated when the *VFM* data that it ordinarily employs in its *SWB* is replaced with measured, site-specific climate data. The *VFM* provided an adequate prediction of *ET* (R^2= 0.79, *bias*= –0.19 mm d^{-1}, *MSE*= 0.28 mm d^{-1} and *RMSE*= 0.53 mm d^{-1}) but overestimates local rainfall (+12%). When local data was used with the *VRI–DSS* to simulate results, the *SWD* had very similar trends to those derived from measured θ_v data. This field trial showed that the use of this *VRI–DSS* system allowed two-thirds of the irrigation water to be saved for the high available water content (*AWC*) soil (imperfectly drained) with the same yields as the low *AWC* soil (free draining).

Furthermore, Chapter 9 reported the use of *VRI-DSS* software in a field trail to investigate the effects of irrigating at thresholds of 40% *AWC* and 60% *AWC* compared with a non-irrigated (rainfed) control treatment for a spring wheat crop. The *ET* estimated by *VRI–DSS*–Wheat model data were similar to the values measured at the study site (R^2= 0.91, *RMSE*= 0.22 mm d^{-1}, and *bias*= 0.21 mm d^{-1}). Soil type impacted soil water uptake pattern, which decreased with soil depth for the coarser textured soil and was uniformly proportioned with soil depth for the intermediate texture soil. There were no significant

differences in the plant height, grain yield, biomass, 1000-grain wt, and grain density observed amongst the different irrigation threshold treatments. Generally, both *IWUE* and crop water productivity (*WP*) increased as the irrigation threshold increased. The rainfed treatment had the lowest *WP* in both soil zones. The trial provided evidence to show that in comparison to 40% *AWC* threshold treatment, less water (40 to 80%) was used by the 60% *AWC* threshold treatment with no negative impact on yield. This study in Chapter 8 and 9 discussed the potential to include high resolution spatio-temporal environmental data (rain, soil, crop) with *VRI-DSS* under different irrigation thresholds.

10.2 Recommendations for future research

1- Development of dynamic *DSS* integrated with wireless sensor network (*WSN*)

Wireless soil and crop sensor networks will allow real-time water applications that precisely match the water needs in each area of the field minimising leaching of nutrients or agrichemicals or surface runoff. Future research is needed to evaluate and do a sensitivity analysis to see which sensing technologies should best be integrated into a *DSS* for *VRI* systems equipped with special management and control software.

2- Testing the *VRI* management system with a wider range of soil-topographic associations

This research has tested two *VRI* irrigation systems at different scales on flat land. Future research is recommended to test *VRI* systems under a wider range of topographic, soil, climate and crop combinations to understand their performance and control needs under a wider range of conditions.

3- Irrigation scheduling using *CWSI*

Further research should be conducted using the canopy-air temperature differences approach in conjunction with other scheduling methods developed in this study to see if this combination of methods approach could possibly improve irrigation scheduling methods.

4- Improvements to the *VRI–DSS*

The research undertaken in this study has developed new methods and demonstrated how

irrigation decisions can be accurately made at the local level informed by site-specific needs. The inclusion of site-specific rainfall (*VRI – DSS*) is an obvious recommended improvement, but also site-specific soil and crop sensing could possibly also improve this product, and more research is required to investigate opportunities for this.

5- Determination of societal, environmental and cost benefits for *VRI*

By improving *IWUE*, decreasing deep percolation (*DP*) and the accompanying *N* leaching, adapting *VRI* to spatial heterogeneity of *AWC* and site-specific soil drainage characteristics could reduce not only *N* fertilizer expenses but also *N* loading into groundwater. Further research should be undertaken to verify these positive effects and provide simple methods to quantify the resulting societal and environmental benefits.

6- More dynamic approaches for measuring the impact of crop water stress/status on crop production.

Soil and crop models do not always provide reliable information on the impact of water stress on crop production at sufficient spatial and temporal resolution for precision irrigation methods. In addition, these models do not fully consider the impact of drought on K_{cb} and this leads to inaccurate estimation of the yield reduction. Also, with overwatering and waterlogging, the models consider all water above field capacity goes to *DP* without taking into account the possibility of waterlogging, which consequently effects final yield. Future research is recommended to develop more dynamic approaches using proximal and remote sensing techniques (e.g. soil moisture WSNs, *LiDAR*, *NDVI*) for measuring this stress impact on crop production. In addition, the incorporation of site-specific sensor data into modelling approaches needs further investigation due to the potential benefits illustrated by this study.

References

Adamchuk, V. I., & Rossel, R. A. V. (2011). Precision agriculture: proximal soil sensing. In *Encyclopedia of Agrophysics* (pp. 650-656): Springer.

Akay, A., Oğuz, H., Karas, I., & Aruga, K. (2009). Using LiDAR technology in forestry activities. *Environmental monitoring and assessment, 151*(1), 117-125.

Akay, A., Wing, M., & Sessions, J. (2014). Estimating sediment reduction cost for low-volume forest roads using a Lidar-derived high-resolution DEM/Nesmenu mazinimo kainos skaiciavimas mazo intensyvumo misko keliuose, taikant aukstos rezoliucijos skaitmenini auksciu modeli (DEM) pagal lazerinio skenavimo technologija (Lidar). *The Baltic Journal of Road and Bridge Engineering, 9*(1), 52-52.

Akıncı, Ş., & Lösel, D. (2012). Plant water-stress response mechanisms. In *Water stress*: InTech.

Al-Kaisi, M. M., Berrada, A., & Stack, M. (1997). Evaluation of irrigation scheduling program and spring wheat yield response in southwestern Colorado. *Agricultural Water Management, 34*(2), 137-148.

Al-Karadsheh, E., Sourell, H., & Krause, R. (2002). *Precision Irrigation: New strategy irrigation water management.* Paper presented at the Proceedingd of the Conference on International Agricultural Research for Development, Deutscher Tropentag, Wiltzenhausen, Germany.

Aladenola, O. (2014). *Decision Support System for Irrigation Water Management.* McGill University Libraries,

Alarcón, J., Domingo, R., Green, S., Nicolás, E., & Torrecillas, A. (2003). Estimation of hydraulic conductance within field-grown apricot using sap flow measurements. *Plant and Soil, 251*(1), 125-135.

Alderfasi, A. A., & Nielsen, D. C. (2001). Use of crop water stress index for monitoring water status and scheduling irrigation in wheat. *Agricultural Water Management, 47*(1), 69-75.

Alghabari, F., & Ihsan, M. Z. (2018). Effects of drought stress on growth, grain filling duration, yield and quality attributes of barley (Hordeum vulgare L.). *Bangladesh Journal of Botany, 47*(3), 421-428.

Allen, R., Pereira, L., Raes, D., & Smith, M. (1998). Crop evapotranspiration-Guidelines for computing crop water requirements-FAO Irrigation and drainage paper 56. *FAO, Rome, 300*(9), D05109.

Allred, B., Daniels, J., Fausey, N., Chen, C., Peters, L., & Youn, H. (2005). Important considerations for locating buried agricultural drainage pipe using ground penetrating radar. *Applied engineering in agriculture, 21*(1), 71-87.

Allred, B., Ehsani, M., & Daniels, J. (2008). General considerations for geophysical methods applied to agriculture. *Handbook of Agricultural Geophysics. CRC Press, Taylor and Francis Group, Boca Raton, Florida*, 3-16.

Allred, B., Freeland, R., Farahani, H., & Collins, M. (2010). *Agricultural geophysics: Past, present, and future.* Paper presented at the 23rd EEGS Symposium on the Application of Geophysics to Engineering and Environmental Problems.

Andales, A., & Chavez, J. (2011, February 22-23). [ET-Based Irrigation Scheduling Proceedings of the 23rd Annual Central Plains Irrigation Conference].

Andreo, V. (2013). Remote Sensing and Geographic Information Systems in Precision Farming. In. MEW 9 Seminar, Faculty of Mathematics, Astronomy and Physics - UNC.

Anthony, D., Elbaum, S., Lorenz, A., & Detweiler, C. (2014). *On crop height estimation with UAVs.* Paper presented at the 2014 IEEE/RSJ International Conference on Intelligent Robots and Systems.

Aragon, B., Houborg, R., Tu, K., Fisher, J. B., & McCabe, M. (2018). CubeSats Enable High Spatiotemporal Retrievals of Crop-Water Use for Precision Agriculture. *Remote Sensing, 10*(12), 1867.

Aston, A., & Van Bavel, C. (1972). Soil surface water depletion and leaf temperature. *Agronomy Journal, 64*(3), 368-373.

Austin, P. M. (1987). Relation between measured radar reflectivity and surface rainfall. *Monthly Weather Review, 115*(5), 1053-1070.

Bacanamwo, M., & Purcell, L. C. (1999). Soybean root morphological and anatomical traits associated with acclimation to flooding. *Crop science, 39*(1), 143-149.

Bacci, L., Battista, P., & Rapi, B. (2008). An integrated method for irrigation scheduling of potted plants. *Scientia horticulturae, 116*(1), 89-97.

Balendonck, J., & Hilhorst, M. (2001). *WET-sensor, application note*. Wageningen, The Netherlands: IMAG.

Barker, J. B., Heeren, D. M., Neale, C. M., & Rudnick, D. R. (2018). Evaluation of variable rate irrigation using a remote-sensing-based model. *Agricultural Water Management, 203*, 63-74.

Barradas, J., Matula, S., & Dolezal, F. (2012). A decision support system-fertigation simulator (DSS-FS) for design and optimization of sprinkler and drip irrigation systems. *Computers and Electronics in Agriculture, 86*, 111-119.

Bausch, W. C. (1993). Soil background effects on reflectance-based crop coefficients for corn. *Remote Sensing of Environment, 46*(2), 213-222.

Bausch, W. C., & Neale, C. M. (1987). Crop coefficients derived from reflected canopy radiation: a concept. *Transactions of the ASAE, 30*(3), 703-0709.

Bazzani, G. (2005). An integrated decision support system for irrigation and water policy design: DSIRR. *Environmental modelling & software, 20*(2), 153-163.

Beeson, J., & Brooks, J. (2006). *Evaluation of a model based on reference crop evapotranspiration (ETo) for precision irrigation using overhead sprinklers during nursery production of Ligustrum japonica.* Paper presented at the V International Symposium on Irrigation of Horticultural Crops 792.

Belford, R. K., Cannell, R. Q., Thomson, R. J., & Dennis, C. W. (1980). Effects of waterlogging at different stages of development on the growth and yield of peas (Pisum sativum L.). *Journal of the Science of Food and Agriculture, 31*(9), 857-869.

Bellvert, J., Adeline, K., Baram, S., Pierce, L., Sanden, B., & Smart, D. (2018). Monitoring crop evapotranspiration and crop coefficients over an almond and pistachio orchard throughout remote sensing. *Remote Sensing, 10*(12), 2001.

Bendig, J., Willkomm, M., Tilly, N., Gnyp, M., Bennertz, S., Qiang, C., . . . Bareth, G. (2013). Very high resolution crop surface models (CSMs) from UAV-based stereo images for rice growth monitoring in Northeast China. *Int. Arch. Photogramm. Remote Sens. Spat. Inf. Sci, 40*, 45-50.

Bergez, J.-E., Debaeke, P., Deumier, J.-M., Lacroix, B., Leenhardt, D., Leroy, P., & Wallach, D. (2001). MODERATO: an object-oriented decision tool for designing maize irrigation schedules. *Ecological modelling, 137*(1), 43-60.

Best, S., & Leon, L. (2006). Geoestadística. In: AGRICULTURA DE PRECISIÓN: Integrando conocimientos para una agricultura moderna y sustentable. In (pp. 147-161). Bongiovanni R.; Montovani: E.C.; Best, S.; Roel, A. Eds. PROCISUR/IICA 2006. Montevideo, Uruguay.

Bing, Z., Shouqi, Y., Hong, L., Xiaoqing, C., & Binjuan, Z. (2006). Optimized irrigation-yield model for winter wheat based on genetic algorithm. *Transactions of The Chinese Society of Agricultural Engineering, 8*, 002.

Bittelli, M. (2011). Measuring soil water content: A review. *HortTechnology, 21*(3), 293-300.

Blackmore, L., Searle, P., & Daly, B. (1987). Methods for Chemical Analysis of Soils. New Zealand Soil Bureau Scientific Report No. 80. In: Wellington, New Zealand: Department of Scientific and Industrial Research.

Blonquist, J., Jones, S., & Robinson, D. (2006). Precise irrigation scheduling for turfgrass using a subsurface electromagnetic soil moisture sensor. *Agricultural Water Management, 84*(1), 153-165.

Blonquist, J., Norman, J., & Bugbee, B. (2009). Automated measurement of canopy stomatal conductance based on infrared temperature. *Agricultural and forest meteorology, 149*(12), 2183-2197.

Booker, D., Henderson, R., & Whitehead, A. (2016). *National water allocation statistics for environmental reporting. Prepared for the Ministry for the Environment* (NIWA Client Report no. 2017065CH). Retrieved from www.mfe.govt.nz.

Breneger, S., Reese, P., Grafton Irrigation, Lindsay NZ, PGG WrightsonWater, Trimble Navigation Inc, & WaterForce. (2015). *Precision Irrigation*. Retrieved from New Zealand: http://irrigationnz.co.nz

Brevik, E., Fenton, T., & Lazari, A. (2006). Soil electrical conductivity as a function of soil water content and implications for soil mapping. *Precision Agriculture, 7*(6), 393-404.

Brown, H. E (September 21, 2018). Personal communication.

Brown, P., Cochrane, T., & Krom, T. (2010). Optimal on-farm irrigation scheduling with a seasonal water limit using simulated annealing. *Agricultural Water Management, 97*(6), 892-900.

Buchleiter, G., Heermann, D., & Duke, H. (1995). *Automation of variable irrigation water and chemical applications.* Paper presented at the Clean Water, Clean Environment, 21 Century Team Agriculture, Working to Protect Water Resources Conf. Proceedings, March 5-8, Kansas City, Missouri, St. Joseph, MI:ASAE, v.3 p.49-52.

Calera, A., Campos, I., Osann, A., D'Urso, G., & Menenti, M. (2017). Remote sensing for crop water management: from ET modelling to services for the end users. *Sensors, 17*(5), 1104.

Camp, C., & Sadler, E. (1998). Irrigation Site-specific crop management with a centre pivot. *Journal of Soil and Water Conservation, 53*(4), 312-314.

Camp, C., Sadler, E., & Evans, R. (2006). Precision water management: current realities, possibilities, and trends. *Handbook of precision agriculture*, 153-183.

Cannell, R., Belford, R. K., Gales, K., Thomson, R., & Webster, C. (1984). Effects of waterlogging and drought on winter wheat and winter barley grown on a clay and a sandy loam soil. *Plant and Soil, 80*(1), 53-66.

Cannell, R. Q., Belford, R. K., Gales, K., Dennis, C. W., & Prew, R. D. (1980). Effects of waterlogging at different stages of development on the growth and yield of winter wheat. *Journal of the Science of Food and Agriculture, 31*(2), 117-132.

Car, N. J., Christen, E. W., Hornbuckle, J. W., & Moore, G. A. (2012). Using a mobile phone Short Messaging Service (SMS) for irrigation scheduling in Australia–Farmers' participation and utility evaluation. *Computers and Electronics in Agriculture, 84*, 132-143.

Čermák, J., Kučera, J., & Nadezhdina, N. (2004). Sap flow measurements with some thermodynamic methods, flow integration within trees and scaling up from sample trees to entire forest stands. *Trees, 18*(5), 529-546.

Charlesworth, P. (2005). Irrigation Insights No. 1-Soil Water Monitoring 2nd edition. National Program for Irrigation Research and Development. In: CSIRO Publishing, Melbourne, Australia.

Chatzinikos, A., Gemtos, T., & Fountas, S. (2013). The use of a laser scanner for measuring crop properties in three different crops in Central Greece. In *Precision agriculture'13* (pp. 129-136): Springer.

Chávez, J., Pierce, F., Elliott, T., & Evans, R. (2010a). A remote irrigation monitoring and control system for continuous move systems. Part A: Description and development. *Precision Agriculture, 11*(1), 1-10.

Chávez, J., Pierce, F., Elliott, T., Evans, R., Kim, Y., & Iversen, W. (2010b). A remote irrigation monitoring and control system (RIMCS) for continuous move systems. Part B: Field testing and results. *Precision agriculture, 11*(1), 11-26.

Chávez, J., Pierce, F., & Evans, R. (2010c). Compensating inherent linear move water application errors using a variable rate irrigation system. *Irrigation Science, 28*(3), 203-210.

Chen, F., & Robinson, P. J. (2009). Estimating reference crop evapotranspiration with ETgages. *Journal of irrigation and drainage engineering, 135*(3), 335-342.

Chen, T., & Tang, H. (2012). Remote monitoring and forecasting system of soil moisture based on ARM and GPRS. *Transactions of The Chinese Society of Agricultural Engineering, 28*(3), 162-166.

Cifre, J., Bota, J., Escalona, J., Medrano, H., & Flexas, J. (2005). Physiological tools for irrigation scheduling in grapevine (Vitis vinifera L.): An open gate to improve water-use efficiency? *Agriculture, Ecosystems & Environment, 106*(2-3), 159-170.

Clawson, K., & Blad, B. (1982). Infrared thermometry for scheduling irrigation of corn. *Agronomy Journal, 74*(2), 311-316.

Clawson, K., Jackson, R., & Pinter, P. (1989). Evaluating plant water stress with canopy temperature differences. *Agronomy Journal, 81*(6), 858-863.

Clothier, B., Scotter, D., & Kerr, J. (1977a). Drainage Flux in Permeable Soil Underlain by a Coarse-Textured Layer 1. *Soil Science Society of America Journal, 41*(4), 671-676.

Clothier, B., Scotter, D., & Kerr, J. (1977b). Water retention in soil underlain by a coarse-textured layer: theory and a field application. *Soil Science, 123*(6), 392-399.

Clothier, B., & White, I. (1981). Measurement of Sorptivity and Soil Water Diffusivity in the Field 1. *Soil Science Society of America Journal, 45*(2), 241-245.

CloudCompare. (2016). 3D point cloud and mesh processing software Open Source Project. https://www.danielgm.net/cc/.

Coates, R., & Delwiche, M. (2008). *Site-specific water and chemical application by wireless valve controller network.* Paper presented at the 2008 Providence, Rhode Island, June 29–July 2, 2008.

Cohen Liechti, T., Matos, G. D. S. C., Pedro, J., Boillat, J.-L., & Schleiss, A. (2012). Comparison and evaluation of satellite derived precipitation products for

hydrological modeling of the Zambezi River Basin. *Hydrology and Earth System Sciences, 16*(EPFL-ARTICLE-175211), 489-500.
Cohen, Y., Fuchs, M., Falkenflug, V., & Moreshet, S. (1988). Calibrated heat pulse method for determining water uptake in cotton. *Agronomy Journal, 80*(3), 398-402.
Colaizzi, P., Barnes, E., Clarke, T., Choi, C., & Waller, P. (2003). Estimating soil moisture under low frequency surface irrigation using crop water stress index. *Journal of irrigation and drainage engineering, 129*(1), 27-35.
Conaty, W. (2010). *Temperature time thresholds for irrigation scheduling in precision application and deficit furrow irrigated cotton.* PhD Thesis, Faculty of Agriculture, Food and Natural Resources, The University of Sydney, NSW, Australia,
Connor, R. (2015). *The United Nations world water development report 2015: water for a sustainable world* (Vol. 1): UNESCO Publishing.
Coolong, T., Snyder, J., Warner, R., Strang, J., & Surendran, S. (2012). The relationship between soil water potential, environmental factors, and plant moisture status for poblano pepper grown using tensiometer-scheduled irrigation. *International journal of vegetable science, 18*(2), 137-152.
Corbari, C., Salerno, R., Ceppi, A., Telesca, V., & Mancini, M. (2019). Smart irrigation forecast using satellite LANDSAT data and meteo-hydrological modeling. *Agricultural Water Management, 212*, 283-294.
Corwin, D., & Lesch, S. (2003). Application of soil electrical conductivity to precision agriculture. *Agronomy Journal, 95*(3), 455-471.
Corwin, D., & Lesch, S. (2005). Characterizing soil spatial variability with apparent soil electrical conductivity: I. Survey protocols. *Computers and Electronics in Agriculture, 46*(1), 103-133.
Cremona, M., Stützel, H., & Kage, H. (2004). Irrigation scheduling of kohlrabi (Brassica oleracea var. gongylodes) using crop water stress index. *HortScience, 39*(2), 276-279.
Cressie, N. (1989). Geostatistics. *The American Statistician, 43*(4), 197-202.
Crommelinck, S., & Höfle, B. (2016). Simulating an autonomously operating low-cost static terrestrial LiDAR for multitemporal maize crop height measurements. *Remote Sensing, 8*(3), 205.
D'urso, G., & Santini, A. (1996). *A remote sensing and modeling integrated approach for the management of irrigation distribution systems.* Paper presented at the Proceedings of the international conference on ''Evapotranspiration and Irrigation Scheduling'', San Antonio (USA).
Dabas, M., Tabbagh, J., & Boisgontier, D. (2001). *Multi-depth continuous electrical profiling (MuCep) for characterization of in-field variability.* Paper presented at the Proceedings of the Third European Conference on Precision Agriculture. June 18-20, 2001, Montpellier, France.
Daccache, A., Knox, J. W., Weatherhead, E., Daneshkhah, A., & Hess, T. (2015). Implementing precision irrigation in a humid climate–Recent experiences and on-going challenges. *Agricultural Water Management, 147*, 135-143.
Dane, J. H., & Topp, G. C. (2002). Methods of Soil Analysis. Part 4: Physical Methods. In. Amer. Soc. Soil Sci., Madison, WI.

Dark, A., Birendra, K., & Kashima, A. (2017). *National Irrigated Land Spatial Dataset: Summary of methodology, assumptions and results*. Retrieved from www.mfe.govt.nz

Das, H., Doblas-Reyes, F., Garcia, A., Hansen, J., Mariani, L., Nain, A., . . . Garcia, A. (2010). Weather and climate forecasts for agriculture. *Guide to Agricultural Meteorological Practices*, 5.1-5.57.

Davies, G., Huang, J., Monteiro Santos, F. A., & Triantafilis, J. (2015). Modeling coastal salinity in quasi 2D and 3D using a DUALEM-421 and inversion software. *Groundwater, 53*(3), 424-431.

De Fraiture, C., Wichelns, D., Rockstrom, J., Kemp-Benedict, E., Eriyagama, N., Gordon, L., . . . Karlberg, L. (2007). Looking ahead to 2050: scenarios of alternative investment approaches. In *In Molden, David (Ed.). Water for food, water for life: A Comprehensive Assessment of Water Management in Agriculture* (pp. 91-145). UK: Earthscan; Colombo, Sri Lanka: IWMI.

De Jong, E., Ballantyne, A., Cameron, D., & Read, D. (1979). Measurement of apparent electrical conductivity of soils by an electromagnetic induction probe to aid salinity surveys. *Soil Science Society of America Journal, 43*(4), 810-812.

De Juan, J., Tarjuelo, J., Valiente, M., & Garcia, P. (1996). Model for optimal cropping patterns within the farm based on crop water production functions and irrigation uniformity I: Development of a decision model. *Agricultural Water Management, 31*(1-2), 115-143.

de Lara, A., Khosla, R., & Longchamps, L. (2019). Characterizing spatial variability in soil water content for precision irrigation management. *AGRONOMY, 8*(5), 59. doi:10.3390/agronomy8050059

deGroot-Hedlin, C., & Constable, S. (1990). Occam's inversion to generate smooth, two-dimensional models from magnetotelluric data. *Geophysics, 55*(12), 1613-1624.

DeJonge, K., Kaleita, A., & Thorp, K. (2007). Simulating the effects of spatially variable irrigation on corn yields, costs, and revenue in Iowa. *Agricultural Water Management, 92*(1), 99-109.

Delavar, M., Moghadasi, M., & Morid, S. (2011). Real-time model for optimal water allocation in irrigation systems during droughts. *Journal of irrigation and drainage engineering, 138*(6), 517-524.

Deutsch, C., & Journel, A. (1998). Geostatistical software library and user's guide. *Oxford University Press, New York*.

Diepen, C. v., Wolf, J., Keulen, H. v., & Rappoldt, C. (1989). WOFOST: a simulation model of crop production. *Soil use and management, 5*(1), 16-24.

Djaman, K., & Irmak, S. (2012a). Actual crop evapotranspiration and alfalfa-and grass-reference crop coefficients of maize under full and limited irrigation and rainfed conditions. *Journal of irrigation and drainage engineering, 139*(6), 433-446.

Dobbs, R., Garcia, A., Hansen, J., Mariani, L., Nain, A., Ramesh, K., . . . Venkataraman, R. (2003). Weather and climate forecasts for agriculture. *Guide to agricultural, meteorological practices*, 57.

Dobbs, R., Oppenheim, J., Thompson, F., Brinkman, M., & Zornes, M. (2011). *Resource Revolution: Meeting the world's energy, materials, food, and water needs*. Retrieved from McKinsey Global Institute, McKinsey & Company: http://www.mckinsey.com/insights/energy_resources_materials/resource_revolution.

Doerge, T., Kitchen, N., & Lund, E. (1999). Site-specific management guidelines: Soil electrical conductivity mapping. SSMG-30. *Atlanta, Ga: Potash & Phosphate Institute*.

Doolittle, J., & Brevik, E. (2014). The use of electromagnetic induction techniques in soils studies. *Geoderma, 223*, 33-45.

Doorenbos, J., & Kassam, A. (1979). Yield response to water. *Irrigation and drainage paper, 33*, 257.

Doorenbos, J., & Pruitt, W. O. (1977). Guidelines for Predicting Crop Water Requirements. FAO Irrigation and Drainag. Paper No. 24.FAO, Rome, Italy.

Dougherty, M., Burger, J. A., Feldhake, C. M., & AbdelGadir, A. (2013). Calibration and use of plate meter regressions for pasture mass estimation in an Appalachian silvopasture. *Archives of Agronomy and Soil Science, 59*(2), 305-315.

Douglas-Mankin, K., Srinivasan, R., & Arnold, J. (2010). Soil and Water Assessment Tool (SWAT) model: Current developments and applications. *Transactions of the ASABE, 53*(5), 1423-1431.

Drew, M., & Sisworo, E. (1979). The development of waterlogging damage in young barley plants in relation to plant nutrient status and changes in soil properties. *New Phytologist, 82*(2), 301-314.

Dualem Inc 2008. DUALEM-21S User's Manual. . In. Dualem Inc., Milton, ON, Canada.

Duchemin, B., Hadria, R., Erraki, S., Boulet, G., Maisongrande, P., Chehbouni, A., . . . Kharrou, M. (2006). Monitoring wheat phenology and irrigation in Central Morocco: On the use of relationships between evapotranspiration, crops coefficients, leaf area index and remotely-sensed vegetation indices. *Agricultural Water Management, 79*(1), 1-27.

Dueben, P. D., & Bauer, P. (2018). Challenges and design choices for global weather and climate models based on machine learning. *Geoscientific Model Development, 11*(10), 3999-4009.

Duke, H., Buchleiter, G., Heermann, D., & Chapman, J. (1997). *Site specific management of water and chemicals using self-propelled sprinkler irrigation systems.* Paper presented at the Precision agriculture'97: papers presented at the first European Conference on Precision Agriculture, Warwick University Conference Centre, UK, 7-10 September 1997.

Duke, H., Heermann, D., & Fraisse, C. (1992). *Linear move irrigation system for fertilizer management research.* Paper presented at the Proc. International Exposition and Technical Conference.

Ehlert, D., Adamek, R., & Horn, H.-J. (2009a). Vehicle based laser range finding in crops. *Sensors, 9*(5), 3679-3694.

Ehlert, D., Adamek, R., & Horn, H.-J. (2009b). Laser rangefinder-based measuring of crop biomass under field conditions. *Precision Agriculture, 10*(5), 395-408.

Ehlert, D., & Dammer, K.-H. (2006). Widescale testing of the Crop-meter for site-specific farming. *Precision Agriculture, 7*(2), 101-115.

Ehlert, D., Heisig, M., & Adamek, R. (2010c). *Assessment of a laser scanner on agricultural machinery.* Paper presented at the Engineering for Rural Development-9th International Scientific Conference. University of Agriculture, Jelgava, Latvia.

Ehlert, D., Heisig, M., & Adamek, R. (2010d). Suitability of a laser rangefinder to characterize winter wheat. *Precision Agriculture, 11*(6), 650-663.

Ehrler, W. (1973). Cotton leaf temperatures as related to soil water depletion and meteorological factors. *Agronomy Journal, 65*(3), 404-409.

Eitel, J., Magney, T., Vierling, L., Brown, T., & Huggins, D. (2014). LiDAR based biomass and crop nitrogen estimates for rapid, non-destructive assessment of wheat nitrogen status. *Field Crops Research, 159*, 21-32.

Ekanayake, J. C., & Hedley, C. B. (2018). Advances in Information Provision from Wireless Sensor Networks for Irrigated Crops. *Wireless Sensor Network, 10*(04), 71.

Ekwue, E., & Bartholomew, J. (2011). Electrical conductivity of some soils in Trinidad as affected by density, water and peat content. *Biosystems engineering, 108*(2), 95-103.

El-Naggar, A., Hedley, C. B., Horne, D., Roudier, P., & Clothier, B. (2017). Soil electrical conductivity imaging of the soil profile and its relationship to soil properties. . *7th Asian-Australasian conference on precision agriculture*. doi:http://doi.org/10.5281/zenodo.891095

El Chami D, Knox JW, Daccache A and Weatherhead EK. Assessing the financial and environmental impacts of precision irrigation in a humid climate. Horticultural Science (Czech Republic), Volume 46, Issue 1, 2019, pp. 43-52

EMTOMO. (2014). EM4Soil Version 2. EMTOMO. In. R. Alice Cruz 4, Odivelas, Lisboa,Portugal, http://www.emtomo.com.

Er-Raki, S., Chehbouni, A., Guemouria, N., Duchemin, B., Ezzahar, J., & Hadria, R. (2007). Combining FAO-56 model and ground-based remote sensing to estimate water consumptions of wheat crops in a semi-arid region. *Agricultural Water Management, 87*(1), 41-54.

Erdem, Y., Arin, L., Erdem, T., Polat, S., Deveci, M., Okursoy, H., & Gültaş, H. T. (2010). Crop water stress index for assessing irrigation scheduling of drip irrigated broccoli (Brassica oleracea L. var. italica). *Agricultural Water Management, 98*(1), 148-156.

Erdem, Y., Erdem, T., Orta, A., & Okursoy, H. (2006). Canopy-air temperature differential for potato under different irrigation regimes. *Acta Agriculturae Scandinavica Section B-Soil and Plant Science, 56*(3), 206-216.

Evans, R., Han, S., Kroeger, M., & Schneider, S. (1996). Precision centre pivot irrigation for efficient use of water and nitrogen. *Precision Agriculture*(precisionagricu3), 75-84.

Evans, R., Iversen, W., & Kim, Y. (2011). Integrated decision support, sensor networks, and adaptive control for wireless site-specific sprinkler irrigation. *Applied engineering in agriculture, 28*(3), 377-387.

Evans, R., LaRue, J., Stone, K., & King, B. (2013). Adoption of site-specific variable rate sprinkler irrigation systems. *Irrigation Science*, 1-17.

Evans, R., & Sadler, E. J. (2008). Methods and technologies to improve efficiency of water use. *Water resources research, 44*(7).

Evett, S. R., Heng, L. K., Moutonnet, P., & Nguyen, M. L. (2008). Field Estimation of Soil Water Content: A Practical Guide to Methods, Instrumentation, and Sensor Technology. *IAEA-TCS-30. International Atomic Energy Agency, Vienna, Austria., ISSN 1018–5518*, 131 pp.

Evett, S. R., Lascano, R., & Sojka, R. (2007). Soil water and monitoring technology. *AGRONOMY, 30*(2), 25.

Evett, S. R., Schwartz, R. C., Casanova, J. J., & Heng, L. K. (2012). Soil water sensing for water balance, ET and WUE. *Agricultural Water Management, 104*, 1-9.

Fan, J., McConkey, B., Wang, H., & Janzen, H. (2016). Root distribution by depth for temperate agricultural crops. *Field Crops Research, 189*, 68-74.

Fant, C., Gueneau, A., Strzepek, K., Awadalla, S., Farmer, W., Blanc, E., & Schlosser, C. (2012). CliCrop: A crop water-stress and irrigation demand model for an integrated global assessment modeling approach. Joint Program on the Science and Policy of Global Change, Report 214. In: MIT. http://globalchange. mit. edu/research/publications/2264.

FAO. (2015). Food and Agriculture Organization of the United Nations, Aquastatwebsite. Retrieved from www.fao.org/nr/water/aquastat/wateruse/index.stm. from United Nations www.fao.org/nr/water/aquastat/wateruse/index.stm

Faro Scene. (2013). Focus3D X 330 Documentation Software for terrestrial and handheld Scanners. https://www.faro.com/products/construction-bim-cim/faro-scene/.

Fender, F., Hanneken, M., Linz, A., Ruckelshausen, A., & Spicer, M. (2005). Messende Lichtgitter und Multispektralkameras als bildgebende Systeme zur Pflanzenerkennung [Measuring light grids and multi-spectral cameras as picture-giving systems for plant recognition]. *Bornimer Agrartechnische Berichte, 40*, 7-16.

Fereres, E., Goldhamer, D., & Parsons, L. (2003). Irrigation water management of horticultural crops. *HortScience, 38*(5), 1036-1042.

Fortes, R., Millán, S., Prieto, M., & Campillo, C. (2015). A methodology based on apparent electrical conductivity and guided soil samples to improve irrigation zoning. *Precision Agriculture, 16*(4), 441.

Fraisse, C., Heermann, D., & Duke, H. (1993). *Modified linear move system for experimental water application.* Paper presented at the Advances in planning, design and management of irrigation systems as related to sustainable land use, Leuven (Belgium), 14-17 Sep 1992.

Friedli, M., Kirchgessner, N., Grieder, C., Liebisch, F., Mannale, M., & Walter, A. (2016). Terrestrial 3D laser scanning to track the increase in canopy height of both monocot and dicot crop species under field conditions. *Plant Methods, 12*(1), 9.

Friedman, J., Hastie, T., & Tibshirani, R. (2001). *The elements of statistical learning* (Vol. 1): Springer series in statistics New York.

Fulton, A., Schwankl, L., Lynn, K., Lampinen, B., Edstrom, J., & Prichard, T. (2011). Using EM and VERIS technology to assess land suitability for orchard and vineyard development. *Irrigation Science, 29*(6), 497-512.

FWE, & APHA. (2005). *Standard methods for the examination of water and wastewater* (21st Edition ed.). American Public Health Association (APHA): Washington, DC, USA. Method 4500-NH3 H. Flow Injection Analysis. Method 4500-NO3 I. Flow Injection Analysis. Method 4500-P G. Flow Injection Analysis.

Gao, W., Hodgkinson, L., Jin, K., Watts, C. W., Ashton, R. W., Shen, J., . . . Phillips, A. L. (2016). Deep roots and soil structure. *Plant, cell & environment, 39*(8), 1662-1668.

Gardner, W. (1986). Water Content. In Methods of Soil Analysis. Part I. Physical and Mineralogical Methods (Klute, A., ed.). In *Agronomy Series No 9. 2nd ed* (pp. 493-544).

Gebbers, R., Ehlert, D., & Adamek, R. (2011). Rapid mapping of the leaf area index in agricultural crops. *Agronomy Journal, 103*(5), 1532-1541.

Gebrechorkos, S. H., Hülsmann, S., & Bernhofer, C. (2018). Evaluation of multiple climate data sources for managing environmental resources in East Africa. *Hydrology and Earth System Sciences, 22*(8), 4547-4564.
Gebregiorgis, M. F., & Savage, M. J. (2006). Field, laboratory and estimated soil-water content limits. *Water SA, 32*(2), 155-162.
Gee, G., Zhang, Z., & Ward, A. (2003). A modified vadose zone fluxmeter with solution collection capability. *Vadose Zone Journal, 2*(4), 627-632.
Girona, J., Mata, M., Fereres, E., Goldhamer, D., & Cohen, M. (2002). Evapotranspiration and soil water dynamics of peach trees under water deficits. *Agricultural Water Management, 54*(2), 107-122.
González-Dugo, M., & Mateos, L. (2008). Spectral vegetation indices for benchmarking water productivity of irrigated cotton and sugarbeet crops. *Agricultural Water Management, 95*(1), 48-58.
González-Dugo, M., Moran, M., Mateos, L., & Bryant, R. (2006). Canopy temperature variability as an indicator of crop water stress severity. *Irrigation Science, 24*(4), 233-240.
González, A., Martín, I., & Ayerbe, L. (1999). Barley yield in water-stress conditions.: The influence of precocity, osmotic adjustment and stomatal conductance. *Field Crops Research, 62*(1), 23-34.
Goovaerts, P. (1997). *Geostatistics for natural resources evaluation*: Oxford University Press on Demand.
Gowda, P. H., Chavez, J. L., Colaizzi, P. D., Evett, S. R., Howell, T. A., & Tolk, J. A. (2008). ET mapping for agricultural water management: present status and challenges. *Irrigation Science, 26*(3), 223-237.
Gowing, J., & Ejieji, C. (2001). Real-time scheduling of supplemental irrigation for potatoes using a decision model and short-term weather forecasts. *Agricultural Water Management, 47*(2), 137-153.
Grafton, R. Q., Williams, J., Perry, C., Molle, F., Ringler, C., Steduto, P., . . . Garrick, D. (2018). The paradox of irrigation efficiency. *Science, 361*(6404), 748-750.
Green, S., M. Deurer, B. Clothier, S. Andrews, K. Cauldwell, A. Roberts, M. Wellwood, and P. Thomas 2010. Water and nitrogen movement under agricultural and horticultural land. Proceedings of the Workshop "Farming's Future: Minimising footprints and maximising margins. Fertiliser & Lime Research Centre, Massey University, 10-11 February 2010.
Greenwood, P., & McNamara, R. (1987). Irrigation of field peas on a soil with impeded drainage. *Peas: management for quality. Palmerston North, New Zealand: Agronomy Society of New Zealand, Special Publication*(6), 33-38.
Gregory, P. J. (2004). Agronomic approaches to increasing water use efficiency. *Water use efficiency in plant biology*, 142-167.
Grote, K., Anger, C., Kelly, B., Hubbard, S., & Rubin, Y. (2010). Characterization of soil water content variability and soil texture using GPR groundwave techniques. *Journal of Environmental and Engineering Geophysics, 15*(3), 93-110.
Hadria, R., Duchemin, B. ı., Lahrouni, A., Khabba, S., Er-Raki, S., Dedieu, G., . . . Olioso §, A. (2006). Monitoring of irrigated wheat in a semi-arid climate using crop modelling and remote sensing data: Impact of satellite revisit time frequency. *International Journal of Remote Sensing, 27*(6), 1093-1117.
Hargreaves, G. H., & Samani, Z. A. (1985). Reference crop evapotranspiration from temperature. *Applied engineering in agriculture, 1*(2), 96-99.

Hecht, J. (2011). *Understanding lasers: an entry-level guide* (Vol. 21): John Wiley & Sons.
Hedley, C., Ekanayake, J., & Roudier, P. (2012). *Wireless soil moisture sensor networks for precision irrigation scheduling.* Paper presented at the Workshop abstracts, advanced nutrient management: Gains from the past-goals for the future.
Hedley, C., Roudier, P., Yule, I., Ekanayake, J., & Bradbury, S. (2013). Soil water status and water table depth modelling using electromagnetic surveys for precision irrigation scheduling. *Geoderma, 199*, 22-29.
Hedley, C., & Yule, I. (2009a). A method for spatial prediction of daily soil water status for precise irrigation scheduling. *Agricultural Water Management, 96*(12), 1737-1745.
Hedley, C., & Yule, I. (2009b). Soil water status mapping and two variable-rate irrigation scenarios. *Precision Agriculture, 10*(4), 342-355.
Hedley, C., Yule, I., Eastwood, C., Shepherd, T., & Arnold, G. (2004). Rapid identification of soil textural and management zones using electromagnetic induction sensing of soils. *Soil Research, 42*(4), 389-400.
Heeren, D., Werner, H., & Trooien, T. (2006). *Evaluation of irrigation strategies with the DSSAT cropping system model.* Paper presented at the ASABE/CSBE North Central Intersectional Meeting.
Heilman, J., Heilman, W., & Moore, D. G. (1982). Evaluating the Crop Coefficient Using Spectral Reflectance 1. *Agronomy Journal, 74*(6), 967-971.
Heng, L., Cayci, G., Kutuk, C., Arrillaga, J., & Moutonnet, P. (2002). *Comparison of soil moisture sensors between neutron probe, Diviner 2000 and TDR under tomato crops.* Paper presented at the Proceedings 17th World Congress of Soil Science.
Hewitt, A. E. (2004). Soil properties for plant growth. *Landcare research science series, 26*.
Hewitt, A. E. (2010). New Zealand soil classification. *Landcare research science series*(1).
Hezarjaribi, A., & Sourell, H. (2007). Feasibility study of monitoring the total available water content using non-invasive electromagnetic induction-based and electrode-based soil electrical conductivity measurements. *Irrigation and Drainage, 56*(1), 53-65.
Hillel, D. (1982). Advances in Irrigation. *Vol. 1, Academic Press, New York.*
Hillel, D. (1998). *Environmental soil physics: Fundamentals, applications, and environmental considerations*: Academic press, 771 pp. Elsevier (USA).
Hillyer, C., & Higgins, C. (2014). *A Demonstration of Energy & Water Savings Potential of Variable Rate Irrigation.* Paper presented at the 2014 Montreal, Quebec Canada July 13–July 16, 2014.
Hoedjes, J., Chehbouni, A., Jacob, F., Ezzahar, J., & Boulet, G. (2008). Deriving daily evapotranspiration from remotely sensed instantaneous evaporative fraction over olive orchard in semi-arid Morocco. *Journal of hydrology, 354*(1-4), 53-64.
Hofle, B. (2014). Radiometric correction of terrestrial LiDAR point cloud data for individual maize plant detection. *IEEE Geoscience and Remote Sensing Letters, 11*(1), 94-98.
Holder, M., Brown, K., Thomas, J., Zabcik, D., & Murray, H. (1991). Capillary-wick unsaturated zone soil pore water sampler. *Soil Science Society of America Journal, 55*(5), 1195-1202.
Holmes, G., Bodley, J., Meadows, J., & Poilve, H. (2004). *Integrating synthetic aperture radar with optical information for crop management applications.*

Paper presented at the Proceedings of the Seventh International Conference on Precision Agriculture.
Hosoi, F., & Omasa, K. (2009). Estimating vertical plant area density profile and growth parameters of a wheat canopy at different growth stages using three-dimensional portable lidar imaging. *ISPRS Journal of Photogrammetry and Remote Sensing, 64*(2), 151-158.
Howell, T. (2002). Irrigation Efficiency. Lal, R. In I. Marcel Dekker (Ed.), *Encyclopedia of Soil Science* (pp. 736-741). New York, NY.
Howell, T. A. (2001). Enhancing water use efficiency in irrigated agriculture. *Agronomy Journal, 93*(2), 281-289.
Huang, J., Davies, G., Bowd, D., Santos, F. M., & Triantafilis, J. (2014). Spatial prediction of the exchangeable sodium percentage at multiple depths using electromagnetic inversion modelling. *Soil use and management, 30*(2), 241-250.
Huang, J., McBratney, A., Minasny, B., & Triantafilis, J. (2017b). 3D soil water nowcasting using electromagnetic conductivity imaging and the ensemble Kalman filter. *Journal of hydrology, 549*, 62-78.
Huang, J., Scudiero, E., Choo, H., Corwin, D., & Triantafilis, J. (2016). Mapping soil moisture across an irrigated field using electromagnetic conductivity imaging. *Agricultural Water Management, 163*, 285-294.
Huang, J., Scudiero, E., Clary, W., Corwin, D., & Triantafilis, J. (2017a). Time-lapse monitoring of soil water content using electromagnetic conductivity imaging. *Soil use and management, 33*(2), 191-204.
Huang, J., Taghizadeh-Mehrjardi, R., Minasny, B., & Triantafilis, J. (2015). Modeling soil salinity along a hillslope in Iran by inversion of EM38 data. *Soil Science Society of America Journal, 79*(4), 1142-1153.
Hudak, A., Evans, J., & Stuart Smith, A. (2009). LiDAR utility for natural resource managers. *Remote Sensing, 1*(4), 934-951.
Hunink, J., Vila, M., & Baille, A. (2011). *REDSIM: Approach to soil water modelling*. Retrieved from http://www.futurewater.nl
Hunsaker, D., Pinter, P. J., & Kimball, B. A. (2005). Wheat basal crop coefficients determined by normalized difference vegetation index. *Irrigation Science, 24*(1), 1-14.
Idso, S., Jackson, R., Pinter Jr, P., Reginato, R., & Hatfield, J. (1981). Normalizing the stress-degree-day parameter for environmental variability. *Agricultural meteorology, 24*, 45-55.
Irmak, S., Haman, D., & Bastug, R. (2000). Determination of crop water stress index for irrigation timing and yield estimation of corn. *Agronomy Journal, 92*(6), 1221-1227.
Irmak, S., Irmak, A., Allen, R., & Jones, J. (2003). Solar and net radiation-based equations to estimate reference evapotranspiration in humid climates. *Journal of irrigation and drainage engineering, 129*(5), 336-347.
Isaaks, E., & Srivastava, R. (1989). Applied geostatistics: Oxford University Press. *New York*, 561.
Jackson, M. (1979). Rapid injury to peas by soil waterlogging. *Journal of the Science of Food and Agriculture, 30*(2), 143-152.
Jackson, R., Idso, S., Reginato, R., & Pinter, P. (1981). Canopy temperature as a crop water stress indicator. *Water resources research, 17*(4), 1133-1138.

Jackson, R., Kustas, W., & Choudhury, B. (1988). A reexamination of the crop water stress index. *Irrigation Science, 9*(4), 309-317.
Jamieson, P., Martin, R., & Francis, G. (1995). Drought influences on grain yield of barley, wheat, and maize. *New Zealand journal of crop and horticultural science, 23*(1), 55-66.
Jha, M., & Chowdary, V. (2007). Challenges of using remote sensing and GIS in developing nations. *Hydrogeology Journal, 15*(1), 197-200.
Jia, X., Dukes, M. D., Jacobs, J. M., & Irmak, S. (2006). Weighing lysimeters for evapotranspiration research in a humid environment. *Transactions of the ASABE, 49*(2), 401-412.
Jinyao, L., & Shaolong, L. (2003). Research Progress of Water Saving Irrigation Theory and Technique of Facility Agriculture in Chin [J]. *Water Saving Irrigation, 3*, 111-113.
Joffre R., Rambal S., Winkel Thierry. (2001). Respuestas de las plantas mediterraneas a la limitacion de agua : desde la hoja hasta el dosel. In : Zamora R. (ed.), Pugnaire F.I. (ed.) Ecosistemas mediterraneos : analisis funcional. Madrid (ESP) ; Séville : CSIC ; AEET, 37-65.
Johnson, A. (1962). Methods of measuring soil moisture in the field. *Geol. Survey Water Supply, Paper 1619-U*.
Jones, H. (2004a). Irrigation scheduling: advantages and pitfalls of plant-based methods. *Journal of experimental botany, 55*(407), 2427-2436.
Jones, H. (2004b). Application of thermal imaging and infrared sensing in plant physiology and ecophysiology. *Advances in Botanical Research, 41*, 107-163.
Jones, H. (2006). *Irrigation scheduling–Comparison of soil, plant and atmosphere monitoring approaches.* Paper presented at the V International Symposium on Irrigation of Horticultural Crops 792.
Jones, J., Hoogenboom, G., Porter, C. H., Boote, K. J., Batchelor, W. D., Hunt, L., . . . Ritchie, J. T. (2003). The DSSAT cropping system model. *European journal of agronomy, 18*(3-4), 235-265.
Jones, S., Wraith, J., & Or, D. (2002). Time domain reflectometry measurement principles and applications. *Hydrological Processes, 16*(1), 141-153.
Journel, A., & Huijbregts, C. (1978). *Mining geostatistics*: Academic press.
Kabenge, I., Irmak, S., Meyer, G., Gilley, J., Knezevic, S., Arkebauer, T. J., . . . Moravek, M. (2013). Evapotranspiration and surface energy balance of a common reed-dominated riparian system in the Platte River Basin, Central Nebraska. *Transactions of the ASABE, 56*(1), 135-153.
Kachanoski, R., WESENBEECK, I. V., & Gregorich, E. (1988). Estimating spatial variations of soil water content using noncontacting electromagnetic inductive methods. *Canadian Journal of Soil Science, 68*(4), 715-722.
Kang, S., Zhang, L., Liang, Y., Hu, X., Cai, H., & Gu, B. (2002). Effects of limited irrigation on yield and water use efficiency of winter wheat in the Loess Plateau of China. *Agricultural Water Management, 55*(3), 203-216.
Kaufman, A., & Keller, G. (1983). Frequency and Transient Soundings *Elsevier. New York*.
Kaye-Blake, B., Schilling, C., Nixon, C., & Destremau, K. (2014). *Water management in New Zealand: A road map for understanding water value* (1176-4384). Retrieved from New Zealand Institute of Economic Research: http://hdl.handle.net/11540/6416

Keating, B., Carberry, P., Hammer, G., Probert, M., Robertson, M., Holzworth, D., . . . Hochman, Z. (2003). An overview of APSIM, a model designed for farming systems simulation. *European journal of agronomy, 18*(3), 267-288.

Khalilian, A., Han, Y., & Farahani, H. (2008). Site-specific irrigation management in coastal plain soils. *In Proc. 2008 South Carolina Water Resources Conf. Clemson, S.C.: Clemson University*.

Khan, M. J., Sarwar, T., Shahzadi, A., & Malik, A. (2007). Effect of different irrigation schedules on water use and yield of wheat. *Sarhad Journal of Agriculture, 23*(4), 1055.

Kim, Y., & Evans, R. (2009). Software design for wireless sensor-based site-specific irrigation. *Computers and Electronics in Agriculture, 66*(2), 159-165.

Kim, Y., Evans, R., & Iversen, W. (2007). Decision support and monitoring for wireless sensor-based site-specific sprinkler irrigation. *ASABE Paper*(073078).

Kim, Y., Evans, R., & Iversen, W. (2008). Remote sensing and control of an irrigation system using a distributed wireless sensor network. *IEEE transactions on instrumentation and measurement, 57*(7), 1379-1387.

King, B., & Kincaid, D. (1996). *Variable flow sprinkler for site-specific water and nutrient management.* Paper presented at the Presentation at the 1996 ASAE Annual International Meeting.

King, B., McCann, I., Eberlein, C., & Stark, J. (1999). Computer control system for spatially varied water and chemical application studies with continuous-move irrigation systems. *Computers and Electronics in Agriculture, 24*(3), 177-194.

King, B., Stark, J., & Wall, R. (2006). Comparison of site-specific and conventional uniform irrigation management for potatoes. *Applied engineering in agriculture, 22*(5), 677-688.

Klute, A., & Dirksen, C. (1986). Hydraulic conductivity and diffusivity: Laboratory methods. *Methods of soil analysis: part 1—physical and mineralogical methods*(methodsofsoilan1), 687-734.

Kodikara, J., Rajeev, P., Chan, D., & Gallage, C. (2013). Soil moisture monitoring at the field scale using neutron probe. *Canadian Geotechnical Journal, 51*(3), 332-345.

Koganti, T., Moral, F., Rebollo, F., Huang, J., & Triantafilis, J. (2017). Mapping cation exchange capacity using a Veris-3100 instrument and invVERIS modelling software. *Science of the Total Environment, 599*, 2156-2165.

Köksal, E. (2008). Irrigation water management with water deficit index calculated based on oblique viewed surface temperature. *Irrigation Science, 27*(1), 41-56.

Köksal, E., Artik, C., & Tasan, M. (2019). Crop Evapotranspiration Estimations of Red Pepper Using Field Level Remote Sensing Data and Energy Balance. *Polish Journal of Environmental Studies, 28*(1).

Krabill, W., Collins, J., Link, L., Swift, R., & Butler, M. (1984). Airborne laser topographic mapping results. *Photogrammetric Engineering and Remote Sensing, 50*(6), 685-694.

Kullberg, E. G., DeJonge, K. C., & Chávez, J. L. (2017). Evaluation of thermal remote sensing indices to estimate crop evapotranspiration coefficients. *Agricultural Water Management, 179*, 64-73.

Lachat Instruments. (1998c). Quik Chem Method 12-107-06-3-A. *Milwaukee, WI, USA*.

Lachat Instruments. (1998f). Quik Chem Method 12-115-01-1-A. *Milwaukee, WI, USA*.

Lati, R. N., Manevich, A., & Filin, S. (2013). Three-dimensional image-based modelling of linear features for plant biomass estimation. *International Journal of Remote Sensing, 34*(17), 6135-6151.
Lawes, R., Oliver, Y., & Robertson, M. (2009). Integrating the effects of climate and plant available soil water holding capacity on wheat yield. *Field Crops Research, 113*(3), 297-305.
Lea-Cox, J. D. (2012). Using wireless sensor networks for precision irrigation scheduling. *Problems, perspectives and challenges of agricultural water management. InTech Press, Rijeka, Croatia*, 233-258.
Leco. (2003). *Total/organic carbon and nitrogen in soils*. Retrieved from LECO Corporation, St. Joseph, MO, Organic Application Note 203-821-165:
Lefsky, M., Cohen, W., Parker, G., & Harding, D. (2002). Lidar remote sensing for ecosystem studies. *AIBS Bulletin, 52*(1), 19-30.
Lenka, S., Singh, A. K., & Lenka, N. (2009). Water and nitrogen interaction on soil profile water extraction and ET in maize–wheat cropping system. *Agricultural Water Management, 96*(2), 195-207.
Li, W., Niu, Z., Huang, N., Wang, C., Gao, S., & Wu, C. (2015). Airborne LiDAR technique for estimating biomass components of maize: A case study in Zhangye City, Northwest China. *Ecological indicators, 57*, 486-496.
Liang, Q., Yuan, D., Wang, Y., & Chen, H.-H. (2007). A cross-layer transmission scheduling scheme for wireless sensor networks. *Computer Communications, 30*(14), 2987-2994.
Liang, X., Liakos, V., Wendroth, O., & Vellidis, G. (2016). Scheduling irrigation using an approach based on the van Genuchten model. *Agricultural Water Management, 176*, 170-179.
Lilley, J., & Kirkegaard, J. (2011). Benefits of increased soil exploration by wheat roots. *Field Crops Research, 122*(2), 118-130.
Liping, C., Chunjiang, Z., Xuexin, L., & Xiaohong, D. (2002). Design and implementation of intelligent decision support system for precision agriculture [J]. *Transactions of The Chinese Society of Agricultural Engineering, 2*, 036.
Liu, D., & Feng, J. (2006). Analysis of precision irrigation and its perspective. *Water Saving Irrigation, 1*, 43-44.
Liu, X., Xu, Y., Zhong, X., Zhang, W., Porter, J. R., & Liu, W. (2012). Assessing models for parameters of the Ångström–Prescott formula in China. *Applied energy, 96*, 327-338.
Lokhorst, C., & Kasper, G. (1998). Site specific grassland management: measuring techniques, spatial-and temporal variation in grass yields. In *Proceedings of the VDI-MEG Tagung Landtechnik, 15-16 Oktober 1998, Garching, Germany, p. 209-214*.
Lu, J., Sun, G., McNulty, S. G., & Amatya, D. M. (2005). A Comparison of Six Potential Evapotranspiration Methods for Regional Use in the Southeastern United States 1. *JAWRA Journal of the American Water Resources Association, 41*(3), 621-633.
Lukangu, G., Savage, M. J., & Johnston, M. A. (1999). Use of sub-hourly soil water content measured with a frequency-domain reflectometer to schedule irrigation of cabbages. *Irrigation Science, 19*(1), 7-13.
Lumme, J., Karjalainen, M., Kaartinen, H., Kukko, A., Hyyppä, J., Hyyppä, H., . . . Kleemola, J. (2008). Terrestrial laser scanning of agricultural crops. *The International Archives of the Photogrammetry, Remote Sensing and Spatial Information Sciences, 37*(B5), 563-566.

Lund, E., Christy, C., & Drummond, P. (1999). *Practical applications of soil electrical conductivity mapping.* Paper presented at the Europe: 2nd European Conference of Precision Agric.

Ly, S., Charles, C., & Degré, A. (2013). Different methods for spatial interpolation of rainfall data for operational hydrology and hydrological modeling at watershed scale. A review. *Biotechnologie, Agronomie, Société et Environnement, 17*(2), 392.

Lynch, J. P. (2013). Steep, cheap and deep: an ideotype to optimize water and N acquisition by maize root systems. *Annals of botany, 112*(2), 347-357.

Marek, T., Almas, L., Amosson, S., & Cox, E. (1998). *The feasibility of variable rate irrigation with centre pivot systems in the northern Texas High Plains.* Paper presented at the 2001 ASAE Annual Meeting.

Marsal, J., Johnson, S., Casadesus, J., Lopez, G., Girona, J., & Stöckle, C. (2014). Fraction of canopy intercepted radiation relates differently with crop coefficient depending on the season and the fruit tree species. *Agricultural and forest meteorology, 184*, 1-11.

Marsal, J., & Stöckle, C. (2012). Use of CropSyst as a decision support system for scheduling regulated deficit irrigation in a pear orchard. *Irrigation Science, 30*(2), 139-147.

McCann, I., King, B., & Stark, J. (1997). Variable rate water and chemical application for continuous-move sprinkler irrigation systems. *Applied engineering in agriculture, 13*(5), 609-615.

McCarthy, A., Hancock, N., & Raine, S. (2010). VARIwise: A general-purpose adaptive control simulation framework for spatially and temporally varied irrigation at sub-field scale. *Computers and Electronics in Agriculture, 70*(1), 117-128.

McKenzie, H., & Wallace, H. S. (1954). The Kjeldahl determination of nitrogen: a critical study of digestion conditions-temperature, catalyst, and oxidizing agent. *Australian Journal of Chemistry, 7*(1), 55-70.

McMaster, G. S., & Wilhelm, W. (1997). Growing degree-days: one equation, two interpretations. *Agricultural and forest meteorology, 87*(4), 291-300.

McNeill, J. (1980). Electromagnetic terrain conductivity measurement at low induction numbers. *Technical Note TN-6. Geonics Limited, Mississauga, Ontario, Canada.*

McQueen, D. (1993). *Glossary of soil physical terms. Lower Hutt*. New Zealand: Landcare Research.

Meisinger, J., & Delgado, J. (2002). Principles for managing nitrogen leaching. *Journal of Soil and Water Conservation, 57*(6), 485-498.

Meron, M., Assaf, R., Bravdo, B., Wallach, R., Hallel, R., Levin, A., & Dahan, I. (1995). *Soil sensor actuated microirrigation of apples.* Paper presented at the Proceedings of the 5th International Microirrigation Congress, ASABE.

Mertens , M., Pätzold, S., & Welp, G. (2008). Spatial heterogeneity of soil properties and its mapping with apparent electrical conductivity. *Journal of Plant Nutrition and Soil Science, 171*(2), 146-154.

Ministry for the Environment. (2014). National policy statement for freshwater management 2014.

Michéli, E., Schad, P., Spaargaren, O., Dent, D., & Nachtergaele, F. (2006). World Reference Base for Soil Resources: A Framework for International Classification, Correlation and Communication. *FAO (Food and Agriculture Organization)*.

Miller, D., & Aarstad, J. (1972). Estimating Deep Drainage Between Irrigations 1. *Soil Science Society of America Journal, 36*(1), 124-127.

Moazami, S., Golian, S., Kavianpour, M. R., & Hong, Y. (2013). Comparison of PERSIANN and V7 TRMM Multi-satellite Precipitation Analysis (TMPA) products with rain gauge data over Iran. *International Journal of Remote Sensing, 34*(22), 8156-8171.

Moghaddasi, M., Morid, S., Araghinejad, S., & Alikhani, M. A. (2010). Assessment of irrigation water allocation based on optimization and equitable water reduction approaches to reduce agricultural drought losses: the 1999 drought in the Zayandeh Rud irrigation system (Iran). *Irrigation and Drainage, 59*(4), 377-387.

Molden, D., Oweis, T., Pasquale, S., Kijne, J., Hanjra, M., Bindraban, P., . . . Farahani, H. (2007). Pathways for increasing agricultural water productivity. In *A Comprehensive Assessment of Water Management in Agriculture* (pp. 279-310). London, UK: Earthscan; Colombo, Sri Lanka: International Water Management Institute.

Moral, F., Terrón, J., & Da Silva, J. M. (2010). Delineation of management zones using mobile measurements of soil apparent electrical conductivity and multivariate geostatistical techniques. *Soil and Tillage Research, 106*(2), 335-343.

Mulla, D. J. (2013). Twenty five years of remote sensing in precision agriculture: Key advances and remaining knowledge gaps. *Biosystems engineering, 114*(4), 358-371.

Neale, C. M., Bausch, W. C., & Heermann, D. F. (1990). Development of reflectance-based crop coefficients for corn. *Transactions of the ASAE, 32*(6), 1891-1900.

Nelson, R., Krabill, W., & Tonelli, J. (1988). Estimating forest biomass and volume using airborne laser data. *Remote Sensing of Environment, 24*(2), 247-267.

Nielsen, D. (1990). Scheduling irrigations for soybeans with the crop water stress index (CWSI). *Field Crops Research, 23*(2), 103-116.

Nielsen, D., Biggar, J., & Erh, K. (1973). Spatial variability of field-measured soil-water properties. *California Agriculture, 42*(7), 215-259.

Nijbroek, R., Hoogenboom, G., & Jones, J. (2003). Optimizing irrigation management for a spatially variable soybean field. *Agricultural Systems, 76*(1), 359-377.

Nikolidakis, S., Kandris, D., Vergados, D., & Douligeris, C. (2015). Energy efficient automated control of irrigation in agriculture by using wireless sensor networks. *Computers and Electronics in Agriculture, 113*, 154-163.

NIWA. (2018). Virtual climate station data and products. Retrieved from www.niwa.co.nz. Retrieved 29 May 2017 www.niwa.co.nz

Nolz, R. (2016). A review on the quantification of soil water balance components as a basis for agricultural water management with a focus on weighing lysimeters and soil water sensors/Ein Überblick über die Ermittlung von Wasserhaushaltsgrößen als Basis für die landeskulturelle Wasserwirtschaft mit Fokus auf Lysimeter und Bodenwassersensoren. *Die Bodenkultur: Journal of Land Management, Food and Environment, 67*(3), 133-144.

O'Shaughnessy, S., & Evett, S. (2008). *Integration of wireless sensor networks into moving irrigation systems for automatic irrigation scheduling.* Paper presented at the 2008 Providence, Rhode Island, June 29–July 2, 2008.

O'Shaughnessy, S., & Evett, S. (2010). Developing wireless sensor networks for monitoring crop canopy temperature using a moving sprinkler system as a platform. *Applied engineering in agriculture, 26*(2), 331-341.
O'Toole, J., Turner, N., Namuco, O., Dingkuhn, M., & Gomez, K. (1984). Comparison of some crop water stress measurement methods. *Crop science, 24*(6), 1121-1128.
Olea, R. (2000). Geostatistics for engineers and earth scientists. In. Norwell, MA: Kluwer Academic Publishers. .
Oliveiria, C., Yoder, R., & Larson, J. (2005). *Evaluating the returns to site-specific irrigation.* Paper presented at the Proc. 7th Intl. Conf. on Precision Agriculture.
Omary, M., Camp, C., & Sadler, E. (1997). Centre pivot irrigation system modification to provide variable water application depths. *Applied engineering in agriculture, 13*(2), 235-239.
Orta, A., Erdem, Y., & Erdem, T. (2003). Crop water stress index for watermelon. *Scientia horticulturae, 98*(2), 121-130.
Oswald, J., Werner, H., & Trooien, T. (2006). Automated water management for centre pivot irrigation systems. *In Proc. Intl. Exposition and Technical Conf., 349-356. Falls Church, Va.: The Irrigation Association., 45*(01).
Papadavid, G., Hadjimitsis, D., Michaelides, S., & Nisantzi, A. (2011). Crop evapotranspiration estimation using remote sensing and the existing network of meteorological stations in Cyprus. *Advances in Geosciences, 30*, 39-44.
Pardossi, A., Incrocci, L., Incrocci, G., Malorgio, F., Battista, P., Bacci, L., . . . Balendonck, J. (2009). Root zone sensors for irrigation management in intensive agriculture. *Sensors, 9*(4), 2809-2835.
Paulus, S., Dupuis, J., Riedel, S., & Kuhlmann, H. (2014). Automated analysis of barley organs using 3D laser scanning: An approach for high throughput phenotyping. *Sensors, 14*(7), 12670-12686.
Pebesma, E. J. (2004). Multivariable geostatistics in S: the gstat package. *Computers & Geosciences, 30*(7), 683-691.
Peijin, H., Ting, J., & Yandong, Z. (2011). Monitoring system of soil water content based on zigbee wireless sensor network. *Transactions of The Chinese Society of Agricultural Engineering, 2011*(4).
Penny, M., Billard, B., & Abbot, R. (1989). LADS—the Australian laser airborne depth sounder. *International Journal of Remote Sensing, 10*(9), 1463-1479.
Perea, R. G., Daccache, A., Díaz, J. R., Poyato, E. C., & Knox, J. W. (2018). Modelling impacts of precision irrigation on crop yield and in-field water management. *Precision Agriculture, 19*(3), 497-512.
Peters, R., & Evett, S. (2004). *Complete Centre Pivot Automation Using the Temperature-Time Threshold Method of Irrigation Scheduling.* Paper presented at the 2004 ASAE Annual Meeting.
Peters, R., & Evett, S. (2005). *Mechanized irrigation system positioning using two inexpensive GPS receivers.* Paper presented at the 2005 ASAE Annual Meeting.
Peters, R., & Evett, S. (2007). Spatial and temporal analysis of crop conditions using multiple canopy temperature maps created with centre-pivot-mounted infrared thermometers. *Transactions of the ASABE, 50*(3), 919-927.
Peters, R., & Evett, S. (2008). Automation of a centre pivot using the temperature-time-threshold method of irrigation scheduling. *Journal of irrigation and drainage engineering, 134*(3), 286-291.

Phene, C. (1986). Operation principles: automation. In Trickle Irrigation for Crop Production: Design, Operation, and Management, ed. F.S. *Nakayama and D.A. Bucks, Elsevier, Tokyo, pp. 188-215.*

Phene, C., & Howell, T. (1984). Soil sensor control of high-frequency irrigation systems. *Transactions of the ASAE, 27*(2), 392-0396.

Phene, C., Hutmacher, R., & Davis, K. (1992). *Subsurface drip irrigation: cotton does not need to be a high water user.* Paper presented at the Proceedings Beltwide Cotton Production Research Conferences, vol. I. D.J. Herber, 489-493. Memphis, Tenn. National Cotton Council of America.

Picón-Toro, J., González-Dugo, V., Uriarte, D., Mancha, L., & Testi, L. (2012). Effects of canopy size and water stress over the crop coefficient of a "Tempranillo" vineyard in south-western Spain. *Irrigation Science, 30*(5), 419-432.

Pierce, F. (2010). Precision Irrigation. *Advanced Engineering Systems for Specialty Crops: A Review of Precision Agriculture for Water, Chemical, and Nutrient Application, and Yield Monitoring, Upadhyaya, SK, Giles, DK, Haneklaus, S. and Schnug, E.(Eds). Landbauforschung, vTI-Agriculture and Forestry Research, special*(340).

Pittman, J., Arnall, D., Interrante, S., Moffet, C., & Butler, T. (2015). Estimation of biomass and canopy height in bermudagrass, alfalfa, and wheat using ultrasonic, laser, and spectral sensors. *Sensors, 15*(2), 2920-2943.

Plant, R. (2001). Site-specific management: the application of information technology to crop production. *Computers and Electronics in Agriculture, 30*(1), 9-29.

Pollok, J., Nelson, P., Touhy, M., Gillingham, S., & Alexander, M. (2003). *Massey University Soil Map, arcgisweb.massey.ac.nz*. Retrieved from Massey University.

Priestley, C. H. B., & Taylor, R. (1972). On the assessment of surface heat flux and evaporation using large-scale parameters. *Monthly Weather Review, 100*(2), 81-92.

Probert, M., Dimes, J., Keating, B., Dalal, R., & Strong, W. (1998). APSIM's water and nitrogen modules and simulation of the dynamics of water and nitrogen in fallow systems. *Agricultural Systems, 56*(1), 1-28.

R Core Team. (2018). R: A language and environment for statistical computing. R Foundation for Statistical Computing, Vienna, Austria. URL https://www.R-project.org/.

Raine, S., Meyer, W., Rassam, D., Hutson, J. L., & Cook, F. (2007). Soil–water and solute movement under precision irrigation: knowledge gaps for managing sustainable root zones. *Irrigation Science, 26*(1), 91-100.

Ratliff, L. F., Ritchie, J. T., & Cassel, D. K. (1983). Field-Measured Limits of Soil Water Availability as Related to Laboratory-Measured Properties 1. *Soil Science Society of America Journal, 47*(4), 770-775.

Reginato, R., & Howe, J. (1985). Irrigation scheduling using crop indicators. *Journal of irrigation and drainage engineering, 111*(2), 125-133.

Remorini, D., & Massai, R. (2003). Comparison of water status indicators for young peach trees. *Irrigation Science, 22*(1), 39-46.

Reyes-González, A., Kjaersgaard, J., Trooien, T., Hay, C., & Ahiablame, L. (2018). Estimation of crop evapotranspiration using satellite remote sensing-based vegetation index. *Advances in Meteorology, 2018*.

Rhoades, J., Manteghi, N., Shouse, P., & Alves, W. (1989). Soil electrical conductivity and soil salinity: New formulations and calibrations. *Soil Science Society of America Journal, 53*(2), 433-439.

Richards, Q., Bange, M., & Johnston, S. (2008). HydroLOGIC: An irrigation management system for Australian cotton. *Agricultural Systems, 98*(1), 40-49.
Rico-Ramirez, M., Cluckie, I., Shepherd, G., & Pallot, A. (2007). A high-resolution radar experiment on the island of Jersey. *Meteorological Applications, 14*(2), 117-129.
Rinaldi, M., Garofalo, P., Rubino, P., & Steduto, P. (2011). Processing tomatoes under different irrigation regimes in Southern Italy: agronomic and economic assessments in a simulation case study. *Journal of Agrometeorology, 3*(2011).
Rinaldi, M., & He, Z. (2014). Decision support systems to manage irrigation in agriculture. *Adv. Agron, 123*, 229-279.
Robinson, D., Lebron, I., Kocar, B., Phan, K., Sampson, M., Crook, N., & Fendorf, S. (2009). Time-lapse geophysical imaging of soil moisture dynamics in tropical deltaic soils: An aid to interpreting hydrological and geochemical processes. *Water resources research, 45*(4).
Rocha, J., Perdigão, A., Melo, R., & Henriques, C. (2012). Remote sensing based crop coefficients for water management in agriculture. *Sustainable Development-Authoritative and Leading Edge Content for Environmental Management*, 167-192.
Rouse Jr, J. W., Haas, R., Schell, J., & Deering, D. (1974). Monitoring vegetation systems in the Great Plains with ERTS. NASA. Goddard Space Flight Center 3d ERTS-1 Symp., Vol. 1, Sect. A"; p. p 309-317
Ruiz-Garcia, L., Lunadei, L., Barreiro, P., & Robla, I. (2009). A review of wireless sensor technologies and applications in agriculture and food industry: state of the art and current trends. *Sensors, 9*(6), 4728-4750.
Sadler, E., Bauer, P., & Busscher, W. (2000a). Site-specific analysis of a droughted corn crop: I. Growth and grain yield. *Agronomy Journal, 92*(3), 395-402.
Sadler, E., Camp, C., Evans, D., & Usrey, L. (1996). A site-specific centre pivot irrigation system for highly-variable coastal plain soils. *Precision Agriculture*(precisionagricu3), 827-834.
Sadler, E., Evans, R., Buchleiter, G., King, B., & Camp, C. (2000b). *Design considerations for site specific irrigation.* Paper presented at the National irrigation symposium. Proceedings of the 4th Decennial Symposium, Phoenix, Arizona, USA, November 14-16, 2000.
Saeys, W., Lenaerts, B., Craessaerts, G., & De Baerdemaeker, J. (2009). Estimation of the crop density of small grains using LiDAR sensors. *Biosystems Engineering, 102*(1), 22-30.
Saha, S., Moorthi, S., Pan, H.-L., Wu, X., Wang, J., Nadiga, S., . . . Behringer, D. (2010). The NCEP climate forecast system reanalysis. *Bulletin of the American Meteorological Society, 91*(8), 1015-1058.
Salter, P., & Haworth, F. (1961). The available-water capacity of a sandy loam soil: I. A critical comparison of methods of determining the moisture content of soil at field capacity and at the permanent wilting percentage. *Journal of Soil Science, 12*(2), 326-334.
Salunkhe, R., Patil, M., & G. Deshmukh, M. (2014). *Irrigation Scheduling (Response of Wheat to IW/CPE)*.
Samarah, N. H. (2005). Effects of drought stress on growth and yield of barley. *Agron. Sustain. Develop. 25: 145-149.*
Sanderson, M. A., Rotz, C. A., Fultz, S. W., & Rayburn, E. B. (2001). Estimating forage mass with a commercial capacitance meter, rising plate meter, and pasture ruler. *Agronomy Journal, 93*(6), 1281-1286.

Santos, C., Lorite, I., Tasumi, M., Allen, R., & Fereres, E. (2010). Performance assessment of an irrigation scheme using indicators determined with remote sensing techniques. *Irrigation Science, 28*(6), 461-477.
Santos, M. (2004). 1-D laterally constrained inversion of EM34 profiling data. *Journal of Applied Geophysics, 56*(2), 123-134.
Santos, M., Triantafilis, J., & Bruzgulis, K. (2011). A spatially constrained 1D inversion algorithm for quasi-3D conductivity imaging: Application to DUALEM-421 data collected in a riverine plain. *Geophysics, 76*(2), B43-B53.
Santos, M., Triantafilis, J., Taylor, R., Holladay, S., & Bruzgulis, K. (2010). Inversion of conductivity profiles from EM using full solution and a 1-D laterally constrained algorithm. *Journal of Environmental & Engineering Geophysics, 15*(3), 163-174.
Sasaki, Y. (1989). Two-dimensional joint inversion of magnetotelluric and dipole-dipole resistivity data. *Geophysics, 54*(2), 254-262.
Schmidt, J., Kienzle, S. W., & Srinivasan, M. (2009). Estimating increased evapotranspiration losses caused by irrigated agriculture as part of the water balance of the Orari Catchment, Canterbury, New Zealand. *Journal of Hydrology (New Zealand)*, 73-94.
Schume, H., Hager, H., & Jost, G. (2005). Water and energy exchange above a mixed European Beech–Norway Spruce forest canopy: a comparison of eddy covariance against soil water depletion measurement. *Theoretical and applied climatology, 81*(1-2), 87-100.
Scotford, I., & Miller, P. (2003). *Monitoring the growth of winter wheat using measurements of normalised difference vegetation index (NDVI) and crop height.* Paper presented at the 4th European Conference on Precision Agriculture. Eds. J Stafford and A Werner.
Scott, R. L. (2010). Using watershed water balance to evaluate the accuracy of eddy covariance evaporation measurements for three semiarid ecosystems. *Agricultural and forest meteorology, 150*(2), 219-225.
Senay, G., Budde, M. E., & Verdin, J. P. (2011). Enhancing the Simplified Surface Energy Balance (SSEB) approach for estimating landscape ET: Validation with the METRIC model. *Agricultural Water Management, 98*(4), 606-618.
Serrano, J., Shahidian, S., & Silva, J. (2014). Spatial and temporal patterns of apparent electrical conductivity: DUALEM vs. Veris sensors for monitoring soil properties. *Sensors, 14*(6), 10024-10041.
Sezen, S. M., Yazar, A., Daşgan, Y., Yucel, S., Akyıldız, A., Tekin, S., & Akhoundnejad, Y. (2014). Evaluation of crop water stress index (CWSI) for red pepper with drip and furrow irrigation under varying irrigation regimes. *Agricultural Water Management, 143*, 59-70.
Sezen, S. M., Yazar, A., & Eker, S. (2006). Effect of drip irrigation regimes on yield and quality of field grown bell pepper. *Agricultural Water Management, 81*(1-2), 115-131.
Shock, C., Feibert, E. B., & Saunders, M. (1998). Irrigation Management for drip-irrigated onions. *Oregon State University Agricultural Experiment Station, Special Report, 988*, 42-48.
Shrivastav, M. (2015). *Using ArcGIS hydrologic modeling and LiDAR digital elevation data to evaluate surface runoff interception performance of riparian vegetative filter strip buffers in central Iowa.* Iowa State University,
Siebert, S., Henrich, V., Frenken, K., & Burke, J. (2013). Update of the digital global map of irrigation areas to version 5. *Rheinische Friedrich-Wilhelms-Universität,*

Bonn, Germany and Food and Agriculture Organization of the United Nations, Rome, Italy.
Slowik, K., Labanauskas, C., Stolzy, L., & Zentmyer, G. (1979). Influence of rootstocks, soil oxygen, and soil moisture on the uptake and translocation of nutrients in young avocado. *J. Am. Soc. Hortic. Sci, 104*, 172-175.
Sluiter, R. (2008). *Interpolation methods for climate data: literature review. KNMI, R&D Information and Observation Technology,…(pp. 1–28)*. Retrieved from https://www.snap.uaf.edu/sites/default/files/files/Interpolation_methods_for_climate_data.pdf:
Smajstrla, A., & Harrison, D. (1998). Tensiometers for soil moisture measurement and irrigation scheduling. Circular 487. *Inst. Food Agr. Sci., Univ. of Fla., Gainesville*.
Smith, K. (2000). *Soil and environmental analysis: physical methods, revised, and expanded*: CRC Press.
Smith, M. (1992). *CROPWAT: A computer program for irrigation planning and management. FAO Irrigation and Drainage Paper No. 46.*: Food & Agriculture Org.
Smith, M., & Allen, S. (1996). Measurement of sap flow in plant stems. *Journal of experimental botany, 47*(12), 1833-1844.
Statistics NZ. (2019). Agricultural Production Statistics. Retrieved from http://www.stats.govt.nz/browse_for_stats/industry_sectors/agriculture-horticultureforestry/AgriculturalProduction_final_HOTPJun12final.aspx. http://www.stats.govt.nz/browse_for_stats/industry_sectors/agriculture-horticultureforestry/AgriculturalProduction_final_HOTPJun12final.aspx
Steduto, P., Hsiao, T., Raes, D., & Fereres, E. (2009). AquaCrop—The FAO crop model to simulate yield response to water: I. Concepts and underlying principles. *Agronomy Journal, 101*(3), 426-437.
Steduto, P., Hsiao, T. C., Fereres, E., & Raes, D. (2012). *Crop yield response to water* (Vol. 1028): fao Rome.
Stewart, C., McBratney, A., & Skerritt, J. (2002). Site-specific durum wheat quality and its relationship to soil properties in a single field in northern New South Wales. *Precision Agriculture, 3*(2), 155-168.
Stockle, C., & Dugas, W. (1992). Evaluating canopy temperature-based indices for irrigation scheduling. *Irrigation Science, 13*(1), 31-37.
Stone, K., Smajstria, A., & Zazueta, F. (1985). Microcomputer: based data acquisition system for continuous soil water potential measurements. *Proceedings-Soil and Crop Science Society of Florida (USA)*.
Su, H., McCabe, M., Wood, E. F., Su, Z., & Prueger, J. (2005). Modeling evapotranspiration during SMACEX: Comparing two approaches for local-and regional-scale prediction. *Journal of hydrometeorology, 6*(6), 910-922.
Sudduth, K., Kitchen, N., Wiebold, W., Batchelor, W., Bollero, G., Bullock, D., . . . Schuler, R. (2005a). Relating apparent electrical conductivity to soil properties across the north-central USA. *Computers and Electronics in Agriculture, 46*(1), 263-283.
Sudduth, K., Kitchen, N., Wiebold, W., Batchelor, W., Bollero, G. A., Bullock, D., . . . Schuler, R. (2005b). Relating apparent electrical conductivity to soil properties across the north-central USA. *Computers and electronics in agriculture, 46*(1-3), 263-283.

Sudduth, K., Myers, D. B., Kitchen, N. R., & Drummond, S. T. (2013). Modeling soil electrical conductivity–depth relationships with data from proximal and penetrating ECa sensors. *Geoderma, 199*, 12-21.

Svobodová, I., & Misa, P. (2004). Effect of drought stress on the formation of yield elements in spring barley and the potential of stress expression reduction by foliar application of fertilizers and growth stimulator. *Plant Soil and Environment, 50*(10), 439-446.

Taherparvar, M., & Pirmoradian, N. (2018). Estimation of Rice Evapotranspiration Using Reflective Images of Landsat Satellite in Sefidrood Irrigation and Drainage Network. *Rice Science, 25*(2), 111-116.

Testezlaf, R., Zazueta, F., & Yeager, T. (1997). A real-time irrigation control system for greenhouses. *Applied engineering in agriculture, 13*(3), 329-332.

Thi, D., Ha, N. T. T., Tran Dang, Q., Koike, K., & Trong, N. M. (2019). Effective Band Ratio of Landsat 8 Images Based on VNIR-SWIR Reflectance Spectra of Topsoils for Soil Moisture Mapping in a Tropical Region. *Remote Sensing, 11*(6), 716.

Thompson, R., Gallardo, M., Valdez, L., & Fernández, M. (2007). Using plant water status to define threshold values for irrigation management of vegetable crops using soil moisture sensors. *Agricultural Water Management, 88*(1-3), 147-158.

Thorp, K. R., DeJonge, K. C., Kaleita, A. L., Batchelor, W. D., & Paz, J. O. (2008). Methodology for the use of DSSAT models for precision agriculture decision support. *Computers and Electronics in Agriculture, 64*(2), 276-285.

Thysen, I., & Detlefsen, N. (2006). Online decision support for irrigation for farmers. *Agricultural Water Management, 86*(3), 269-276.

Tilly, N., Hoffmeister, D., Cao, Q., Lenz-Wiedemann, V., Miao, Y., & Bareth, G. (2013). *Precise plant height monitoring and biomass estimation with terrestrial laser scanning in paddy rice.* Paper presented at the Proceedings of the ISPRS Annals of the Photogrammetry, Remote Sensing and Spatial Information Sciences Conference, Antalya, Turkey.

Tomczak, M. (1998). Spatial interpolation and its uncertainty using automated anisotropic inverse distance weighting (IDW)-cross-validation/jackknife approach. *Journal of Geographic Information and Decision Analysis, 2*(2), 18-30.

Topp, G., & Davis, J. (1985). Time-domain reflectometry (TDR) and its application to irrigation scheduling. In *Advances in irrigation* (Vol. 3, pp. 107-127): Elsevier.

Topp, G., Davis, J., & Annan, A. (1980). Electromagnetic determination of soil water content: Measurements in coaxial transmission lines. *Water resources research, 16*(3), 574-582.

Torre-Neto, A., Schueller, J., & Haman, D. (2000). Networked sensing and valve actuation for spatially-variable microsprinkler irrigation. *Networked sensing and valve actuation for spatially-variable microsprinkler irrigation.*, 1-17.

Triantafilis, J., Ribeiro, J., Page, D., & Santos, F. M. (2013b). Inferring the location of preferential flow paths of a leachate plume by using a DUALEM-421 and a Quasi-Three-Dimensional inversion model. *Vadose Zone Journal, 12*(2).

Triantafilis, J., & Santos, F. M. (2010). 2-dimensional soil and vadose-zone representation using an EM38 and EM34 and a laterally constrained inversion model. *Soil Research, 47*(8), 809-820.

Triantafilis, J., & Santos, F. M. (2013c). An inversion approach to generate electromagnetic conductivity images from signal data. *Environmental modelling & software, 43*, 88-95.

Triantafilis, J., Terhune, C., & Santos, F. M. (2013a). Electromagnetic conductivity imaging (EMCI) of soil using a DUALEM-421 and inversion modelling software (EM4Soil). *Geoderma, 211*, 28-38.

UNEP. (2011). Investing in Natural Capital. UNEP, Towards a Green Economy: Pathways to Sustainable Development and Poverty Eradication. Nairobi, UNEP.

USDA, & Soil Conservation Service. (1975). *Soil taxonomy: a basic system of soil classification for making and interpreting soil surveys*: US Department of Agriculture.

User Manual for Scene. (2019). https://faro.app.box.com/s/uivkgf3jyrxcxn5ofazlohjnadddknhr.

Vachaud, G., Passerat de Silans, A., Balabanis, P., & Vauclin, M. (1985). Temporal Stability of Spatially Measured Soil Water Probability Density Function 1. *Soil Science Society of America Journal, 49*(4), 822-828.

Van Dam, J., Huygen, J., Wesseling, J., Feddes, R., Kabat, P., Van Walsum, P., . . . Van Diepen, C. (1997). *Theory of SWAP version 2.0; Simulation of water flow, solute transport and plant growth in the soil-water-atmosphere-plant environment. .* Retrieved from Report 71, Subdep. Water Resources, Wageningen University, Technical document 45, Alterra Green World Research, Wageningen:

van Iersel, M., Dove, S., & Burnett, S. (2009). *The use of soil moisture probes for improved uniformity and irrigation control in greenhouses.* Paper presented at the International Symposium on High Technology for Greenhouse Systems: GreenSys2009 893.

Vellidis, G., Liakos, V., Andreis, J., Perry, C., Porter, W., Barnes, E., . . . Migliaccio, K. (2016). Development and assessment of a smartphone application for irrigation scheduling in cotton. *Computers and Electronics in Agriculture, 127*, 249-259.

Vellidis, G., Tucker, M., Perry, C., Kvien, C., & Bednarz, C. (2008). A real-time wireless smart sensor array for scheduling irrigation. *Computers and Electronics in Agriculture, 61*(1), 44-50.

Vermeiren, L., & Jobling, G. (1980). *Localized irrigation: design, installation, operation, evaluation*: FAO Irrigation and Drainage Paper No.36, Rome, 203p.

Vicente, M. A., Gallardo, J. F., Moreno, G., & González, M. I. (2003). Comparison of soil water-contents as measured with a neutron probe and time domain reflectometry in a Mediterranean forest ("Sierra de Gata", Central Western Spain). *Annals of forest science, 60*(3), 185-193.

von Hebel, C., Rudolph, S., Mester, A., Huisman, J. A., Kumbhar, P., Vereecken, H., & van der Kruk, J. (2014). Three-dimensional imaging of subsurface structural patterns using quantitative large-scale multiconfiguration electromagnetic induction data. *Water resources research, 50*(3), 2732-2748.

Wall, R., King, B., & McCann, I. (1996). Centre-pivot irrigation system control and data communications network for real-time variable water application. *Precision Agriculture*(precisionagricu3), 757-766.

Wang, D., & Cai, X. (2009). Irrigation scheduling—Role of weather forecasting and farmers' behavior. *Journal of water resources planning and management, 135*(5), 364-372.

Wang, D., & Gartung, J. (2010). Infrared canopy temperature of early-ripening peach trees under postharvest deficit irrigation. *Agricultural Water Management, 97*(11), 1787-1794.
Wasson, A., Rebetzke, G., Kirkegaard, J., Christopher, J., Richards, R., & Watt, M. (2014). Soil coring at multiple field environments can directly quantify variation in deep root traits to select wheat genotypes for breeding. *Journal of experimental botany, 65*(21), 6231-6249.
Webster, R., & Oliver, M. A. (2007). Statistics in Practice. *Geostatistics for Environmental Scientists, Second Edition*, 316-317.
Weiss, M., Troufleau, D., Baret, F., Chauki, H., Prevot, L., Olioso, A., . . . Brisson, N. (2001). Coupling canopy functioning and radiative transfer models for remote sensing data assimilation. *Agricultural and forest meteorology, 108*(2), 113-128.
Wessels, W., Steyn, W., & Moolman, J. (1995). *Automatic microirrigation and salt injection system for research and commercial applications.* Paper presented at the Proceeding of the fifth international microirrigation Congress. Orlando Fl., USA. ASAE.
Wheeler, D. M., & Rutherford, K. (2014). Hydrology. OVERSEER® Technical manual. *2253-461X. 51 p. Retrieved 10 February 2015, from*

http://www.overseer.org.nz/OVERSEERModel/Information/Technicalmanual.aspx.
White, R. (2003). *Soils for fine wines*: Oxford University Press.
White, S., & Raine, S. (2008). A grower guide to plant based sensing for irrigation scheduling.
Widmoser, P. (2009). A discussion on and alternative to the Penman–Monteith equation. *Agricultural Water Management, 96*(4), 711-721.
Widmoser, P. (2010). An alternative to define canopy surface temperature bounds. *Agricultural Water Management, 97*(2), 224-230.
Williams, B., & Hoey, D. (1987). The use of electromagnetic induction to detect the spatial variability of the salt and clay contents of soils. *Soil Research, 25*(1), 21-27.
Williams, L., & Ayars, J. (2005). Water use of Thompson Seedless grapevines as affected by the application of gibberellic acid (GA3) and trunk girdling–practices to increase berry size. *Agricultural and forest meteorology, 129*(1-2), 85-94.
Wilson, K. B., Hanson, P. J., Mulholland, P. J., Baldocchi, D. D., & Wullschleger, S. D. (2001). A comparison of methods for determining forest evapotranspiration and its components: sap-flow, soil water budget, eddy covariance and catchment water balance. *Agricultural and forest meteorology, 106*(2), 153-168.
Wong, M., & Asseng, S. (2006). Determining the causes of spatial and temporal variability of wheat yields at sub-field scale using a new method of upscaling a crop model. *Plant and Soil, 283*(1-2), 203-215.
Wong, M., Asseng, S., Robertson, M., & Oliver, Y. (2008). Mapping subsoil acidity and shallow soil across a field with information from yield maps, geophysical sensing and the grower. *Precision Agriculture, 9*(1-2), 3-15.
Woods, M., Pitt, D., Penner, M., Lim, K., Nesbitt, D., Etheridge, D., & Treitz, P. (2011). Operational implementation of a LiDAR inventory in Boreal Ontario. *The Forestry Chronicle, 87*(4), 512-528.
Wraith, J. M., Robinson, D. A., Jones, S. B., & Long, D. S. (2005). Spatially characterizing apparent electrical conductivity and water content of surface soils

with time domain reflectometry. *Computers and Electronics in Agriculture, 46*(1-3), 239-261.
Wright, J. L. (1982). New evapotranspiration crop coefficients. *Proceedings of the American Society of Civil Engineers, Journal of the Irrigation and Drainage Division, 108*(IR2), 57-74.
Xiao, K., Xiao, D., & Luo, X. (2010). Smart water-saving irrigation system in precision agriculture based on wireless sensor network. *Transactions of The Chinese Society of Agricultural Engineering, 26*(11), 170-175.
Xu, C.-Y., & Singh, V. (2005). Evaluation of three complementary relationship evapotranspiration models by water balance approach to estimate actual regional evapotranspiration in different climatic regions. *Journal of hydrology, 308*(1-4), 105-121.
Xu, J., Peng, S., Ding, J., Wei, Q., & Yu, Y. (2013). Evaluation and calibration of simple methods for daily reference evapotranspiration estimation in humid East China. *Archives of Agronomy and Soil Science, 59*(6), 845-858.
Xue, Q., Zhu, Z., Musick, J., Stewart, B., & Dusek, D. (2003). Root growth and water uptake in winter wheat under deficit irrigation. *Plant and Soil, 257*(1), 151-161.
Xuejun, Y., Yongxin, L., Tiansheng, H., Yefu, W., Dongping, Q., & Zhuliang, C. (2013). Design and experiment of automatic irrigation control system based on soil moisture meter. *Transactions of the Chinese Society for Agricultural Machinery, 44*(S2), 241-246,250.
Yadav, M., Tripathi, J., Bhatt, R., & Rawal, N. (2018). Tensiometer based irrigation scheduling in wheat for improved water use efficiency in Nepal. *Journal of Soil and Water Conservation, 17*(3), 275-279.
Yang, M. (2015). *Benchmarking rainfall interpolation over the Netherlands*: University of Twente Faculty of Geo-Information and Earth Observation (ITC).
Yazar, A., Howell, T., Dusek, D., & Copeland, K. (1999). Evaluation of crop water stress index for LEPA irrigated corn. *Irrigation Science, 18*(4), 171-180.
Yildirim, M., Demirel, K., & Bahar, E. (2012). Effect of restricted water supply and stress development on growth of bell pepper (Capsicum Annuum L.) under drought conditions. *Journal of Agro Crop Science, 3*(1), 1-9.
Yu, X., Wu, P., Han, W., & Zhang, Z. (2013). A survey on wireless sensor network infrastructure for agriculture. *Computer Standards & Interfaces, 35*(1), 59-64.
Yuan, G., Luo, Y., Sun, X., & Tang, D. (2004). Evaluation of a crop water stress index for detecting water stress in winter wheat in the North China Plain. *Agricultural Water Management, 64*(1), 29-40.
Yuan, X., Wood, E. F., Luo, L., & Pan, M. (2011). A first look at Climate Forecast System version 2 (CFSv2) for hydrological seasonal prediction. *Geophysical research letters, 38*(13).
Yule, I., Hedley, C., & Bradbury, S. (2008). *Variable-rate irrigation.* Paper presented at the 12th Annual Symposium on Precision Agriculture Research & Application in Australasia. Sydney.
Zazueta, F., & Smajstrla, A. (1992). Microcomputer-based control of irrigation systems. *Applied engineering in agriculture, 8*(5), 593-596.
Zhang, L., & Grift, T. (2012). A LIDAR-based crop height measurement system for Miscanthus giganteus. *Computers and Electronics in Agriculture, 85*, 70-76.
Zhang, Y., & Feng, L. (2009). *CropIrri: A decision support system for crop irrigation management.* Paper presented at the International Conference on Computer and Computing Technologies in Agriculture.

Zhang, Y., Kendy, E., Qiang, Y., Changming, L., Yanjun, S., & Hongyong, S. (2004). Effect of soil water deficit on evapotranspiration, crop yield, and water use efficiency in the North China Plain. *Agricultural Water Management, 64*(2), 107-122.

Zhu, C., Peng, S., & Sun, J. (2003). Reseach on optimal irrigation scheduling of winter what with water-saving and high efficiency. *Journal of Irrigation and Drainage, 22*(5), 77-80.

Zhu, Y., Hu, J., Cao, W., & Zhang, J. (2005). Decision support system for field water management based on crop growth model. *Journal of Soil and Water Conservation, 19*(2), 160-162.

Appendix

The description of inversion algorithm (EM4Soil) by Santos (2004)

The nonlinear, smoothness-constrained inversion algorithm described by Santos (2004) was adopted in EM4Soil. The earth model used in the inversion process consists in a set of 1D models distributed according to the locations of the measurement sites. All the models have number of layers whose thickness is kept constant. Two forward modeling subroutines, one based on the cumulative response (McNeill, 1980; Wait, 1962) and another based on the full solution of the Maxwell equations (Kaufman & Keller, 1983), are used optionally to calculate the σa responses of the model.

Two inversion algorithms are available: in the S1 algorithm the optimization equations are represented as follows (Sasaki, 1989):

$$[(J^T J + \lambda\, C^T C)]\delta p = J^T b \qquad [1]$$

In the second algorithm S2 the equations are (Sasaki, 2001):

$$[(J^T J + \lambda\, C^T C)]\delta p = J^T b + \lambda\, C^T C(p - p_o) \qquad [2]$$

where δp is the vector containing the corrections applicable to the parameters (logarithm of block conductivities, pj) of an initial model, p_o is a reference model, b is the vector of the differences between the logarithm of the observed and calculated σa [$bi = \ln(\sigma a^o) - \ln(\sigma a^c)$], J is the Jacobian matrix whose elements are given by $(\sigma_j/\sigma_{ai}^c)(\partial\sigma_{ai}^c/\partial\sigma_j)$, the superscript T denotes the transpose operation, and λ is a Lagrange multiplier that controls the amplitude of the parameter corrections and whose best value is determined empirically. The value can be determined empirically by comparing the models calculated using different values with the available information. The elements of the matrix C are the coefficients of the values of the roughness in each parameter, which is defined in terms of the four neighbors parameters. The elements of C are -4, 1, or 0. An iterative process allows the final model to be obtained, with its response fitting the data set in a least square sense.

The misfit between data and model response is measured through the rmse (expressed in mS m^{-1}) defined by:

$$rmse = \sqrt{\frac{1}{N}\sum(\sigma_{ai}^{o} - \sigma_{ai}^{c})^2} \quad [3]$$

Cumulative Response of a Multilayered Earth

At low induction numbers, the magnetic coupling between ground current loops induced by the primary field is negligible and, for this reason, the secondary magnetic field measured at the receiver is the sum of the independent magnetic fields from each individual induced current loop (McNeill, 1980). In this case, and properly normalizing the measured fields, the depth of investigation depends only on the transmitter–receiver separation and not on the frequency or σ (Kaufman & Keller, 1983). It is then possible to construct a mathematical function of depth that describes the relative contribution to the secondary magnetic field, measured at the receiver, due to the homogeneous material within a thin horizontal layer at a depth d (Callegary et al., 2007; Gómez-Treviño et al., 2002; Kaufman & Keller, 1983; McNeill, 1980). It is worth mentioning that this approach is only valid for fairly resistive environments. For highly conductive structures, the instrument response is not linear and the use of the cumulative function will produce biased models (the conductivity of deeper layers will be underestimated if covered by highly conductive layers). In the presence of a layered-earth model, the relative contribution to the secondary magnetic field from all material up to a depth d below the sensor can be expressed by the cumulative function R (for HCP or PRP configurations used in the DUALEM instruments) as defined the (McNeill, 1980) and (Wait, 1962):

$$R_{HCP} = 1 - \frac{1}{\sqrt{4z^2 + 1}} \quad [4]$$

$$R_{PRP} = 1 - \frac{2z}{\sqrt{4z^2 + 1}} \quad [5]$$

where z (= d/s) represents the depth normalized by the coil spacing s. Taking into account these definitions, the response of an M-layer earth is calculated by adding the contribution

from each layer independently, weighted according to its conductivity and depth as

$$\sigma_a^c = \sigma_1 R(z_1) + \sum_{i=2}^{M-1} \sigma_i [R(z_i) - R(z_{i-1})] + \sigma_M [1 - R(z_{M-1})] \quad [6]$$

The derivatives of the apparent conductivity σac with respect to the layer conductivities are

$$\frac{\partial \sigma_a^c}{\partial \sigma_1} = R(z_1) \quad [7]$$

$$\frac{\partial \sigma_a^c}{\partial \sigma_1} = [R(z_1) - R(z_{i-1})] \quad i = 2, \ldots . M - 1 \quad [8]$$

$$\frac{\partial \sigma_a^c}{\partial \sigma_M} = [R(z_{M-1})] \quad [9]$$

Similar equations can be written for GEONICS instruments, EM31, EM38 and EM34 (McNeill, 1980):

$$R_{VDM} = \frac{1}{\sqrt{4z^2 + 1}} \quad [10]$$

$$R_{HDM} = \sqrt{4z^2 + 1 - 2z} \quad [11]$$

and,

$$\sigma_a^c = \sigma_1 [1 - R(z_1)] + \sum_{i=2}^{M-1} \sigma_i [R(z_i) - R(z_{i-1})] + \sigma_M [1 - R(z_{M-1})] \quad [12]$$

For the apparent conductivity calculations

Usually the initial thickness of the layers is kept constant in the inversion process. The use of the cumulative response to calculate the model response at each measuring site means that we are not considering the EM interaction between constituent blocks of the model; however, the smooth inversion algorithm constrains each block σ to be somewhat dependent on its neighbours. That is, the method represents a one-dimensional, laterally constrained approach and the final model is a rough representation of a two-dimensional model (Quasi-2D).

Full Solution of the Maxwell Equations

Forward calculations based on the work of Keller and Frischknecht (1966), Wait (1962) and Anderson (1979) are used to calculate sensor responses at each measuring site, assuming a 1-D model. For a vertical dipole as primary source the secondary components of the magnetic field measured at a site with coordinates (x, y, h) over a N-layer model are given by Keller and Frischknecht (1966)

$$H_{zs} = -\frac{m}{4\pi\delta^3} T_o(A, B) \qquad [13]$$

$$H_{xs} = -\frac{m}{4\pi\delta^3} \frac{x}{r} T_1(A, B) \qquad [14]$$

where m is the magnetic moment of the source and r is the transmitter-receiver distance. A, B and δ are given by

$$A = \frac{h}{\delta} \qquad [15]$$

$$B = \frac{r}{\delta} \qquad [16]$$

$$\delta = \sqrt{2/\sigma_1 \mu_0 \omega} \qquad [17]$$

and

$$T_o = -\int_0^\infty R_0(g)g^2 e^{-gA} J_0(gB)dg \qquad [18]$$

$$T_1 = -\int_0^\infty R_0(g)g e^{-gA} J_1(gB)dg \qquad [19]$$

Here, J_0 ( ) and J_1 ( ) are Bessel functions of the first kind of order 0 and 1, respectively. $R_0(g)$ is calculated recursively taking into account the conductivity and thickness of each layer.

Integrals in Equations (36) are evaluated using a subroutine developed by Anderson (1979).

The predicted values of the Quadrature component for HCP and PRP configurations at height h above the ground are given by

$$Q_{HCP} = \mathrm{Im}\left(\frac{H_{zs}}{H_{zp}}\right) \qquad [20]$$

$$Q_{PRP} = \mathrm{Im}\left(\frac{H_{ys}}{H_{zp}}\right) \qquad [21]$$

MASSEY UNIVERSITY
GRADUATE RESEARCH SCHOOL

STATEMENT OF CONTRIBUTION
DOCTORATE WITH PUBLICATIONS/MANUSCRIPTS

We, the candidate and the candidate's Primary Supervisor, certify that all co-authors have consented to their work being included in the thesis and they have accepted the candidate's contribution as indicated below in the *Statement of Originality*.

Name of candidate:	Ahmed El-Naggar
Name/title of Primary Supervisor:	Associate Professor David Horne
Name of Research Output and full reference:	
El-Naggar, A.G., Hedley, C.B., Horne, D., Roudier, P. and Clothier, B.E., 2019. Soil sensing technology improves application of irrigation water. Agricultural Water Management, p. 105901.https://doi.org/10.1016/j.agwat.2019.105901	
In which Chapter is the Manuscript /Published work:	Chapter 5
Please indicate:	
• The percentage of the manuscript/Published Work that was contributed by the candidate:	85%
and	
• Describe the contribution that the candidate has made to the Manuscript/Published Work:	
The candidate designed and performed all of the field work in this publication. He conducted all of the statistical analysis. He also took the lead role in interpreting the data. The candidate wrote the paper and oversaw its publication in the journal.	
For manuscripts intended for publication please indicate target journal:	
Chapter 4: Precision Agriculture – Chapter 6: Remote Sensing – Chapter 8 and 9: Irrigation and Drainage	
Candidate's Signature:	Ahmed El-Naggar Digitally signed by Ahmed El-Naggar Date: 2019.12.12 08:13:50 +13'00'
Date:	12 December 2019
Primary Supervisor's Signature:	David John Horne Digitally signed by David John Horne Date: 2019.12.11 22:17:34 +13'00'
Date:	11 December 2019

(This form should appear at the end of each thesis chapter/section/appendix submitted as a manuscript/ publication or collected as an appendix at the end of the thesis)